

**STRUCTURE BASED DESIGN AND DEVELOPMENT OF
KINASE INHIBITORS AND DENDRIMERIC NANOPROBE
BASED ON 2-AMINOTHIAZOLE TEMPLATE**

*A Thesis submitted
in partial fulfillment for the Degree of*

Doctor of Philosophy

by

SARAH TITUS



Department of Chemistry

**INDIAN INSTITUTE OF SPACE SCIENCE AND TECHNOLOGY
THIRUVANANTHAPURAM**

JUNE, 2016

CERTIFICATE

This is to certify that the thesis entitled **Structure Based Design and Development of Kinase Inhibitors and Dendrimeric Nanoprobe Based on 2-aminothiazole Template** submitted by **Sarah Titus** to the Indian Institute of Space Science and Technology, Thiruvananthapuram, in partial fulfillment for the award of the degree of **Doctor of Philosophy** is a *bona fide* record of research work carried out by her under my supervision. The contents of this thesis, in full or in parts, have not been submitted to any other Institution or University for the award of any degree or diploma.

Dr. K. G. Sreejalekshmi
Supervisor
Department of Chemistry

Thiruvananthapuram
June, 2016

Counter signature of HOD with seal

DECLARATION

I declare that this thesis entitled **Structure Based Design and Development of Kinase Inhibitors and Dendrimeric Nanoprobe Based on 2-aminothiazole Template** submitted in partial fulfillment of the degree of **Doctor of Philosophy** is a record of original work carried out by me under the supervision of Dr. K. G. Sreejalekshmi, and has not formed the basis for the award of any other degree or diploma, in this or any other Institution or University. In keeping with the ethical practice in reporting scientific information, due acknowledgements have been made wherever the findings of others have been cited.

Sarah Titus
SC11D004

Thiruvananthapuram – 695547
16/06/2016

ACKNOWLEDGEMENTS

I owe many people whom, without their support and cooperation this thesis would not have been possible. I take this opportunity to express my sincere gratitude towards each one of them.

The foremost person I would like to thank is my supervisor Dr. K. G. Sreejalekshmi, the one who inspired me both professionally and personally. It has been an honor to be the first Ph.D. student in her career. Her positive attitude and her way of handling the students always amazed me. Being a passionate researcher and an excellent supervisor, she taught me to stick in to professional and scientific ethics and to keep respect towards mine as well as my colleague's works. Without her motivation and patience this thesis would not have been possible. I express my sincere gratitude and obligation for her eminent guidance, constant encouragement, incredible patience and understanding throughout my Ph.D. programme.

I would like to thank IIST for the financial assistance and I am thankful to Director, IIST for providing me the facilities to carry out the work. I would like to thank all the faculty members of Department of Chemistry for their moral support and encouragement along the way. I would like to specially thank Dr. Honey John for all her help and support especially during the early days of my Ph.D. I sincerely thank my doctoral committee members Dr. S. Baskaran, IIT, Madras, Dr. Mangalam S. Nair, NIIST, Thiruvananthapuram and Dr. S. Moosath, IIST, Thiruvananthapuram for the constant monitoring and timely assessment of my research work.

I am thankful to all the staff members of Department of Chemistry Mr. Sreekumaran Nair, Mr. Dileep, Mr. Loveson, Mrs. Rehna, Mrs. Jayasree L, Mrs. Jayasree, Mrs Remya and Mrs. Bindu for all the help they extended at the time of need. I express my words of acknowledgements towards the staff of library, administration, accounts, stores and purchase department for all their cooperation.

I am thankful to all my fellow research scholars for their sincere help and support. I would like to specially thank Mr. Rakesh, my group member, for all the help he extended during my research programme and most importantly for the constant encouraging words. I am taking this opportunity to thank all my friends Raneesh, Arun, Narasimman, Remya, Jalaja, Kavitha, Haripadmam, Dhanya, Aneesha, Harsha, Resmi and especially Dhanyechi and Sarika for making my Ph.D. days a memorable one.

I am expressing my words of gratitude to NIIST, IISER, RGCB, NCESS Thiruvananthapuram, IIT Madras and IIT Bombay for the characterizations of the samples. I would like to thank ACTREC, Mumbai for the *in vitro* anticancer screening studies and the technical and scientific support team of Schrodinger software for their timely help.

I would like to thank all my teachers without whom none of my success would be possible. I sincerely thank all those who directly or indirectly helped me for the completion of this work.

I could never have done this without the support and encouragement from my family. No words can describe my gratitude and affection towards my parents and my brother Emil for their unconditional love and care throughout my life. I would also like to thank my chechi Geethu for being a support ever since she became our family. I express my love and gratitude towards my late grandparents who have always been an inspiration for me. My heartfelt thanks to all my family members for their strong support and encouragement and I specially thank my aunt Pennamma and my uncle Philip for their guidance from the very first step towards my educational career.

At last but not least, I bow my head to ‘The God Almighty’ for this blessed life.

Sarah Titus

ABSTRACT

Small-ring heterocycles are considered to be '*privileged medicinal scaffolds*' which offer ideal properties for quality lead compounds or fragments for drug discovery due to their low molecular weight, desirable physical properties as well as their ability to accommodate substituents around the core in defined three dimensional orientations. The interactions of these designer small molecular systems with the target can often be tailored which offers a high degree of diversity and has proven to be useful for the search of new therapeutic agents. The understanding of molecular reasons for the activity of a drug or drug candidate is one of the priorities of modern medicinal chemistry. In this regard rational drug discovery or *omics*-guided drug design could be used to achieve the molecular design of new structures where the selection of a specific and druggable biological target, which is well identified as associated with a disease and whose activity could be modulated by a small molecule is considered to be inevitable. In the present work we decided to explore this target based approach which include the exploration of the medicinally relevant chemical as well as biological space.

Among various heterocyclic systems, thiazole ring, especially aminothiazole is bestowed with wide spectrum of biological activities and has attracted considerable attention as a scaffold for drug discovery. Following clear insights on the role of kinase proteins in cell cycle and tumorigenesis, Aurora kinases emerged as a major class of therapeutic targets for anticancer drug development. The different kinase inhibitory activities of aminothiazole derivatives have been explored by many research groups including their potential as Aurora kinase inhibitors. The results of *in vitro* studies also indicated very good cytotoxicity of such derivatives against many of the cancer cell lines. Thus aminothiazoles store the potential to be used as an effective scaffold for the design of more potent drug candidates and can also be explored in the development of materials for biomedical applications.

Driven by the anticancer activity of reported 2-aminothiazole derivatives, in part A of the present study, we felt it worth examining the possibilities of developing unexplored members from this family by expanding the chemical space around the template. Well-supported by the reported bioactivity of different hydrazone containing heterocyclic compounds, especially that of 2-hydrazinothiazoles, we have selected hydrazone moiety as a suitable fragment for the modification of 2-aminothiazole core. Thus combining the hydrazone fragment with the 2-aminothiazole ring we have designed novel class of 2-aminothiazoles bearing hydrazono unit at the C4 of thiazole ring to afford 4-hydrazinothiazoles with four sites for diversity multiplication. The plausible routes for the synthesis of the designed core were investigated and [4+1] ring synthesis route using aminoamidinothiourea as the C-N-C-S fragment and α -haloketone as the C5 contributor was designed and formulated for the target compounds. The required aminoamidinothiourea was generated in two successive condensations of binucleophilic aminoguanidine with a carbonyl compound and an isothiocyanate. The synthetic protocol offered a huge advantage of accommodating a large number of commercially available carbonyl compounds, isothiocyanates and α -haloketones as fragments for the construction of our proposed 4-hydrazinothiazoles and thus found to be well suited for drug design.

Utilizing the possibility of diversity multiplication in the designed scaffold a virtual library of 120 molecules was designed by varying the carbonyl component, isothiocyanate and α -haloketone ($4 \times 6 \times 5 = 120$) to generate four families of compounds belonging to isopropylidene, isobutylidene, cyclohexylidene and benzylidene classes of 4-hydrazinothiazoles. The potential of the designed scaffold as Aurora kinase inhibitor was identified by the preliminary molecular docking studies on three different class of anticancer drug targets *viz*; estrogen receptor, cyclin dependent kinase and Aurora kinase. Encouraged by the promising results from *in silico* screening, the feasibility of the chemical synthesis was investigated and two-step as well as *one-pot* sequential multicomponent synthesis for the desired compounds were developed. The versatility of the synthetic protocol was proven by the synthesis of 54 derivatives of 4-hydrazinothiazoles (yield >80%) among which structural elucidation was carried out for 26 compounds. Single crystal X-ray diffraction studies on selected members of 4-hydrazinothiazole family revealed interesting solvation patterns which were guided by the hydrazone capping unit on the C4 position of the thiazole ring. Detailed investigations on the crystal landscapes further suggested the potential of these molecules to be tested in materials science applications for the development of synthetic water/ion channels.

In vitro screening of 36 derivatives in six human cancer cell lines (MCF-7, A549, HL-60, OVCAR-3, SK-MEL-2, SW620) using Sulphorhodamine B assay with Adriamycin as the positive control had identified three hits, one compound in the cyclohexylidene family against A549 cell line and two compounds-one each from isobutylidene and benzylidene family - were found to be active against MCF-7 with GI₅₀ values in micromolar concentrations. With a view of generating novel lead like molecules, presently, we focused on one of the families, 4-benzylidenehydrazinothiazoles, for the hit to lead generation. Accordingly, the virtual library was expanded to 22500 molecules of 4-benzylidenehydrazinothiazoles by utilizing diversity multiplication available in the core scaffold and by considering the commercial availability of reagents for synthesis. The *in silico* screening of the expanded library in the active sites of 7 different Aurora proteins (six from Aurora kinase A and one from Aurora kinase B) showed promising results comparable with well-known Aurora inhibitors in the clinical and preclinical studies and also with anticancer drugs already available in the market. Detailed investigation of the interactions of the hit molecule in the active sites of target proteins suggested it to be an ATP competitive Type I inhibitor. The effect of ring substitution on the binding pattern of the molecule was studied in detail as a preliminary step towards the hit to lead generation. The computation of pharmaceutically relevant descriptors showed that most of the ligands from the virtual library were within the recommended range of that for 95% of drugs with little or no violation from Lipinski's 'rule of five' which proved the 'drug-likeness' of the designed derivatives.

As a first step towards our long term goal of developing a multifunctional dendrimer system for drug delivery, along with the small molecule drug discovery process we have carried out preliminary steps toward the development of suitable carrier system for the designed scaffold. To contribute to that, development of a multifunctional carrier system based on polyamidoamine dendrimer was initiated by investigating the possibility of constructing heterocyclic ring systems on to the periphery of the dendrimers. Owing to the specific interest in 2-aminothiazole core,

in part B of the present work, we have designed polyamidoamine-2-aminothiazole conjugate as a tunable template.

A potential precursor platform for building different heterocycles on to the periphery of polyamidoamine dendrimer was obtained through a divergent covalent amidine transfer strategy. The applicability of the synthon in heterocyclic nanovectorization was demonstrated by the design and formulation of synthetic routes for anchoring of 2-aminothiazole template through [4+1] ring closure. With an intension of developing the conjugate as a potential nanoprobe for imaging applications, we attempted to impart useful photophysical properties to the conjugate. To this end, we used coumarin moiety as a photounit, which was introduced through the α -halo component during the thiazole ring synthesis. Following the optimized reaction procedure, we have synthesized generation zero of polyamidoamine-coumarinoyl-2-aminothiazole conjugate and was characterized using spectroscopic techniques.

The molecular dynamics simulations (5ns) on the dendrimer conjugate in DMSO and water as well in different pH conditions predicted the detailed internal structure of the dendrimer including the free-space and distribution of solvent molecules. The change in the structural features with change in solvent environment was noticed whereby the conjugate showed a larger radius of gyration in DMSO than in water. The pH dependence studies provided useful insights on the use of such systems as carriers. The larger internal cavity radius observed for the conjugate at pH 4 has given a preliminary idea about the encapsulation efficiency and thereby the release mechanism of suitable guest molecules.

The polyamidoamine-coumarinoyl-2-aminothiazole conjugate was highly soluble in most of the organic solvents and the fluorescence emission studies of the conjugate in different solvents revealed it as an excellent solvent polarity indicator which suggested its potential to be developed as labelling agents for cell membranes, protein binding sites and liposomes. The conjugate was identified with positive solvatochromism with emission maxima ranging from 467 to 557nm depending upon the polarity of solvent with exceptionally large Stokes shift values ranging from 98 to 175nm along with moderate to good quantum yield (0.05-0.77).

The present study has contributed to the development of synthetic routes to a highly privileged scaffold for drug discovery based on 2-aminothiazole template which is discussed in part A of the thesis. The chemical library based on the scaffold was identified with three hits in the anticancer drug screening against human cancer cell lines. The expanded library, during *in silico* screening, indicated promising results comparable with well-known Aurora inhibitors and also with marketed anticancer drugs. Detailed investigations suggested the hit molecule to be an ATP competitive Type I inhibitor. In the second part of the thesis, development of a divergent strategy for the covalent immobilization of various heterocycles onto polyamidoamine dendrimer was proposed following the accomplishment of a universal amidinothiourea platform on the dendrimer periphery through amidine transfer. The utility of amidinothiourea anchored dendrimer in heterocycle synthesis was demonstrated by the construction of 2-aminothiazole unit following a [4+1] ring construction strategy and a conjugate with a coumarin unit was identified with excellent photophysical properties. The study is first of its kind to develop a versatile platform for heterocycles on polyamidoamine dendrimer with tunable properties and hence potential applications in biomedical field.

TABLE OF CONTENTS

DESCRIPTION	PAGE NUMBER
CERTIFICATE	iii
DECLARATION	iv
ACKNOWLEDGEMENTS	v
ABSTRACT	vii
LIST OF FIGURES	xx
LIST OF SCHEMES	xxv
LIST OF TABLES	xxvi
ABBREVIATIONS	xxvii
NOTATIONS	xxx
1. INTRODUCTION	1
1.1. Heterocycles as anticancer agents	3
1.2. Anticancer activity of aminothiazoles	5
1.3. The hydrazone linkage: significance in therapeutics	7
1.4. Biological activity of hydrazinethiazoles	9
1.5. Computer-aided drug design (CADD)	10

1.6. Scope and objectives	12
1.7. Organization of thesis	15
PART A	17
Specific objectives of part A	18
2. DESIGN AND DEVELOPMENT OF 4-HYDRAZINOTHIAZOLES AS NIVEL SCAFFOLD FOR ANTICANCER DRUG DISCOVERY	19
2.1. Background	19
2.2. Results and discussion	20
2.2.1. Exploration of medicinally relevant chemical space	20
2.2.2. Design of novel scaffold based on 2-aminothiazole template	23
2.2.3. Retrosyntheis of novel scaffold	24
2.2.4. Design of virtual library of 4-hydrazinothiazoles	26
2.2.5. Selection of anticancer drug targets	27
2.2.6. Virtual screening by molecular docking	28
2.2.7. Validation of retrosynthetic routes to 4-hydrazinothiazoles	30
2.3. Experimental details	33
2.3.1. General reagent information	33
2.3.2. General analytical information	33

2.3.3. General computational details	34
2.4. Synthesis	34
2.4.1. General procedure for the synthesis of amino amidinothiourea (AATU)	34
2.4.2. General procedure for [4+1] ring closure of AATU	34
2.4.3. General procedure for <i>one-pot</i> synthesis of HAT	35
2.4.4. Characterization of AATU	35
2.4.4.1. N-(Isopropylideneamino)-N'- (phenylthiocarbamoyl)guanidine (IPAATU-1)	35
2.4.4.2. N-(Isopropylideneamino)-N'- (p-methoxyphenylthiocarbamoyl)guanidine (IPAATU-2)	36
2.4.4.3. N-(Isobutylideneamino)-N'- (phenylthiocarbamoyl)guanidine (IBAATU-1)	36
2.4.4.4. N-(Isobutylideneamino)-N'-(p- methoxyphenylthiocarbamoyl)guanidine (IBAATU-2)	36
2.4.4.5. N-(Cyclohexylideneamino)-N'- (phenylthiocarbamoyl)guanidine (CyAATU-1)	37
2.4.4.6. N-(Cyclohexylideneamino)-N'-(p- methoxyphenylthiocarbamoyl)guanidine (CyAATU-2)	37
2.4.4.7. N-(Benzylideneamino)-N'- (phenylthiocarbamoyl)guanidine (BzAATU-1)	37
2.4.4.8. N-(Benzylideneamino)-N'-(p- methoxyphenylthiocarbamoyl)guanidine (BzAATU-2)	38

2.4.4.9. N-(Benzylideneamino)-N'-(p-methylphenylthiocarbamoyl)guanidine (BzAATU-3)	38
2.4.5. Characterization of HATs	39
2.4.5.1. 5-benzoyl-4-isopropylidenehydrazino-2-phenylaminothiazole (IPHAT-1)	39
2.4.5.2. 5-(4-chlorobenzoyl)-4-isopropylidenehydrazino-2-phenylaminothiazole (IPHAT-2)	41
2.4.5.3. 5-(4-fluorobenzoyl)-4-isopropylidenehydrazino-2-phenylaminothiazole (IPHAT-3)	43
2.4.5.4. 4-isopropylidenehydrazino-2-phenylamino-5-(4-nitrobenzoyl)thiazole (IPHAT-4)	44
2.4.5.5. 4-isopropylidenehydrazino-5-(4-methoxybenzoyl)-2-phenylaminothiazole (IPHAT-5)	46
2.4.5.6. 5-benzoyl-4-isopropylidenehydrazino-2-(4-methoxyphenylamino)thiazole (IPHAT-6)	48
2.4.5.7. 4-isopropylidenehydrazino-5-(naphth-2-oyl)-2-phenylaminothiazole (IPHAT-7)	49
2.4.5.8. 4-isopropylidenehydrazino-2-(4-methoxyphenylamino)-5-(naphth-2-oyl)-thiazole (IPHAT-8)	51
2.4.5.9. 5-(benzoyl)-4-isobutylidenehydrazino-2-phenylaminothiazole (IBHAT-1)	53
2.4.5.10. 5-(4-chlorobenzoyl)-4-isobutylidenehydrazino-2-phenylaminothiazole (IBHAT-2)	55
2.4.5.11. 5-(4-fluorobenzoyl)-4-isobutylidenehydrazino-2-phenylaminothiazole (IBHAT-3)	57

2.4.5.12. 4-isobutylidenehydrazino-5-(4- nitrobenzoyl)- 2-phenylaminothiazole (IBHAT-4)	59
2.4.5.13. 4-isobutylidenehydrazino-5-(4-methoxybenzoyl)- 2-phenylaminothiazole (IBHAT-5)	60
2.4.5.14. 5-benzoyl-4-isobutylidenehydrazino- 2-(4-methoxyphenylamino) thiazole (IBHAT-6)	62
2.4.5.15. 4-isobutylidenehydrazino-5-(naphth- 2-oyl)-2-phenylaminothiazole (IBHAT-7)	64
2.4.5.16. 5-(benzoyl)-4-cyclohexylidenehydrazino- 2-phenylaminothiazole (CyHAT-1)	66
2.4.5.17. 5-(4-chlorobenzoyl)-4-cyclohexylidenehydrazino- 2-phenylaminothiazole (CyHAT-2)	68
2.4.5.18. 4-cyclohexylidenehydrazino-5- (4-methoxybenzoyl)-2-phenylaminothiazole (CyHAT-3)	70
2.4.5.19. 4-cyclohexylidenehydrazino-5- (4-methoxybenzoyl)-2-phenylaminothiazole (CyHAT-4)	72
2.4.5.20. 5-benzoyl-4-benzylidenehydrazino- 2-phenylaminothiazole (BzHAT-1)	74
2.4.5.21. 4-benzylidenehydrazino-5-(4-chlorobenzoyl)- 2-phenylaminothiazole (BzHAT-2)	75
2.4.5.22. 4-benzylidenehydrazino-5-(4-nitrobenzoyl)- 2-phenylaminothiazole (BzHAT-3)	77
2.4.5.23. 4-benzylidenehydrazino-5-(4-methoxybenzoyl)- 2-phenylaminothiazole (BzHAT-4)	79

2.4.5.24. 5-benzoyl-4-benzylidenehydrazino-2-(4-methoxyphenylamino)thiazole (BzHAT-5)	81
2.4.5.25. 4-benzylidenehydrazino-5-(4-bromobenzoyl)-2-(4-chlorophenylamino)thiazole (BzHAT-6)	82
2.4.5.26. 4-benzylidenehydrazino-2-(4-methylphenylamino)5-(4-nitrobenzoyl)thiazole (BzHAT-7)	84
2.5. Conclusions	85
3. EXPLORATION OF SOLID STATE LANDSCAPE OF 4-HYDRAZINOTHIAZOLES AND EVALUATION OF ‘DRUG-LIKENESS’	87
3.1. Background	87
3.2. Results and discussion	88
3.2.1. Solid-state landscape of 4-hydrazinothiazoles	88
3.2.1.1. Hydrate formation in 4-alkylidenehydrazinothiazoles	89
3.2.1.2. Solvate/hydrate formation in 4-arylidenehydrazinothiazoles	98
3.2.1.3. 4-Cycloalkylidenehydrazinothiazoles	102
3.2.2. ‘Drug-likeness’ of 4-hydrazinothiazoles: ADME property calculation	106
3.2.3. <i>In vitro</i> anticancer screening of 4-hydrazinothiazoles	112
3.3. Experimental details	116
3.3.1. Single crystal X-ray diffraction	116

3.3.2. ADME property calculation	119
3.3.3. <i>In vitro</i> anticancer screening	119
3.4. Conclusions	120
4. VIRTUAL SCREENING OF 4-BENZYLIDENEHYDRAZINOTHIAZOLES IN AURORA KINASE PROTEINS	122
4.1. Background	122
4.1.1. Structure and function of AURK-A and AURK-B	123
4.1.2. Different modes of kinase inhibition	125
4.2. Results and discussion	127
4.2.1. Expansion of virtual library	127
4.2.2. <i>In vitro</i> anticancer screening of BzHATs	129
4.2.3. <i>In silico</i> ADME property calculation	132
4.2.4. <i>In silico</i> binding studies of 4-benzylidenehydrazinothiazoles	136
4.2.4.1. Binding interactions of the core structure	138
4.2.4.2. Binding interactions of the active compound, 5-benzoyl-4-benzylidenehydrazino-2-(4-methoxyphenylamino)thiazole	141
4.2.4.3. Effect of substitution on ring A of active compound 5-benzoyl-4-benzylidenehydrazino-2-(4-methoxyphenylamino)thiazole	145

4.2.4.4. Effect of substitution on ring C of active compound 5-benzoyl-4-benzylidenehydrazino-2-(4-methoxyphenylamino)thiazole	147
4.3. Conclusions	149
PART B	151
Specific objectives of part B	152
5. PAMAM DENDRIMERS AS MULTIFUNCTIONAL CARRIERS IN BIOMEDICAL APPLICATIONS	153
5.1. Background	153
5.1.1. Dendrimers and their unique structural features	154
5.1.2. PAMAM dendrimer in biomedical applications	156
5.1.3. Fluorescent dendritic nanoprobe (FDNs)	158
5.1.4. Molecular dynamics simulation studies on dendrimers	160
6. DESIGN, SYNTHESIS AND MD SIMULATIONS OF PAMAM-2-AMINOTHIAZOLE CONJUGATE	163
6.1. Background	163
6.2. Results and discussion	165
6.2.1. Design of PAMAM based versatile synthon for heterocyclic ring construction	165
6.2.2. Retrosynthesis of amidinothiourea conjugated PAMAM	167

6.2.3. Validation of retrosynthetic routes to PAMAM-ATU	168
6.2.4. Synthesis of PAMAM-2-aminothiazole conjugate	170
6.2.5. Molecular dynamics simulation studies on PAMAM-CouTz	175
6.2.5.1. Structural minimization of G0 and G0-CouTz	175
6.2.5.2. Effect of solvent on the structure and dynamics of G0	179
6.2.5.3. Effect of solvent on the structure and dynamics of G0-CouTz	181
6.2.5.4. Effect of pH on the structure and dynamics of G0	185
6.2.5.5. Effect of pH on the structure and dynamics of G0-CouTz	188
6.3. Experimental details	192
6.3.1. General reagent information	192
6.3.2. General analytical information	192
6.3.3. General computational details	193
6.4. Synthesis	194
6.4.1. Synthesis of PAMAM G0	194
6.4.2. Synthesis of G0-ATU	196
6.4.3. Synthesis of G0-ATU-2	198
6.4.4. Synthesis of G0-CouTz	198

6.5. Conclusions	200
7. EVALUATION OF THE POTENCY OF NOVEL FLUORESCENT DENDRIMERIC NANOPROBE (FDN) FOR IMAGING APPLICATIONS	201
7.1. Background	201
7.2. Results and discussion	202
7.2.1. Absorption characteristics of the conjugates	202
7.2.2. Emission characteristics of the conjugates	206
7.3. Experimental details	212
7.3.1. UV-Vis absorption studies	212
7.3.2. Fluorescence emission studies	212
7.4. Conclusions	213
8. CONCLUSIONS AND FUTURE PERSPECTIVES	214
8.1. Conclusions	214
8.2. Future perspectives	216
REFERENCES	218
LIST OF PATENTS/PUBLICATIONS BASED ON THESIS	252

LIST OF FIGURES

FIGURE	TITLE	PAGE NUMBER
1.1	Plant-derived anticancer agents	2
1.2	Examples of naturally occurring heterocyclic drugs	3
1.3	Thiazole containing pharmaceutical agents	5
1.4	Structural features of hydrazone moiety	8
1.5	Computer aided drug design	11
2.1	The main steps in the ‘reductionist-target-based approach’ of drug design	20
2.2	Chemical structure of thiazole containing biomolecules	21
2.3	2-Aminothiazole core containing drug molecules	22
2.4	Structure of 4-hydrazinothiazole	23
2.5	Thiazole ring synthesis	24
2.6	Structures of designed classes of 4-hydrazinothiazoles	26
2.7	¹ H NMR spectrum of IPHAT-1	40
2.8	¹³ C NMR spectrum of IPHAT-1	40
2.9	HR-MS spectrum of IPHAT-2	41
2.10	¹ H NMR spectrum of IPHAT-2	42
2.11	¹³ C NMR spectrum of IPHAT-2	42
2.12	¹ H NMR spectrum of IPHAT-3	43
2.13	¹³ C NMR spectrum of IPHAT-3	44
2.14	HR-MS spectrum of IPHAT-4	45
2.15	¹ H NMR spectrum of IPHAT-4	45
2.16	¹³ C NMR spectrum of IPHAT-4	46
2.17	¹ H NMR spectrum of IPHAT-5	47
2.18	¹³ C NMR spectrum of IPHAT-5	47
2.19	¹ H NMR spectrum of IPHAT-6	49
2.20	¹³ C NMR spectrum of IPHAT-6	49
2.21	LC-MS spectrum of IPHAT-7	50
2.22	¹ H NMR spectrum of IPHAT-7	50
2.23	¹³ C NMR spectrum of IPHAT-7	51
2.24	LC-MS spectrum of IPHAT-8	52
2.25	¹ H NMR spectrum of IPHAT-8	52
2.26	¹³ C NMR spectrum of IPHAT-8	53
2.27	¹ H NMR spectrum of IBHAT-1	54
2.28	¹³ C NMR spectrum of IBHAT-1	54
2.29	ESI-MS spectrum of IBHAT-2	55
2.30	¹ H NMR spectrum of IBHAT-2	56
2.31	¹³ C NMR spectrum of IBHAT-2	56
2.32	ESI-MS spectrum of IBHAT-3	57
2.33	¹ H NMR spectrum of IBHAT-3	58

2.34	¹³ C NMR spectrum of IBHAT-3	58
2.35	¹ H NMR spectrum of IBHAT-4	59
2.36	¹³ C NMR spectrum of IBHAT-4	60
2.37	HR-MS spectrum of IBHAT-5	61
2.38	¹ H NMR spectrum of IBHAT-5	61
2.39	¹³ C NMR spectrum of IBHAT-5	62
2.40	¹ H NMR spectrum of IBHAT-6	63
2.41	¹³ C NMR spectrum of IBHAT-6	63
2.42	LC-MS spectrum of IBHAT-7	64
2.43	¹ H NMR spectrum of IBHAT-7	65
2.44	¹³ C NMR spectrum of IBHAT-7	65
2.45	ESI-MS spectrum of CyHAT-1	66
2.46	¹ H NMR spectrum of CyHAT-1	67
2.47	¹³ C NMR spectrum of CyHAT-1	67
2.48	ESI-MS spectrum of CyHAT-2	68
2.49	¹ H NMR spectrum of CyHAT-2	69
2.50	¹³ C NMR spectrum of CyHAT-2	69
2.51	ESI-MS spectrum of CyHAT-3	70
2.52	¹ H NMR spectrum of CyHAT-3	71
2.53	¹³ C NMR spectrum of CyHAT-3	71
2.54	ESI-MS spectrum of CyHAT-4	72
2.55	¹ H NMR spectrum of CyHAT-4	73
2.56	¹³ C NMR spectrum of CyHAT-4	73
2.57	¹ H NMR spectrum of BzHAT-1	74
2.58	¹³ C NMR spectrum of BzHAT-1	75
2.59	¹ H NMR spectrum of BzHAT-2	76
2.60	¹³ C NMR spectrum of BzHAT-2	76
2.61	ESI-MS spectrum of BzHAT-3	77
2.62	¹ H NMR spectrum of BzHAT-3	78
2.63	¹³ C NMR spectrum of BzHAT-3	78
2.64	LC-MS spectrum of BzHAT-4	79
2.65	¹ H NMR spectrum of BzHAT-4	80
2.66	¹³ C NMR spectrum of BzHAT-4	80
2.67	¹ H NMR spectrum of BzHAT-5	81
2.68	¹³ C NMR spectrum of BzHAT-5	82
2.69	¹ H NMR spectrum of BzHAT-6	83
2.70	¹³ C NMR spectrum of BzHAT-6	83
2.71	ESI-MS spectrum of BzHAT-7	84
2.72	¹ H NMR spectrum of BzHAT-7	85
2.73	¹³ C NMR spectrum of BzHAT-7	85
3.1	Propeller shaped 4-hydrazinotiazole scaffold	89
3.2	ORTEP diagram of IPHAT monohydrates	90
3.3	H-bonding interactions formed by water molecules in DAS hydrate and IPHAT	91
3.4	Butterfly shaped dimer formed by IPHAT	92
3.5	Intra- and inter-molecular H-bonding interactions in IPHAT with dD...A	93

3.6	Comparison of 1D water chains in aquaporin and IPHAT	95
3.7	(a) Parallel water chains in the crystal lattice of IPHAT monohydrates, (b) Dipolar orientation of water molecules	96
3.8	(a) View of N-rich left handed helix enclosing 1D water wire in IPHAT, (b) Single file water chain observed in the crystal lattice	97
3.9	(a) View of packing diagram of IPHAT crystal lattice, (b) N-rich channel area enclosing water molecules	98
3.10	(a) Solvent molecules enclosed in the hydrophobic cavity formed by phenyl rings in the crystal lattice of BzHAT, (b) N-rich channel area enclosing solvent molecules.	99
3.11	H-bonding interactions in BzHAT-2. alcoholates	101
3.12	(a) Supramolecular assembly of BzHAT alcoholates in the <i>ac</i> plane, (b) Centroid-centroid distance between adjacent layers marked with black dotted line, (c) <i>Herringbone</i> arrangement of NRC of BzHAT-2.alcoholates	101
3.13	(a) Triangular wave arrangement of solvent molecules in molecular packing of BzHAT alcoholate along <i>bc</i> plane, (b) 'Z' like arrangement of thiazole S atoms in the plane	102
3.14	View of H-bonding interactions (dashed line) in CyHAT along <i>a</i> axis	103
3.15	Pincer-shaped channels of CyHAT-1 viewed along <i>ac</i> plane	104
3.16	Calixarene type of arrangement of CyHAT-1 along <i>a</i> axis	105
3.17	Views of hydrophobic cavity observed along <i>c</i> axis of CyHAT-1 crystal packing	105
3.18	(a) The derivatives of BzHAT and CyHAT having similarity with gefetinib; (b) Derivatives of CyHAT showing similarity with raloxifene	111
3.19	Growth inhibition curve of active compounds against (a) MCF-7; b) A549	113
3.20	GI ₅₀ chart of the active compounds in six cancer cell lines	116
4.1	Domain organisation of AURK-A and B	124
4.2	2D representation of the kinase binding site	126
4.3	The structure of the core compound used for the expansion of virtual library	128
4.4	Comparison of GI ₅₀ values of active compound and methyl derivative of BzHAT	130
4.5	Phase contrast images of cell lines treated with methyl derivative of BzHAT	132

4.6	The predicted 2D interaction diagram of native ligands in active sites of (a) 2BMC, (b) 4AF3	137
4.7	The 3D binding site of BzHAT-1(core structure) in AURK-A proteins	139
4.8	The 3D binding site of BzHAT-1 (core structure) in AURK-B protein 4AF3	140
4.9	The 3D binding site of the BzHAT-5 (active molecule) in AURK-A proteins	143
4.10	Binding modes of (a) dasatinib in the active site of c-Abl, (b) BzHAT-5 in the active site of AURK-A	143
4.11	The 3D binding site of BzHAT-1(core structure) in AURK-B protein 4AF3	144
4.12	Effect of ring A substitution on the binding pattern of BzHAT-5 in AURK-A proteins	146
4.13	Effect of ring A substitution on the binding pattern of BzHAT-5 in AURK-B protein	147
4.14	Effect of ring C substitution on the binding pattern of BzHAT-5 in AURK-A proteins	148
4.15	Substituent and orientation effect of –NO ₂ and -Br derivatives of BzHAT-5 (red) in 4AF3	149
5.1	Schematic representation of structural components of dendrimer architecture	154
5.2	Applications of dendrimers in cancer therapy	156
5.3	Chemical structure of PAMAM generation 3	157
5.4	Classification of FNSs based on their chemical composition	159
6.1	Designed PAMAM-2-aminothiazole conjugate	164
6.2	Designed divergent strategies for PAMAM-2-aminothiazole conjugate	165
6.3	PAMAM dendrimer bearing amidinothiourea unit as a universal platform for nanovectorization of diverse heterocycles	166
6.4	Topographic AFM images (1μm x 1μm) and corresponding cross sectional analysis of G0-CouTz on mica surface	174
6.5	Energy minimized structures of G0 and G0-CouTz at pH 4, 7.4 and 10	176
6.6	Snapshots of G0 during simulations in DMSO and water at pH7.4	179
6.7	Time-evolution of radius of gyration of G0 in DMSO and water during the course of 5ns molecular dynamics simulations	180
6.8	Variation of energy components of G0 in DMSO and water during the course of molecular dynamics simulations	181
6.9	Snapshots of G0-CouTz during simulations in DMSO and water at pH7.4	182

6.10	Time-evolution of the distance and angle between the core and modified terminal N-atom	183
6.11	Time-evolution of intramolecular H-bonding interactions formed in G0-CouTz in DMSO and water	183
6.12	Variation of energy components of G0-CouTz in DMSO and water during the course of molecular dynamics simulations	184
6.13	Time-evolution of radius of gyration of G0-CouTz in DMSO and water during the course of 5ns molecular dynamics simulations	185
6.14	Snapshots of G0 during simulations under different pH in water	187
6.15	Time-evolution of radius of gyration of G0 in under different pH conditions during the course of 5ns molecular dynamics simulations	187
6.16	Time-evolution of intramolecular H-bonding interactions formed in G0 in water under different pH	188
6.17	Snapshots of G0-CouTz during simulations under different pH in water	190
6.18	Time-evolution of radius of gyration of G0-CouTz in under different pH conditions during the course of 5ns molecular dynamics simulations	191
6.19	¹ H NMR spectrum of PAMAM G0	195
6.20	¹³ C NMR spectrum of PAMAM G0	195
6.21	ESI-MS spectrum of PAMAM G0	196
6.22	¹ H NMR spectrum of G0-ATU	197
6.23	MALDI-TOF-MS spectrum of G0-ATU	197
6.24	¹ H NMR spectrum of G0-CouTz	199
6.25	MALDI-TOF-MS spectrum of G0-CouTz	199
7.1	Comparison of UV-visible absorption spectra of PAMAM G0 and the conjugates in DMF	203
7.2	Schematic representation of possible charge transfer in G0-CouTz	204
7.3	UV-visible absorption spectra of G0-CouTz in different solvents	205
7.4	Photographs of solid state green fluorescence (left) and positive solvatochromism obtained for G0-CouTz conjugate at an excitation wavelength of 365nm	207
7.5	Emission spectra of G0-CouTz in different solvents	207
7.6	Lippert-Mataga plot of G0-CouTz	209
7.7	Fluorescence decay profile of G0-CouTz in different solvents	210
7.8	Change in fluorescence intensity with time at an irradiation wavelength of 365nm	212

LIST OF SCHEMES

SCHEME	TITLE	PAGE NUMBER
2.1	Retrosynthesis of HAT through [4+1] ring synthesis route	25
2.2	Chemical synthesis of 4-hydrazinothiazoles	31
2.3	Mechanism of formation of 4-hydrazinothiazoles	32
6.1	Retrosynthesis of amidinothiourea conjugated PAMAM (PAMAM-ATU)	167
6.2	Divergent synthesis of amino terminated PAMAM	168
6.3	Divergent synthesis of G0-ATU	169
6.4	Synthetic route for 2-aminothiazole conjugated PAMAM G0	171
6.5	Mechanism of heterocyclization of PAMAM-ATU	172
6.6	Chemical synthesis of coumarinoyl-2-aminothiazole conjugated PAMAM	173

LIST OF TABLES

TABLE	TITLE	PAGE NUMBER
2.1	Designed virtual library of 4-hydrazinothiazoles	27
2.2	Target proteins selected for preliminary virtual screening	28
2.3	Comparison of dock scores in the protein binding sites	29
3.1	H-bonding interactions in IPHAT-1 and IPHAT-2	94
3.2	H-bonding interactions in BzHAT-2. EtOH and BzHAT-2.MeOH	100
3.3	H-bonding interactions in CyHAT-1	104
3.4	The preferred range of physical descriptor values in Lipinski's RO5	107
3.5	The physical descriptors of top scored ligands of 4-hydrazinothiazoles in 3LAU	109
3.6	The predicted permeability properties of top scored ligands of 4-hydrazinothiazoles in 3LAU	110
3.7	Cell lines used for the anticancer screening	112
3.8	<i>In vitro</i> screening results of tested compounds	114
3.9	Summary of crystallographic data and structure refinement summary	118
4.1	List of functional groups used for the expansion of virtual library	128
4.2	<i>In vitro</i> screening results of tested BzHAT derivatives	130
4.3	The physical descriptors of BzHAT derivatives screened for anticancer activity	133
4.4	The predicted permeability properties of BzHAT derivatives screened for anticancer activity	134
4.5	Details of the protein crystal structures used for molecular docking	136
6.1	Distances and angles obtained for minimized structures of G0 and G0-CouTz	178
6.2	Distances and angles obtained for G0-CouTz after 5ns of simulations	184
6.3	Mean values of various energy components of G0-CouTz obtained during MD simulation.	189
6.4	The values of distances and angles obtained in G0-CouTz after 5ns at different pH	191
7.1	Solvatochromic shift in the absorption spectra of G0-CouTz	205
7.2	Stokes shift values calculated for G0-CouTz in different solvents	208
7.3	Fluorescence lifetime and QY of G0-CouTz	211

ABBREVIATIONS

1D	One dimensional
2D	Two dimensional
3D	Three dimensional
AATU	Aminoamidinothiourea
Abl	Abelson murine leukemia
ACN	Acetonitrile
ADME	Absorption, distribution, metabolism and excretion
ADR	Adriamycin
AP	Adenine pocket
APC/C	Anaphase-promoting complex/cyclosome
APIs	Active pharmaceutical ingredients
ATP	Adenosine triphosphate
ATU	Amidinothiourea
AURK	Aurora kinase
BBB	Blood brain barrier
BzHAT	4-benzylidenehydrazinothiazole
CADD	Computer-aided drug design
CCDC	Cambridge crystallographic data centre
CDCl ₃	Chloroform-d
Cdh1	Cadherin-1
CDK	Cyclin-dependent kinase
Chk	Checkpoint kinase
CML	Chronic myelogenous leukemia
CNS	Central nervous system
CyHAT	4-cyclohexylidenehydrazinothiazole
DAS	Dasatinib
DDS	Drug delivery systems
DFG	Asp-Phe-Gly
DFT	Density functional theory

DMAc	Dimethylacetamide
DMF	N,N-dimethylformamide
DMSO	Dimethyl sulphoxide
DNA	Deoxyribonucleic acid
EDA	Ethylenediamine
EI-MS	Electron ionization mass spectrometry
EPR	Enhanced permeability and retention
ESI-MS	Electron spray ionization mass spectrometry
Et ₃ N	Triethylamine
EtOH	Ethanol
FDA	Food and drug administration
FDN	Fluorescent dendritic nanoprobe
FNSs	Fluorescent nanostructures
FP-1	Front pocket-1
FT-IR	Fourier transform infrared spectroscopy
GI	Growth inhibition
GK	Gate keeper
H ₂ O	Water
HAT	4-Hydrazinothiazole
HOMO	Highest occupied molecular orbital
HR-MS	High resolution mass spectrometry
HTS	High-throughput screening
IBHAT	4-isobutylidenehydrazinothiazole
IPHAT	4-isopropylidenehydrazinothiazole
KBr	Potassium bromide
LBDD	Ligand-based drug design
LC	Lethal concentration
LC/MS	Liquid chromatography- mass spectrometry
LG	Leaving group
LUMO	Lowest unoccupied molecular orbital
MAOI	Mitochondrial monoamine oxidase inhibitory
MCRs	Multicomponent reactions

MD	Molecular dynamics
MDCK	Madin-Darby canine kidney epithelial
MeOH	Methanol
Mp	Melting point
MRI	Magnetic resonance imaging
MW	Molecular weight
NaOH	Sodium hydroxide
NCI	National cancer institute
NMR	Nuclear magnetic resonance
NRC	Nitrogen rich channel
OPLS	Optimized potential for liquid simulations
ORTEP	Oak ridge thermal-ellipsoid plot
PAMAM	Polyamidoamine
PDB	Protein data bank
PDK1	Phosphoinositide-dependent kinase-1
PK	Pharmacokinetic
Ppm	Parts per million
PSA	Polar surface area
QSAR	Quantitative structure activity relationship
QY	Quantum yield
RDD	Rational drug design
RES	Reticuloendothelial system
RNA	Ribonucleic acid
RO5	Rule of five
SANS	Small angle neutron scattering
SAXS	Small angle X-ray scattering
SBDD	Structure based drug design
SRB	Sulforhodamine B
TCT	Thiocarbamoylamidine transfer
TGI	Total growth inhibition
TLC	Thin layer chromatography
UATR	Universal attenuated total reflectance

UV

Ultraviolet

vHTS

Virtual high-throughput screening

XRD

X-ray diffraction

NOTATIONS

α	Alpha
\AA	Angstrom
β	Beta
$^{\circ}$	Degree
$^{\circ}\text{C}$	Degree Centigrade
Δ	Delta
γ	Gamma
g	Gram
Hz	Hertz
K	Kelvin
μg	Microgram
mg	Milligram
mL	Millilitre
mm	Millimetre
mmol	Millimol
%	Percentage
ϕ	Phi
π	Pi
ρ	Rho
σ	Sigma
V	Volume

CHAPTER 1

INTRODUCTION

Cancer is a generic term for a large group of diseases that can affect any part of the body. It is considered as the aberrant growth of cells or the rapid creation of abnormal cells that grow beyond their usual boundaries, and which can then invade adjoining parts of the body and spread to other organs, referred to as metastasizing (Gupta & Massagué, 2006). Metastases are the major cause of death from cancer and are often caused by the localized, uncontrolled cell proliferation due to a defect in regulating the cell cycle. According to the latest reports of cancer statistics a total of 1,658,370 new cancer cases and 589,430 cancer deaths are projected to occur in the United States in 2015 (Siegel *et al.*, 2015). The growing statistics of the disease make the development of effective and economically viable treatment techniques inevitable. Chemotherapy is the most commonly used treatment technique for many cancers including breast cancer, lung cancer, colon cancer and leukemia. The commonly used chemotherapeutic drugs like doxorubicin (C. Carvalho *et al.*, 2009; F. S. Carvalho *et al.*, 2014), methotrexate (Gaies *et al.*, 2012; Zachariae, 1990) and 5-fluorouracil (Goette, 1981; Takimoto *et al.*, 1996) among many others are associated with many undesirable side effects such as pain, hair loss, depression of immune system, nausea, vomiting and can even lead to heart damage and liver damage. Hence research in this area continuously seek discovery of selective anticancer agents that will eliminate cytotoxicity towards normal cells, a drawback associated with conventional cancer chemotherapeutics. This give an impetus for the search for new lead compounds in modern anticancer research.

In earlier days, the development of anticancer agents solely focused on natural products obtained from plants and marine organisms which was inspired by their recognition as potential anticancer agents recognized in the 1950's by the U.S National Cancer Institute (NCI) under the leadership of the late Dr. Jonathan Hartwell. The discovery of the cytostatic effect of N-mustard (Auerbach &

Falconer, 1949; Da *et al.*, 1948) had made a remarkable impact on anticancer research and the observations opened way for the synthesis of various alkylating agents (Benitez *et al.*, 1960; DeGraw & Goodman, 1964), antimetabolites (Parker, 2009; Peters *et al.*, 2000) and antimitotics (Jiang *et al.*, 1990; Kamal *et al.*, 2015) with antitumor activity against several human malignancies. Plant-derived compounds, especially colchicines, vinca alkaloids (vincristine and vinblastine) and taxanes (paclitaxel and docetaxel), had made huge impact in modern cancer chemotherapy (Figure 1.1).

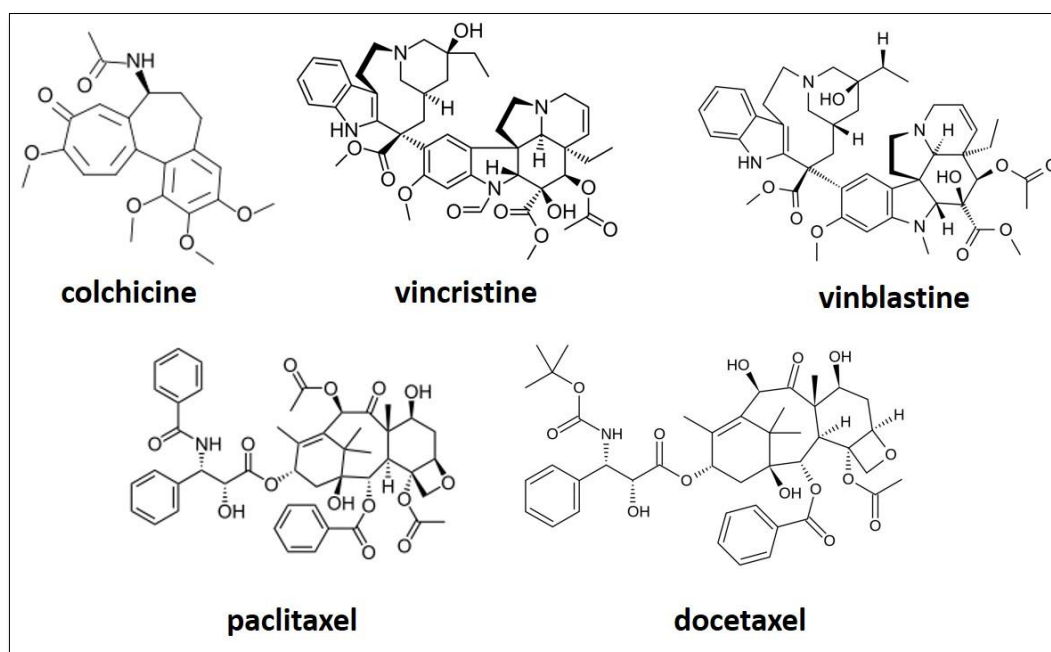


Figure 1.1. Plant-derived anticancer agents

Later on, drug discovery and development witnessed a paradigm shift when chemically synthesized small molecules demonstrated their potential as anticancer agents. However, the non-specificity and non-selectivity of existing drug molecules continued to challenge drug discovery research until Rational Drug Design (RDD) was proposed as a possible move in the right direction. RDD or reverse pharmacology requires the identification of a specific and druggable biological target, which is well identified as associated with a disease and whose activity could be modulated by a small molecule. Currently this target based approach, empowered by the advancements in the field of synthetic organic

chemistry as well as expanding knowledge domain in cell biology, has become a key area in modern anticancer research. Subsequently, the modern era of medicinal practice is witnessing enormous applications of these small molecule therapeutic agents that have critical role in the treatment and prevention of various diseases (B. Lu & Atala, 2014). Interestingly, over 80% of the potential small molecules screened for medicinal applications belongs to the heterocyclic family suggesting an unparalleled role played by these fragments in drug design.

1.1. Heterocycles as Anticancer Agents

Heterocycles have great importance in nature. About one half of all natural products contain heterocyclic components. Many of them, especially nitrogen-containing heterocycles (N-heterocycles) have vital functions in the human body. For example, the purine and pyrimidine bases of deoxyribonucleic acid (DNA), carrier of genetic information in all living beings, are N-heterocycles. The alkaloids are another special class of naturally occurring N-heterocycles. More over many natural drugs (Butler *et al.*, 2014; Koehn & Carter, 2005) shown in Figure 1.2 contain heterocycles. Since a wide spectrum of heterocycles is known with well-established chemistries and proven physiological action, they are often chosen as lead compounds for drug discovery and development.

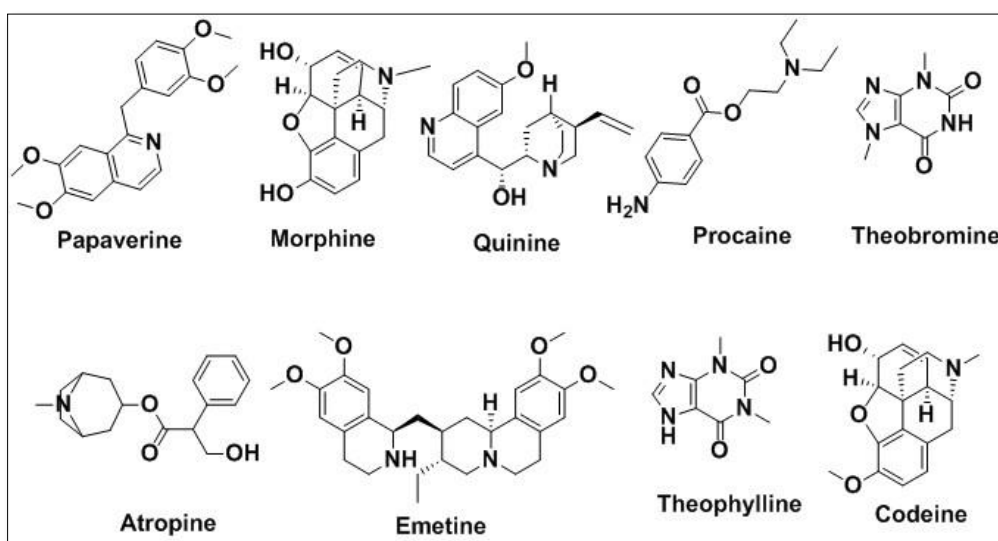


Figure 1.2. Examples of naturally occurring heterocyclic drugs

Further, the ability of these ring systems to accommodate substituents around a core in defined three dimensional orientations for target binding make them '*privileged medicinal scaffolds*' as termed by Merck researchers. The majority of cytostatic drugs in use, for example, alkylating agents, antimetabolites, alkaloids and antitumor antibiotics, are heterocyclic in nature and they inhibit tumor progression mostly by interfering with DNA (Tokarski *et al.*, 2006). Recently RNA as well as a number of proteins have also been reported (Maeda *et al.*, 2000; Torchilin, 2012) to be effective targets for anticancer drug discovery.

To have better interactions with the targets and hence improving the reactivity profile of anticancer agents, research in the past few decades identified modification of chemical space around heterocycles as a successful strategy. After identifying triazoles as promising DNA alkylating agents (De las Heras *et al.*, 1979), intense research has been done on the anticancer activity of different N-heterocycles. To name them, pyrrole (Gupton, 2006; La Regina *et al.*, 2014), pyrimidine (Kamal *et al.*, 2011; Shiau & Chen, 2015), indole (Patil *et al.*, 2012; Sidhu *et al.*, 2015) and quinoline (Al-Said *et al.*, 2011; Heiniger *et al.*, 2010; R Solomon & Lee, 2011) are a few that have shown promising cytotoxicity profile towards the cancer cells. Apart from N-heterocycles, various other heterocyclic ring systems were reported to be serving as the core in potential anticancer agents (Kidwai *et al.*, 2002; Martins *et al.*, 2015; Sherer & Snape, 2014). Among all the classes, thiazole ring, a five membered heterocycle of the 1,3-azole family containing sulphur and nitrogen, have found widespread applications in the field of medicine varying from antimicrobial sulphathiazole, antifungal abafungin to antineoplastic bleomycin and tiazofurin (Figure 1.3).

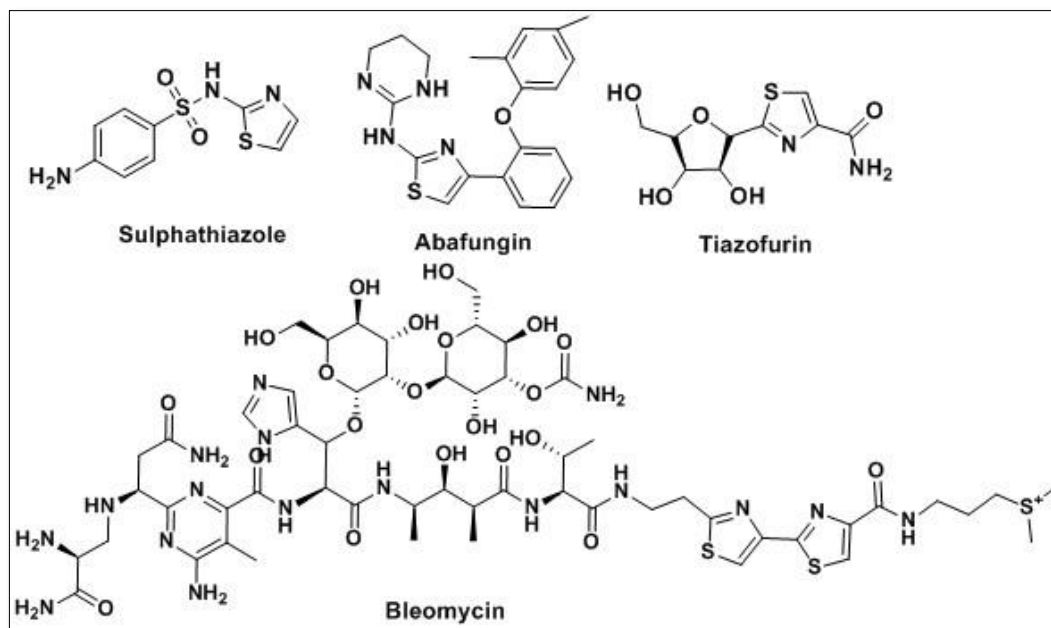


Figure 1.3. Thiazole containing pharmaceutical agents

The following discussion will focus on the biological activities of one of the prominent members of the thiazole family *viz.* aminothiazoles with a special emphasis to their anticancer activity.

1.2. Anticancer Activity of Aminothiazoles

Thiazole is present as a subunit of Vitamin B₁ (Thiamine) and in a large number of biologically active marine compounds. These class of compounds were reported to possess antitumor (Al-Omary *et al.*, 2012; El-Messery *et al.*, 2012; Hassan *et al.*, 2012; Ramírez *et al.*, 2015), antiproliferative (Cai *et al.*, 2012; Prashanth *et al.*, 2014; Romagnoli *et al.*, 2012; Vicini *et al.*, 2003; Zhou *et al.*, 2015), DNA cleaving (Cejudo *et al.*, 2006; Hamamichi *et al.*, 1992; Y. Li *et al.*, 2004; Reddy *et al.*, 2015; Stubbe *et al.*, 1996) and angiogenesis inhibiting (Bhat *et al.*, 2013; Knox *et al.*, 2003; Zheng *et al.*, 2013; Zheng *et al.*, 2014) activities. The quest for chemotherapeutic activity of thiazoles was initiated by the discovery of natural chemotherapeutic antibiotics such as tiazofurin (Ahluwalia *et al.*, 1984; Melink *et al.*, 1985; O'Dwyer *et al.*, 1984; Robins *et al.*, 1982; Tricot *et al.*, 1990) and bleomycin (Blum *et al.*, 1973; Sikic *et al.*, 2013).

Motivated by the anticancer activity of naturally occurring epothilone derivatives (Bollag *et al.*, 1995; Ferrandina *et al.*, 2012; Lee *et al.*, 2001; Lee *et al.*, 2008; Nettles *et al.*, 2004; E. Thomas *et al.*, 2007; Trivedi *et al.*, 2008), a microtubule stabilizer containing thiazole ring, a series of research followed exploring the antimitotic activity of thiazole containing compounds which induce apoptosis by inhibiting tubulin polymerization (C.-M. Li *et al.*, 2010; Lin *et al.*, 2015; Y. Lu *et al.*, 2011; Mahboobi *et al.*, 2006; Salehi *et al.*, 2013; D. M. Wang *et al.*, 2014). Among the various reported thiazole derivatives, aminothiazoles have gained considerable attention and are proven to have excellent inhibitory activity against many cancer specific targets. Several groups have reported on the synthesis and evaluation of the anticancer activity of aminothiazole derivatives (Gorczynski *et al.*, 2004; Prasanna *et al.*, 2010; Romagnoli *et al.*, 2011; S. A. Thomas *et al.*, 2013). Recent studies on a diaminothiazole derivative reported by Rajasekharan *et al.* (1986) have indicated the antimitotic and antiangiogenic activities (Juneja *et al.*, 2013; Paul *et al.*, 2013; Romagnoli *et al.*, 2009; Sengupta *et al.*, 2005; N. E. Thomas *et al.*, 2014; Vasudevan *et al.*, 2015) which further encourage the studies on the applicability of aminothiazole to serve as a potential scaffold in the development of anticancer drugs with very good efficacy.

As mentioned earlier, the selection of a specific biological target, which is druggable and well identified as associated with cancer is inevitable in rational anticancer drug discovery. Protein kinases are reported to be key regulators of mitosis and the clear understanding of the role of kinase proteins in cell cycle and tumorigenesis have made them excellent therapeutic targets for anticancer drug development (Lapenna & Giordano, 2009). For example, Cyclin-dependent kinases (CDKs) are the driving force behind the cell cycle and cell proliferation (Sherr, 1996) with individual CDKs performing distinct roles in cell cycle progression. Deregulation of the functions of these proteins induce unscheduled proliferation as well as genomic and chromosomal instability (Malumbres & Barbacid, 2009) as noticed in many solid tumors. Thus CDKs and their regulatory pathways are found to be potential targets for the development of novel chemotherapeutic agents. Many reports are available for the potential CDK inhibitory activity of aminothiazole

derivatives (L. Chen *et al.*, 2005; R. Chen *et al.*, 2009; Hirai *et al.*, 2010; Kyoung S Kim *et al.*, 2001; Kyoung Soon Kim *et al.*, 2002; Misra *et al.*, 2004; Schonbrunn *et al.*, 2013; Shimamura *et al.*, 2006). Apart from CDK inhibition, this class of compounds were reported to inhibit other protein kinases like Chk1 (Dudkin *et al.*, 2012; Gomha *et al.*, 2015), Src family kinases (Das *et al.*, 2006; Francini *et al.*, 2015; Lindauer & Hochhaus, 2014; Nam *et al.*, 2005; Shah *et al.*, 2004) and very recently Sphingosine kinases (Sphk) (Vogt *et al.*, 2014), the aberrant activity of which is associated with the growth and progression of cancer. Aurora kinases (AURKs) are another major class of protein kinases that are found to be strongly expressed at a high frequency in a broad range of tumor types as compared to their concentrations in normal cells and hence are widely accepted as excellent targets for novel anticancer drug development (Keen & Taylor, 2004). It is found that the aminothiazole derivatives which act as AURK inhibitors (Andersen *et al.*, 2008; Arbitrario *et al.*, 2010; Jung *et al.*, 2006; Qin *et al.*, 2010) show very good cytotoxicity against many of the cancer cell lines and thus stores the potential to be used as an effective scaffold for the development of more potent candidates. With this background, in the present study, we selected 2-aminothiazole as the template on which the design of the novel derivatives as potential anticancer agents using fragment based approach was envisaged and discussed in the subsequent sections.

1.3. The Hydrazone Linkage: Significance in Therapeutics

Hydrazones, with their highly reactive azomethine -NHN=CH- group, are versatile linkers for connecting various classes of organic compounds and have gained considerable significance in the drug discovery portal. The ease of synthesis, increased hydrolytic stability and tendency towards crystallinity made them desirable for applications in various fields. The characteristic structural features, hydrogen bonding donor and acceptor region (Figure 1.4) in combination with other functional groups leads to potent molecules with unique properties.

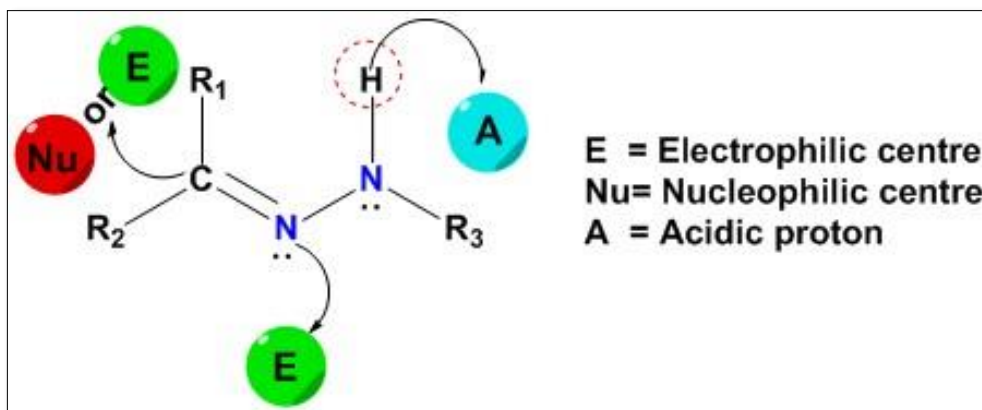


Figure 1.4. Structural features of hydrazone moiety

Different classes of hydrazones like acylhydrazones and their metal complexes have recently attracted great attention due to their therapeutic properties (Sedaghat *et al.*, 2015; Sedaghat *et al.*, 2013; Shujah *et al.*, 2014). The biological importance of hydrazones ranges from antiinflammatory (Kandpal *et al.*, 2015; Özkay *et al.*, 2010; Salgın-Gökşen *et al.*, 2007; Vasantha *et al.*, 2015), analgesic (N. Kumar *et al.*, 2014; Rajitha *et al.*, 2014; Sondhi *et al.*, 2006), anticonvulsant (Amir *et al.*, 2014; P. Kumar *et al.*, 2012), antituberculous (Gemma *et al.*, 2009; Mahajan *et al.*, 2011; Manvar *et al.*, 2011; Mao *et al.*, 2007), antitumor (Congiu & Onnis, 2013; Easmon *et al.*, 2006; Green *et al.*, 2001; Kaplánek *et al.*, 2015) to anti-HIV (Ma *et al.*, 2011; Vicini *et al.*, 2009) activities.

In earlier days hydrazone were commonly used as an intermolecular linkage for making stable protein or peptide conjugates for various biochemical studies (King *et al.*, 1986). To reduce the toxicity caused by the chemotherapeutic drugs towards normal cells various carriers were used in drug delivery among which monoclonal antibodies were the commonly used vehicle. Followed by the successful study on selective cytotoxicity of daunorubicin- anti T cell monoclonal antibody conjugate with acid sensitive cis- aconityl linkage (Dillman *et al.*, 1988), Greenfield *et al.* (1990) reported on the improved *in vitro* efficacy of adriamycin-immunoconjugate through hydrazone linkage in human tumor cells. Hydrazones undergo rapid hydrolysis at pH5 that increases its solubility. This characteristic amplifies the use of hydrazones in antitumor studies. Of late, the use of nanoscale delivery vehicles was identified as an alternative to overcome the drawbacks of

chemotherapeutic drugs such as low solubility and normal cell cytotoxicity. Tumor targeting and enhanced tumor accumulation of drug added more flavour to the nanoconjugate development. In anticancer therapy, the utility of hydrazone as a pH sensitive linker in drug-carrier conjugate is a well-studied area (Du *et al.*, 2011; Hrubý *et al.*, 2005; Lai *et al.*, 2007; Prabakaran *et al.*, 2009). Apart from the use of hydrazones as acid sensitive linkages, efforts have been made in combining hydrazone moiety to many small molecules to afford better pharmaceutical properties.

1.4. Biological Activity of Hydrazinothiazoles

Among various hydrazone based biologically active small molecules, hydrazone containing thioureas and thiazoles are receiving greater attention in recent years. The antifungal property of hydrazine dithiocarbamoyl, thiourea derivative, was reported earlier in 1950's (Tager & Danowski, 1948). The first clinically approved antiviral agent methisazone, active against pox viruses, is a hydrazone containing thiourea. In the last decade, research on the biological activities of thiosemicarbazones (Beraldo & Gambino, 2004; Hall *et al.*, 2009) and hydrazone containing thioureas are gaining prominence. El-Gaby *et al.* (2002) reported the synthesis of a series of hydrazone derivatives of benzene sulphonylthioureas with significant antibacterial property. The antimicrobial activity of thiourea derivative of isonicotinyl hydrazone was reported by Sriram *et al.* (2006). In 1990's a group of researchers have established the synthesis of thiazole hydrazones and thiazole halohydrazones (Denisova & Andronnikova, 1995; Usol'tseva & Andronnikova, 1994a, 1994b; Usol'tseva *et al.*, 1993) that could be used as precursors of biologically active compounds. A number of 2-thiazolylhydrazones are reported to be having mitochondrial monoamine oxidase inhibitory (MAOI) activity (Raciti *et al.*, 1995), antibacterial activity and antifungal activity (Bharti *et al.*, 2010; Cukurovali *et al.*, 2006; Holla *et al.*, 2003; Karegoudar *et al.*, 2008). A number of derivatives from this class of molecules are proven to be excellent candidates showing antitubercular (Özdemir, 2010) as well as antimalarial (Makam *et al.*, 2014) activities and very recently a number of phenyl thiazole

hydrazone derivatives were reported to possess activity against glycation proteins (Khan *et al.*) which is a promising therapeutic approach for the prevention of diabetes. Earlier in 1990's Andronnikova *et al.* (1988) reported on the synthesis and antitumor activity studies of 2-hydrazinothiazoles derivatives. In the recent past, the synthesis and the anticancer activities of 2-hydrazinothiazoles derivatives were reported (Ignat *et al.*, 2012; Manivel & Khan, 2009; Zaharia *et al.*, 2010). The expanding spectrum of the biological activity of hydrazinothiazoles would suggest the possible expansion of the chemical space around the scaffold in a rational drug design (RDD) approach to develop novel drug candidates.

1.5. Computer Aided Drug Design (CADD)

Conventional drug design is an iterative process which starts with the identification of compounds with interesting biological activity, followed by chemical synthesis, clinical studies, approval from the Food and Drug Administration (FDA) and finally marketing. The series of processes are resource as well as time intensive, whereas the success of the strategy are often very limited. Considering the existing drawbacks of current chemotherapeutic drugs, identification of novel, potent, selective and specific drugs is very much essential in anticancer therapy. But, with the availability of huge number of potential lead molecules as well as targets, the discovery and development process for a new anticancer compound with the right combination of activity, specificity, stability and safety is a long term and still expensive task. In this context, the introduction of computational modelling techniques could make the drug design comparatively easier one by decreasing the laboratory illness and expense for the discovery of the drug candidates. Recently, there has been an increased focus on computer aided drug design (CADD) due to the rising downstream costs resulting from high clinical failure rates associated with conventional drug design. Figure 1.5 demonstrates the general protocol followed in CADD.

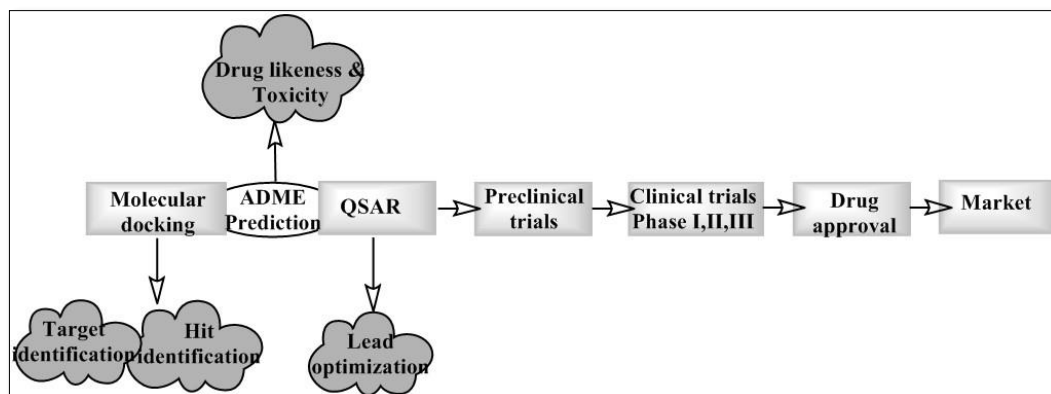


Figure 1.5. Computer aided drug design

To encourage modern drug discovery researchers, there are many reports on the successful stories of using CADD. To list a few, in 2004 a new group of pyrazolo[3.4.d]pyrimidine compounds with antiproliferative activity against human leukemia cell lines (Carraro *et al.*, 2004) were identified, but with poor solubility and substandard pharmacokinetic properties such as cell permeability. Hence, a series of more soluble pyrazolo[3.4.d]pyrimidine derivatives with better activity were rationally designed with the help of molecular modelling (Radi *et al.*, 2011). Kalani *et al.* (2012) reported on the quantitative structure activity relationship (QSAR) on ursolic acid analogues by ADME (Absorption, Distribution, Metabolism and Excretion) property screening. They found that the *in vitro* studies of the screened compounds on the cancer cell lines to be matching with their computational results. Further Qin *et al.* (2010) carried out QSAR studies on various aminothiazole derivatives (as AURK-A inhibitors) to study the structural features affecting the biological activity of the compounds. Over the past decade, there have been remarkable advances in the area of CADD, which has been applied during almost all stages in the drug discovery pipeline (Ooms, 2000; Xiang *et al.*, 2012).

Even though quantum mechanical calculations like *ab initio* and density functional theories (DFT) give accurate results, they are associated with high computational cost. Hence, molecular mechanics is used extensively in drug development in which molecular docking and molecular dynamics are the most commonly used tools for elucidating cancer targets. Molecular docking predicts the

preferred orientation of small molecules inside the structures of macromolecular targets. The knowledge of the preferred orientation may be used to predict the strength of association between the ligand and target protein using a scoring function. Following molecular docking, one can quickly screen large databases of potential drugs to identify molecules with comparable binding affinity with the target protein, the relative orientation of the ligand in the active site of the protein, and thereby more potent and selective analogues with better selectivity can be designed. This method is widely used for both hit identification and lead optimization (Kitchen *et al.*, 2004) as exemplified by the discovery of potent anticancer agents (X. Li *et al.*, 2012; Madadi *et al.*, 2015; Penthala *et al.*, 2015; H.-H. Wang *et al.*, 2013; Xing *et al.*, 2014).

Molecular modelling studies offer dual advantage, prediction of biological activity of the newly developed compound as well as identification of the core which is responsible for the activity. By recognising the core one can easily design analogues of the compound with better predicted activity and solubility. Thus the computational approaches would make the drug design a much easier task with low cost.

1.6. Scope and Objectives

As described in the introduction despite of the immense research on the development of novel anticancer agents, lack of selectivity and specificity towards the cancer cells is still a major drawback. As part of our longstanding research interest in the design and development of heterocyclic small molecule drug-carrier conjugates with specificity and selectivity towards targeted drug delivery for cancer therapy, our current research topic is focussing on the exploration of novel heterocyclic derivatives with promising biological activity. Success stories on the antitumor activity of thiazole containing Aurora inhibitors such as SNS-314 (Robert *et al.*, 2008) and CYC-116 (Griffiths *et al.*, 2008) made us to think about elaborating the chemical space around thiazole, more specifically 2-aminothiazole, for anticancer drug design. Encouraged by the success stories on the anticancer activity

of 2-aminothiazole derivatives such as DAT1, we felt it worth examining the possibilities of developing unexplored members from this family in a fragment based design approach. Well supported by the reported bioactivity of different hydrazone containing heterocyclic compounds, especially that of 2-hydrazinothiazoles (Bharti et al., 2010; Chimenti *et al.*, 2007; Secci *et al.*, 2012; Zaharia et al., 2010) we have selected hydrazone moiety as a fragment of our choice for the modification of the chemical space around 2-aminothiazole core. Thus, we envisaged combining the hydrazone fragment with the 2-aminothiazole ring through *C4* position which would afford a novel class of thiazoles, 4-hydrazinothiazoles, for which the synthetic feasibility could be explored following a retrosynthetic analysis.

In the present work, which we planned in two parts, the first part would focus on the design of a virtual library of 4-hydrazinothiazoles followed by the evaluation of their potential as anticancer agents through molecular docking studies by choosing appropriate target proteins. Design of facile synthetic routes for the chemical synthesis of potential small molecules followed by their *in vitro* screening and detailed *in silico* binding studies on target proteins are also planned as part of the work. Once we are successful in finding potential systems for drug development, our next objective will be to initiate studies on developing a drug delivery platform utilising the 2-aminothiazole core with a long term objective of developing materials for biomedical applications. As a first step towards this goal we thought of developing a multifunctional PAMAM dendrimer system, on to which the 2-aminothiazole fragment can be attached covalently. This would lead to the design and synthesis of polyamidoamine (PAMAM)-2-aminothiazole conjugate as a tunable template which was also planned as part of the work. Time dependent change in the structure and dynamics of the dendrimer and the designed conjugate under different pH and solvent conditions through molecular dynamics (MD) simulations would further provide useful insight for design optimization and was hence scheduled.

To systematically proceed with our research plans, the following specific objectives were put forth and discussed in two distinct parts in the thesis- Part A and Part B.

Part A

- Design of a novel scaffold based on 2-aminothiazole template for anticancer drug development.
- Design of virtual library of 4-hydrazinothiazole with tunable sites allowing for diversity multiplication.
- Formulating synthetic routes to these 4-hydrazinothiazoles, their chemical synthesis, characterization and *in vitro* screening against selected human cancer cell lines.
- Expansion of virtual library, molecular docking assisted virtual screening and detailed *in silico* binding studies in Aurora kinase family of proteins.
- Identifying lead-like structures from the library for the development of kinase inhibitors.

Part B

- Design of PAMAM -2-aminothiazole conjugate with tunable sites.
- Formulation of divergent synthetic strategy, chemical synthesis and characterization of conjugate.
- Development of the conjugate as fluorescent nanoprobe.
- Photophysical studies on the conjugate to evaluate its potential as a fluorescent probe.
- Molecular dynamics simulation of the conjugate under different pH and solvent conditions.

1.7. Organization of Thesis

The thesis composed of eight chapters and are organized as follows

Chapter 1 begins with an introduction which provides an outline of the background and current state of the art of research problem. It provides the importance for the search of novel potent anticancer agents. It gives an outlook on the role of heterocycles in medicinal chemistry specifically 2-aminothiazole scaffold in anticancer drug development. It also brief the significant results obtained by the formation of hydrazone hybrids of thiazole. The importance of computer aided drug design is also included. This chapter further contains the scope and objectives of the current research problem and the entire organization of thesis.

Chapter 2 deals with the design of novel heterocyclic scaffold based on 2-aminothiazole template for small molecule drug design. Retrosynthetic analysis for the designed scaffold, their chemical synthesis and estimation of the generality of the designed synthetic routes followed by characterization of synthesized derivatives are included in this chapter. The chapter also include *in silico* analysis of the scaffold to identify its potential in anticancer drug design by molecular docking studies.

Chapter 3 include the solid-state screening of the molecules by single crystal XRD studies and the role of hydrazone moiety in the solvate formation. The chapter also contain *in vitro* anticancer screening of synthesized derivatives and the *in silico* ADME property prediction for determining the ‘drug-likeness’ of the molecules.

Chapter 4 deals with the design of expanded library of 4-benzylidenehydrazinothiazoles and their binding studies in the active sites of Aurora kinase proteins. The chapter also contain the *in vitro* anticancer screening of representative examples from the designed library and their ADME property evaluation.

Chapter 5 is the introduction about polyamidoamine dendrimers. A brief literature survey on the biomedical applications of this class of dendrimers and their modifications are included in the chapter. It also give an insight to the increased interest of molecular dynamics simulation studies in the field of drug design.

Chapter 6 contain the design and development of a novel versatile synthon for the construction of a number of heterocyclic ring systems on to the periphery of PAMAM. Design of synthetic routes for the synthon, chemical synthesis and characterization of the synthesized conjugate are part of the chapter. The utility of the synthon in heterocyclic ring construction was proven by the synthesis of PAMAM-2-aminothiazole conjugate and is included in the chapter. Demonstration of property tuning of the novel thiazolyl conjugate was done by the introduction of coumarin moiety and the role of solvent and pH of solution on the structure and interactions of the conjugate was studied using MD simulations and included in the chapter.

Chapter 7 deals with the photophysical studies of the coumarinoyl-2-aminothiazole conjugated PAMAM. The fluorescence solvatochromism observed in the conjugate is studied in detail.

Chapter 8 include the summary and conclusion of the current research problem.

PART A

*Exploring chemical space around 2-aminothiazole core:
design of 4-hydrazino-2-aminothiazoles
as potential anticancer agents in a structure based drug
discovery approach: hit identification to lead
optimization*

Specific Objectives of Part A

- Design of a novel scaffold based on 2-aminothiazole template for anticancer drug development.
- Design of virtual library of 4-hydrazinothiazole with tunable sites allowing for diversity multiplication.
- Formulating synthetic routes to these 4-hydrazinothiazoles, their chemical synthesis, characterization and *in vitro* screening against selected human cancer cell lines.
- Expansion of virtual library, molecular docking assisted virtual screening and detailed *in silico* binding studies in aurora kinase family of proteins.
- Identifying lead-like structures from the library for the development of kinase inhibitors.

CHAPTER 2

DESIGN AND DEVELOPMENT OF 4-HYDRAZINOTHIAZOLES AS NOVEL SCAFFOLD FOR ANTICANCER DRUG DISCOVERY

2.1. Background

Drug discovery is a process by which a drug candidate or a lead molecule, often a small molecule, is identified and partially validated for the treatment of a specific disease. It is a time consuming and expensive process estimating a time average of 12-15 years and a cost of \$600-800 million (Silverman & Holladay, 2014). The advancements in the field of genomics and molecular biology has motivated the researchers to identify novel molecular frameworks with minimal structural subunits for biological targets of interest. In contrast to the traditional laborious trial and error methods, drug discovery today focuses on the aspects of structural identification, design and synthesis of therapeutically interesting compounds in a ‘reductionist-target-based approach’ (Collins & Workman, 2006; Terstappen *et al.*, 2007). In this approach, drug discovery process can be broken down in to four steps namely target selection and validation, chemical hit to lead generation, and lead optimization followed by clinical trials (Figure 2.1). For the execution of this rational drug design, exploration of the chemical (Reymond *et al.*, 2010) as well as the biological space (Stockwell, 2004) are considered to be the fundamental requirements which will improvise the suitability and robustness of the agents that enter the clinic.

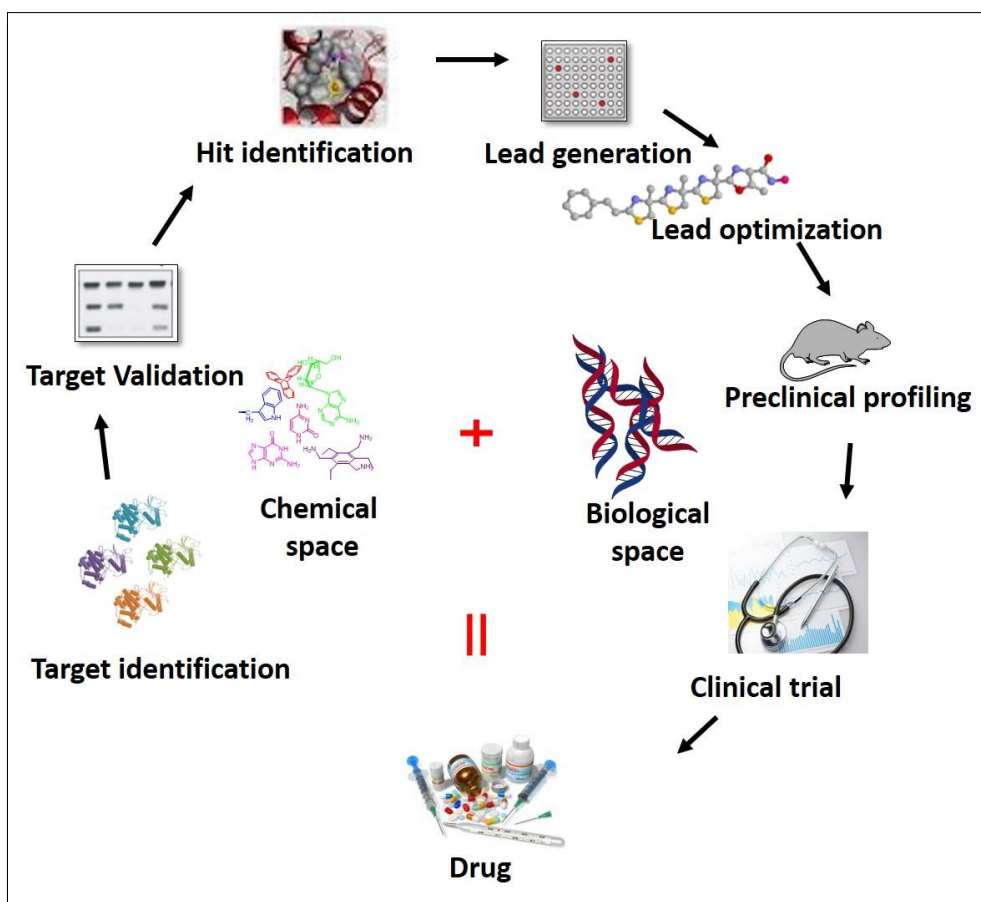


Figure 2.1. The main steps in the ‘reductionist-target-based approach’ of drug design

2.2. Results and Discussion

2.2.1. Exploration of medicinally relevant chemical space

Chemical space, the ensemble of all organic molecules, reported so far comprise around 10^{60} molecules (Bohacek *et al.*, 1996) and is a key concept in drug discovery. Even though the chemical space is vast, there is limited access to the medicinally relevant chemical space with appropriate synthetic and design techniques (Deng *et al.*, 2013). Despite the presence of numerous recurring molecular frameworks in bioactive molecules, design of novel scaffolds (Welsch *et al.*, 2010) able to direct functional groups in a well-defined three dimensional (3D) space is very much essential in small molecule drug discovery. In this context, heterocycles, the common structural motif present in over 80% of top small

molecule drugs hold a significant position (Dua *et al.*, 2011) and considering their presence in overall bioactive compound population and the ability to present functional groups in a favorable arrangement they are considered to be privileged structures in drug development (Song *et al.*, 2014). Among various heterocyclic ring systems, 1,3-thiazole is a well-represented five member ring heterocycle in the azole family. Thiazole ring is found in a variety of natural products and biomolecules like vitamin B1, fire fly chemical luciferin and in a number of marine alkaloids such as mycothiazole, camalexin and also in the well-studied class of anticancer agents, epothilones (Figure 2.2).

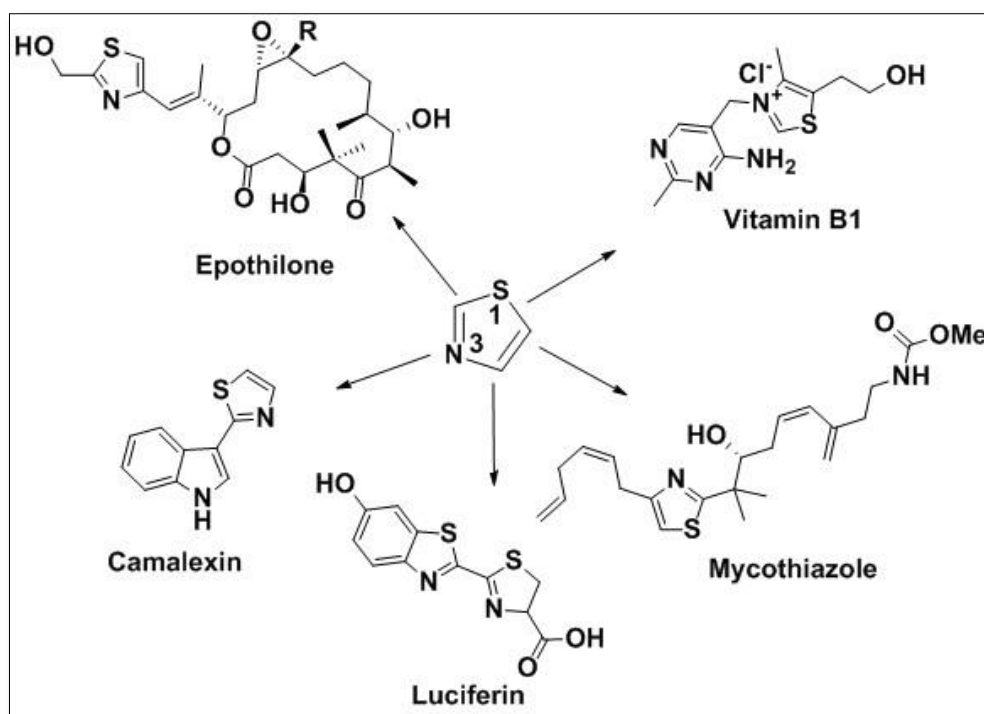


Figure 2.2. Chemical structure of thiazole containing biomolecules

Biological importance of thiazole ring structure varies from pharmacophoric and bioisosteric elements to spacer that made them a suitable core scaffold in design and development of novel therapeutic agents (Ayati *et al.*, 2015). For example, this ring system is an important pharmacophore in many clinically used drugs such as ravuconazole (anti-fungal agent), ritonavir (anti-HIV), fentiazac (anti-inflammatory agent), nizatidine (anti-ulcer agent) and dasatinib (anticancer). Among different synthetic derivatives of thiazoles, 2-aminothiazoles have found to

be an attractive moiety in medicinal chemistry with a wide spectrum of biological activities such as antibacterial, antifungal, antitubercular, anti-HIV and anti-inflammatory (Das *et al.*, 2016). Different drug molecules containing 2-aminothiazole core are given in Figure 2.3.

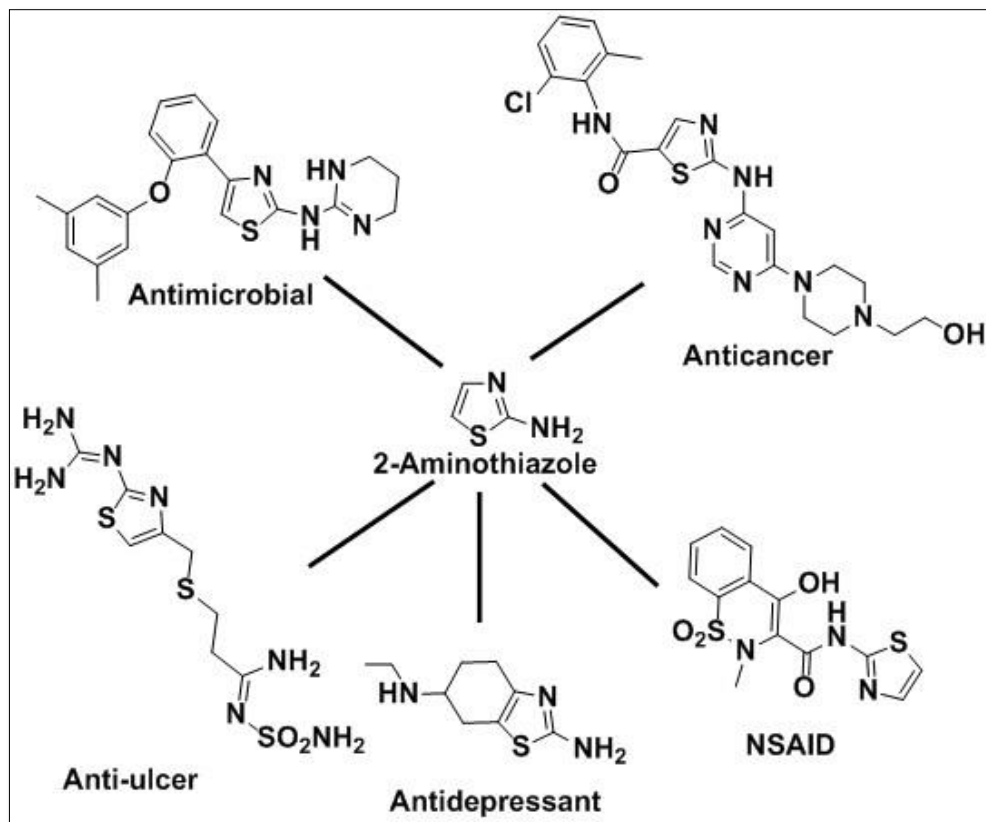


Figure 2.3. 2-aminothiazole core containing drug molecules (Das *et al.*, 2016)

Structural modification of compounds with known physiological or pharmacological effects for the production of novel and high quality lead molecules is an important aspect in medicinal chemistry. Such type of structural alterations with biologically relevant molecular entities that can provide diversity to the core is considered to be a key factor in drug development. The recurrence of 2-aminothiazole motif in a number of compounds which target members of different gene families along with reported anticancer activities of compounds such as DAT1 (Sengupta *et al.*, 2005) and related compounds has motivated us to select 2-aminothiazole as a template for the design of a novel anticancer drug design scaffold.

2.2.2. Design of novel scaffold based on 2-aminothiazole template

As discussed before, driven by the success stories on the anticancer activity of reported 2-aminothiazole derivatives (Nam *et al.*, 2005), we felt it worth examining the possibilities of developing unexplored members from this family. The biological activity of heterocyclic compounds clearly depends on the functional groups situated around the core. Search for suitable fragments for the modification of heterocyclic cores identified the role of hydrazone libraries especially hydrazone containing heterocycles in drug discovery (Rollas & Küçükgül, 2007; Verma *et al.*, 2014). Moreover the reported bioactivities of different hydrazone containing thiazoles especially 2-hydrazinothiazoles (Bharti *et al.*, 2010; Chimenti *et al.*, 2007; Secci *et al.*, 2012; Zaharia *et al.*, 2010) inspired us to select the moiety as a suitable fragment for the modification of 2-aminothiazole core for the present study. For that we have decided to modify the *C4* position of 2-aminothiazole ring in with hydrazone fragment to afford a novel class of thiazoles, 4-hydrazinothiazoles (**HATs**) (Figure 2.4).

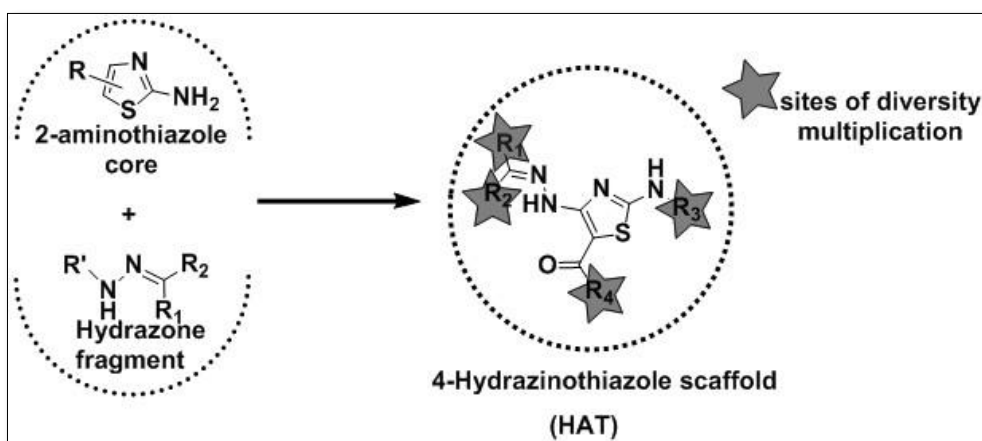


Figure 2.4. Structure of 4-hydrazinothiazole

The structural diversity plays key role in the hit to lead generation and thus scaffolds with sites prone to structural modifications are much significant in drug design. The designed scaffold, 4-hydrazinothiazole (**HAT**), provides four sites for the structural modifications through the R_n groups. Apart from this, a number of

nucleophilic sites and an acid labile hydrazone bond are part of the structure which give additional advantage in the field of drug design. Since synthetic feasibility is a crucial factor in drug discovery process, we next proceeded with the design of appropriate synthetic routes to our designed 4-hydrazinothiazoles.

2.2.3. Retrosynthesis of novel scaffold

Thiazole ring can be attained through a number of synthetic routes (Figure 2.5) in which [4+1] ring closure (Rajasekharan *et al.*, 1986) is a widely accepted procedure for the synthesis of 2,4-diamino-5-ketothiazoles.

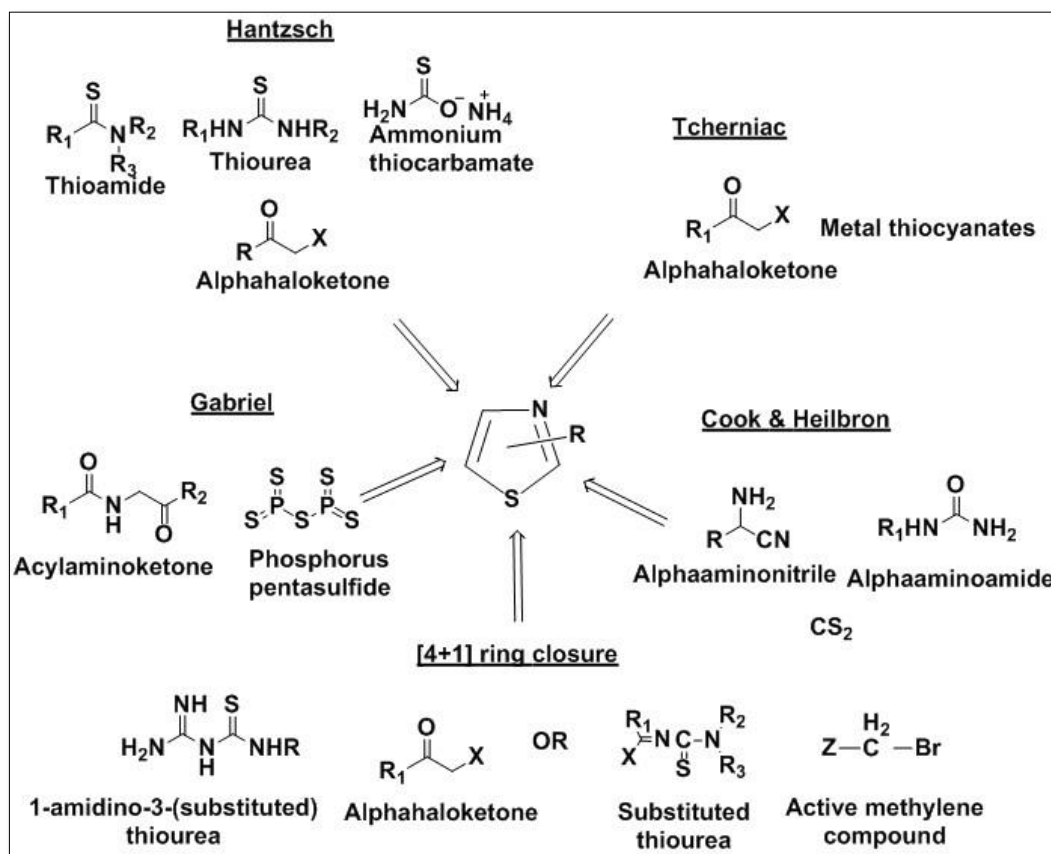
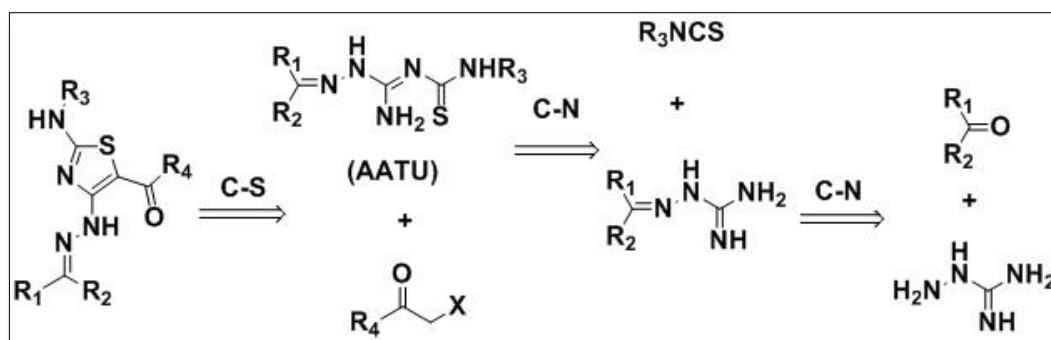


Figure 2.5. Thiazole ring synthesis

Along similar lines, following a retrosynthetic analysis (Scheme 2.1), we envisaged the access to designed core (**HAT**) through [4+1] ring synthesis route

which would recognise a C-N-C-S fragment which typically should contain the hydrazine fragment. Such a C-N-C-S fragment for the thiazole ring construction could be afforded by an aminoamidinothiourea (**AATU**) precursor unit which accommodate the hydrazone part.



Scheme 2.1. Retrosynthesis of **HAT** through [4+1] ring synthesis route

In this route the required **AATU** could be generated in two successive condensations of aminoguanidine with a carbonyl compound and an isothiocyanate (Sreejalekshmi, 2010). The C5 for thiazole ring formation could be afforded by a fragment containing an active methylene group such as α-haloketones. The ring closure between the precursor units **AATU** and α-haloketones is expected to lead to thiazole ring formation subsequent to an eliminative aromatization that largely depends on the leaving group (LG) propensities of substituents on amidino carbon with unsymmetric substituents. The hypothesized synthetic route would suggest an easy access to 4-hydrazinothiazoles, provided there is exclusive elimination of ammonia in the ring closure step, with a huge advantage in providing a large number derivatives through commercially available fragments carbonyl compounds (R₁ & R₂), isothiocyanates (R₃) and α-haloketones (R₄) and thus would be well suited for drug design purpose. On the contrary, elimination of the hydrazine fragment would lead to the established class of 2,4-diamino-5-ketothiazoles, whereas probability of ending up in a mixture of products also exists. However, to evaluate the potential of the scaffold, **HAT**, in anticancer drug discovery we next proceed with the design of a virtual library and planned for the virtual screening of the library against established anticancer drug targets.

2.2.4. Design of virtual library of 4-hydrazinothiazoles

Chemical compound library design is the basic and fundamental step in the drug discovery process and high-throughput screening (HTS) of this compound is necessary to identify promising lead molecules. Our retrosynthesis suggested a possibility of generating different classes of 4-hydrazinothiazoles by the suitable selection of carbonyl compounds which appears in the hydrazone part in the designed core. Hence giving special emphasis on to the hydrazone part, in the present work four classes of **HAT** were designed by considering the diversity attainable through R_1 and R_2 in the scaffold (Figure 2.6). From a synthetic point of view, this diversity can be realized through the appropriate selection of the carbonyl compounds which are available in plenty (commercially). Hence, the vast structural diversity that could be achieved clearly explain the potential of the designed scaffold in drug design.

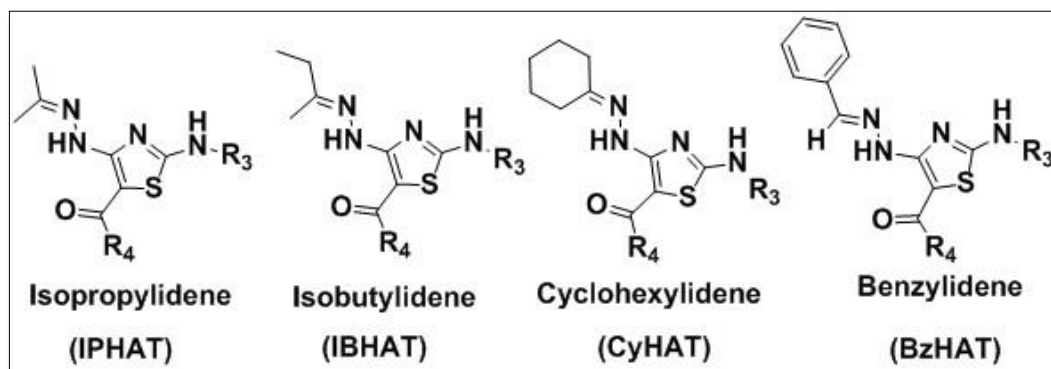
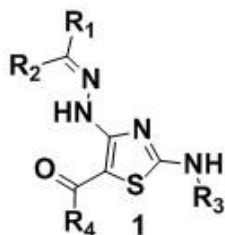


Figure 2.6. Structures of designed classes of 4-hydrazinothiazoles

To start with the structure based drug design (SBDD), following a skeletal diversity oriented design protocol, a 120 ($R_1/R_2 \times R_3 \times R_4: 4 \times 5 \times 6$) member virtual library of 4-hydrazinothiazoles has been created by varying the R_3 and R_4 fragments in the core scaffold **1** (Table 2.1).

Table 2.1. Designed virtual library of 4-hydrazinothiazoles



R₁	-CH ₃	-C ₂ H ₅	-C ₆ H ₅	-C ₆ H ₁₀		
R₂	-CH ₃	-CH ₃	-H			
R₃	-H	-NO ₂	-OCH ₃	-F	-Cl	-CH ₃
R₄	-H	-NO ₂	-OCH ₃	-F	-Cl	

The designed structures of the compounds were then optimized using OPLS_2005 (Optimized Potential for Liquid Simulations) as the force field and the 3D geometries were generated for the virtual screening purpose. To evaluate the potential of the designed scaffold in anticancer drug development we proceeded with the next step of SBDD, *i.e.*, the selection of suitable target proteins.

2.2.5. Selection of anticancer drug targets

The selection of biological targets (Knowles & Gromo, 2003) has much significance in anticancer drug discovery and development. Cancer is typically associated with the genomic instability caused by errors in mitosis (Hartwell & Kastan, 1994), the central process of growth that follows a multi-phase mechanism by which parental DNA is completely separated in to two identical daughter cells. This extremely important biological process is controlled and regulated by different proteins and inhibition of these protein activities are found to be very effective in treatment of cancer. Thus the current era of anticancer therapy is mainly focusing on drugs that disrupt mitotic progression with the identification and inhibition of new target proteins associated with specific functions in different phases of mitotic pathways.

Progress in molecular biology led to the identification of molecules targeting such proteins with key roles in mitosis. Accordingly, a number of therapeutic targets have been reported in the literature for developing anticancer

drugs (Landry & Gies, 2008). Since protein phosphorylation plays an important role in regulation of cell cycle, protein kinases have emerged as one of the most important targets for anticancer drug discovery (Cohen, 2002). Estrogen receptors are another well-known class of targets especially against hormone responsive cancers (Jordan, 2003). To investigate the potential of our designed scaffold in anticancer drug development three targets were selected from well-established families of target proteins (Table 2.2) for the preliminary screening of the designed library of compounds.

Table 2.2. Target proteins selected for preliminary virtual screening

Entry	Protein family	PDB ID	Resolution(Å)	Biological function
1	Estrogen receptor	3ERT	1.90	Transcription
2	Cyclin dependent kinase	4CFN	2.20	G1/S transition of mitotic cell division
3	Aurora kinase A	3LAU	2.10	G2/M mitotic cell division

The X-ray crystal structures of the selected proteins obtained from protein data bank (PDB) were prepared by adding hydrogens and optimized for the purpose of virtual screening. To investigate the potential of designed library of 4-hydrazinothiazoles in anticancer drug development and to select suitable targets for the hit to lead generation molecular docking was selected as a tool for virtual screening.

2.2.6. Virtual screening by molecular docking

Molecular docking is one of the widely used tool in drug design to predict the binding of small molecules to protein targets (Meng *et al.*, 2011). The approach is used to model the interactions between the small molecule and protein binding site for elucidating the fundamental biochemical processes. The binding affinity is estimated with a scoring function based on the ligand conformation as well as its

position and orientation inside the protein active sites. This scoring function will delineate the correct poses from incorrect ones or binders from inactive compounds.

In order to explore the possible binding modes of the compounds and to evaluate their binding affinity towards the target protein, the optimized ligand structures were screened in the active sites of individual proteins in a grid based ligand docking protocol using GLIDE. The preliminary docking has revealed a better affinity of the cyclohexylidene derivatives of 4-hydrazinotiazoles, in terms of their binding energy, towards the estrogen receptor protein whereas the benzylidene class of compounds showed a better affinity towards the cyclin dependent kinase protein. But, all the four classes of designed compounds, isopropylidene, isobutylidene, cyclohexylidene and benzylidene, were found to be having comparatively good affinity towards the active site of Aurora kinase protein 3LAU. The comparison of dock scores of top scored ligands in the active sites of 3LAU protein is given in Table 2.3.

Table 2.3. Comparison of dock scores in the protein binding sites

Entry	Class of compound	R ₃	R ₄	Glide score		
				3LAU	3ERT	4CFN
1	IPHAT	-CH ₃	-Cl	-7.28	-6.08	-4.58
2	IPHAT	-NO ₂	-Cl	-7.17	-5.60	-4.52
3	IPHAT	-Cl	-NO ₂	-7.16	-6.32	-1.86
4	IPHAT	-H	-NO ₂	-7.15	-3.44	-4.91
5	IPHAT	-OCH ₃	-OCH ₃	-7.15	-2.84	-5.05
6	IBHAT	-OCH ₃	-H	-7.57	-2.60	-1.721
7	IBHAT	-CH ₃	-H	-7.39	-5.24	-3.37

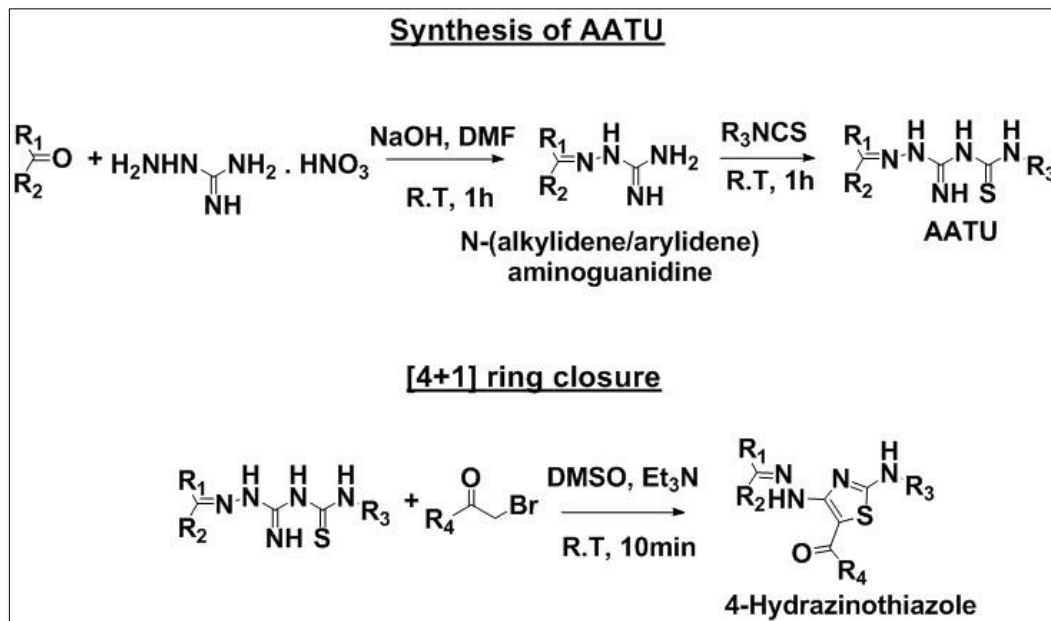
8	IBHAT	-NO ₂	-Cl	-7.38	-5.53	-5.66
9	IBHAT	-Cl	-F	-7.26	-3.19	-2.93
10	IBHAT	-NO ₂	-F	-7.59	-3.28	-5.05
11	CyHAT	-OCH ₃	-F	-7.30	-3.37	-2.12
12	CyHAT	-OCH ₃	-H	-7.03	-1.69	0.776
13	BzHAT	-OCH ₃	-H	-7.75	-4.94	-0.53
14	BzHAT	-CH ₃	-NO ₂	-7.17	-6.60	-6.42

Since the preliminary virtual screening of the designed library of molecules revealed the better affinity of the scaffold towards the active sites of AURK protein, we have selected Aurora kinase family as the target protein for our further hit to lead generation studies. Prior to the molecular docking studies, we next proceeded with the evaluation of the feasibility of attaining the scaffold, **HAT**, following the hypothesized synthetic route.

2.2.7. Validation of retrosynthetic routes to 4-hydrazinotiazoles

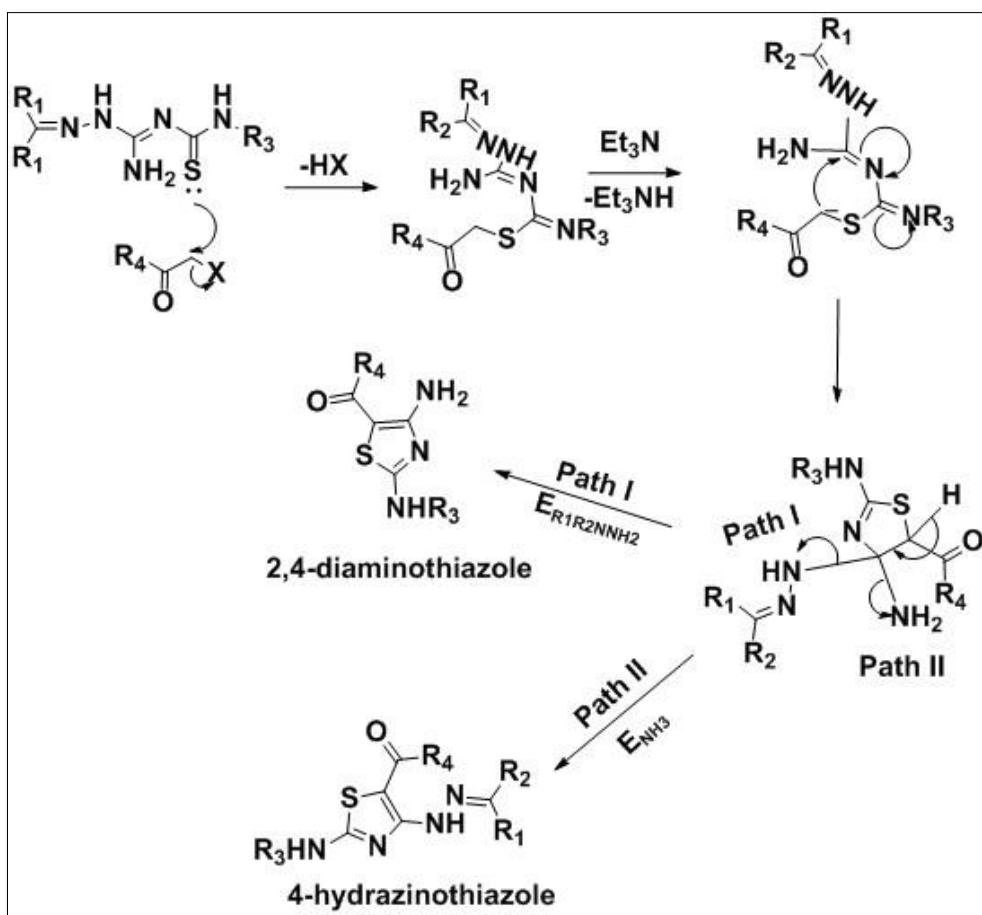
As mentioned earlier, synthetic feasibility of the scaffolds is an essential factor in anticancer drug development and the current drug discovery process relies on the ability of synthetic chemistry to deliver libraries of small molecules with increasing levels of structural diversity. Since the retrosynthesis of the core scaffold suggested the feasibility of a [4+1] ring closure between **AATU** and α -haloketone for the formation of the target **HAT** compound we next decided to validate our scheme. The chemical synthesis of different derivatives of **HAT** was accomplished following the procedure shown in Scheme 2.2 which further established the versatility of the designed scaffold. The first step was the synthesis of **AATU** which could be achieved by the selective blocking of amino functionality in aminoguanidine by carbonyl compound through Schiff base formation to generate corresponding N-(alkylidene/arylidene)aminoguanidines and their subsequent

condensation with isothiocyanates (Sreejalekshmi, 2010). Then the [4+1] ring closure of the resulting **AATU** with α -haloketone followed by base assisted eliminative aromatization afforded the target compound. In view of the greater reactivity in nucleophilic substitution and the commercial availability, α -bromoketones were selected as the C5 fragment contributor during the cyclization.



Scheme 2.2. Chemical synthesis of 4-hydrazinothiazoles

The reaction is expected to proceed through the S-alkylation of the **AATU** (Scheme 2.3) resulting in the formation of an acyclic S-alkylthiourea intermediate **2** which can cyclize in presence a base to thiazoline **3**. This further undergo a base assisted eliminative aromatization to yield the target compound, **HAT**. But, the end product(s) of such an eliminative process is largely decided by the leaving group propensities of the competing species present at the amidino carbon which suffer the nucleophilic attack. The aromatisation can proceed with either the elimination of hydrazone moiety (Path I) which give rise to the formation of well-known 2,4-diaminothiazoles or with the elimination of ammonia (Path II) giving rise to compounds of our virtual library *i.e.*, **HAT**.



Scheme 2.3. Mechanism of formation of 4-hydrazinothiazoles

The success of the reaction to form exclusively 4-hydrazinothiazoles would be rationalized by comparing the basicity and the pKa value of the leaving groups (~ 36 for NH_3 and ~ 21 for hydrazine). The elimination of more basic ammonia molecule probably suggest a retro-Michael addition during the aromatization step.

In order to prove the versatility of the synthesis, 54 derivatives of 4-hydrazinothiazoles were synthesized in the two-step protocol (Scheme 2.2) from which structural elucidation was carried out for 26 compounds using spectroscopic and analytical techniques. Considering the recent applications of multicomponent reactions (MCRs) in medicinal chemistry (Slobbe *et al.*, 2012) we also developed a one-pot four component ring synthesis strategy for the designed **HAT** scaffold and the versatility of the synthesis was demonstrated by the synthesis of seven

derivatives of 4-hydrazinothiazoles (Titus & Sreejalekshmi, 2014). The yield of the synthesized compounds was found to be good to excellent and the designed procedure proceeded under very mild conditions and could accommodate large number of commercially available starting materials to afford densely functionalized **HAT** derivatives.

2.3. Experimental Details

2.3.1. General reagent information

Aminoguanidine nitrate, isothiocyanates and α -bromoketones were purchased from Aldrich chemical company and were used as such. Ketones/aldehydes and NaOH were purchased from Merck chemicals. The solvents DMF and DMSO, and organic base Et₃N were obtained from Merck chemicals and were used after purification using general procedure. CDCl₃ for NMR spectroscopy was obtained from Aldrich chemical company.

2.3.2. General analytical information

Purity of the compounds were checked using thin layer chromatography (TLC) on silica coated plates obtained from Merck, India and spots were visualized under UV light or in iodine chamber. All the synthesized compounds were characterized by spectroscopic techniques (¹H NMR, ¹³C NMR, MS, FT-IR), melting point determination and elemental analysis. Melting point determination was carried out using Thermoscientific melting point determination apparatus. NMR spectra were recorded using Bruker AV III 500 MHz FT-NMR spectrometer using CDCl₃ as solvent. LC/MS spectra were recorded on Varian Inc LC/MS spectrometer. HR-MS was obtained using Waters Micromass Q-Tof microTM (YA105) spectrometer. ESI-MS was recorded using Thermoscientific Exactive Orbitrap mass spectrometer. IR spectra were obtained using Perkin Elmer Spectrum 100 FT-IR spectrometer. Elemental analysis was carried out with Perkin Elmer 2400 Series CHNS/O Analyser.

2.3.3. General computational details

The virtual screening of the compounds were carried out using Schrodinger software Suite 2012. The chemical structures of compounds in the virtual library were created using Maestro panel available in the software. The optimization of the ligand structures were carried out using Ligprep (Version 2.9) with OPLS_2005 force field. The hydrogen addition and preparation of proteins were done using protein preparation wizard. GLIDE (Version 6.2) was used for the molecular docking studies and the binding energy of the compounds were calculated using PRIME/MM-GBSA.

2.4. Synthesis

2.4.1. General procedure for the synthesis of aminoamidino thiourea (AATU)

A suspension of NaOH (10mmol, 0.40g) was made in DMF and to this aminoguanidine nitrate (10mmol, 1.37g) was added and the reaction mixture was stirred for 10min at room temperature. It was followed by the addition of 10mmol of the ketone/aldehyde and the stirring was continued for 45-50min. To this mixture 9mmol (1.21g) isothiocyanate in DMF was added drop wise and stirred for 1h. The reaction mixture was then added to crushed ice for the precipitation of the solid products. The product obtained was filtered and dried in air. Recrystallization was carried out in appropriate solvents to obtain the pure products.

2.4.2. General procedure for the [4+1] ring closure of AATU

Aminoamidinothiourea (10mmol) was dissolved in DMSO and to this α -bromoketone (10mmol) was added followed by the addition of 1.2 molar excess of Et₃N. The reaction mixture was stirred for 10min at room temperature and then was added to crushed ice. The solid obtained was collected by filtration and dried in air.

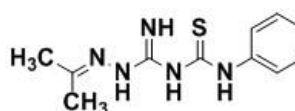
Appropriate solvents were used for the recrystallization of the compounds to obtain pure products.

2.4.3. General procedure for *one-pot* synthesis of HAT

The sequential one-pot four-component synthesis of the target compounds was carried out as follows. To a stirred suspension of NaOH (10mmol, 0.40g) in DMSO 10mmol (1.37g) of aminoguanidine nitrate was added followed by the addition of equimolar quantity of ketone/aldehyde (10mmol). The mixture was stirred for 1h at room temperature and then 9mmol isothiocyanate in DMSO was added in drops over 10min and the stirring continued for another 1h. Subsequently, α -bromoketone (9mmol) was added followed by Et₃N (10mmol, 1.39mL) and stirred for 15min. Completion of the reaction was monitored by TLC on silica coated plate and the reaction mixture was poured into crushed ice with vigorous stirring. The solid products obtained were filtered and dried in air. Purification of the products was done by recrystallization in appropriate solvents.

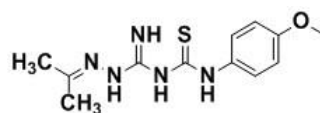
2.4.4. Characterization of AATU

2.4.4.1. N-(Isopropylideneamino)-N'-(phenylthiocarbamoyl)guanidine (IPAATU-1)



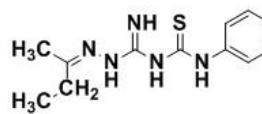
Off-white shining crystals from ethanol-water (1:1). Yield 85%. Mp 166-167°C. Lit. Mp 167-168 °C (Sreejalekshmi, 2010). IR (UATR) ν cm⁻¹: 3300, 3200 (N-H), 2840 (C-H aliphatic), 1620 (C=N), 1550, 1400 (C-H aromatic), 1300, 1230, 1185 (C-N), 1100 (C=S), 830, 735 (aromatic); ¹H NMR (300 MHz, CDCl₃): δ (ppm) 2.02 (s, 3H, CH₃), 2.07 (s, 3H, CH₃), 6.43 (br, 2NH), 7.10 (t, 1ArH, J= 6.9Hz), 7.31 (t, 2ArH, J= 9Hz), 7.47 (d, 2ArH, J = 9Hz), 7.90 (br, 1NH), 12.95 (br, 1NH); Anal. calcd. for C₁₁H₁₅N₅S (249.33): C, 52.99; H, 6.06; N, 28.09%. Found: C, 52.77; H, 6.23; N, 28.30%.

2.4.4.2. N-(Isopropylideneamino)-N'-(p-methoxyphenylthiocarbamoyl)guanidine (IPAATU-2)



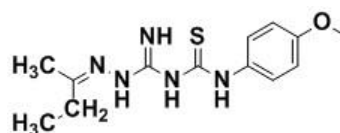
Off-white shining crystals from ethanol-water (1:1). Yield 69%. Mp 160–161°C. Lit. Mp 161-163°C (Sreejalekshmi, 2010). IR (UATR) ν cm^{-1} : 3387, 3235 (N-H), 2821 (C-H aliphatic), 1646, 1629 (C=N), 1528, 1438, 1426 (C-H aromatic), 1297, 1177 (C-N), 1110, 1034 (C=S), 823 (aromatic); ^1H NMR (500 MHz, CDCl_3): δ (ppm) 2.05 (s, 6H, CH_3), 3.79 (s, 3H, OCH_3), 6.45 (br, 2NH), 6.72–7.02 (m, 2ArH), 7.29–7.61 (m, 2ArH), 7.84 (br, 1NH), 12.25 (br, 1NH); ^{13}C NMR (125 MHz, CDCl_3): 18.6 ($-\text{CH}_3$), 25.2 ($-\text{CH}_3$), 55.5 ($-\text{OCH}_3$), 113.8 (aromatic), 124.3 (aromatic), 132.2 (aromatic), 154.1 (C=N), 156.5 (aromatic), 158.4 (C=NH), 185.5 (C=S); Anal. calcd. for $\text{C}_{12}\text{H}_{17}\text{N}_5\text{OS}$ (279.36): C, 51.58; H, 6.13; N, 25.07%. Found: C, 51.45; H, 6.04; N, 25.02%.

2.4.4.3. N-(Isobutylideneamino)-N'-(phenylthiocarbamoyl)guanidine (IBAATU-1)



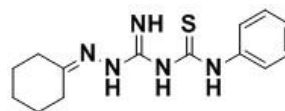
Off-white shining crystals from ethanol-water (1:1). Yield 65%. Mp 153–154°C. Lit. Mp 153-154°C (Sreejalekshmi, 2010). IR (UATR) ν cm^{-1} : 3395, 3283 (N-H), 3140 (C-H aromatic), 2839 (C-H aliphatic), 1626 (C=N), 1558, 1449, 1354 (C-H aromatic), 1111, 1026 (C=S), 842, 763 (aromatic); Anal. calcd. for $\text{C}_{12}\text{H}_{17}\text{N}_5\text{S}$ (263.36): C, 54.73; H, 6.51; N, 26.59%. Found: C, 54.94; H, 6.71; N, 26.79%.

2.4.4.4. N-(Isobutylideneamino)-N'-(p-methoxyphenylthiocarbamoyl)guanidine (IBAATU-2)



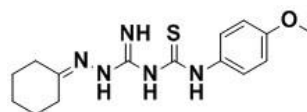
Off-white shining crystals from ethanol-water (1:1). Yield 60%. Mp 150–151°C. IR (UATR) ν cm^{-1} : 3395, 3282 (N-H), 3138 (C-H aromatic), 2830 (C-H aliphatic), 1622 (C=N), 1556, 1447, 1350 (C-H aromatic), 1111, 1024 (C=S), 840, 760 (aromatic).

2.4.4.5. N-(Cyclohexylideneamino)-N'-(phenylthiocarbamoyl)guanidine (CyAATU-1)



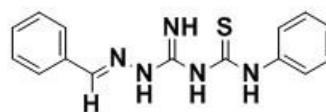
Off-white shining crystals from ethanol-water (1:1). Yield 75%. Mp 161–162°C. Lit. Mp 160-162°C (Sreejalekshmi, 2010). IR (UATR) ν cm^{-1} : 3426, 3197 (N-H), 2971, 2824 (C-H aliphatic), 1640 (C=N), 1560, 1493 (C-H aromatic), 1189, 1019 (C=S), 841, 743 (aromatic); ^1H NMR (300MHz, CDCl_3): δ (ppm) 1.62–1.77 (m, 6H, cyclohexyl), 2.33–2.46 (m, 4H, cyclohexyl), 6.29–6.47 (br, 2NH), 7.09 (t, 1ArH, $J = 6\text{Hz}$), 7.30 (t, 2ArH, $J = 6\text{Hz}$), 7.47 (d, 2ArH, $J = 9\text{Hz}$), 7.87 (br, 1NH), 12.50 (br, 1NH); EI-MS: m/z (%): 289 (10), 256 (17), 255 (27), 197 (39), 196 (10), 192 (29), 154 (36), 135 (100), 119 (10), 111 (26), 102 (10), 98 (18), 96 (31), 93 (31), 86 (14), 77 (80); Anal. calcd. for $\text{C}_{14}\text{H}_{19}\text{N}_5\text{S}$ (289.39): C, 58.10; H, 6.62; N, 24.20%. Found: C, 58.32; H, 6.47; N, 23.96%.

2.4.4.6. N-(Cyclohexylideneamino)-N'-(p-methoxyphenylthiocarbamoyl)guanidine (CyAATU-2)



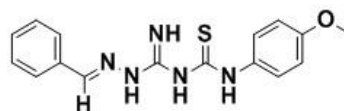
Off-white shining crystals from ethanol-water (1:1). Yield 66%. Mp 175–176°C. IR (UATR) ν cm^{-1} : 3321, 3195 (N-H), 2972, 2820 (C-H aliphatic), 1638 (C=N), 1560, 1493 (C-H aromatic), 1189, 1019 (C=S), 847, 740 (aromatic).

2.4.4.7. N-(Benzylideneamino)-N'-(phenylthiocarbamoyl)guanidine (BzAATU-1)



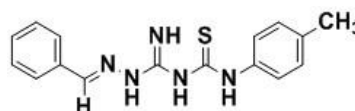
Pale green shining crystals from ethanol-water (1:1). Yield 65%. Mp 168–169°C. Lit. Mp 169-170°C (Sreejalekshmi, 2010). IR (UATR) ν cm^{-1} : 3417, 3398 (N-H), 3088 (C-H aromatic), 1619 (C=N), 1591, 1560, 1464 (C-H aromatic), 1095 (C=S), 807, 748, 686 (aromatic); Anal. calcd. for $\text{C}_{15}\text{H}_{15}\text{N}_5\text{S}$ (297.37): C, 60.58; H, 5.08; N, 23.55%. Found: C, 60.83; H, 5.26; N, 23.75%.

2.4.4.8. N-(Benzylideneamino)-N'-(p-methoxyphenylthiocarbamoyl)guanidine (BzAATU-2)



Pale green shining crystals from ethanol-water (1:1). Yield 62%. Mp 169–170°C. Lit. Mp 165–166°C (Sreejalekshmi, 2010). IR (KBr) ν cm^{-1} : 3427, 3225 (N-H), 3093, 2830, 1720, 1621 (C=N), 1534, 1509 (C-H aromatic), 1110, 1099 (C=S), 835, 800, 751, 690 (aromatic); Anal. calcd. for $\text{C}_{16}\text{H}_{17}\text{N}_5\text{OS}$ (327.40): C, 58.69; H, 5.23; N, 21.39%. Found: C, 58.42; H, 5.48; N, 21.27%.

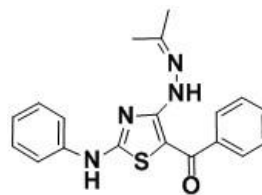
2.4.4.9. N-(Benzylideneamino)-N'-(p-methylphenylthiocarbamoyl)guanidine (BzAATU-3)



Pale green shining crystals from ethanol-water (1:1). Yield 58%. Mp 156–158°C. Lit. Mp 156–158°C (Sreejalekshmi, 2010). IR (KBr) ν cm^{-1} : 3400 (N-H), 3080 (C-H aromatic), 1610, 1600 (C=N), 1580, 1550, 1500, 1435 (C-H aromatic), 1090 (C=S), 805, 750, 680 (aromatic); ^1H NMR (300 MHz, CDCl_3): δ (ppm) 2.33 (s, 3H, - CH_3), 6.6 (br, 1NH), 7.43 (m, 3ArH), 7.65 (m, 2ArH), 7.93 (br, 2NH), 8.51 (br, 1NH); EI- MS: m/z (%): 195 (9), 162 (35), 161 (20), 150 (14), 149 (100), 148 (42), 119 (15), 117 (12), 106 (12), 92 (13), 91 (97), 90 (34), 89 (30), 85 (25), 77 (20); Anal. calcd. for $\text{C}_{16}\text{H}_{17}\text{N}_5\text{S}$ (311.40): C, 61.71; H, 5.50; N, 22.49%. Found: C, 61.52; H, 5.63; N, 22.30 %.

2.4.5. Characterization of HATs

2.4.5.1. 5-benzoyl-4-isopropylidenehydrazino-2-phenylaminothiazole (IPHAT-1)



The compound **IPHAT-1** was synthesized using acetone (580mg, 10mmol), phenylisothiocyanate (1.21g, 9mmol) and phenacylbromide (1.79g, 9mmol) and following the general procedure. The crude product was purified by recrystallization using ethanol-acetone (1:1) mixture to obtain the product as yellow solid (97%). Mp 206-208°C. IR (UATR) ν cm^{-1} : 3350, 3220 (N-H), 3060 (aromatic), 1676 (C=O), 749, 690 (aromatic); ^1H NMR (500 MHz, CDCl_3) : δ (ppm) 2.10 (s, 6H, CH_3), 7.21-7.24 (m, 1ArH), 7.28-7.29 (m, 3ArH), 7.40-7.48 (m, 5ArH), 7.76-7.77 (m, 1ArH), 8.45 (s, 1ArNH), 12.09 (s, 1NH); ^{13}C NMR (67.9 MHz, CDCl_3): δ (ppm) 17.2, 25.2, 94.4, 120.9, 125.6, 127.2, 128.4, 129.7, 130.7, 138.2, 141.3, 152.3, 161.8, 184.2; EI-MS: m/z (%): 350 (41), 245 (6), 119 (21), 105 (37), 77 (100), 56 (19); Anal. calcd. for: $\text{C}_{19}\text{H}_{18}\text{N}_4\text{O}_2\text{S}$ (350.44): C, 65.12; H, 5.18; N, 15.99%. Found: C, 65.08; H, 5.14; N, 15.83%.

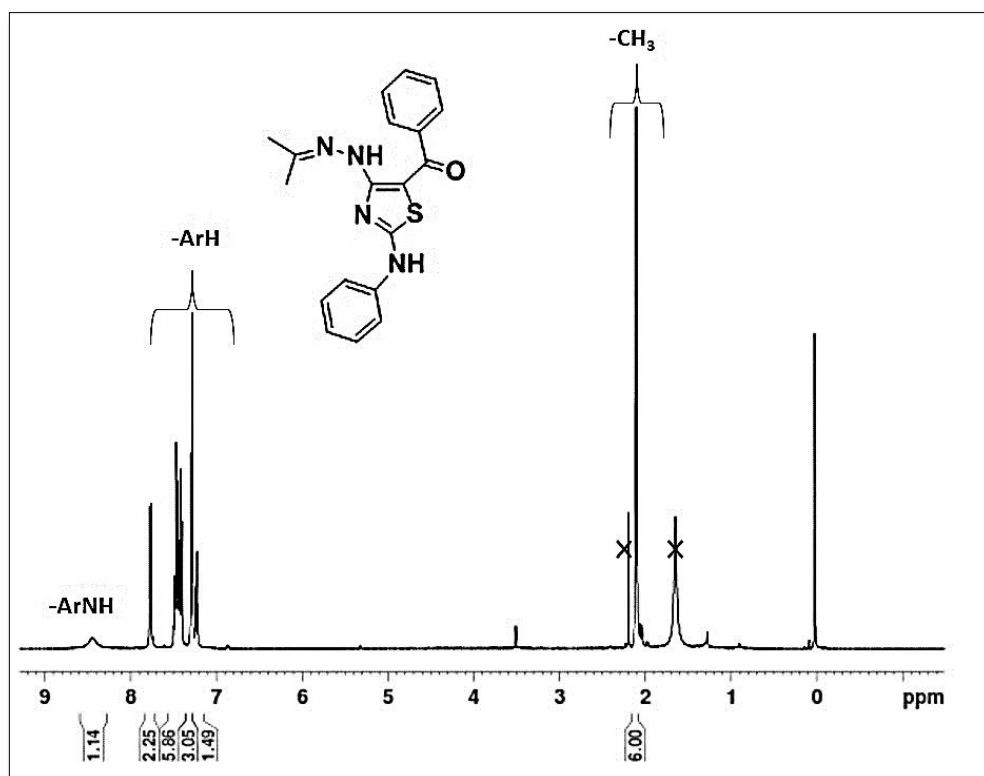


Figure 2.7. ^1H NMR spectrum of **IPHAT-1**

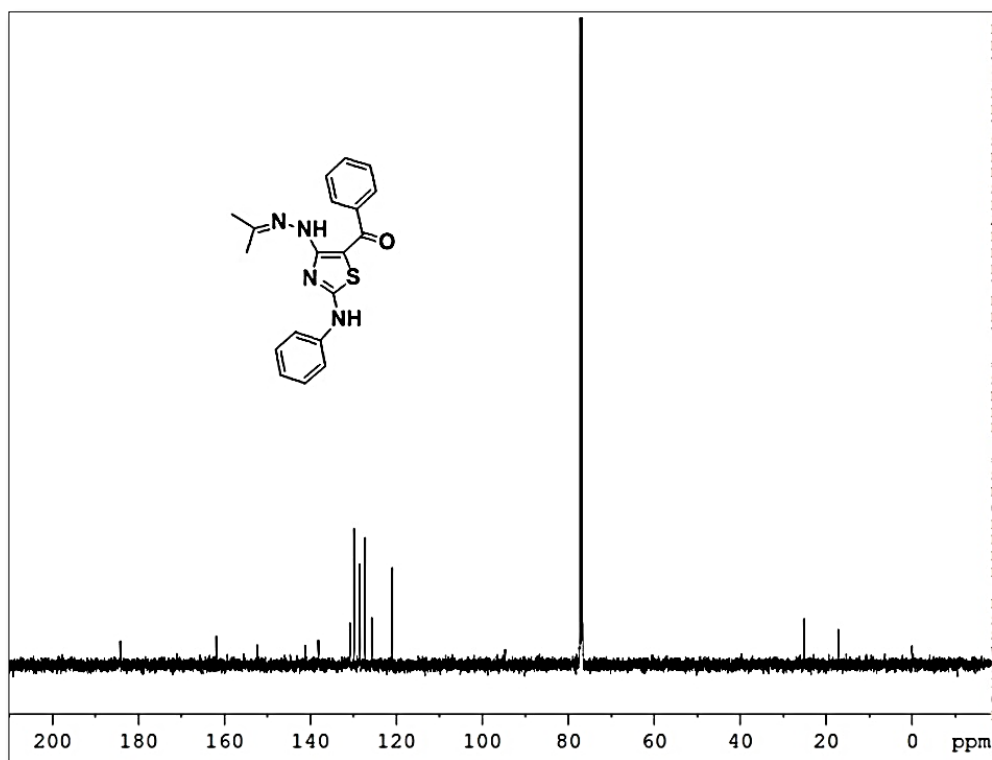
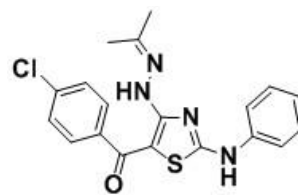


Figure 2.8. ^{13}C NMR spectrum of **IPHAT-1**

2.4.5.2. 5-(4-chlorobenzoyl)-4-isopropylidenehydrazino-2phenylaminothiazole (IPHAT-2)



Compound was synthesized using acetone (580mg, 10mmol), phenylisothiocyanate (1.216g, 9mmol) and 4-chlorophenacylbromide (2.10g, 9mmol) and following the general procedure. The crude product was purified by recrystallization using ethanol-acetone (1:1) mixture to obtain the product as yellow solid (94%). Mp 236-237°C. IR (UATR) ν cm^{-1} : 3224 (N-H), 3008, 2972 (aromatic), 1681 (C=O), 840, 748 (aromatic); ^1H NMR (500 MHz, CDCl_3): δ (ppm) 2.07 (s, 6H, $-\text{CH}_3$), 7.23-7.26 (m, 1ArH), 7.28-7.30 (m, 2ArH), 7.41-7.44 (m, 4ArH), 7.71-7.72 (m, 2ArH), 8.60 (s, 1ArNH), 12.09 (s, 1NH); ^{13}C NMR (125 MHz, CDCl_3): δ (ppm) 17.2, 25.1, 121.2, 125.9, 128.6, 128.7, 129.7, 136.7, 138.1, 139.5, 152.7, 162.1, 171.2, 182.5; HR-MS calcd. for $(\text{M}+\text{H})^+$: 385.0890; Found: 385.0875.

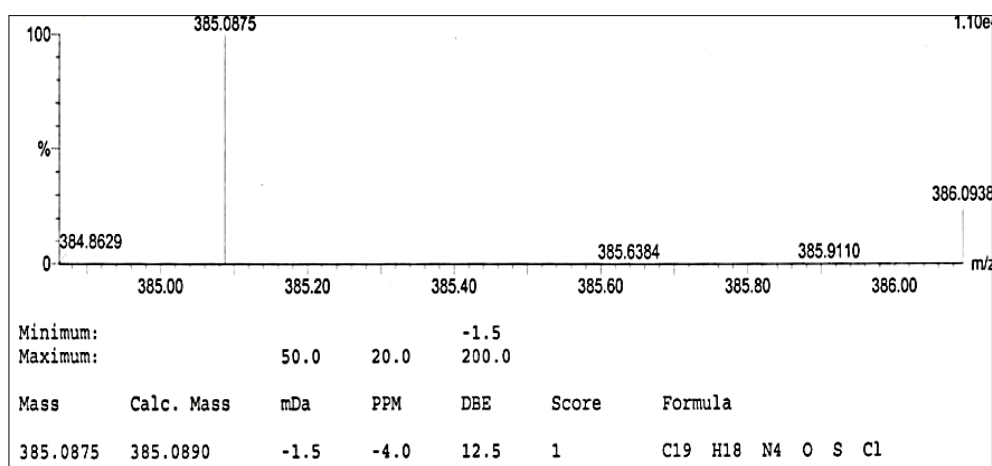


Figure 2.9. HR-MS spectrum of **IPHAT-2**

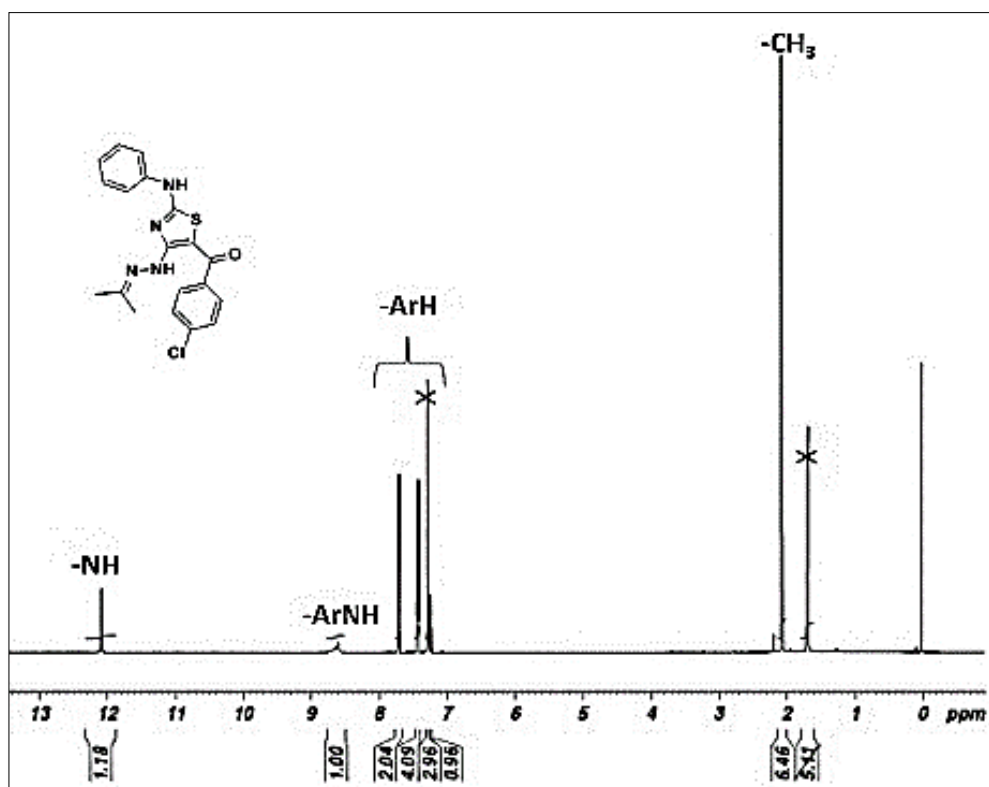


Figure 2.10. ¹H NMR spectrum of **IPHAT-2**

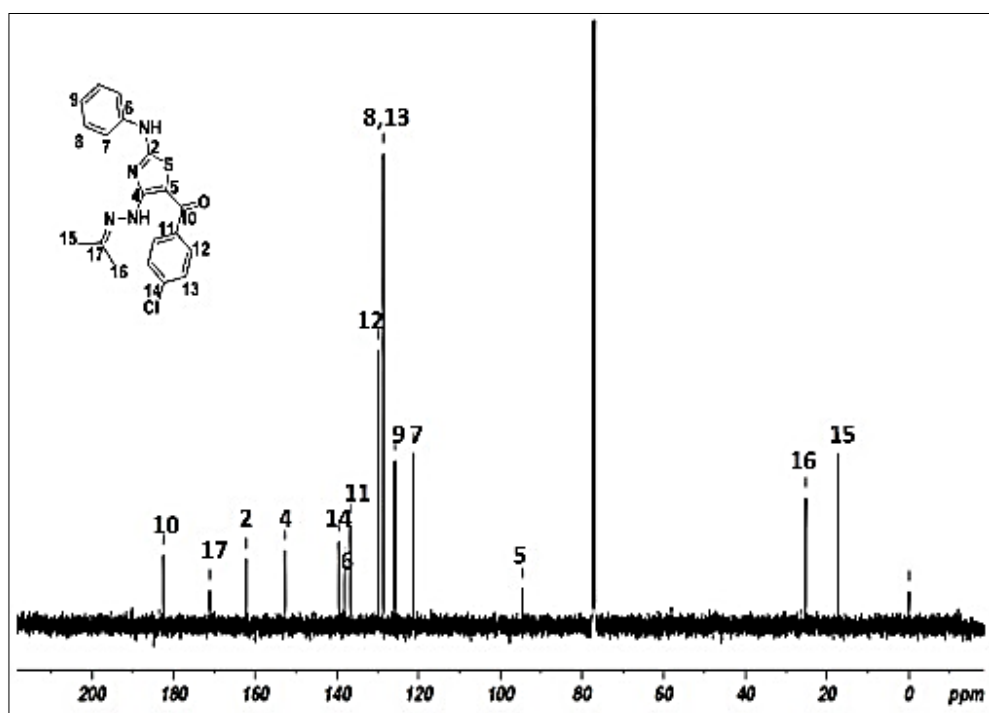
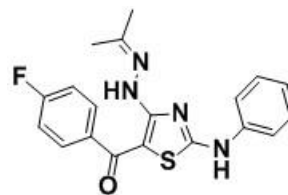


Figure 2.11. ¹³C NMR spectrum of **IPHAT-2**

2.4.5.3. 5-(4-fluorobenzoyl)-4-isopropylidenehydrazino-2-phenylaminothiazole (IPHAT-3)



IPHAT-3 was synthesized using acetone (580mg, 10mmol), phenylisothiocyanate (1.21mg, 9mmol), 4-fluorophenacylbromide (1.95mg, 9mmol) and following the general procedure. The crude product was purified by recrystallization using ethanol-acetone (1:1) mixture to obtain the product as yellow solid (90%). Mp 224-225°C. IR (UATR) ν cm^{-1} : 3340, 3279 (N-H), 3062, 2945 (aromatic), 1670 (C=O), 847, 755 (aromatic); ^1H NMR (500MHz, CDCl_3): δ (ppm) 1.96 (s, 3H, CH_3), 2.03 (s, 3H, CH_3), 7.12 (t, $J=8.5\text{Hz}$, 2ArH), 7.21-7.24 (m, 1ArH), 7.28-7.30 (m, 2ArH), 7.38-7.42 (m, 2ArH), 7.76-7.80 (m, 2ArH), 9.10 (s, 1ArNH), 12.08 (s, 1NH); ^{13}C NMR (125 MHz, CDCl_3): δ (ppm) 17.1, 24.9, 115.4, 115.5, 121.4, 125.8, 129.5, 137.4, 138.4, 152.4, 162.1, 163.0, 165.0, 171.4, 182.6; Anal. calcd. for $\text{C}_{19}\text{H}_{17}\text{FN}_4\text{OS}$ (368.43): C, 61.94; H, 4.65; N, 15.22%. Found: C, 59.37; H, 3.88; N, 14.45%.

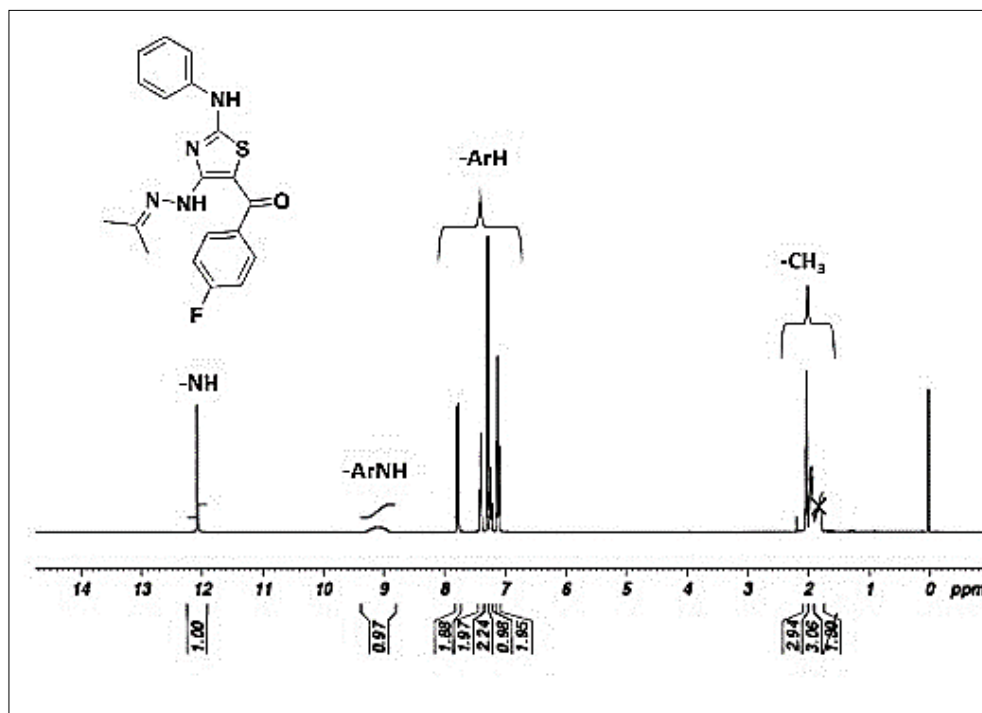


Figure 2.12. ^1H NMR spectrum of **IPHAT-3**

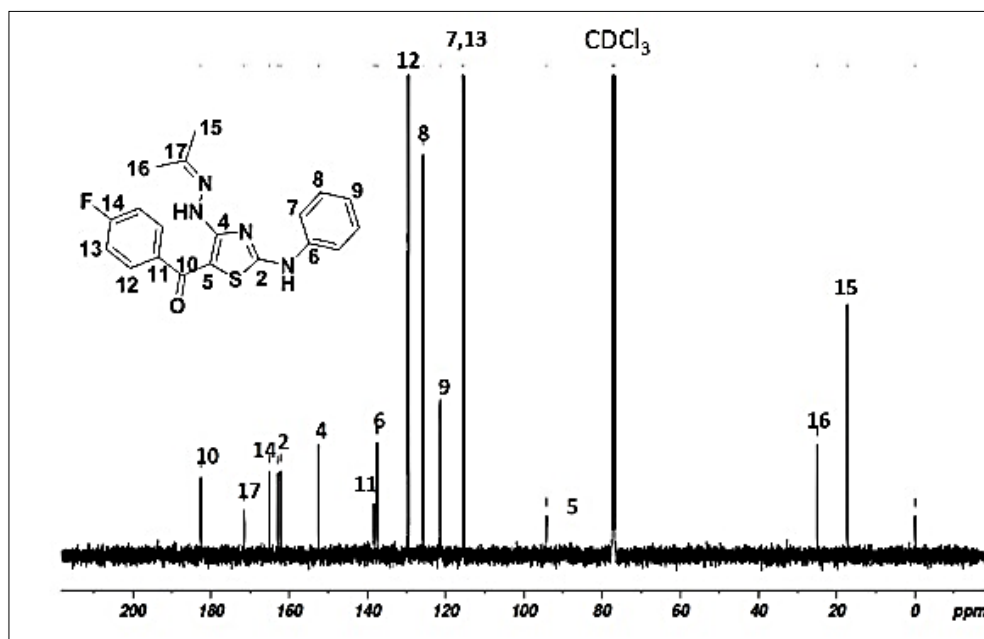
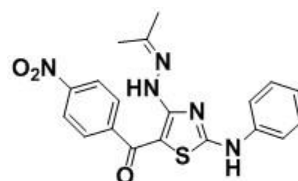


Figure 2.13. ^{13}C NMR spectrum of **IPHAT-3**

2.4.5.4. 4-isopropylidenehydrazino-2-phenylamino-5-(4-nitrobenzoyl)thiazole (IPHAT-4)



The compound **IPHAT-4** was synthesized using acetone (580mg, 10mmol), phenylisothiocyanate (1.216g, 9mmol) and 4-nitrophenacylbromide (2.19g, 9mmol) and following the general procedure. The crude product was purified by recrystallization using ethanol-acetone (1:1) mixture to obtain the product as red solid (75%). Mp 229-230°C. IR (UATR) ν cm^{-1} : 3338, 3232 (N-H), 3062, 2987 (aromatic), 1671 (C=O), 1521, 1339 (ArNO_2), 852 (C-N of ArNO_2); ^1H NMR (500MHz, CDCl_3) : δ (ppm) 2.08 (s, 6H, CH_3), 7.28 (m, 3ArH), 7.43 (m, 2ArH), 7.90 (m, 2ArH), 8.30 (d, $J=6.0\text{Hz}$, 2ArH), 8.71 (s, 1ArNH), 12.13 (s, 1NH); ^{13}C NMR (125 MHz, CDCl_3): δ (ppm) 25.2, 121.5, 123.8, 126.3, 128.2, 129.8, 137.8, 146.7, 148.7, 153.7, 162.6, 171.8, 180.8; HR-MS calcd. for $(\text{M}+\text{H})^+$: 396.1130; Found: 396.1118.

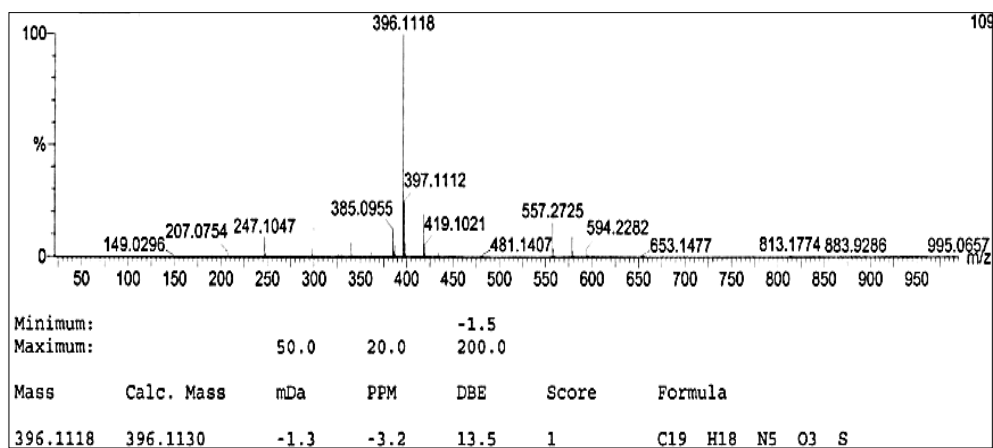


Figure 2.14. HR-MS spectrum of **IPHAT-4**

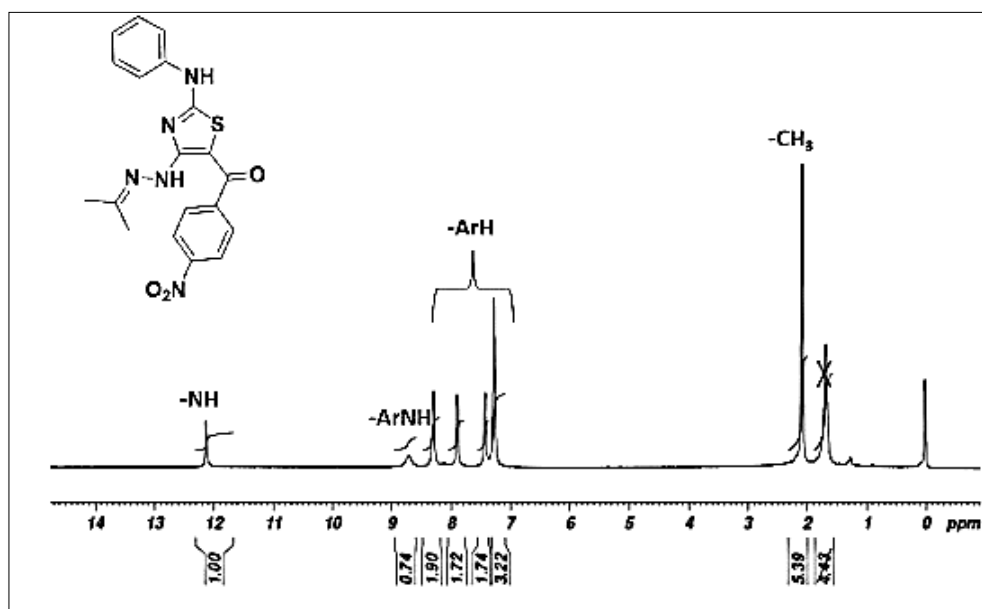


Figure 2.15. ^1H NMR spectrum of **IPHAT-4**

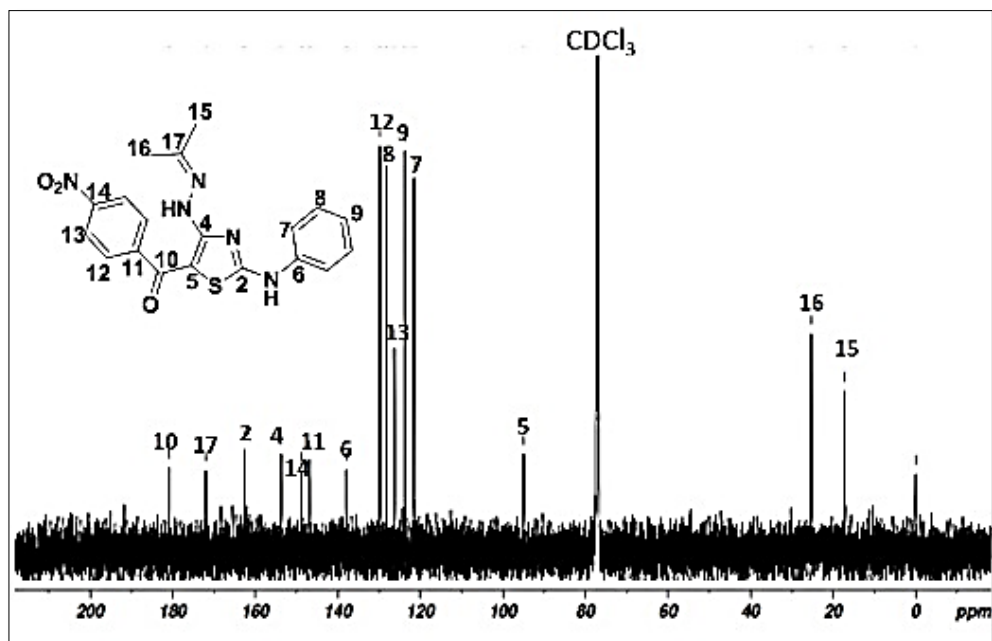
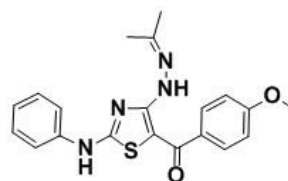


Figure 2.16. ^{13}C NMR spectrum of **IPHAT-4**

2.4.5.5. 4-isopropylidenehydrazino-5-(4-methoxybenzoyl)-2-phenylaminothiazole (**IPHAT-5**)



IPHAT-5 was synthesized using acetone (580mg, 10mmol), phenylisothiocyanate (1.216g, 9mmol) and 4-methoxyphenacylbromide (2.06g, 9mmol) and following the general procedure. The crude product was purified by recrystallization using ethanol-acetone (1:1) mixture to obtain the product as yellow solid (92%). Mp 248-250°C. IR (UATR) ν cm^{-1} : 3273 (N-H), 3077, 2956 (aromatic), 2838 (aliphatic), 1676 (C=O), 1254, 1028 (C-O-C); ^1H NMR (500MHz, CDCl_3): δ (ppm) 2.06 (s, 6H, CH_3), 3.85 (s, 3H, OCH_3), 6.93 (d, $J = 8.6\text{Hz}$, 2ArH), 7.19-7.22 (m, 1ArH), 7.26-7.27 (m, 2ArH), 7.38-7.41 (m, 2ArH), 7.76 (d, $J = 8.6\text{Hz}$, 2ArH), 8.44 (s, 1ArNH), 12.07 (s, 1NH); ^{13}C NMR (125 MHz, CDCl_3): δ (ppm) 17.2, 25.1, 55.4, 94.1, 113.7, 121.1, 125.5, 129.2, 129.7, 133.8, 138.4, 151.9, 161.6, 161.8, 170.8, 183.5; EI-MS: m/z (%): 380 (100), 379 (64), 324 (19), 275 (19), 149 (41), 148 (20), 122 (25), 121 (12), 105 (65), 77 (40), 56 (40); Anal. calcd. for

C₂₀H₂₀N₄O₂S (380.47): C, 63.13; H, 5.30; N, 14.73%. Found: C, 63.06; H, 5.22; N, 14.69%.

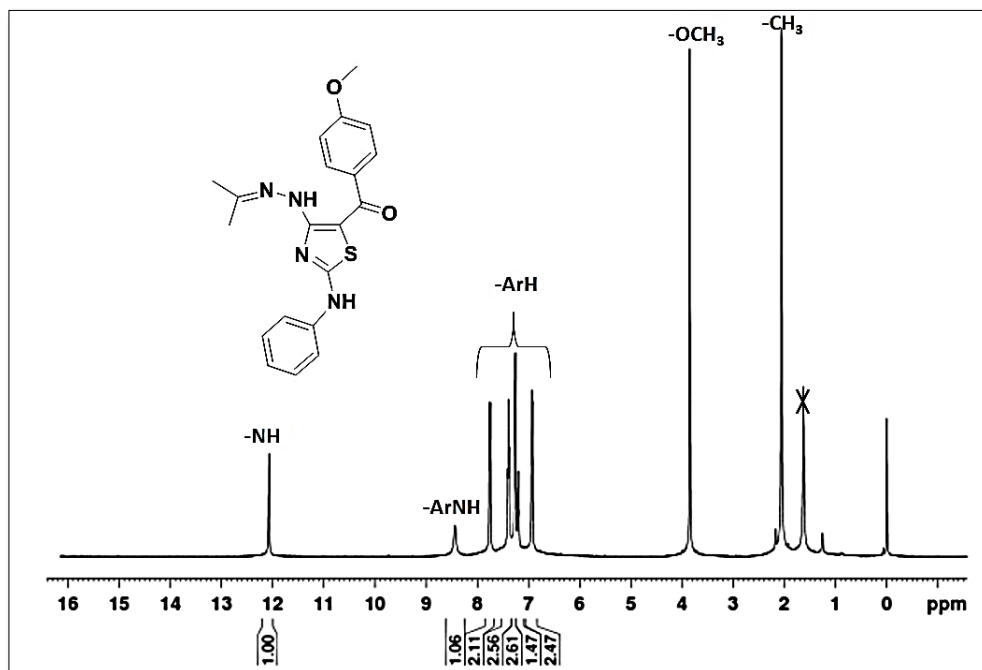


Figure 2.17. ¹H NMR spectrum of **IPHAT-5**

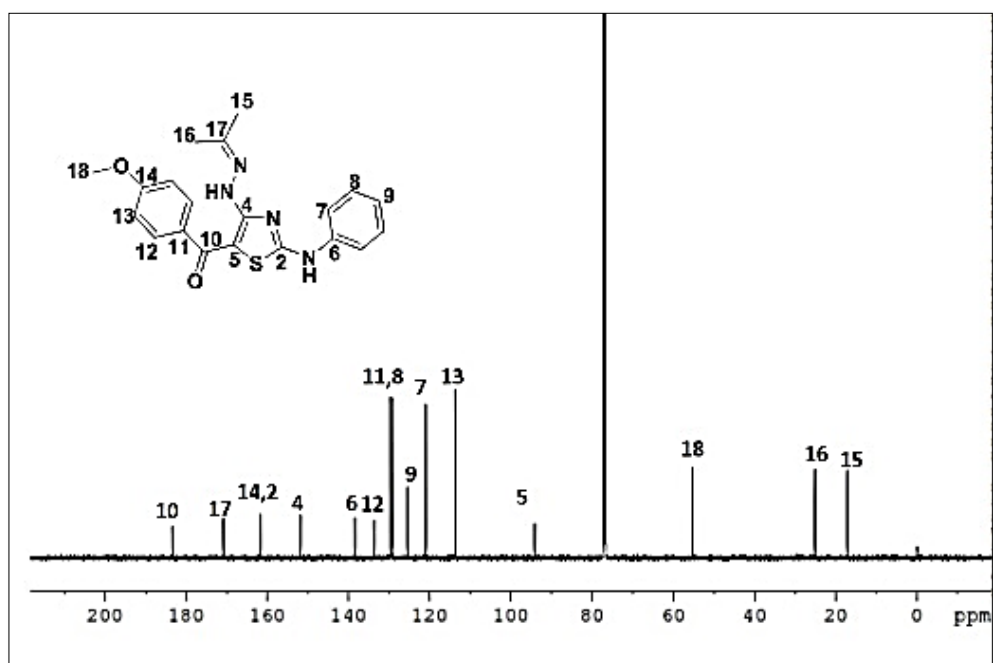
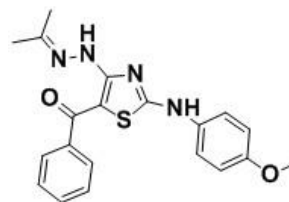


Figure 2.18. ¹³C NMR spectrum of **IPHAT-5**

2.4.5.6. 5-benzoyl-4-isopropylidenehydrazino-2-(4-methoxyphenylamino)thiazole (IPHAT-6)



Compound was synthesized using acetone (580mg, 10mmol), 4-methoxyphenylisothiocyanate (1.48g, 9mmol) and phenacylbromide (1.79g, 9mmol) and following the general procedure. The crude product was purified by recrystallization using ethanol-acetone (1:1) mixture to obtain the product as yellow solid (92%). Mp 238-240°C. IR (UATR) ν cm^{-1} : 3268 (N-H), 3076, 2996 (aromatic) 1695 (C=O), 1231, 1030 (C-O-C); ^1H NMR (500 MHz, CDCl_3): δ (ppm) 1.97 (s, 3H, CH_3), 2.03 (s, 3H, CH_3), 3.79 (s, 3H, OCH_3), 6.72-6.76 (m, 1ArH), 6.82-6.83 (m, 1ArH), 6.86-6.88 (m, 1ArH), 7.25-7.28 (m, 1ArH), 7.41-7.46 (m, 3ArH), 7.74-7.76 (m, 2ArH), 8.95 (s, 1ArNH), 12.08 (s, 1NH); ^{13}C NMR (125 MHz, CDCl_3): δ (ppm) 17.1, 25.0, 55.4, 94.6, 121.5, 127.1, 128.2, 130.2, 130.5, 135.6, 135.8, 141.2, 152.2, 162.0, 171.9, 183.8; EI-MS: m/z (%): 364(100), 308(20), 259(23), 133(48), 132(34), 105(63), 91(16), 77(37), 56(48); Anal. calcd. for $\text{C}_{20}\text{H}_{20}\text{N}_4\text{O}_2\text{S}$ (380.47): C, 65.90; H, 5.53; N, 15.37. Found: C, 65.77; H, 5.46; N, 15.29.

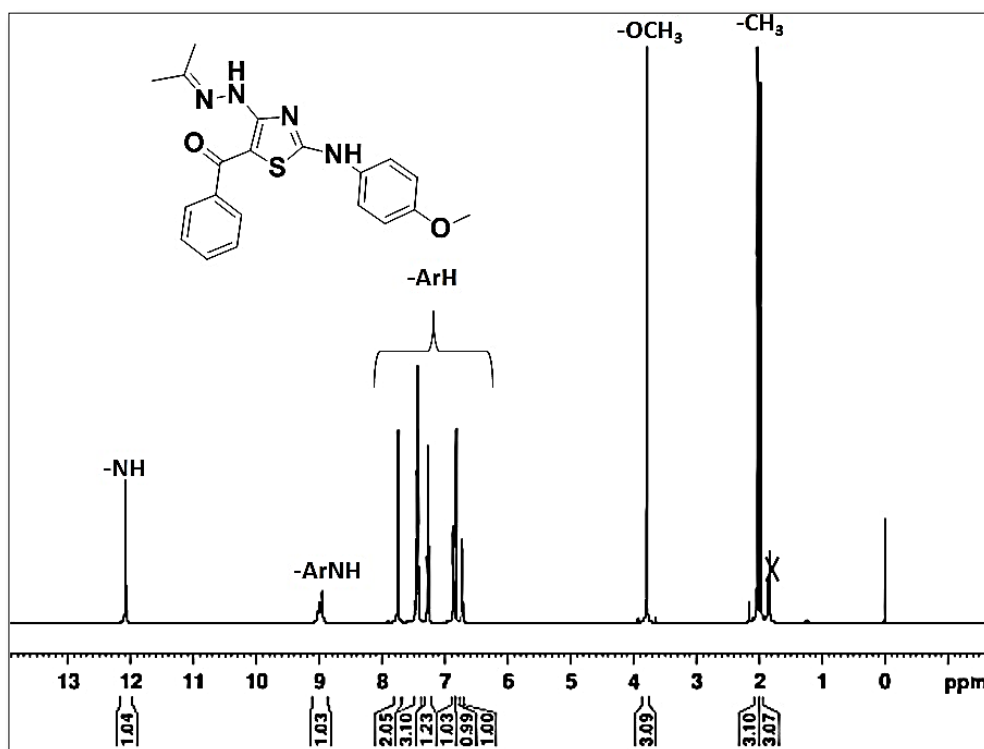


Figure 2.19. ^1H NMR spectrum of IPHAT-6

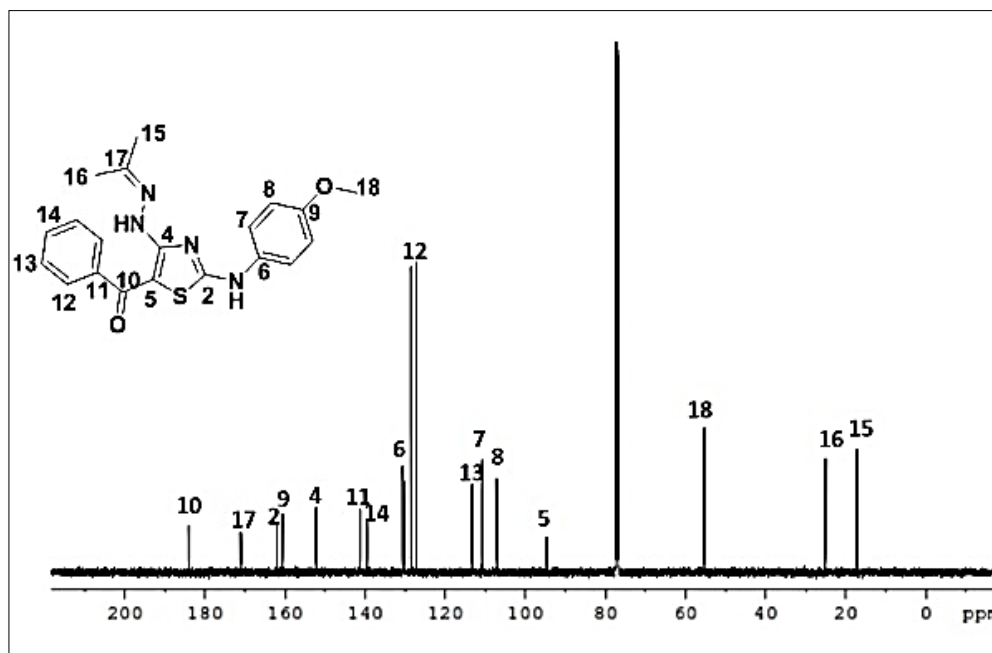
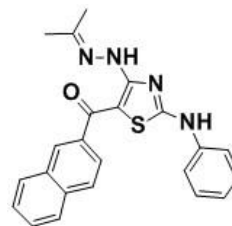


Figure 2.20. ^{13}C NMR spectrum of **IPHAT-6**

2.4.5.7. 4-isopropylidenehydrazino-5-(naphth-2-oyl)-2-phenylaminothiazole (**IPHAT-7**)



IPHAT-7 was synthesized using acetone (580mg, 10mmol), phenylisothiocyanate (1.21g, 9mmol) and 2-bromoacetylnaphthalene (2.24g, 9mmol) and following the general procedure. The crude product was purified by recrystallization using ethanol-acetone (1:1) mixture to obtain the product as yellow solid (90%). Mp 258-259°C. IR (UATR) ν cm^{-1} : 3282 (N-H), 3098, 3052 (aromatic) 1629 (C=O), 832, 759 (aromatic); ^1H NMR (500 MHz, CDCl_3): δ (ppm) 2.12 (s, 3H, CH_3), 2.16 (s, 3H, CH_3), 7.19-7.22 (m, 1ArH), 7.25-7.27 (m, 2ArH), 7.37-7.41 (m, 2ArH), 7.51-7.57 (m, 2ArH), 7.83-7.88 (m, 2ArH), 7.90-7.93 (m, 2ArH), 8.19 (s, 1ArNH), 8.24 (s, 1ArH), 12.15 (s, 1NH); ^{13}C NMR (125 MHz, CDCl_3): δ (ppm) 17.3, 25.2, 95.0, 120.9, 124.3, 125.6, 126.6, 127.4, 127.8, 128.4, 128.9, 129.7, 132.6, 134.4, 138.2, 138.7, 152.4, 161.9, 171.2, 184.1; LC-MS (M^+): m/z : 400.12.

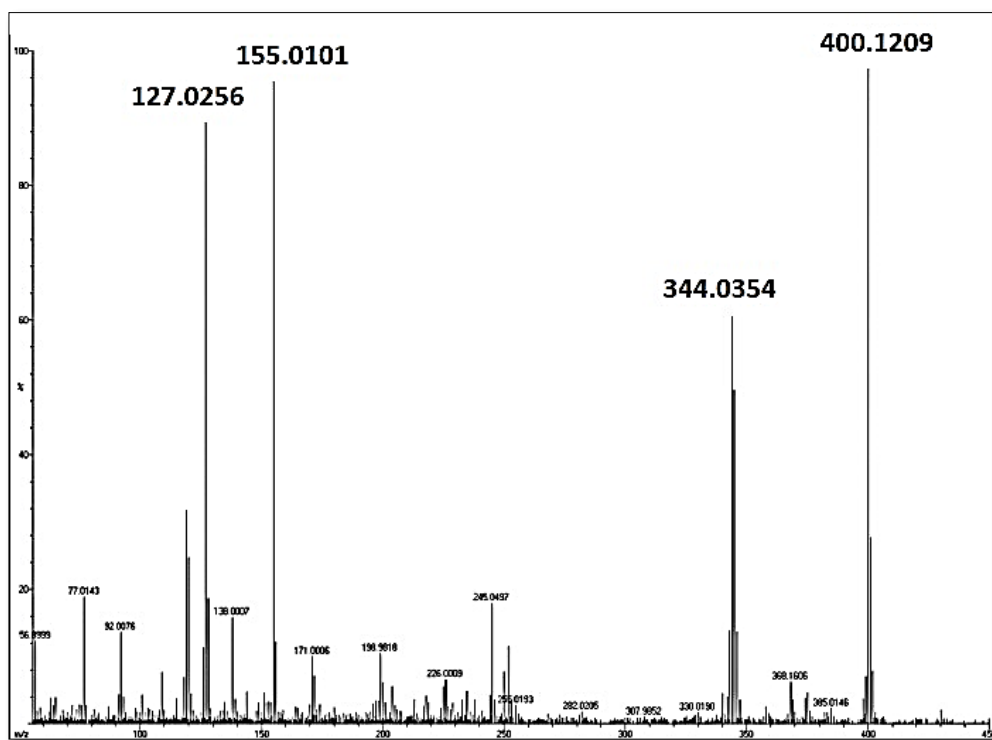


Figure 2.21. LC-MS spectrum of **IPHAT-7**

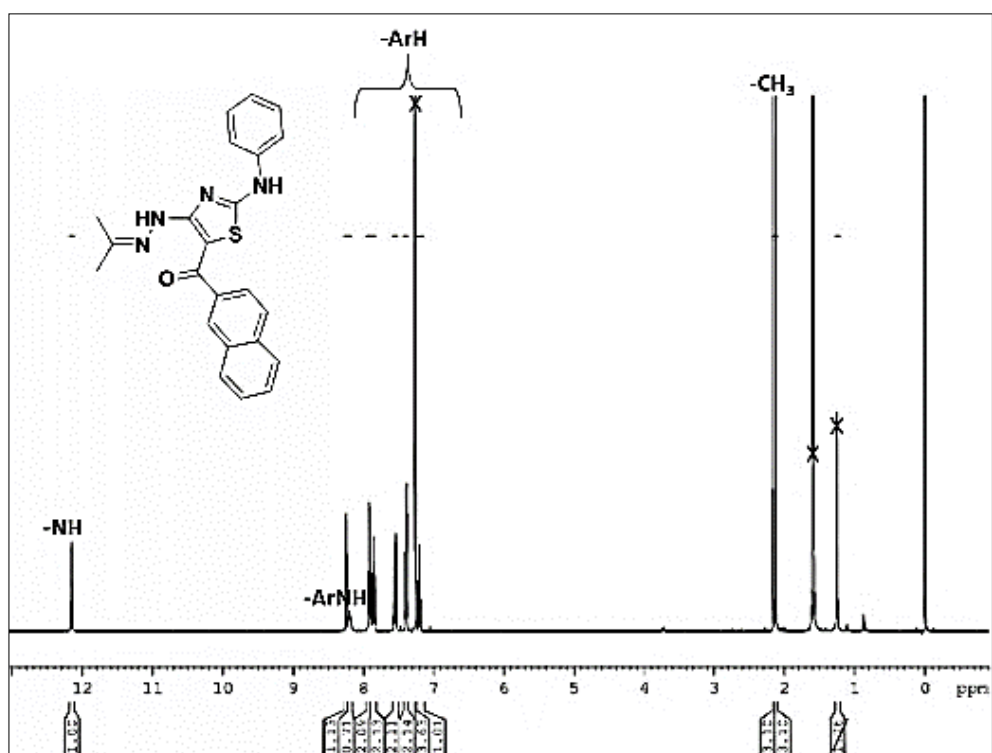


Figure 2.22. ¹H NMR spectrum of **IPHAT-7**

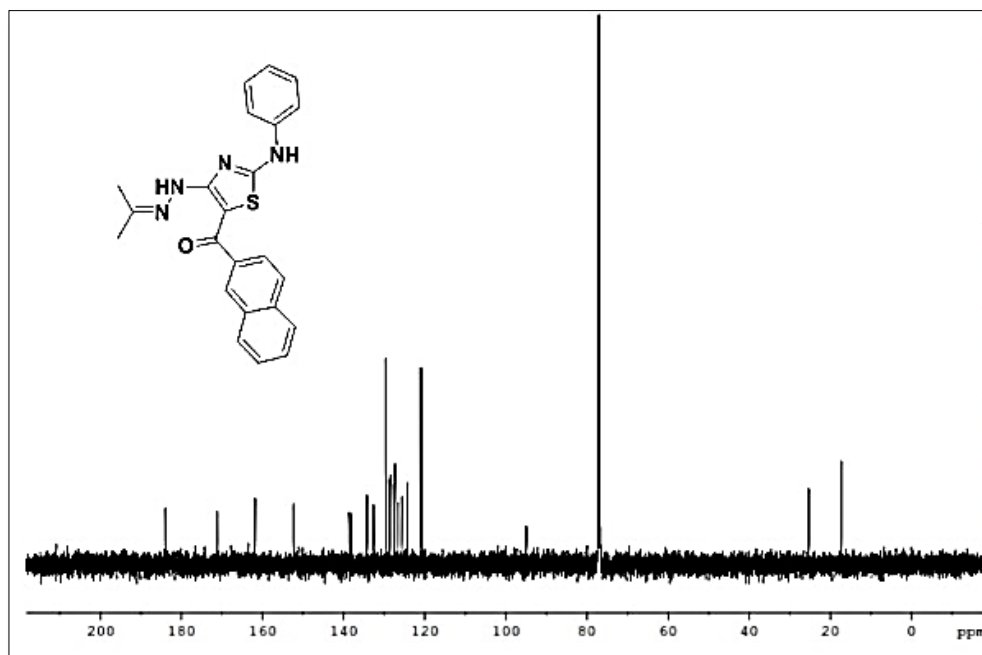
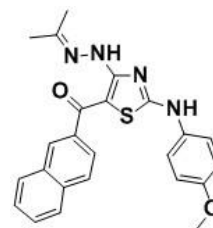


Figure 2.23. ^{13}C NMR spectrum of **IPHAT-7**

2.4.5.8. 4-isopropylidenehydrazino-2-(4-methoxyphenylamino)-5-(naphth-2-oyl)- thiazole (IPHAT-8)



The compound **IPHAT-8** was synthesized using acetone (580mg, 10mmol), 4-methoxyphenylisothiocyanate (1.48g, 9mmol) and 2-bromoacetylnaphthalene (2.24g, 9mmol) and following the general procedure. The crude product was purified by recrystallization using ethanol-acetone (1:1) mixture to obtain the product as yellow solid (90%). Mp 223-224°C. IR (UATR) ν cm^{-1} : 3395, 3269 (N-H), 3054, 2996 (aromatic) 1636 (C=O), 1231, 1030 (C-O-C), 823, 776 (aromatic); ^1H NMR (500 MHz, CDCl_3): δ (ppm) 2.08 (s, 6H, CH_3), 3.80 (s, 3H, OCH_3) 6.89-6.90 (m, 2ArH), 7.21-7.22 (m, 2ArH), 7.49-7.55 (m, 2ArH), 7.80-7.82 (m, 1ArH), 7.84-7.86 (m, 2ArH), 7.87-7.91 (m, 1ArH), 8.20 (s, 1ArH), 8.29 (s, 1ArNH), 12.19 (s, 1NH); ^{13}C NMR (125 MHz, CDCl_3): δ (ppm) 17.3, 25.2, 55.5, 95.0, 114.9, 124.7, 126.5, 127.3, 127.7, 128.3, 128.9, 131.2, 132.6, 134.3, 138.8, 152.3, 158.2, 162.5, 173.4, 183.8; LC-MS (M^+): m/z : 430.15.

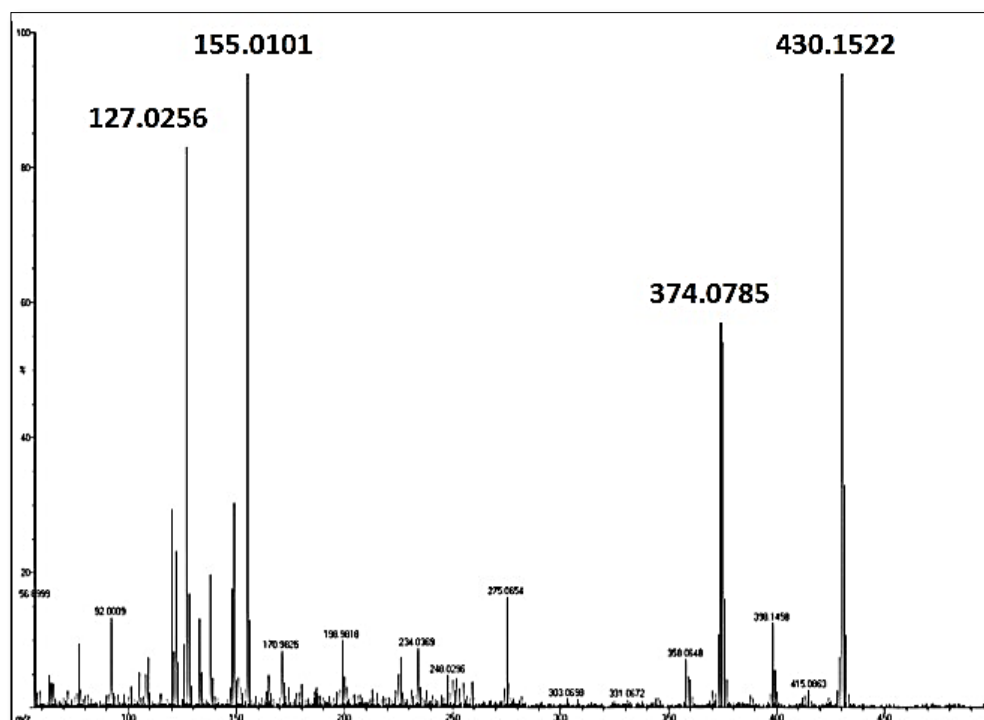


Figure 2.24. LC-MS spectrum of **IPHAT-8**

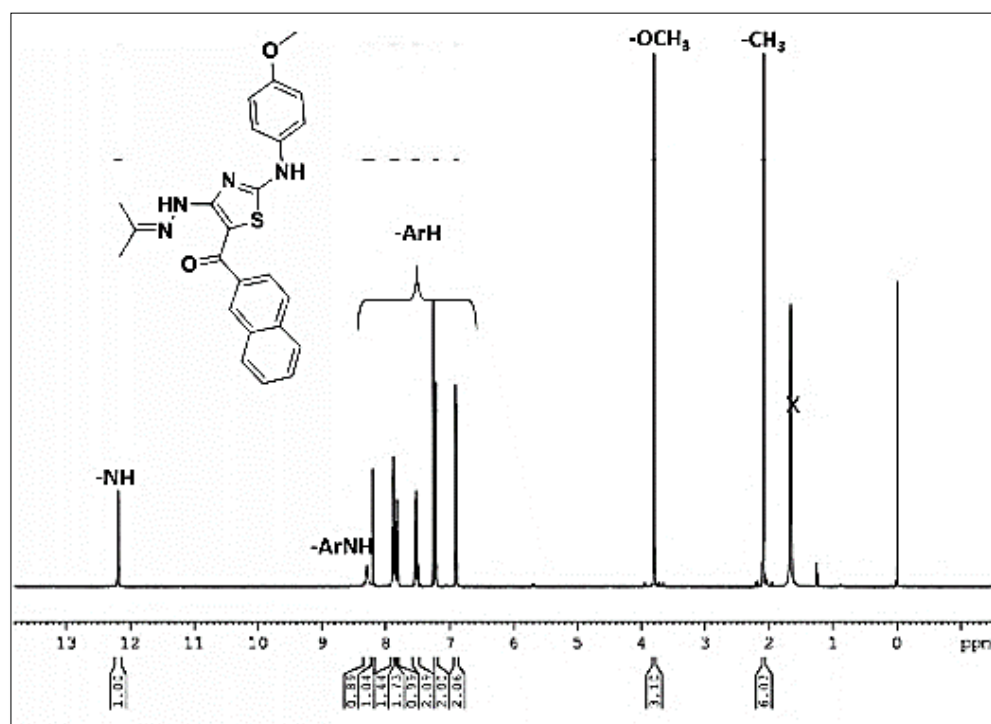


Figure 2.25. ¹H NMR spectrum of **IPHAT-8**

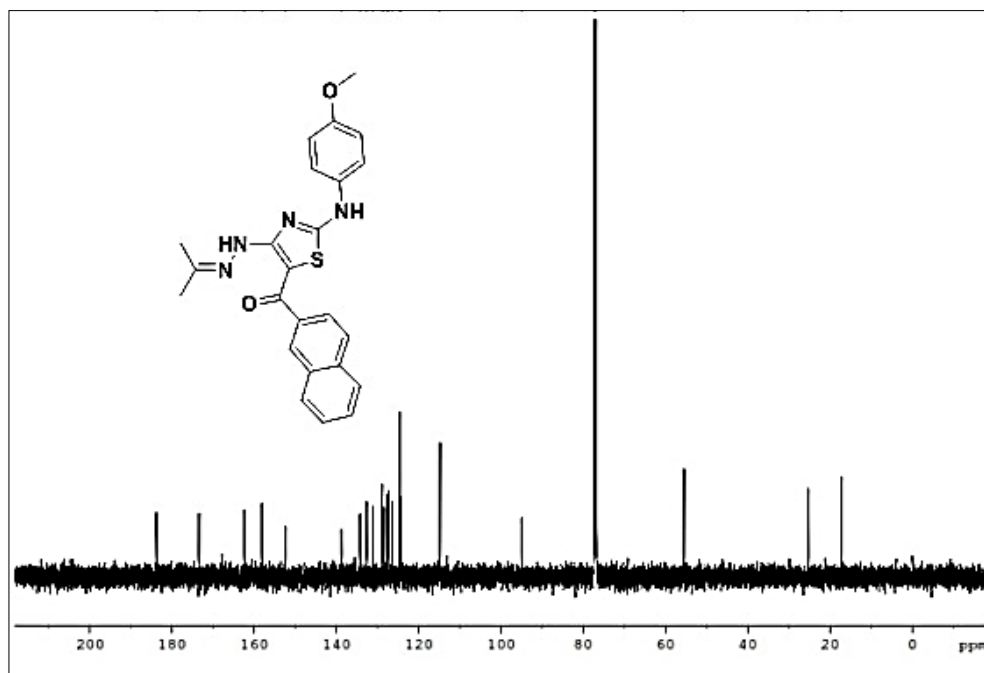
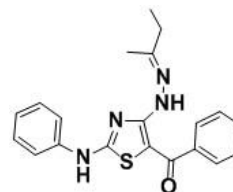


Figure 2.26. ^{13}C NMR spectrum of **IPHAT-8**

2.4.5.9. 5-(benzoyl)-4-isobutylidenehydrazino-2-phenylaminothiazole (**IBHAT-1**)



The compound **IBHAT-1** was synthesized using 2-butanone (721mg, 10mmol), phenylisothiocyanate (1.216g, 9mmol) and phenacylbromide (1.79g, 9mmol) and following the general procedure. The crude product was purified by recrystallization using chloroform-acetone (1:1) mixture to obtain the product as yellow solid (92%). Mp 168-169°C. IR (KBr) ν cm^{-1} : 3260, 3190 (N-H), 2950, 2900 (C-H), 820, 750 (aromatic); ^1H NMR (500 MHz, CDCl_3): δ (ppm) 1.05-1.08 (m, 1H), 1.19-1.22 (m, 1H), 1.82 (s, 3H, CH_3), 1.99-2.04 (m, 3H), 7.17-7.23 (m, 1ArH), 7.28-7.30 (m, 2ArH), 7.37-7.43 (m, 2ArH), 7.45-7.48 (m, 3ArH), 7.74-7.76 (m, 2ArH), 8.95 (s, 1ArNH), 12.08 (s, 1NH); ^{13}C NMR (125 MHz, CDCl_3): δ (ppm) 15.2, 17.2, 25.1, 121.2, 125.7, 127.2, 128.5, 129.6, 130.7, 135.3, 138.4, 141.3, 152.3, 161.9, 171.4, 175.3, 184.1.

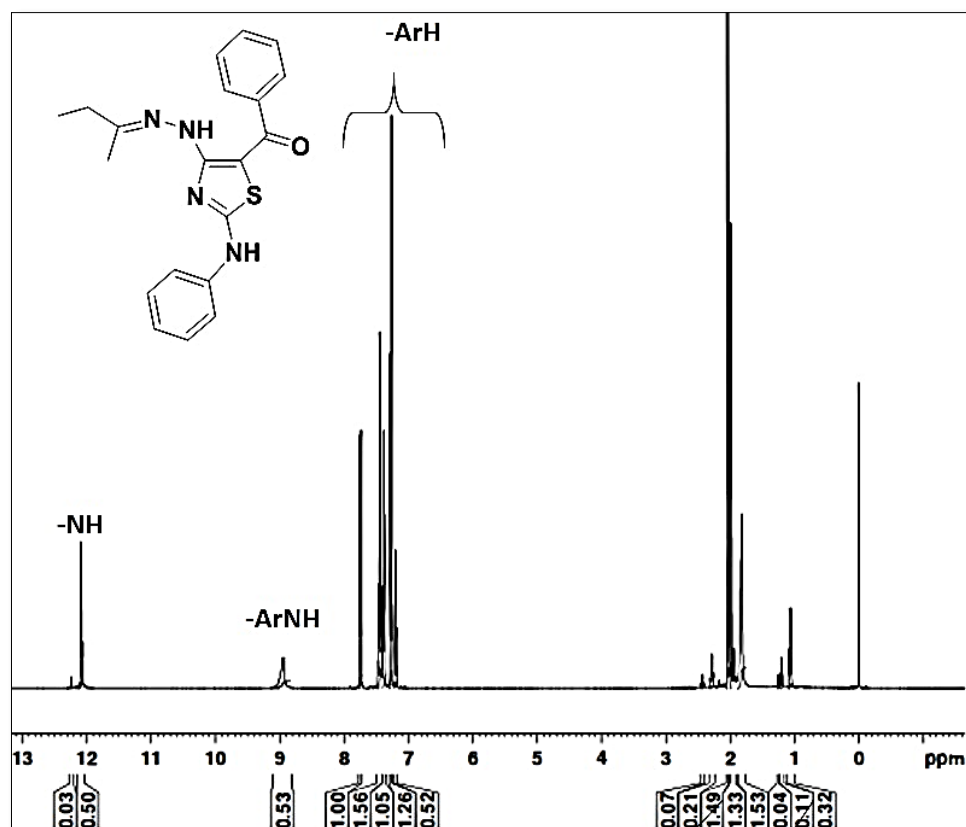


Figure 2.27. ¹H NMR spectrum of **IBHAT-1**

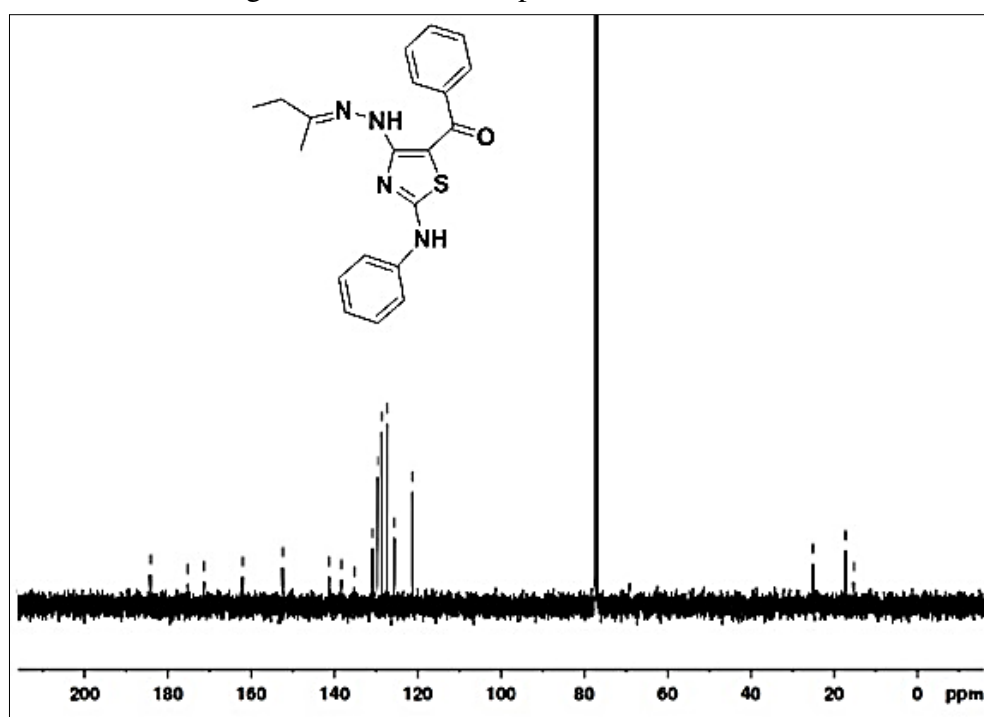
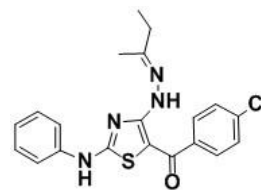


Figure 2.28. ¹³C NMR spectrum of **IBHAT-1**

2.4.5.10. 5-(4-chlorobenzoyl)-4-isobutylidenehydrazino-2-phenylaminothiazole (IBHAT-2)



The compound **IBHAT-2** was synthesized using 2-butanone (721mg, 10mmol), phenylisothiocyanate (1.216g, 9mmol) and 4-chlorophenacylbromide (2.10g, 9mmol) and following the general procedure. The crude product was purified by recrystallization using chloroform-acetone (1:1) mixture to obtain the product as yellow solid (92%). Mp 216-218°C. IR (KBr) ν cm^{-1} : 3260, 3190 (N-H), 2955(C-H), 826, 753 (aromatic); ^1H NMR (500 MHz, CDCl_3): δ (ppm) 1.12-1.15 (m, 1H), 1.22-1.25 (m, 2H), 2.07 (s, 3H, CH_3), 2.40 (dd, $J=7.5\text{Hz}$, 1H), 2.47 (dd, $J=7.5\text{Hz}$, 1H), 7.19-7.27 (m, 2ArH), 7.39-7.47 (m, 4ArH), 7.68-7.70 (m, 2ArH), 8.35 (s, 1ArNH), 12.22 (s, 1NH); ^{13}C NMR (125 MHz, CDCl_3): δ (ppm) 11.3, 15.2, 32.0, 94.4, 121.2, 125.8, 128.7, 129.7, 136.7, 138.3, 139.6, 157.0, 162.2, 171.4, 182.5; ESI-MS ($\text{M}+\text{H}^+$): 399.10; Anal. calcd. for $\text{C}_{20}\text{H}_{19}\text{ClN}_4\text{OS}$ (398.91): C, 60.22; H, 4.80; N, 14.05%. Found: C, 60.42; H, 5.02; N, 14.23%.

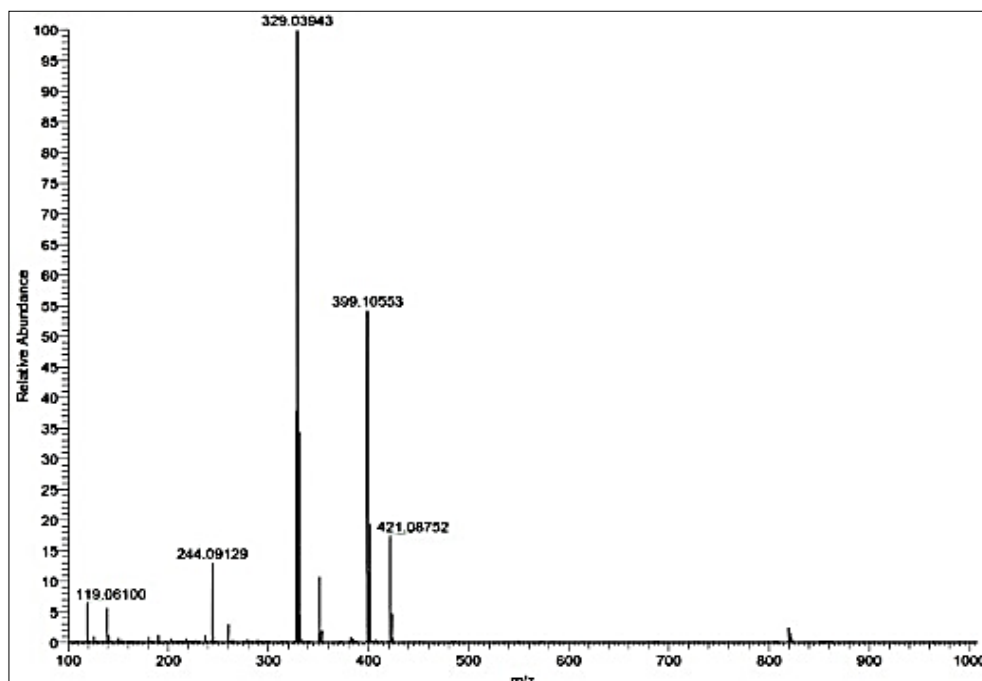


Figure 2.29. ESI-MS spectrum of **IBHAT-2**

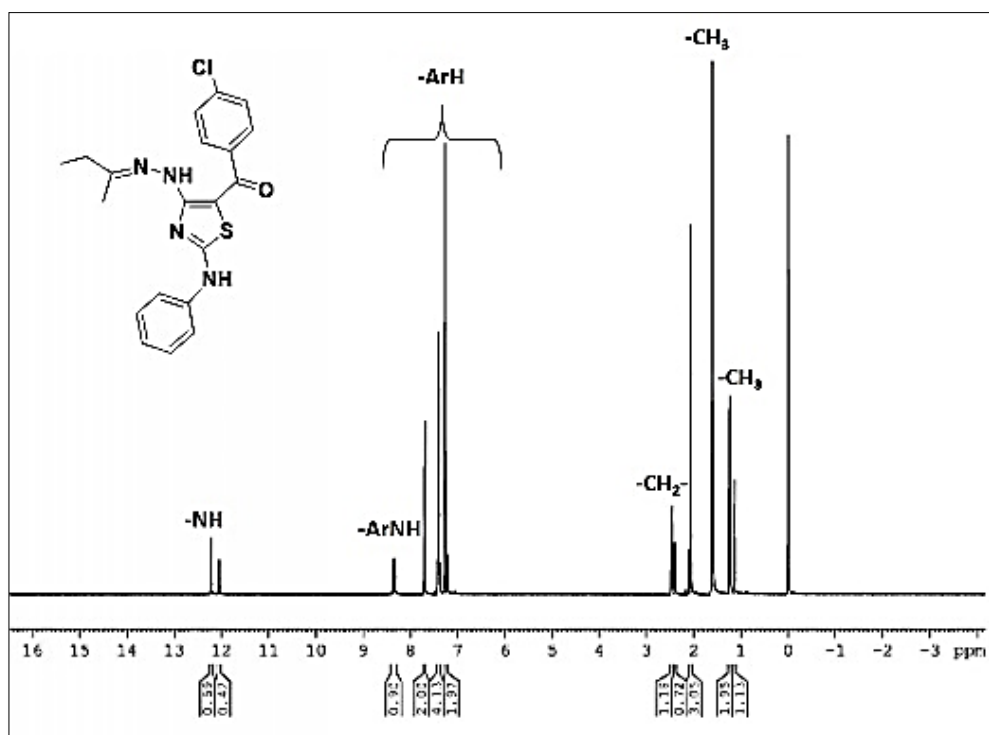


Figure 2.30. ¹H NMR spectrum of **IBHAT-2**

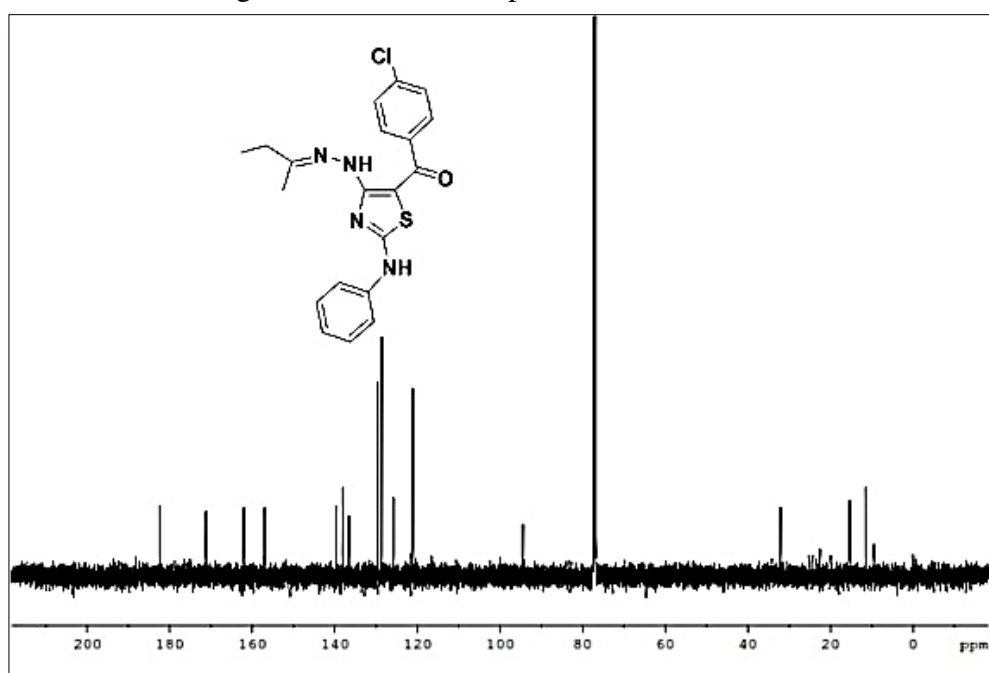
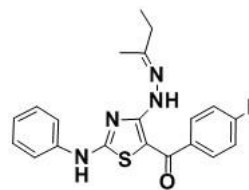


Figure 2.31. ¹³C NMR spectrum of **IBHAT-2**

2.4.5.11. 5-(4-fluorobenzoyl)-4-isobutylidenehydrazino-2-phenylaminothiazole (IBHAT-3)



The above compound was synthesized using 2-butanone (721mg, 10mmol), phenylisothiocyanate (1.216g, 9mmol) and 4-fluorophenacylbromide (1.95mg, 9mmol) following the general procedure. The crude product was purified by recrystallization using chloroform-acetone (1:1) mixture to obtain the product as yellow solid (92%). Mp 194-195°C. IR (KBr) ν cm^{-1} : 3260, 3190 (N-H), 2946 (C-H), 827, 743 (aromatic); ^1H NMR (500 MHz, CDCl_3): δ (ppm) 1.02-1.05 (m, 3H), 1.99 (s, 3H, CH_3), 2.22-2.26 (m, 2H), 7.09-7.12 (m, 2ArH), 7.20-7.22 (m, 1ArH), 7.27-7.28 (m, 2ArH), 7.36-7.39 (m, 2ArH), 7.76-7.78 (m, 2ArH), 9.14 (s, 1ArNH), 12.05 (s, 1NH); ^{13}C NMR (125 MHz, CDCl_3): δ (ppm) 11.2, 15.2, 22.3, 31.9, 94.2, 115.4, 121.3, 125.7, 129.6, 137.5, 138.5, 156.8, 157.2, 162.2, 163.1, 165.1, 171.4, 182.6; HR-MS calcd. for $(\text{M}+\text{H})^+$: 383.1342; Found: 383.1351.

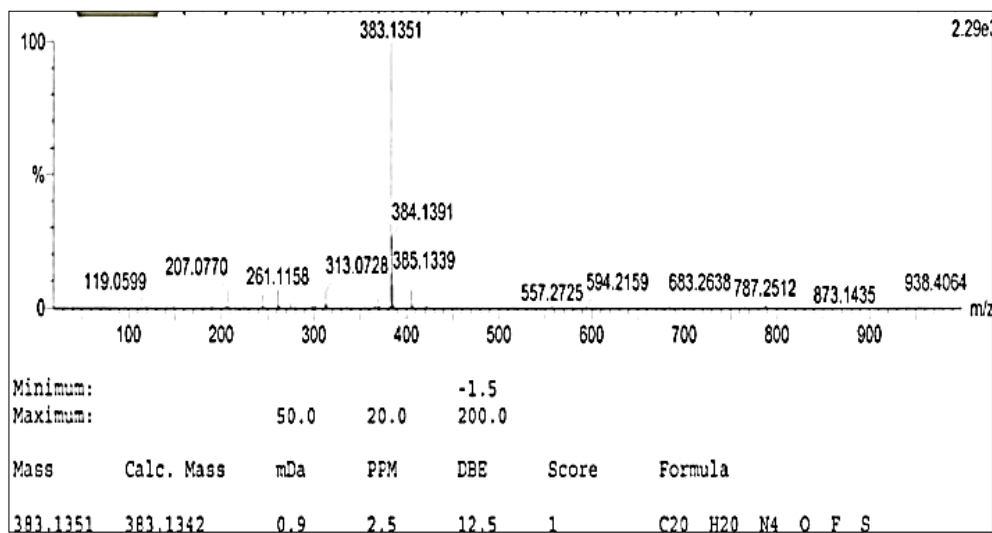


Figure 2.32. ESI-MS spectrum of **IBHAT-3**

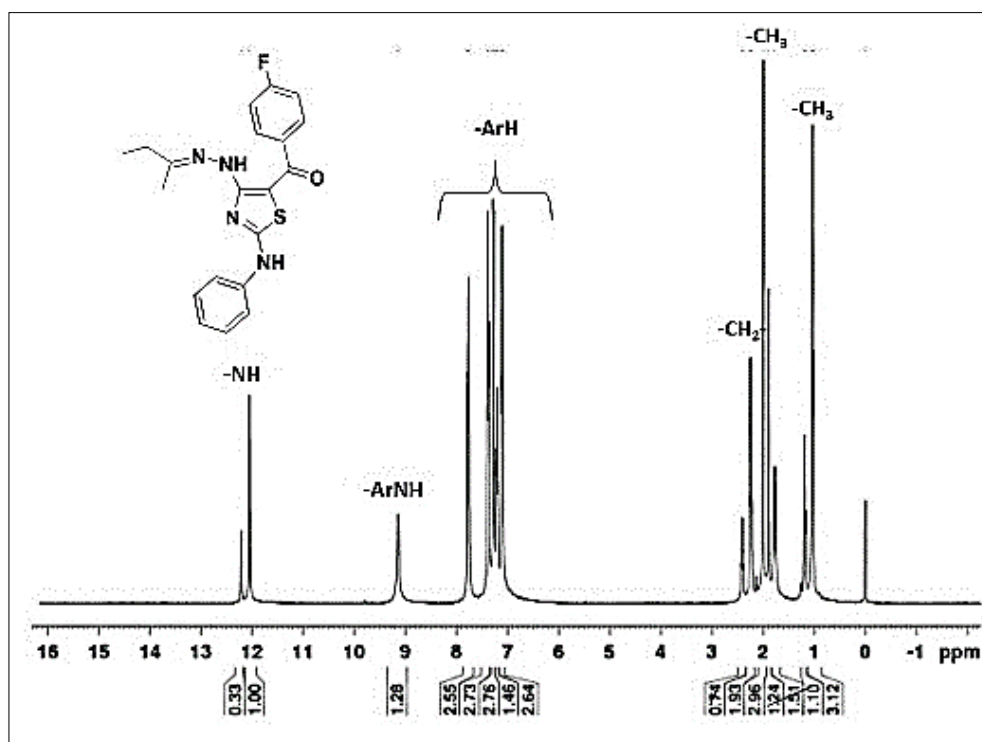


Figure 2.33. ¹H NMR spectrum of **IBHAT-3**

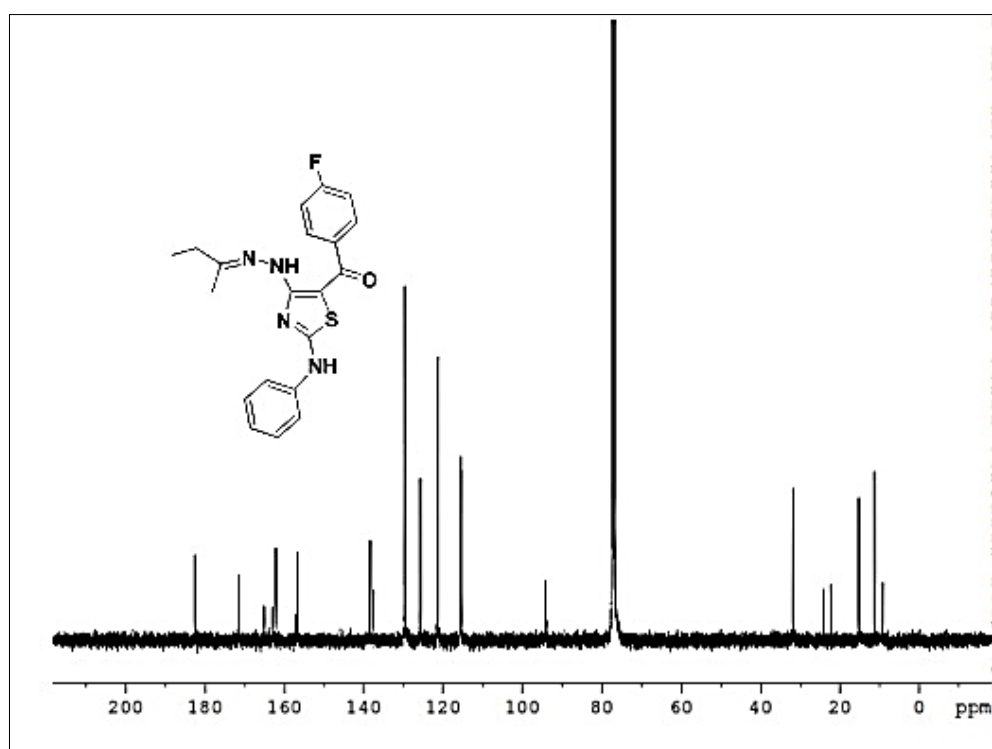
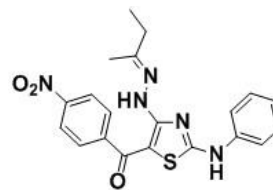


Figure 2.34. ¹³C NMR spectrum of **IBHAT-3**

2.4.5.12. 4-isobutylidenehydrazino-5-(4-nitrobenzoyl)-2-phenylaminothiazole (IBHAT-4)



The compound **IBHAT-4** was synthesized using 2-butanone (721mg, 10mmol), phenylisothiocyanate (1.216g, 9mmol), 4-nitrophenacylbromide (2.19g, 9mmol) following the general procedure. The crude product was purified by recrystallization using ethanol-acetone (1:1) mixture to obtain the product as red solid (80%). Mp. 212-213°C. IR (UATR) ν cm^{-1} : 3480 (N-H), 1599, 1531, 1567, 1378, 852 (aromatic); ^1H NMR (500MHz, CDCl_3): δ (ppm) 1.83 (s, 3H), 2.04 (m, 3H), 2.28 (dd, J = 7.5Hz, 1H), 2.44 (dd, J = 7.5Hz, 1H), 7.24-7.29 (m, 3ArH), 7.40-7.43 (m, 2ArH), 7.90 (d, J = 9Hz, 2ArH), 8.29 (d, J = 8.5Hz, 2ArH), 9.21 (s, 1ArNH), 12.12 (s, 1NH); ^{13}C NMR (125MHz, CDCl_3): δ (ppm) 11.2, 15.3, 17.2, 22.4, 24.2, 25.0, 32.0, 94.8, 121.7, 123.8, 126.2, 128.2, 129.7, 138.0, 146.7, 148.7, 153.6, 157.9, 162.7, 172.1 180.8; LC-MS ($\text{M}+1$) $^+$: m/z : 410.30.

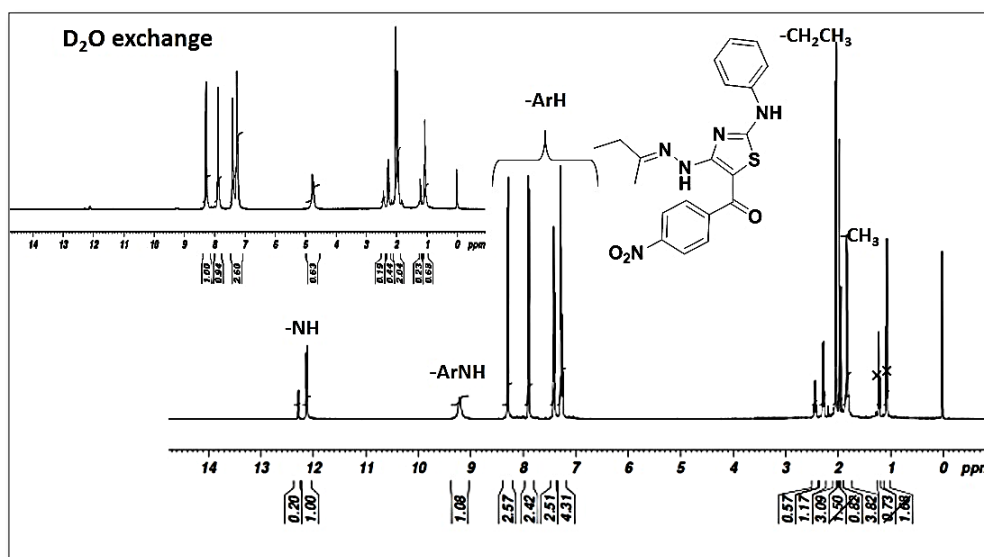


Figure 2.35. ^1H NMR spectrum of **IBHAT-4**

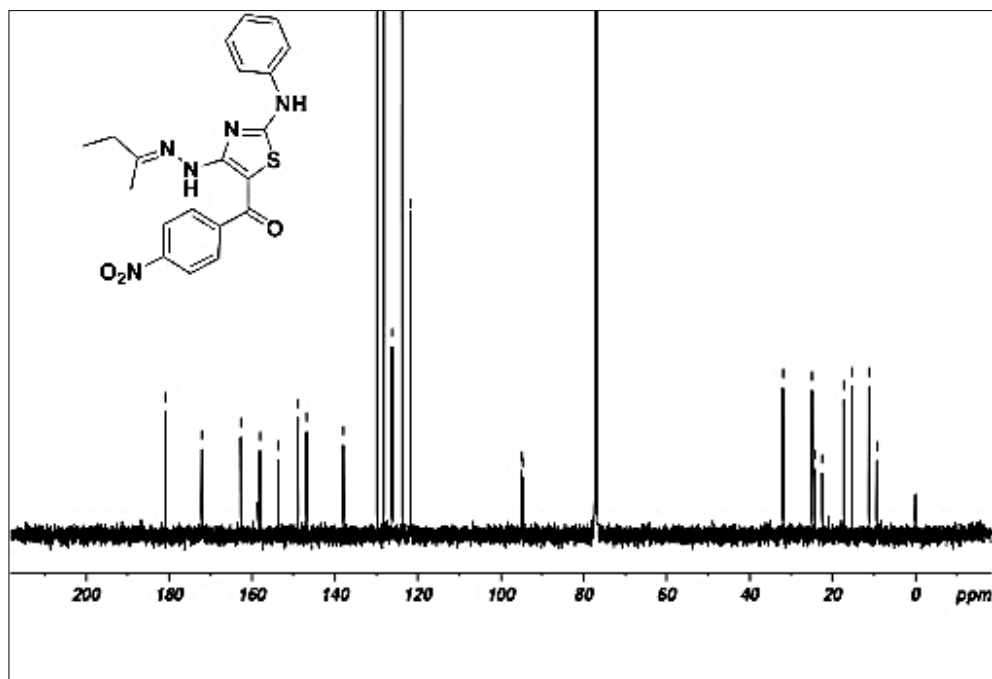
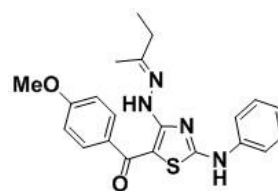


Figure 2.36. ^{13}C NMR spectrum of **IBHAT-4**

2.4.5.13. 4-isobutylidenehydrazino-5-(4-methoxybenzoyl)-2-phenylaminothiazole (IBHAT-5)



The above compound was synthesized using 2-butanone (721mg, 10mmol), phenylisothiocyanate (1.216g, 9mmol) and 4-methoxyphenacylbromide (2.06g, 9mmol) following the general procedure. The crude product was purified by recrystallization using ethanol-acetone (1:1) mixture to obtain the product as yellow solid (88%). Mp 229-230°C. IR (UATR) ν cm^{-1} : 3281, 3212 (N-H), 1601, 1557, 1299, 1252, 1070; ^1H NMR (500MHz, CDCl_3): δ (ppm) 1.05 (s, 2H), 1.21 (s, 1H), 1.79-1.91 (m, 2H), 2.02 (s, 2H), 2.26 (s, 1H), 3.86 (s, 3H, OCH_3), 6.95 (d, $J=7.5\text{Hz}$, 2ArH), 7.20 (m, 1ArH), 7.28-7.30 (m, 2ArH), 7.38-7.39 (m, 2ArH), 7.77-7.79 (m, 2ArH), 9.11 (s, 1ArNH), 12.08 (s, 1NH); ^{13}C NMR (125MHz, CDCl_3): δ (ppm) 11.3, 15.2, 31.9, 55.4, 113.7, 121.1, 125.5, 129.2, 129.6, 133.8, 138.5, 156.2, 161.6, 161.9, 170.9, 183.5; HR-MS calcd. for $(\text{M}+\text{H})^+$: 395.1542; Found: 395.1560.

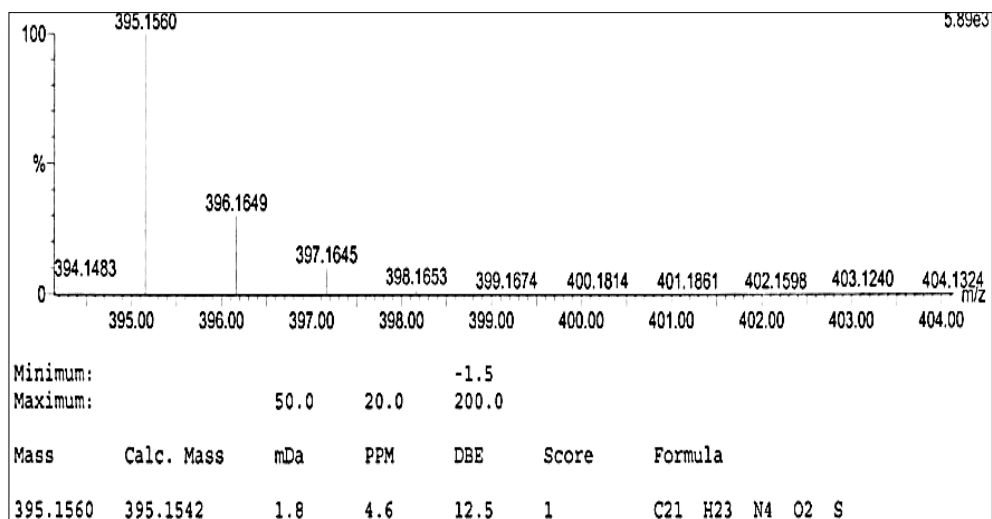


Figure 2.37. HR-MS spectrum of **IBHAT-5**

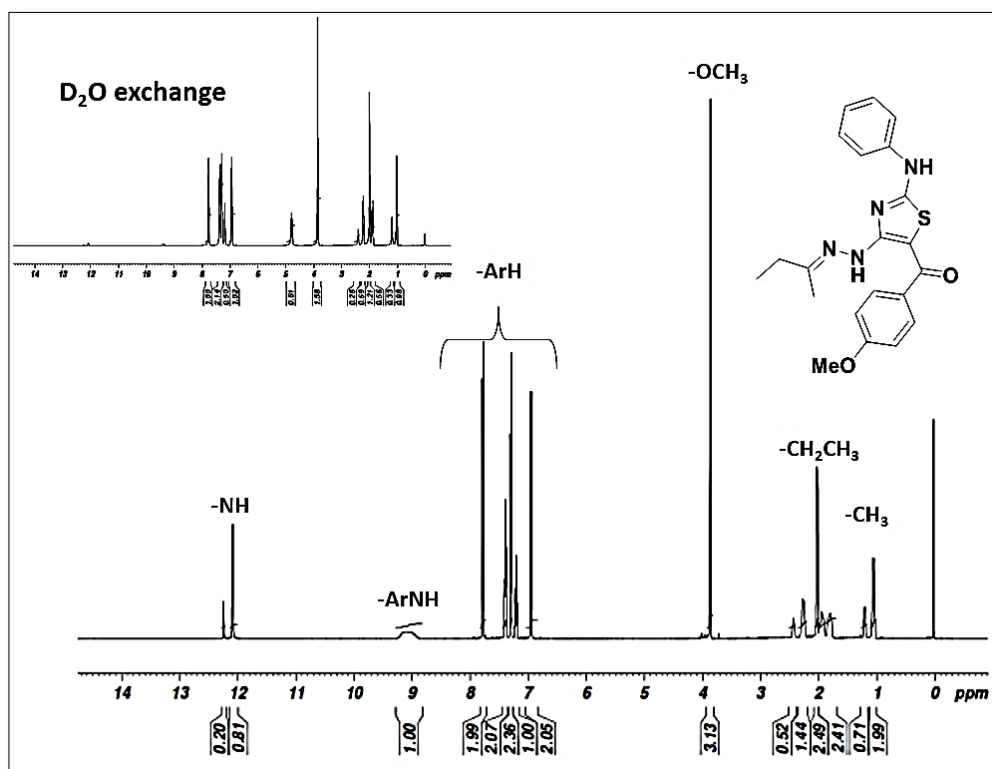


Figure 2.38. ¹H NMR spectrum of **IBHAT-5**

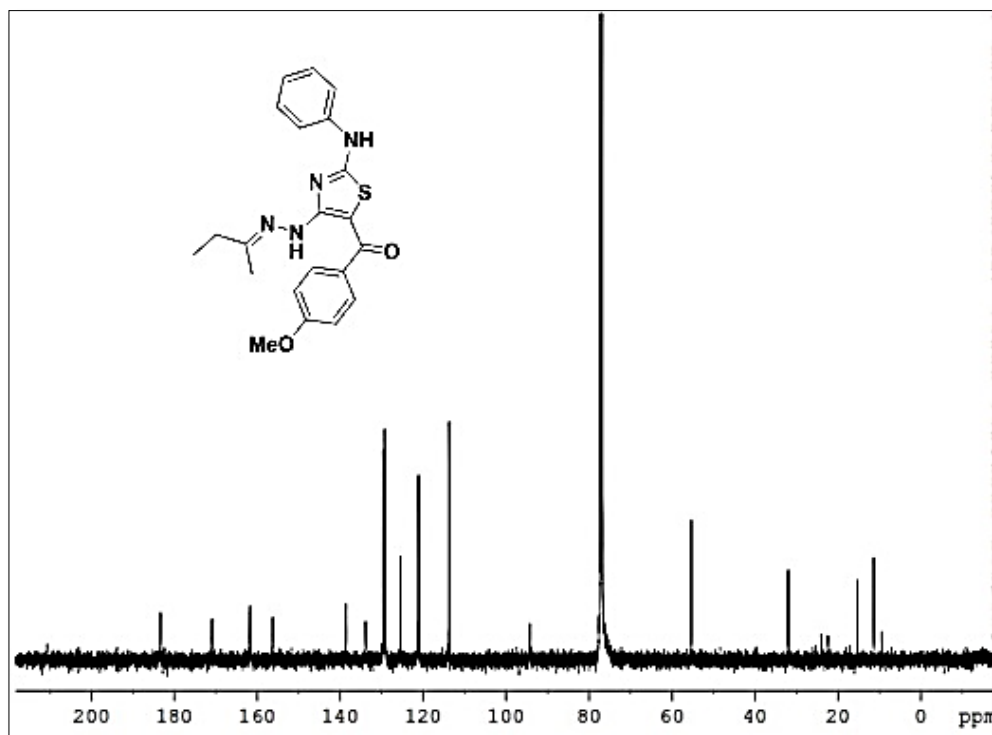
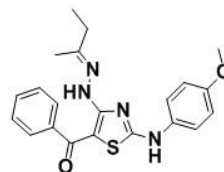


Figure 2.39. ^{13}C NMR spectrum of **IBHAT-5**

2.4.5.14. 5-benzoyl-4-isobutylidenehydrazino-2-(4-methoxyphenylamino)thiazole (**IBHAT-6**)



The compound **IBHAT-6** was synthesized using 2-butanone (721mg, 10mmol), 4-methoxyphenyl isothiocyanate (1.48g, 9mmol) and phenacylbromide (1.79g, 9mmol) following the general procedure. The crude product was purified by recrystallization using ethanol-acetone (1:1) mixture to obtain the product as yellow solid (80%). Mp 217-218°C. IR (UATR) ν cm^{-1} : 3268, 3201 (N-H), 2870 (aliphatic), 1698 (C=O), 836, 729 (aromatic); ^1H NMR (500MHz CDCl_3): δ (ppm) 1.09-1.23 (m, 2H), 2.01-2.05 (m, 1H), 2.06 (s, 3H), 2.33-2.36 (m, 1H), 2.44-2.46 (m, 1H), 3.81 (s, 3H), 6.89-6.93 (m, 2ArH), 7.20-7.22 (m, 2ArH), 7.36-7.45 (m, 3ArH), 7.71 (d, J = 7.0Hz, 2ArH), 8.32 (s, 1ArNH), 12.12 (s, 1NH); ^{13}C NMR (125MHz, CDCl_3): δ (ppm) 17.2, 22.3, 24.1, 31.9, 55.5, 114.7, 124.7, 127.2, 128.4, 130.5, 131.1, 141.4, 152.1, 156.7, 162.5, 173.4, 183.7; LC-MS ($\text{M}-1$) $^+$: m/z : 393.30.

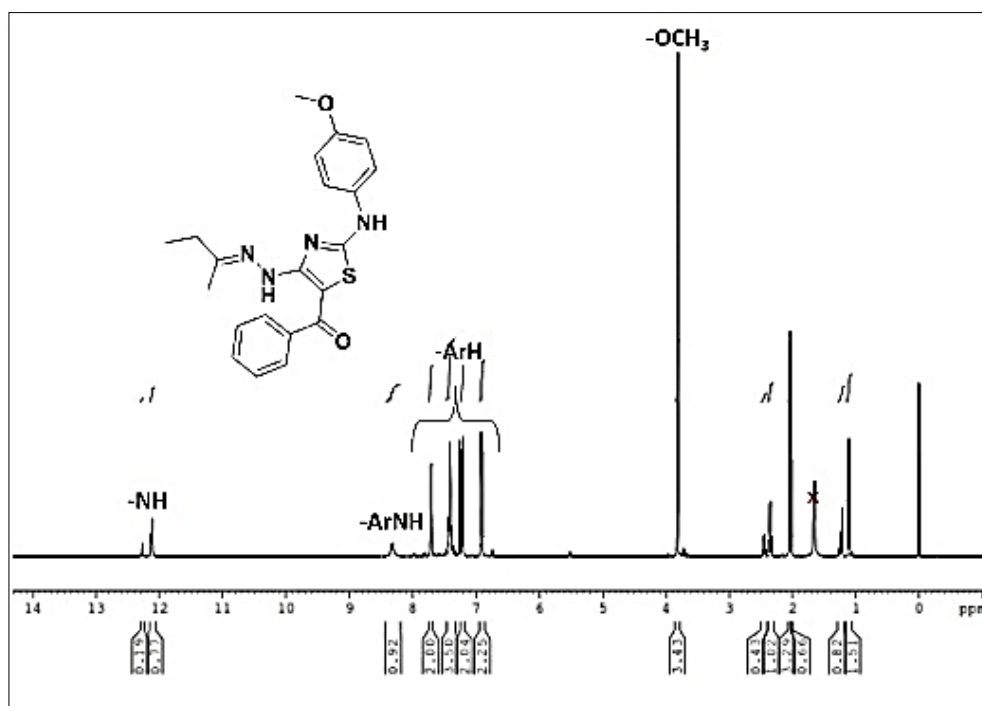


Figure 2.40. ¹H NMR spectrum of **IBHAT-6**

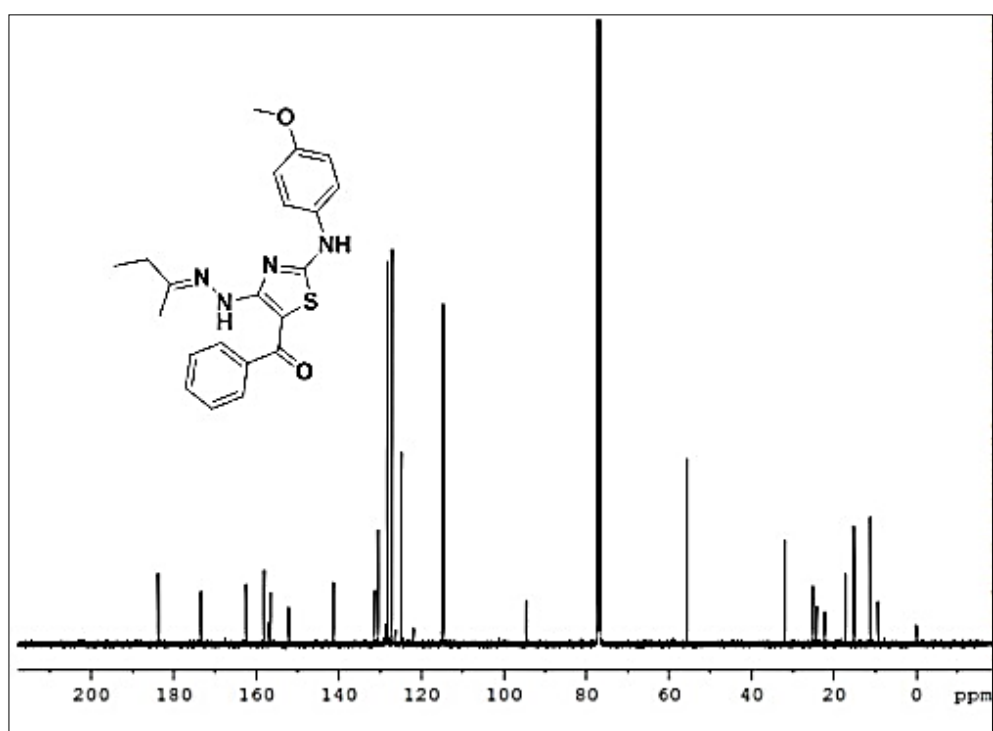
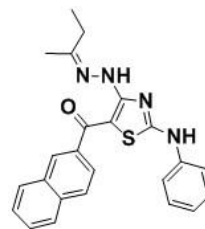


Figure 2.41. ¹³C NMR spectrum of **IBHAT-6**

2.4.5.15. 4-isobutylidenehydrazino-5-(naphth-2-oyl)-2-phenylaminothiazole (IBHAT-7)



IBHAT-7 was synthesized using 2-butanone (721mg, 10mmol), phenylisothiocyanate (1.21g, 9mmol) and 2-bromoacetylnaphthalene (2.24g, 9mmol) following the general procedure. The crude product was purified by recrystallization using ethanol-acetone (1:1) mixture to obtain the product as yellow solid (90%). Mp 237-238°C. IR (UATR) ν cm^{-1} : 3282 (N-H), 3098, 3052 (aromatic) 1629 (C=O), 832, 759 (aromatic); ^1H NMR (500 MHz, CDCl_3): δ (ppm) 1.13 (t, J = 7.5Hz, 3H), 2.08 (s, 3H), 2.39 (dd, J = 7.5Hz, 2H), 7.36-7.39 (m, 2ArH), 7.51-7.57 (m, 3ArH), 7.83-7.88 (m, 3ArH), 7.89-7.92 (m, 3ArH), 8.53 (s, 1ArNH), 8.24 (s, 1ArH), 12.13 (s, 1NH); ^{13}C NMR (125 MHz, CDCl_3): δ (ppm) 11.4, 15.2, 32.1, 95.1, 120.9, 124.3, 125.6, 126.6, 127.4, 127.8, 128.4, 128.9, 129.7, 132.6, 134.4, 138.3, 138.7, 156.8, 161.9, 171.2, 184.1; LC-MS (M) $^+$: m/z : 414.10.

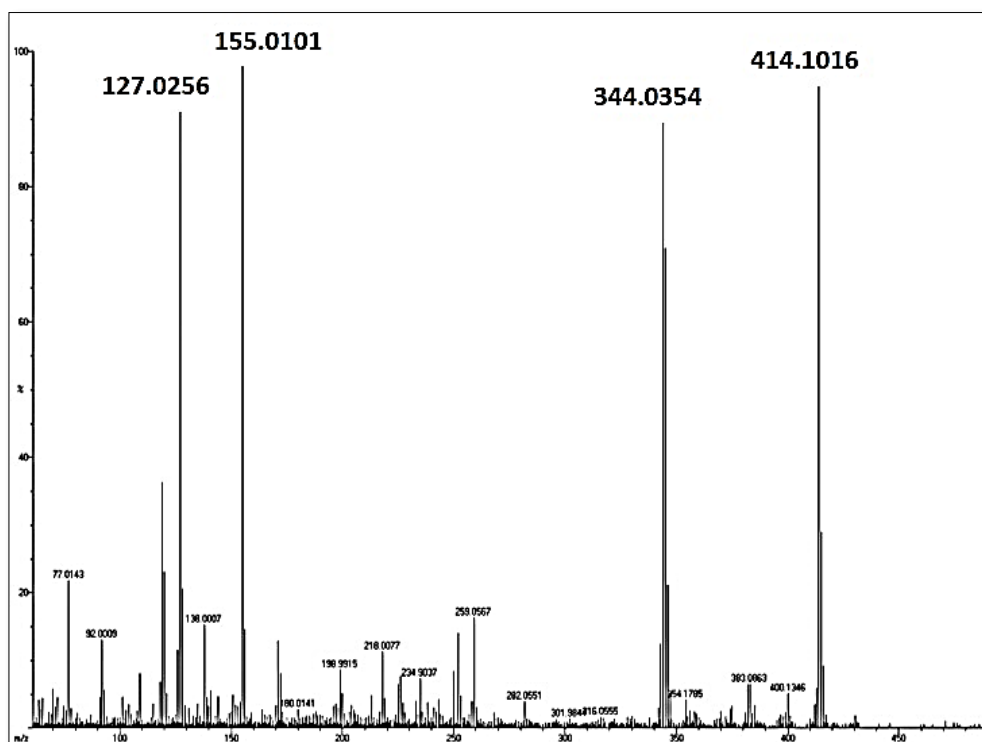


Figure 2.42. LC-MS spectrum of **IBHAT-7**

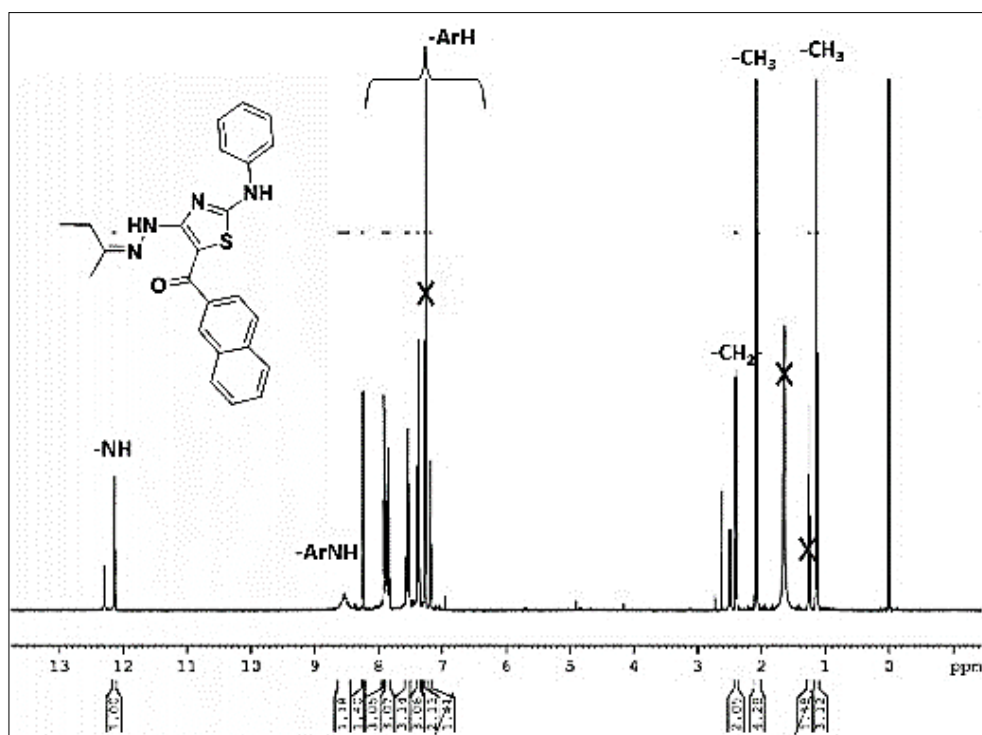


Figure 2.43. ¹H NMR spectrum of **IBHAT-7**

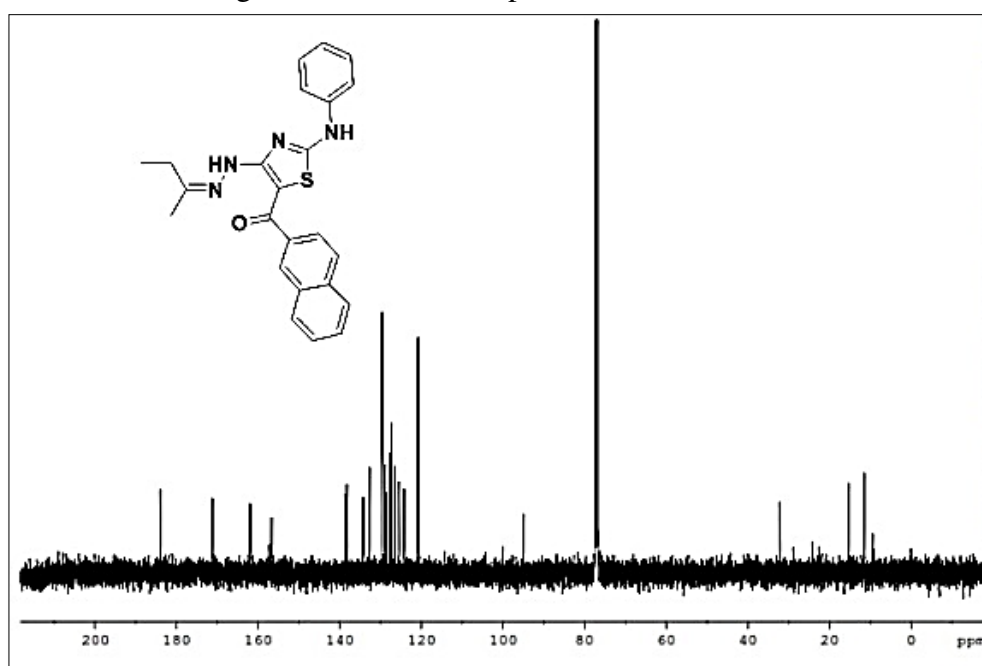
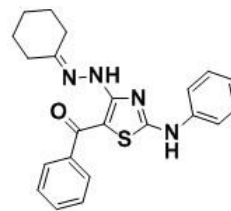


Figure 2.44. ¹³C NMR spectrum of **IBHAT-7**

2.4.5.16. 5-(benzoyl)-4-cyclohexylidenehydrazino-2-phenylaminothiazole (CyHAT-1)



The above compound was synthesized using cyclohexanone (981mg, 10mmol), phenylisothiocyanate (1.216g, 9mmol) and phenacylbromide (1.79g, 9mmol) following the general procedure. The crude product was purified by recrystallization using ethanol-acetone (1:1) mixture to obtain the product as yellow solid (70%). Mp. 205-206°C. IR (UATR) ν cm^{-1} : 3281, 3212 (N-H), 1601, 1557, 1253, 1070 ; ^1H NMR (500MHz, CDCl_3): δ (ppm) 1.53-1.67 (m, 4H), 1.68-1.81 (m, 2H), 2.21-2.41 (m, 2H), 2.42-2.62 (m, 2H), 7.18-7.21 (m, 1ArH), 7.29-7.31 (m, 2ArH), 7.36-7.39 (m, 2ArH), 7.42-7.47 (m, 3ArH), 7.76-7.78 (m, 2ArH), 8.74 (s, 1ArNH), 12.29 (s, 1NH); ^{13}C NMR (125MHz, CDCl_3): δ (ppm) 25.8, 26.8, 27.1, 29.6, 35.2, 94.4, 121.1, 125.6, 127.2, 128.4, 129.7, 130.7, 138.4, 141.3, 158.2, 162.7, 171.3, 184.0; ESI-MS ($\text{M}+\text{H}^+$): 391.16.

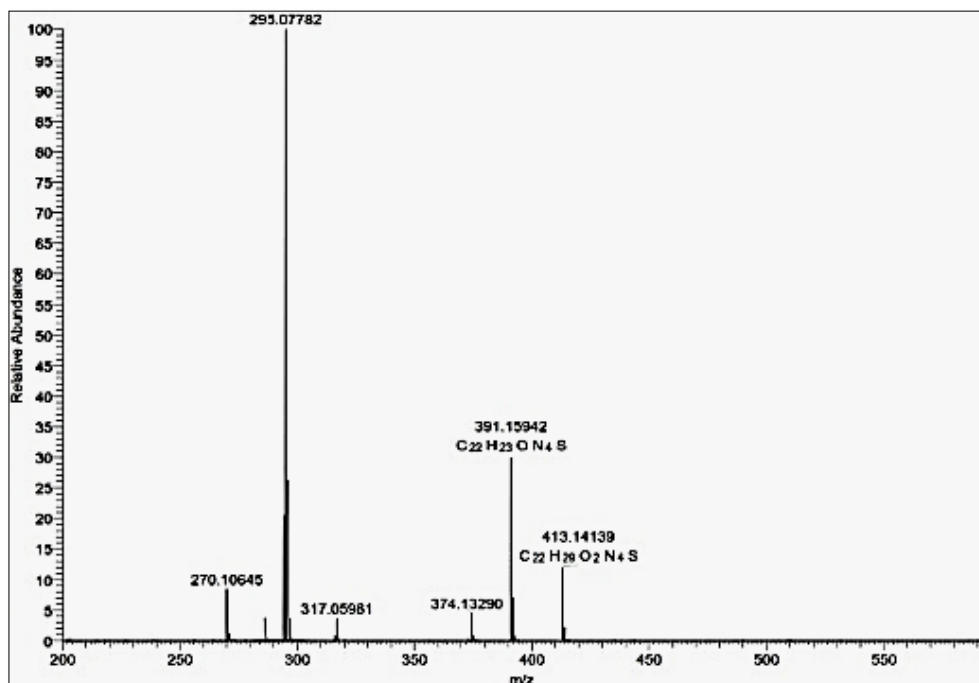


Figure 2.45. ESI-MS spectrum of **CyHAT-1**

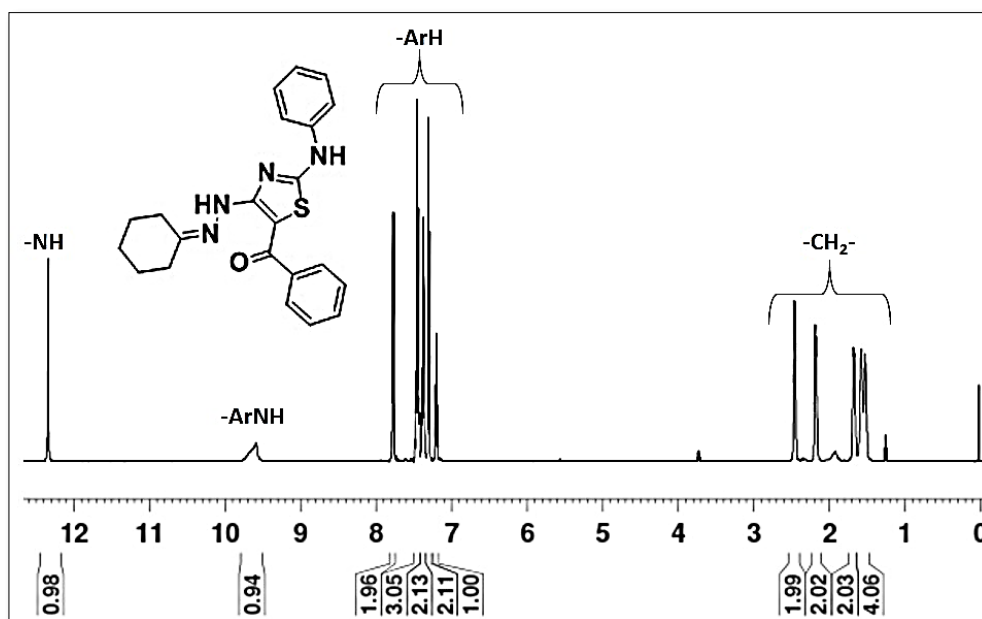


Figure 2.46. ¹H NMR spectrum of CyHAT-1

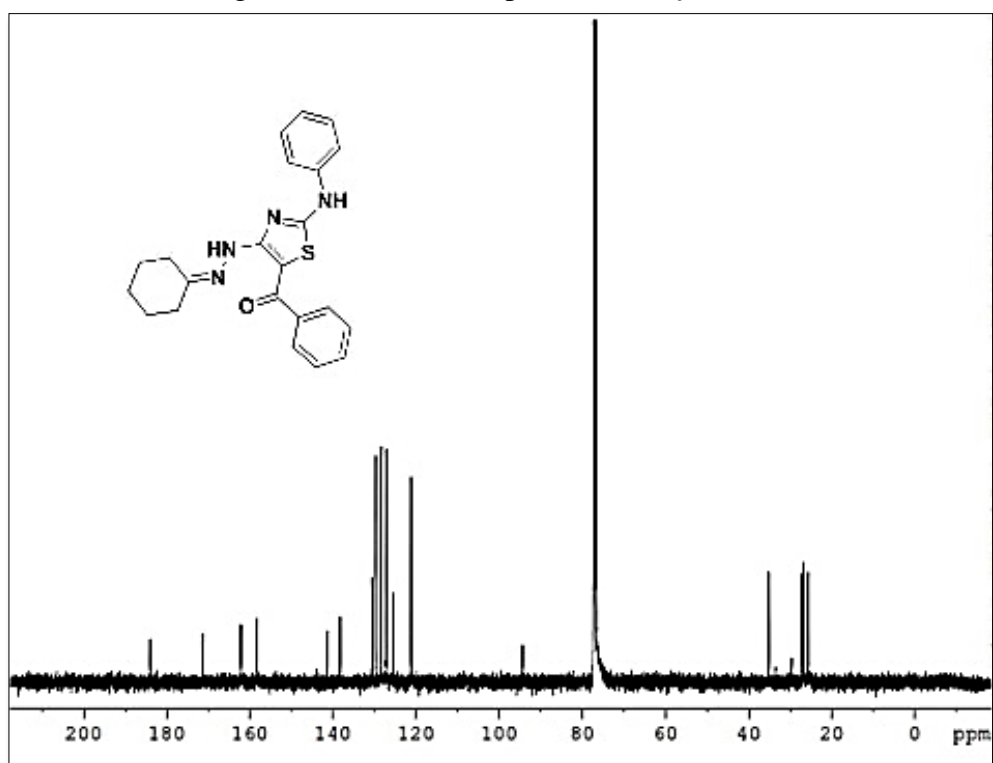
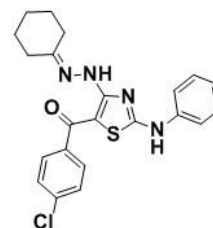


Figure 2.47. ¹³C NMR spectrum of CyHAT-1

2.4.5.17. 5-(4-chlorobenzoyl)-4-cyclohexylidenehydrazino-2-phenylaminothiazole (CyHAT-2)



CyHAT-2 was synthesized using cyclohexanone (981mg, 10mmol), phenylisothiocyanate (1.216g, 9mmol) and 4-chlorophenacylbromide (2.10g, 9mmol) following the general procedure. The crude product was purified by recrystallization using ethanol-acetone (1:1) mixture to obtain the product as yellow solid (70%). Mp. 231-232°C. IR (UATR) ν cm^{-1} : 3293, 3216 (N-H), 1625, 1540, 1076; ^1H NMR (500MHz, CDCl_3): δ (ppm) 1.62-1.70 (m, 6H), 2.17-2.43 (m, 2H), 2.47-2.49 (m, 2H), 7.22-7.27 (m, 2ArH), 7.38-7.41 (m, 5ArH), 7.68-7.70 (m, 2ArH), 8.81 (s, 1ArNH), 12.28 (s, 1NH); ^{13}C NMR (125MHz, CDCl_3): δ (ppm) 25.5, 25.8, 26.8, 27.1, 35.1, 94.2, 121.3, 125.8, 128.6, 128.7, 129.7, 136.7, 138.2, 139.6, 158.6, 162.4, 171.4, 182.3; ESI-MS ($\text{M}+\text{H}$) $^+$: 425.12.

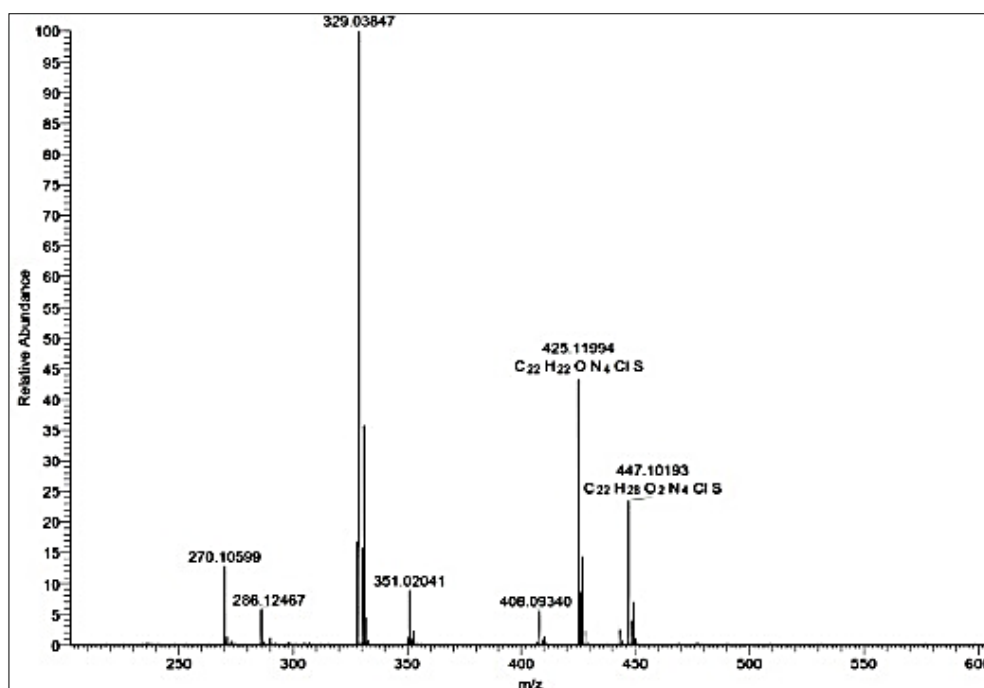


Figure 2.48. ESI-MS spectrum of **CyHAT-2**

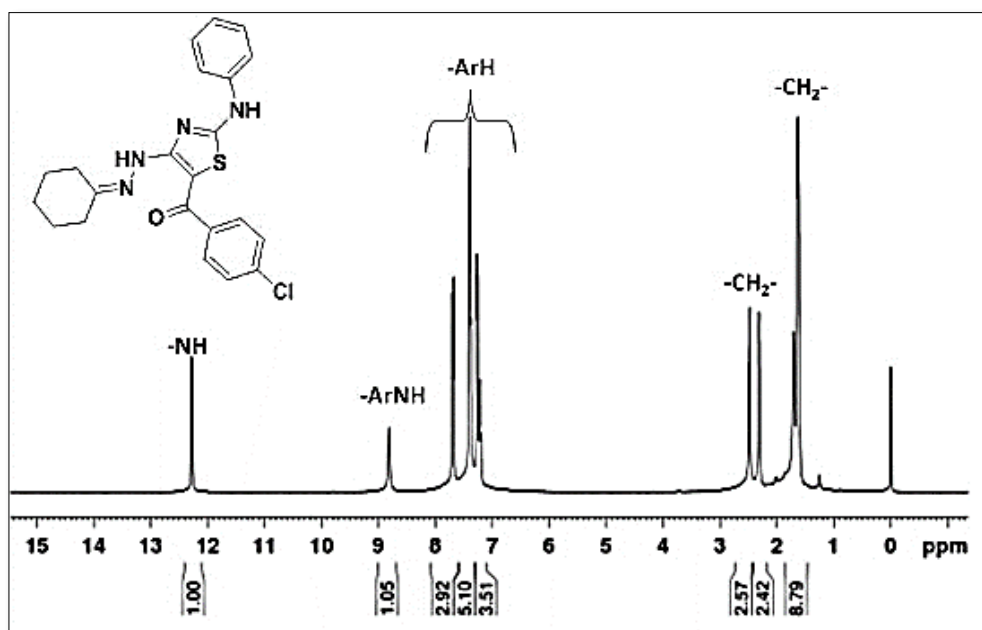


Figure 2.49. ¹H NMR spectrum of CyHAT-2

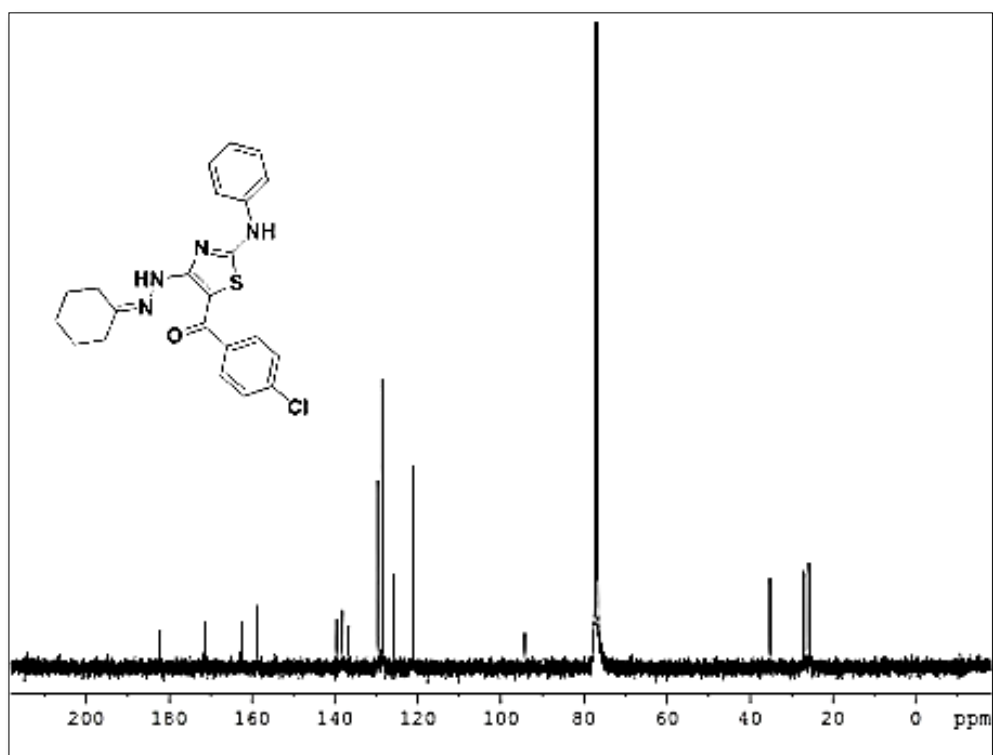
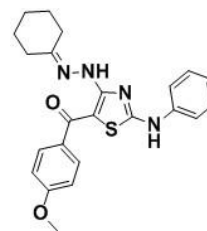


Figure 2.50. ¹³C NMR spectrum of CyHAT-2

2.4.5.18. 4-cyclohexylidenehydrazino-5-(4-methoxybenzoyl)-2-phenylaminothiazole (CyHAT-3)



The compound was synthesized using cyclohexanone (981mg, 10mmol), phenylisothiocyanate (1.21g, 9mmol) and 4-methoxyphenacylbromide (2.06g, 9mmol) following the general procedure. The crude product was purified by recrystallization using ethanol-acetone (1:1) mixture to obtain the product as yellow solid (63%). Mp 224-225°C. IR (UATR) ν cm^{-1} : 3296 (N-H), 1629, 1545, 1244, 1058; ^1H NMR (500MHz, CDCl_3): δ (ppm) 0.69-1.75 (m, 4H), 2.40-2.43 (m, 2H), 2.51-2.53 (m, 2H), 3.85 (s, 3H), 6.92-6.94 (m, 2ArH), 7.19-7.22 (m, 1ArH), 7.27-7.28 (m, 2ArH), 7.38-7.42 (m, 2ArH), 7.75-7.77 (m, 2ArH), 8.38 (s, 1ArNH), 12.29 (s, 1NH); ^{13}C NMR (125MHz, CDCl_3): δ (ppm) 9.3, 11.3, 15.2, 17.2, 24.1, 31.9, 55.4, 113.7, 121.1, 125.5, 129.2, 129.6, 133.8, 138.5, 151.9, 156.2, 161.9, 170.9, 183.4; ESI-MS ($\text{M}+\text{H}^+$): 421.16; Anal. calcd. for $\text{C}_{23}\text{H}_{24}\text{N}_4\text{O}_2\text{S}$ (420.16): C, 65.69; H, 5.76; N, 13.33%. Found: C, 66.18; H, 5.91; N, 13.55%.

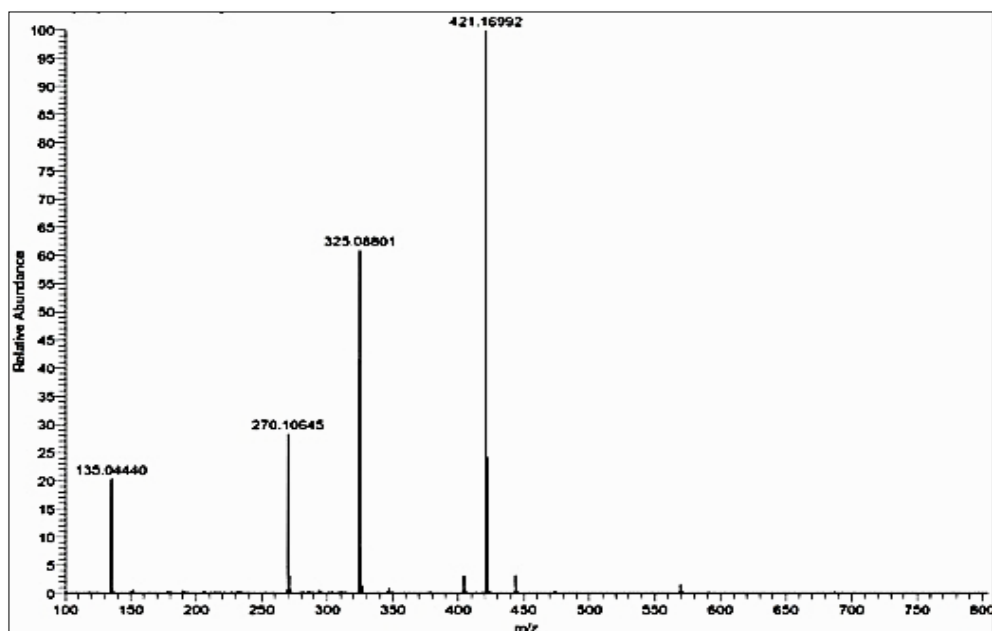


Figure 2.51. ESI-MS spectrum of **CyHAT-3**

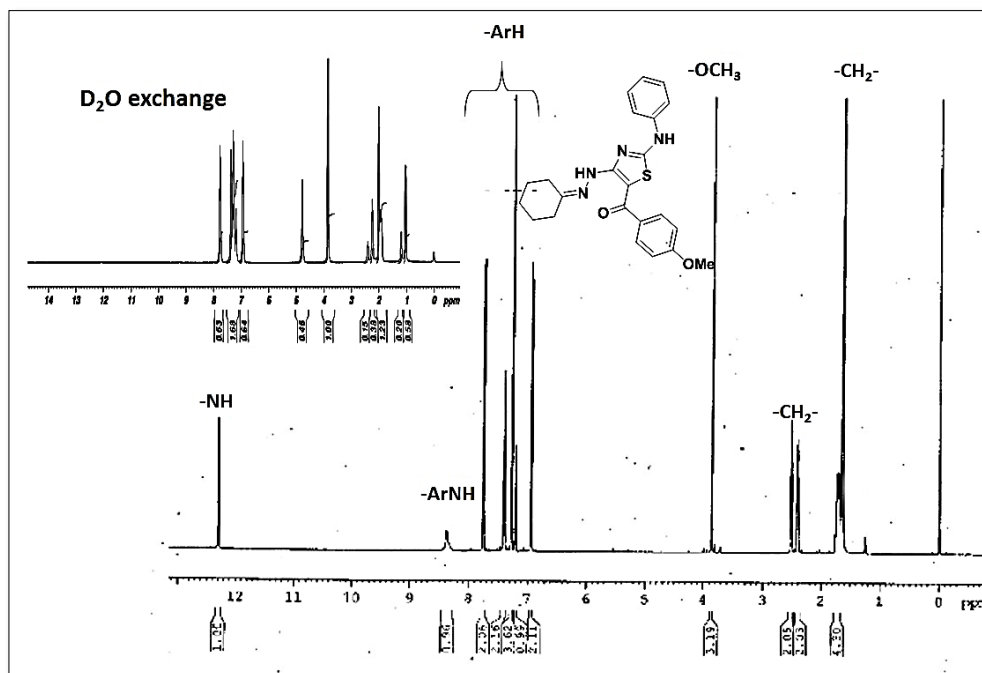


Figure 2.52. ¹H NMR spectrum of CyHAT-3

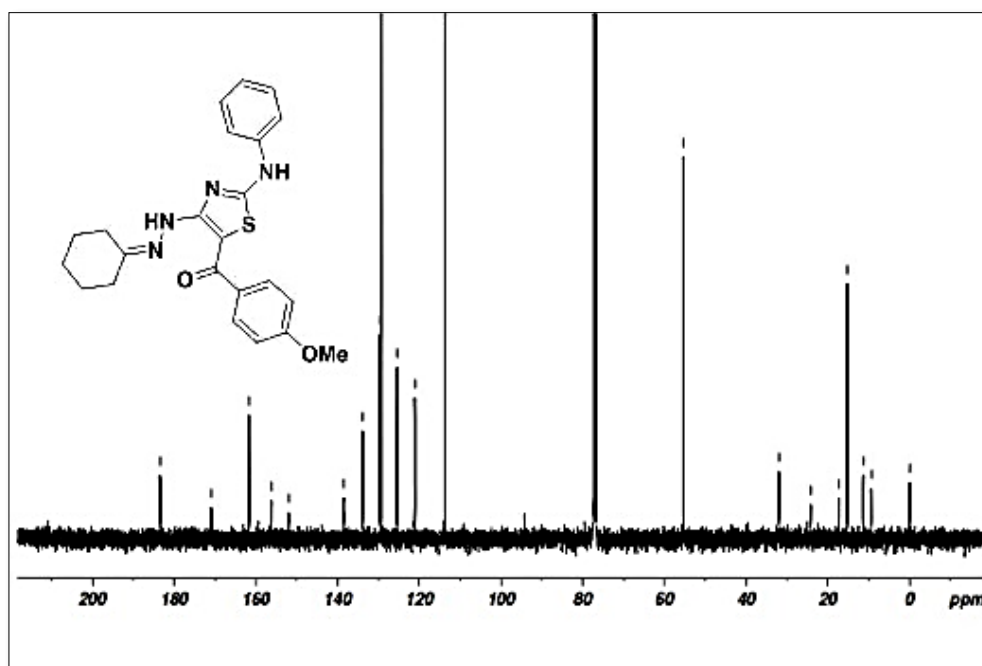
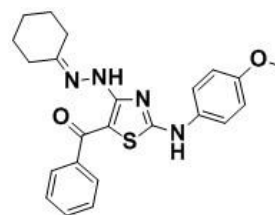


Figure 2.53. ¹³C NMR spectrum of CyHAT-3

2.4.5.19. 4-cyclohexylidenehydrazino-5-(4-methoxybenzoyl)-2-phenylaminothiazole (CyHAT-4)



Compound was synthesized using cyclohexanone (981mg, 10mmol), 4-methoxyphenylisothiocyanate (1.48g, 9mmol) and phenacylbromide (1.79g, 9mmol) following the general procedure. The crude product was purified by recrystallization using ethanol-acetone (1:1) mixture to obtain the product as yellow solid (80%). Mp. 246-247°C. IR (UATR) ν cm^{-1} : 3276, 3198 (N-H), 2938, 2858 (aliphatic), 1678 (C=O), 831, 731 (aromatic); ^1H NMR (500MHz, CDCl_3): δ (ppm) 1.63-1.72 (m, 6H), 2.34-2.38 (m, 2H), 2.49-2.52 (m, 2H), 3.81 (s, 3H), 6.89-6.92 (m, 2ArH), 7.20-7.22 (m, 2ArH), 7.38-7.47 (m, 3ArH), 7.70-7.72 (m, 2ArH), 8.36 (s, 1ArNH), 12.34 (s, 1NH); ^{13}C NMR (125MHz, CDCl_3): δ (ppm) 25.6, 25.9, 26.9, 27.2, 35.2, 55.5, 94.6, 100.0, 114.9, 124.7, 127.2, 128.4, 130.5, 131.2, 141.4, 158.3, 162.8, 173.4, 183.7; LC-MS ($\text{M}+1$) $^+$: m/z : 421.12.

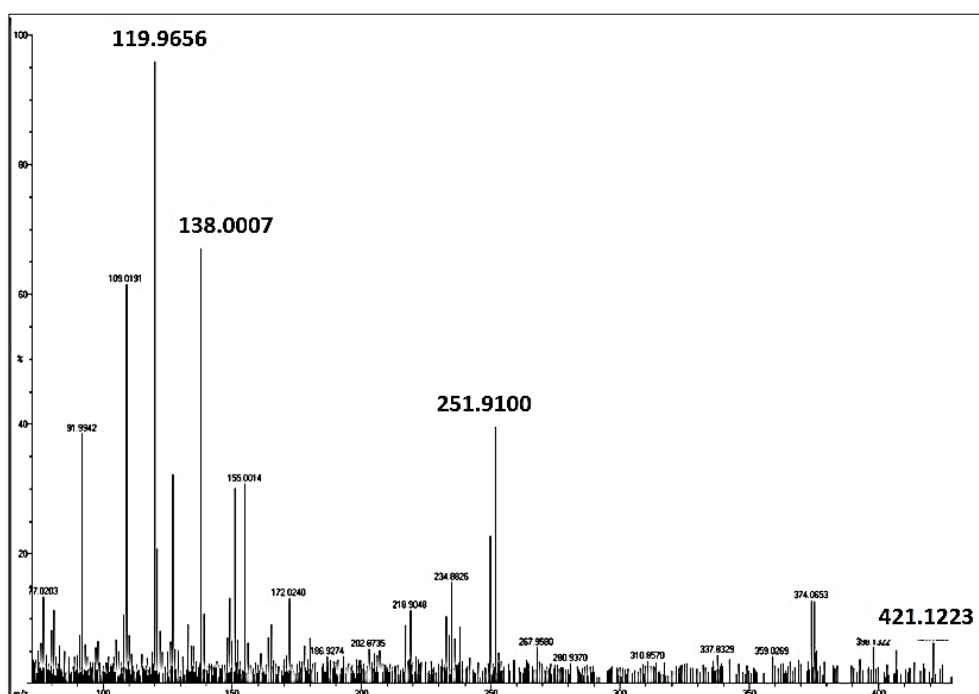


Figure 2.54. ESI-MS spectrum of CyHAT-4

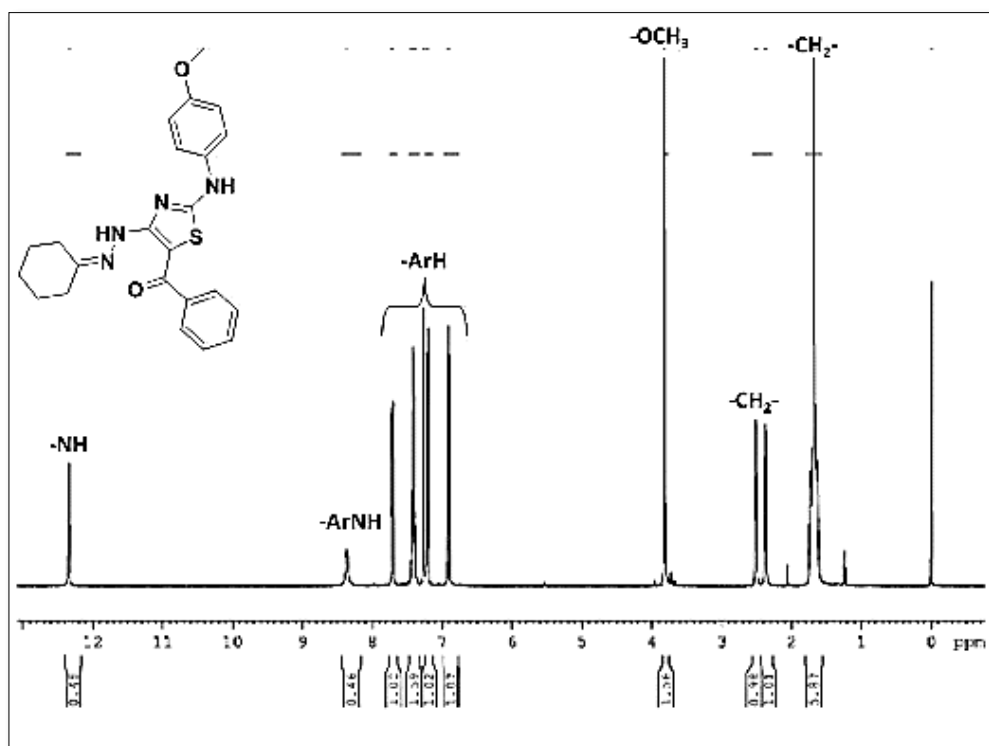


Figure 2.55. ¹H NMR spectrum of CyHAT-4

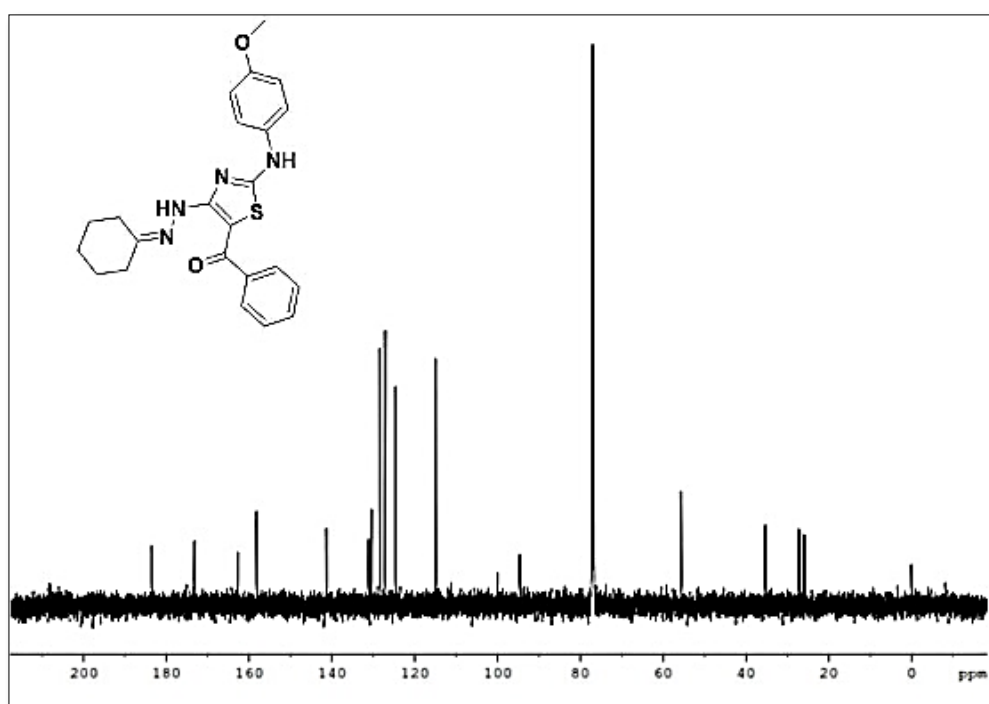
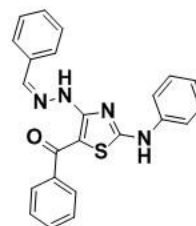


Figure 2.56. ¹³C NMR spectrum of CyHAT-4

2.4.5.20. 5-benzoyl-4-benzylidenehydrazino-2-phenylaminothiazole (BzHAT-1)



The compound **BzHAT-1** was synthesized using benzaldehyde (1.06g, 10mmol), phenylisothiocyanate (1.216g, 9mmol) and phenacylbromide (1.79g, 9mmol) following the general procedure. The crude product was purified by recrystallization using ethanol-acetone (1:1) mixture to obtain the product as yellow solid (90%). Mp 190-192°C. IR (UATR) ν cm^{-1} : 3480-2870, 1697, 1601, 1515, 1249, 751; ^1H NMR (500MHz, CDCl_3): δ (ppm) 7.12-7.15 (m, 1ArH), 7.27-7.35 (m, 7ArH), 7.43-7.49 (m, 3ArH), 7.65-7.67 (m, 2ArH), 7.75-7.77 (m, 2ArH), 7.97-8.01 (s, 1H), 9.11 (s, 1ArNH), 12.37 (s, 1NH); ^{13}C NMR (125MHz, CDCl_3): δ (ppm) 94.6, 125.6, 127.3, 127.4, 128.4, 128.5, 129.4, 129.7, 130.8, 133.8, 138.4, 141.2, 145.5, 161.3, 171.6, 184.5; LC-MS (M^+): m/z : 398.40.

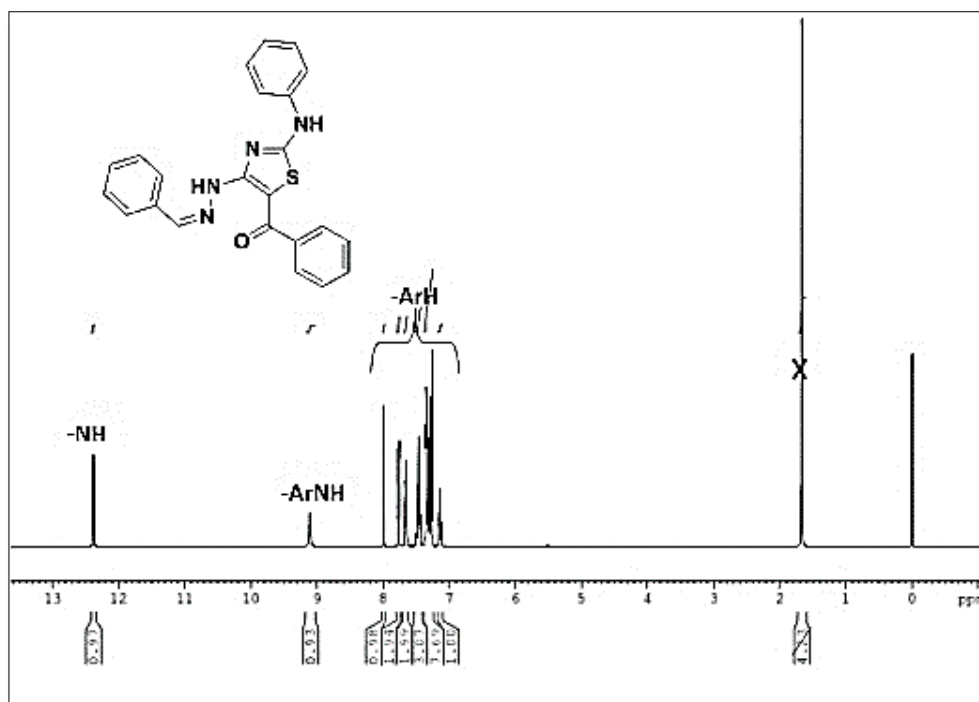


Figure 2.57. ^1H NMR spectrum of **BzHAT-1**

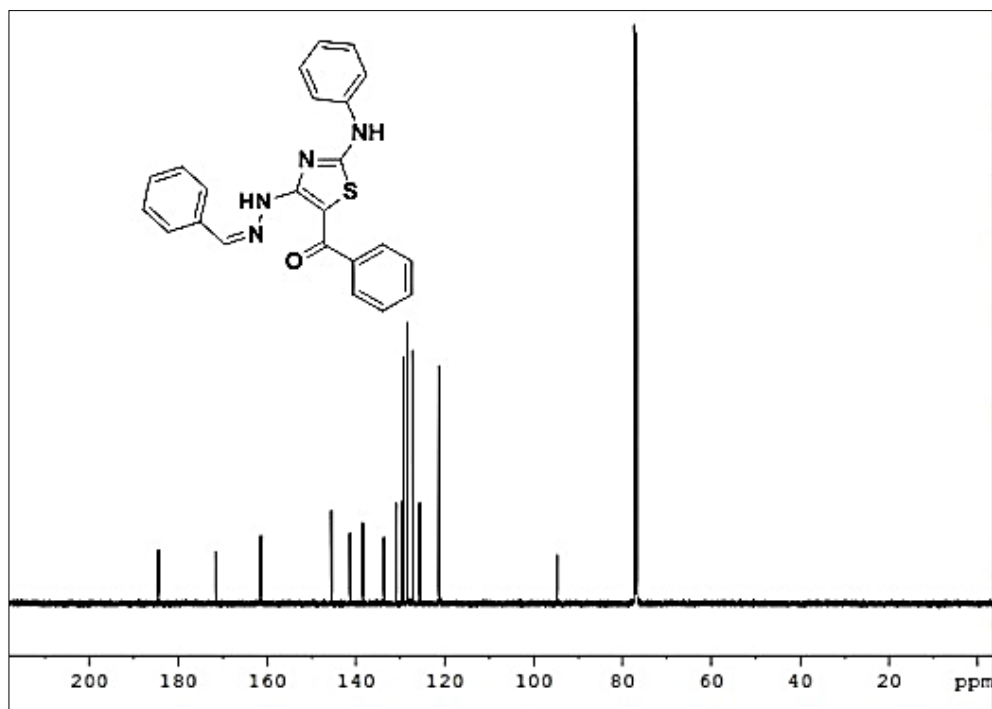
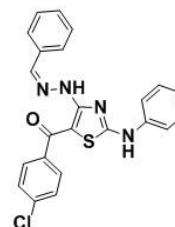


Figure 2.58. ^{13}C NMR spectrum of **BzHAT-1**

2.4.5.21. 4-benzylidenehydrazino-5-(4-chlorobenzoyl)-2-phenylaminothiazole (**BzHAT-2**)



The compound **BzHAT-2** was synthesized using benzaldehyde (1.06g, 10mmol), phenylisothiocyanate (1.216g, 9mmol) and 4-chlorophenacylbromide (2.10g, 9mmol) following the general procedure. The crude product was purified by recrystallization using ethanol-acetone (1:1) mixture to obtain the product as yellow solid (90%). Mp 163-164°C. IR (UATR) ν cm^{-1} : 3450, 3336 (N-H), 1737 (C=O), 840, 753 (aromatic); ^1H NMR (500MHz, CDCl_3): δ (ppm) 6.85-7.16 (m, 2ArH), 7.17-7.50 (m, 9ArH), 7.52-7.66 (m, 2ArH), 7.65-7.67 (m, 2ArH), 7.91 (s, 1H), 9.78 (s, 1ArNH), 12.35 (s, 1NH); ^{13}C NMR (125MHz, CDCl_3): δ (ppm) 94.4, 121.5, 125.9, 127.4, 128.5, 128.7, 128.8, 129.4, 129.9, 133.7, 136.9, 138.2,

139.5, 145.8, 161.5, 171.6, 183.0; Anal. calcd for $C_{23}H_{17}ClN_4OS$ (432.9): C, 57.52; H, 4.39; N, 12.20%. Found: C, 57.36; H, 4.19; N, 12.05%.

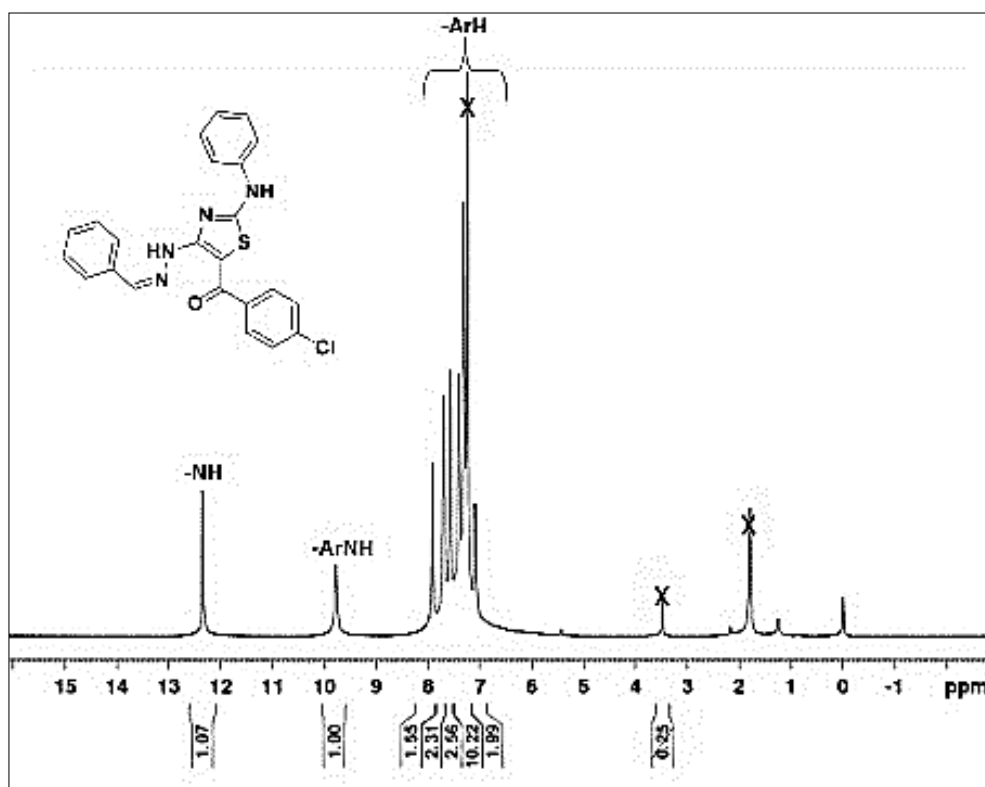


Figure 2.59. 1H NMR spectrum of **BzHAT-2**

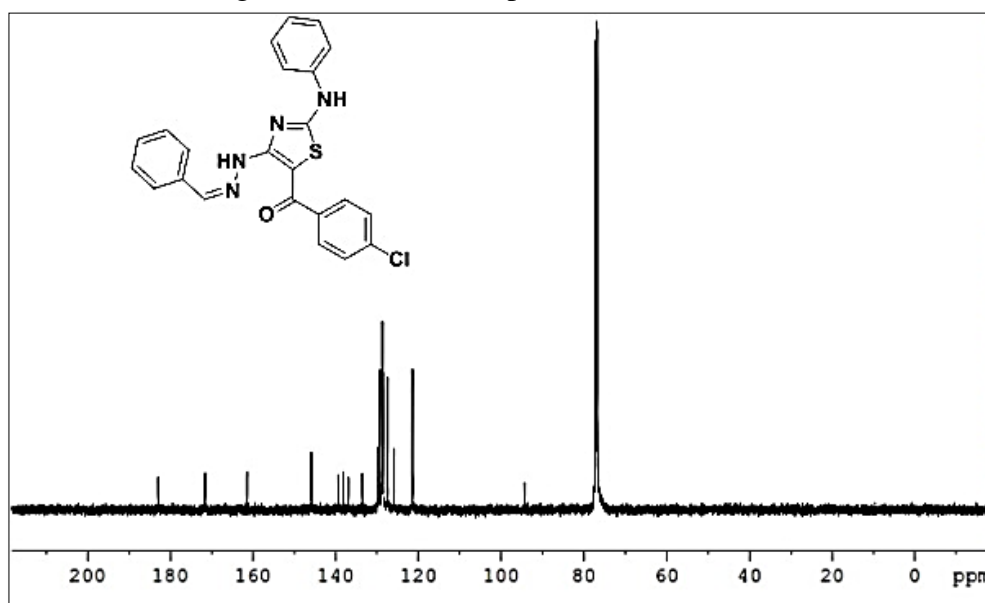
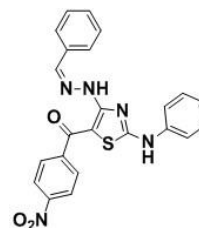


Figure 2.60. ^{13}C NMR spectrum of **BzHAT-2**

2.4.5.22. 4-benzylidenehydrazino-5-(4-nitrobenzoyl)-2-phenylaminothiazole (BzHAT-3)



The compound was synthesized using benzaldehyde (1.06g, 10mmol), phenylisothiocyanate (1.21g, 9mmol) and 4-nitrophenacylbromide (2.19g, 9mmol) following the general procedure. The crude product was purified by recrystallization using ethanol-acetone (1:1) mixture to obtain the product as yellow solid (85%). Mp 126-127°C; IR (UATR) ν cm^{-1} : 3214 (N-H), 3033 (aromatic), 1735 (C=O), 823, 729 (aromatic); ^1H NMR (500MHz, CDCl_3): δ (ppm) 7.21-7.24 (s, 1ArH), 7.27-7.29 (m, 2ArH), 7.37-7.40 (m, 5ArH), 7.72-7.74 (m, 2ArH), 7.88-7.90 (m, 2ArH), 8.07 (s, 1CH), 8.29-8.31 (m, 2ArH), 8.66 (s, 1ArNH), 12.36 (s, 1NH); ^{13}C NMR (125MHz, CDCl_3): δ (ppm) 94.9, 121.6, 123.9, 126.6, 127.5, 128.3, 128.6, 129.7, 130.2, 133.5, 137.9, 146.6, 146.7, 148.9, 162.0, 171.9, 181.4 ; ESI-MS $(\text{M}+\text{H})^+$: 444.11.

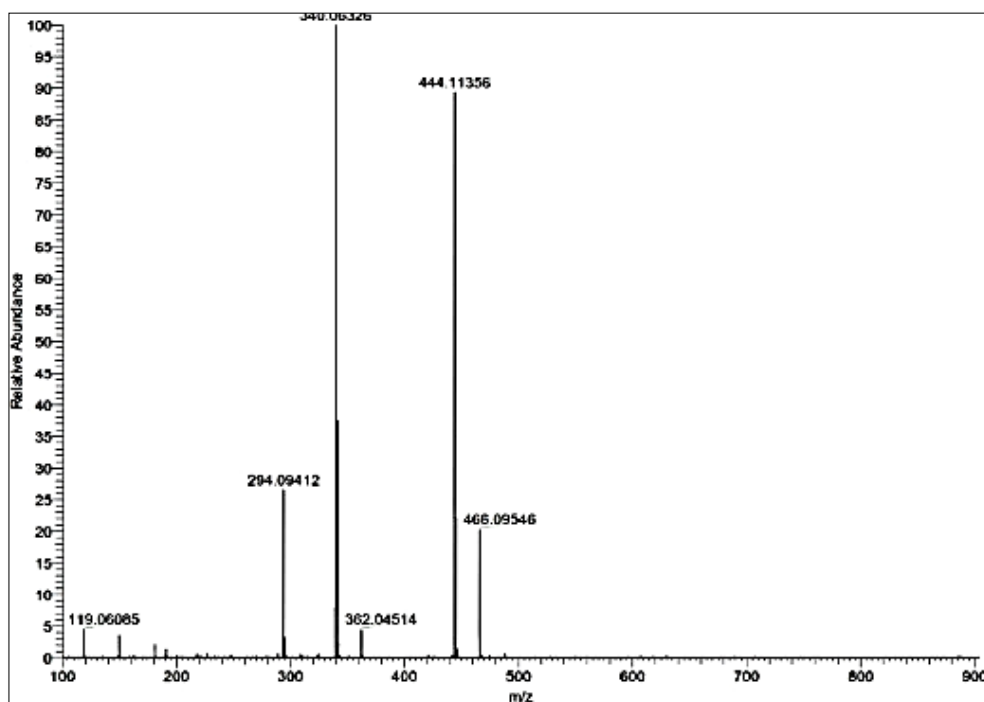
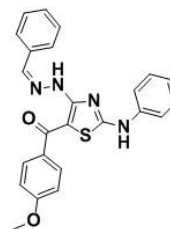


Figure 2.61. ESI-MS spectrum of **BzHAT-3**

2.4.5.23. 4-benzylidenehydrazino-5-(4-methoxybenzoyl)-2-phenylaminothiazole (BzHAT-4)



The compound was synthesized using benzaldehyde (1.06g, 10mmol), phenylisothiocyanate (1.21g, 9mmol) and 4-methoxyphenacylbromide (2.06g, 9mmol) following the general procedure. The crude product was purified by recrystallization using ethanol-acetone (1:1) mixture to obtain the product as yellow solid (85%). Mp 134-135°C; IR (UATR) ν cm^{-1} : 3218 (N-H), 3059 (aromatic), 1728 (C=O), 838, 757 (aromatic); ^1H NMR (500MHz, CDCl_3): δ (ppm) 3.85 (s, 3H), 6.93-6.96 (m, 2ArH), 7.12-7.15 (m, 1ArH), 7.28-7.35 (m, 7ArH), 7.64-7.66 (m, 2ArH), 7.76-7.78 (m, 2ArH), 7.97 (s, 1H), 8.05 (s, 1ArNH) 12.39 (s, 1NH); ^{13}C NMR (125MHz, CDCl_3): δ (ppm) 55.4, 94.5, 113.7, 121.1, 125.5, 127.4, 128.5, 129.4, 129.6, 129.7, 133.7, 134.0, 138.4, 145.2, 161.0, 161.9, 170.5, 183.9; LC-MS ($\text{M}+1$): m/z : 429.30.

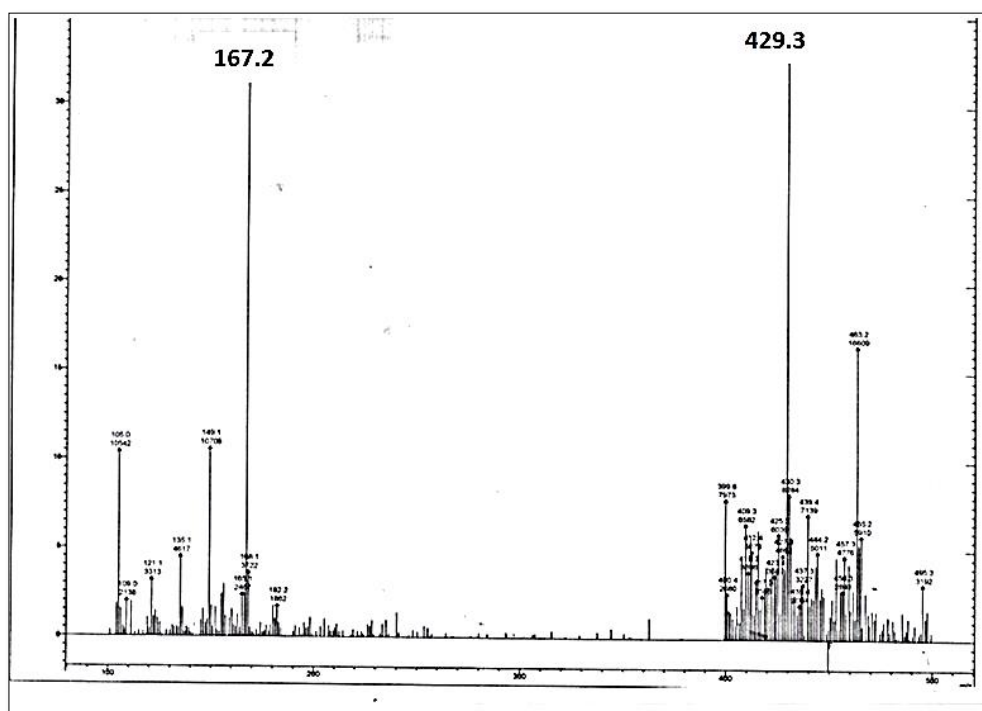


Figure 2.64. LC-MS spectrum of **BzHAT-4**

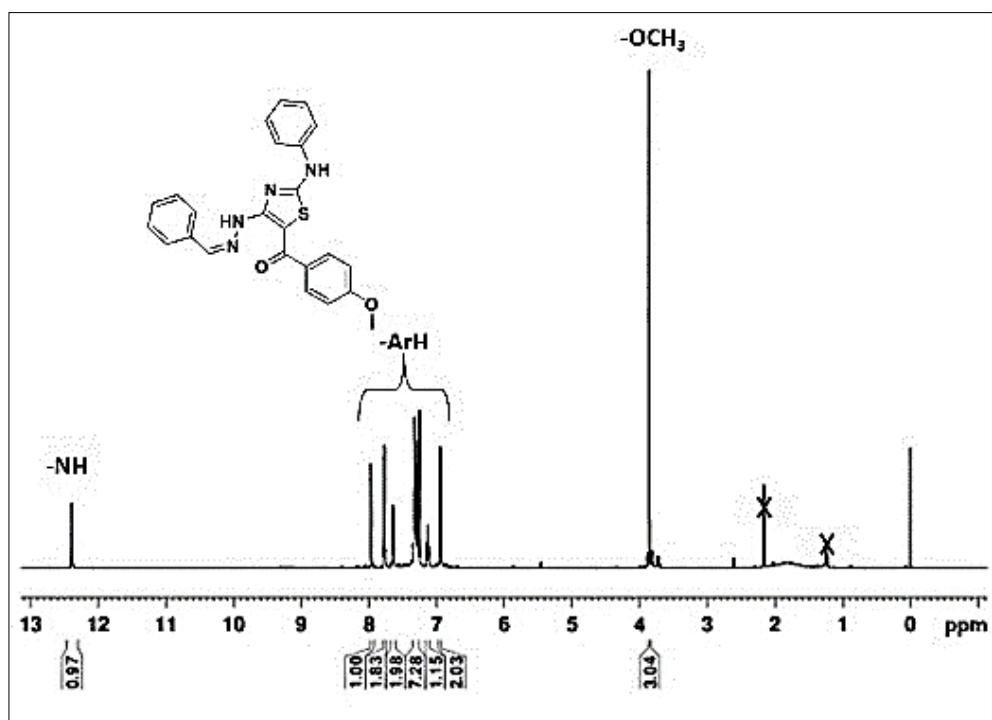


Figure 2.65. ^1H NMR spectrum of **BzHAT-4**

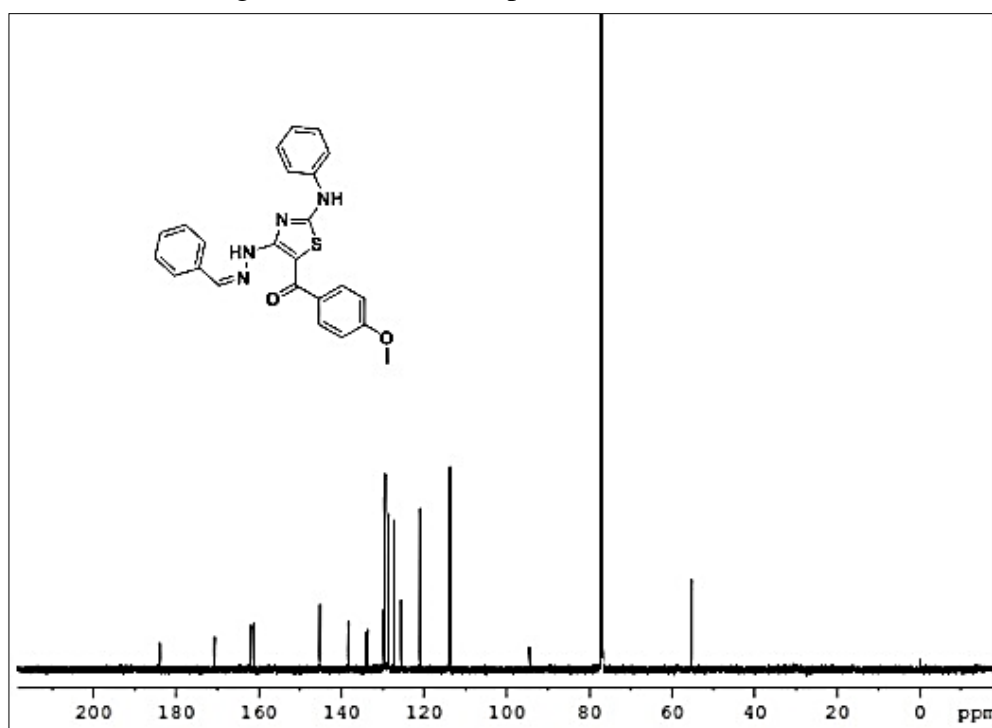
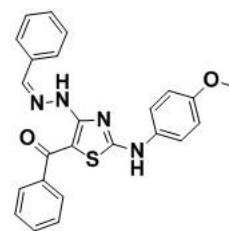


Figure 2.66. ^{13}C NMR spectrum of **BzHAT-4**

2.4.5.24. 5-benzoyl-4-benzylidenehydrazino-2-(4-methoxyphenylamino)thiazole (BzHAT-5)



Compound was synthesized using benzaldehyde (1.06g, 10mmol), 4-methoxyphenyl isothiocyanate (1.48g, 9mmol) and phenacylbromide (1.79g, 9mmol) following the general procedure. The crude product was purified by recrystallization using ethanol-acetone (1:1) mixture to obtain the product as yellow solid (85%). Mp 193-194°C; IR (UATR) ν cm^{-1} : 3220 (N-H), 3040, 1718 (C=O), 826, 725 (aromatic); ^1H NMR (500MHz, CDCl_3): δ (ppm) 3.83 (s, 3H), 6.94 (d, J =9Hz, 2ArH), 7.23-7.31(m, 1ArH), 7.35-7.42 (m, 3ArH), 7.46-7.48 (m, 2ArH), 7.51-7.54 (m, 3ArH), 7.64-7.67 (m, 3ArH), 7.98 (s, 1H), 8.05 (s, 1ArNH) 12.39 (s, 1NH); ^{13}C NMR (125MHz, CDCl_3): δ (ppm) 55.4, 94.6, 114.4, 124.8, 127.2, 127.3, 128.3, 128.4, 129.6, 130.7, 131.3, 133.8, 141.3, 155.4, 158.0, 161.8, 173.6, 184.2; LC-MS ($M+1$): m/z : 429.30.

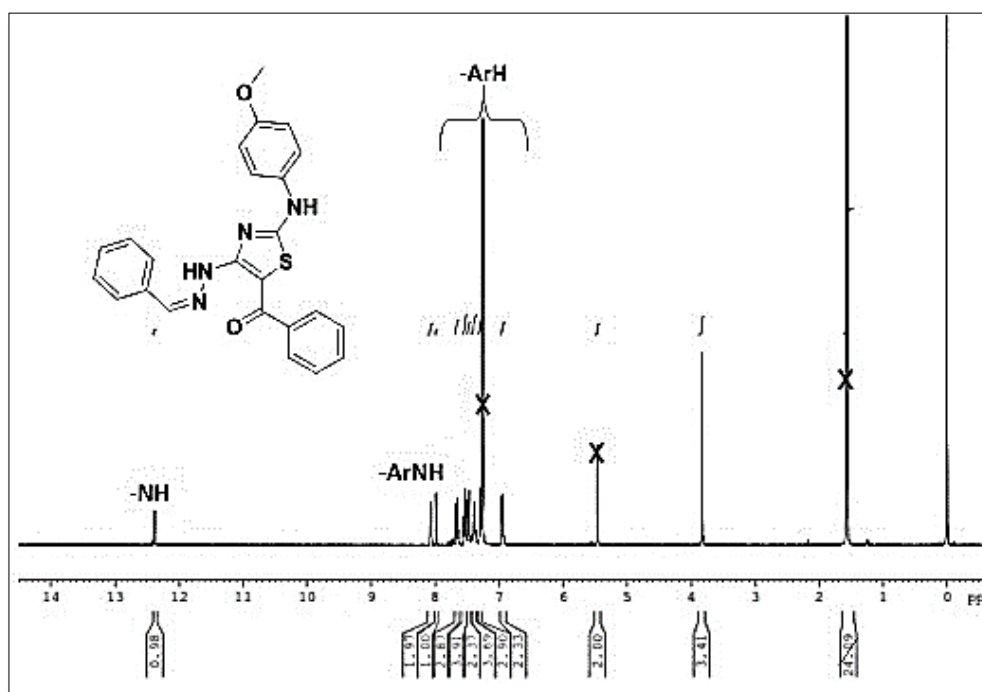


Figure 2.67. ^1H NMR spectrum of **BzHAT-5**

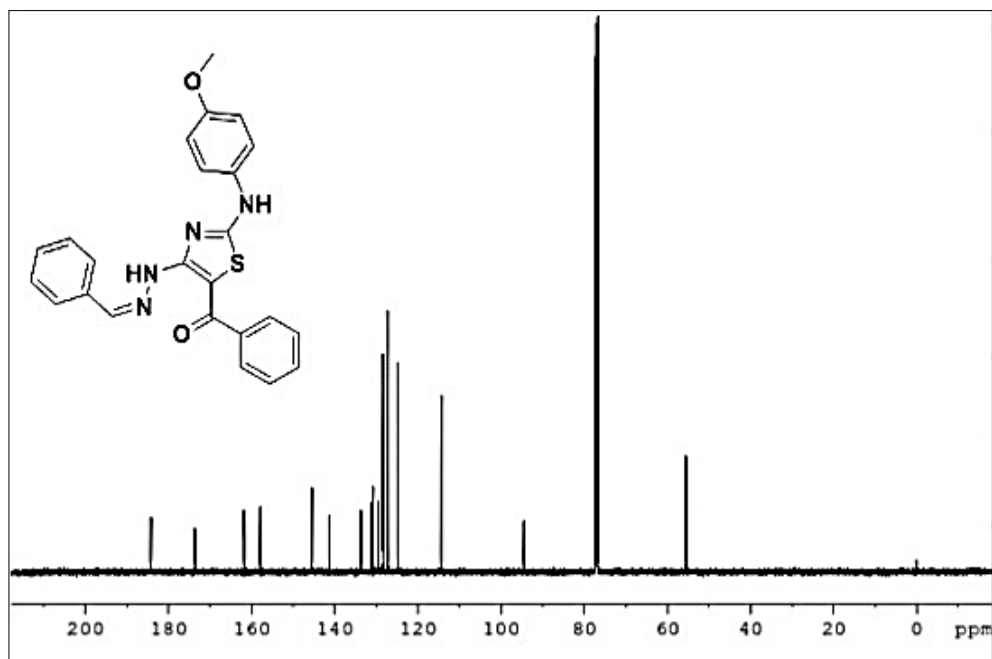
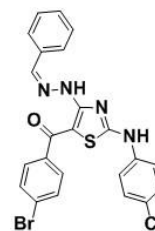


Figure 2.68. ^{13}C NMR spectrum of **BzHAT-5**

2.4.5.25. 4-benzylidenehydrazino-5-(4-bromobenzoyl)-2-(4-chlorophenylamino)thiazole (BzHAT-6)



The compound **BzHAT-6** was synthesized using benzaldehyde (1.06g, 10mmol), 4-chlorophenylisothiocyanate (1.52g, 9mmol) and 4-bromophenacylbromide (2.50g, 9mmol) following the general procedure. The crude product was purified by recrystallization using ethanol-acetone (1:1) mixture to obtain the product as yellow solid (88%). Mp 158-159°C; IR (UATR) ν cm^{-1} : 3224 (N-H), 3040 (aromatic), 1718 (C=O), 840, 725 (aromatic); ^1H NMR (500MHz, CDCl_3): δ (ppm) 7.28-7.38 (m, 3ArH), 7.45-7.47 (m, 4ArH), 7.52-7.55 (m, 1ArH), 7.59-7.69 (m, 5ArH), 8.03 (s, 1H), 7.99 (s, 1ArNH), 12.33 (s, 1NH); ^{13}C NMR (125MHz, CDCl_3): δ (ppm) 94.5, 122.8, 125.6, 127.4, 128.6, 128.9, 129.6, 130.1, 131.2, 131.8, 146.1, 158.1, 158.2, 159.4, 161.3, 171.1 182.1; Anal.

calcd for $C_{23}H_{16}BrClN_4OS$ (511.82): C, 57.52; H, 4.39; N, 12.20%. Found: C, 57.36; H, 4.19; N, 12.05%.

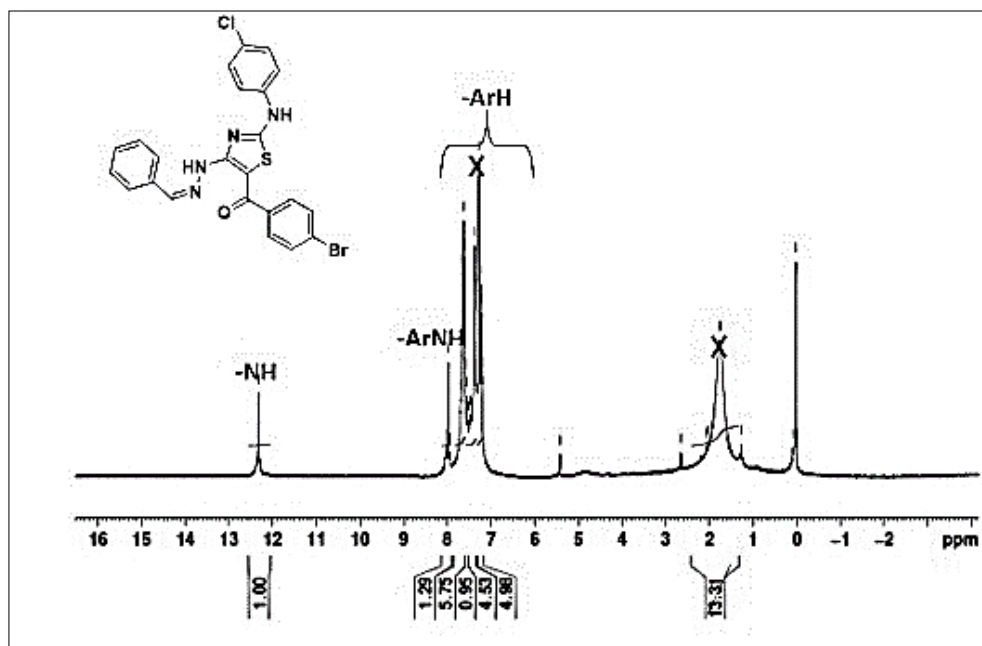


Figure 2.69. 1H NMR spectrum of **BzHAT-6**

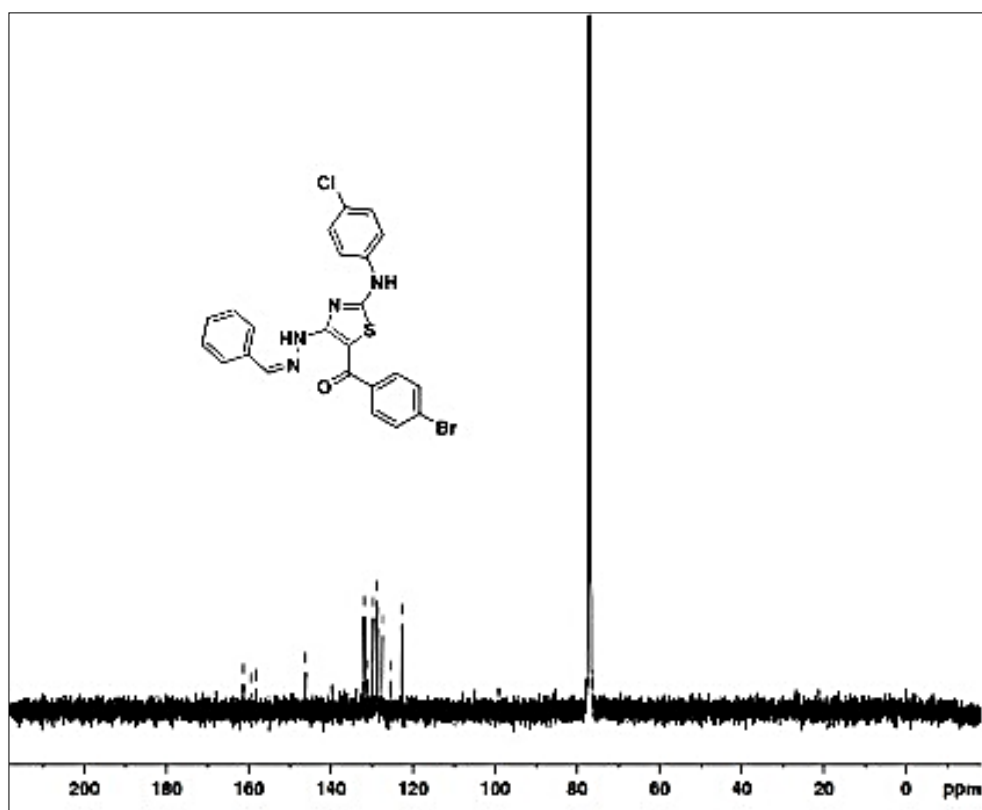
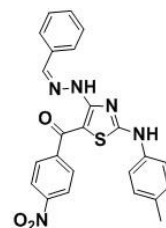


Figure 2.70. ^{13}C NMR spectrum of **BzHAT-6**

2.4.5.26. 4-benzylidenehydrazino-2-(4-methylphenylamino)-5-(4-nitrobenzoyl)thiazole (BzHAT-7)



The compound **BzHAT-7** was synthesized using benzaldehyde (1.06g, 10mmol), 4-methylphenylisothiocyanate (1.34g, 9mmol) and 4-nitrophenacylbromide (2.19g, 9mmol) following the general procedure. The crude product was purified by recrystallization using ethanol-acetone (1:1) mixture to obtain the product as yellow solid (88%). Mp 122-123°C; IR (UATR) ν cm^{-1} : 3220 (N-H), 3028 (aromatic), 1710 (C=O), 836, 747 (aromatic); ^1H NMR (500MHz, CDCl_3): δ (ppm) 2.33 (s, 3H), 7.16-7.20 (m, 4ArH), 7.39-7.40 (m, 3ArH), 7.71-7.73 (m, 2ArH), 7.86-7.88 (m, 2ArH), 8.06 (s, 1H), 8.27-8.29 (m, 2ArH), 8.61 (s, 1ArNH), 12.38 (s, 1NH); ^{13}C NMR (125MHz, CDCl_3): δ (ppm) 20.9, 95.0, 99.9, 122.2, 123.8, 127.5, 128.2, 128.6, 130.1, 130.2, 133.6, 135.2, 136.7, 146.7, 148.8, 162.2, 172.7, 181.3; ESI-MS ($\text{M}+\text{H}^+$): 458.13.

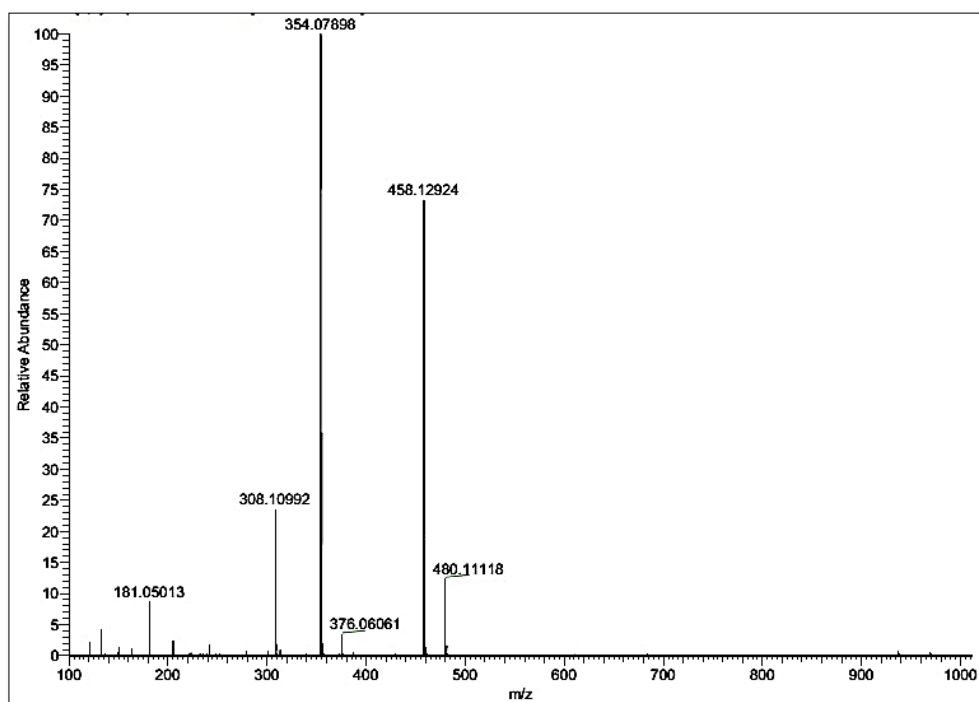


Figure 2.71. ESI-MS spectrum of **BzHAT-7**

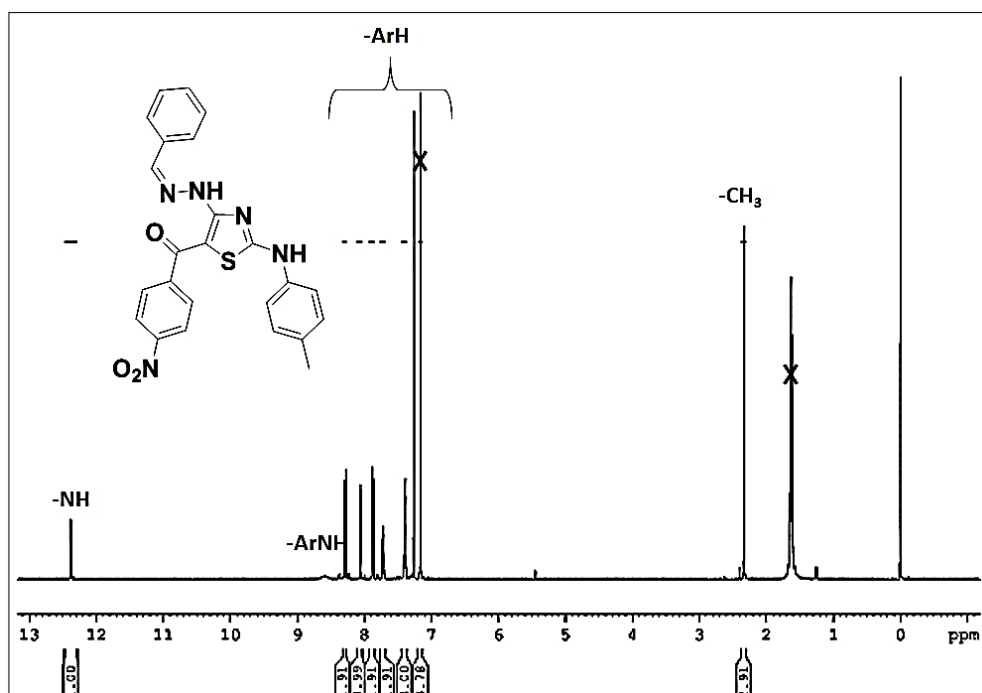


Figure 2.72. ^1H NMR spectrum of **BzHAT-7**

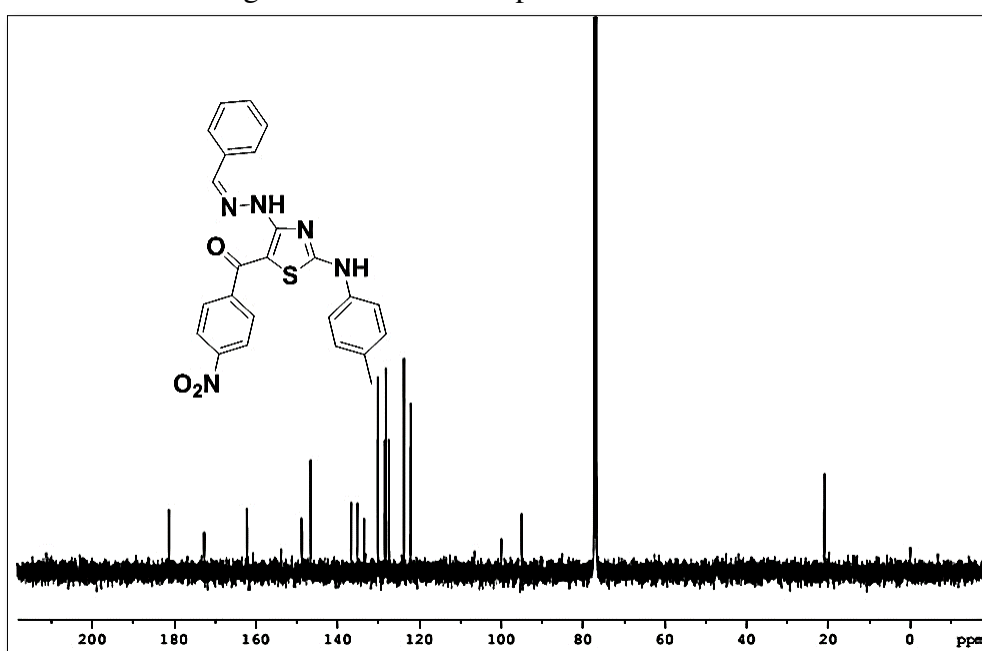


Figure 2.73. ^{13}C NMR spectrum of **BzHAT-7**

2.5. Conclusions

To summarize the work in chapter 2, we have designed and developed a novel 2-aminothiazole template based small molecule drug design scaffold *viz*; 4-

hydrazinothiazoles (**HAT**) with immense scope of diversity multiplication around the core. A 120 member virtual library of **HAT** was designed and preliminary docking studies were conducted by choosing 3LAU, 3ERT and 3CFN proteins. The promising results from the docking studies where the **HAT** derivatives showed significant affinity to 3LAU protein encouraged us to develop retrosynthetic strategies to access these novel ligands. This was followed by the design of the chemical synthesis route where we successfully developed an efficient one-pot four component as well as a two-step ring synthesis routes and optimized them for the highly substituted scaffold in very good to excellent yield. The versatility of the developed [4+1] ring synthesis was established by the synthesis of 54 derivatives of **HAT** of which 26 compounds were characterized with spectroscopic techniques. After identifying Aurora kinase as a promising target for the designed scaffold by virtual screening we then aimed at the *in vitro* screening and *in silico* studies for the ‘drug-likeness’ of the designed library of molecules which is now discussed.

CHAPTER 3

EXPLORATION OF SOLID STATE LANDSCAPE OF 4-HYDRAZINOTHIAZOLES AND EVALUATION OF ‘DRUG-LIKENESS’

3.1. Background

The paradigm of rational anticancer drug design through virtual high-throughput screening (vHTS) has proven to be a successful strategy for the identification and development of many hits and potential candidates in a cost effective way (Bleicher *et al.*, 2003). But, the careful implementation of the computational tools in drug discovery is much important for its success. Most of the identified lead molecules bear the burden ‘of no use’ and are being discarded in the later stages of drug development primarily due to their poor druggability and processability. Hence apart from the traditional potency and selectivity concerns, the developability assessment of potential candidates (Gardner *et al.*, 2004) became an inevitable part in modern medicinal chemistry research especially in the early stages of drug development. The druggability of the bioactive molecules is evaluated by measuring an ensemble of ‘drug-like’ properties that affect its absorption, distribution, metabolism, excretion and toxicity (ADMET) and is often referred to as pharmaceutical profiling (Kerns & Di, 2003). Whereas the processability is assessed by the analysis of different solid-state forms that significantly affect the biopharmaceutical properties such as solubility and permeability which are the key components in determining the bioavailability of a drug/ lead like molecule (Huang & Tong, 2004).

3.2. Results and Discussion

3.2.1. Solid-state landscape of 4-hydrazinothiazoles

The biopharmaceutical properties such as solubility and permeability are the deciding factors of the therapeutic efficacy of a molecule. In this regard, the solid forms in which active pharmaceutical ingredients (APIs) are manufactured and isolated have pivotal role in drug development and pharmaceutical product lifecycle management (Newman & Byrn, 2003). Depending upon the arrangement of molecules in three dimensions the existing pharmaceutical solids can be classified as either crystalline solids with regular arrangement of molecules or amorphous solids with lack of long-range order. The difference in the molecular arrangement is responsible for the changes in physical and chemical properties of these two solid forms (Grant, 1999) which ultimately leads to the change in bioavailability of the molecule. Even though in the case of most of the APIs the most soluble form is the amorphous one, medicinal chemists prefer the crystalline forms due to the well- defined and reproducible physical properties and chemical stability during the formulation (Aaltonen *et al.*, 2009). Polymorphs, solvates/hydrates and co-crystals are the most common crystalline forms of APIs among which solvates and co-crystals are having a significant place. When the unit cell of API is accompanied by solid guest molecule then it is termed as co-crystal and when the guest moiety is a liquid then it is termed as solvate. Due to the small size and multidirectional hydrogen bonding nature of water molecules hydrates are the most common forms of solvates and one third of the APIs are capable of forming hydrates during pharmaceutical processing.

Having identified the designed trivariant scaffold 4-hydrazinothiazoles as suitable template for anticancer drug design, we felt it worthy to proceed with the investigation of solid state structures, especially the crystalline forms of representative members from the synthesized family of compounds. In general, the derivatives adopted a propeller shape (Figure 3.1) with thiazole ring as hub encased by three blades (**B₁**-**B₃**).

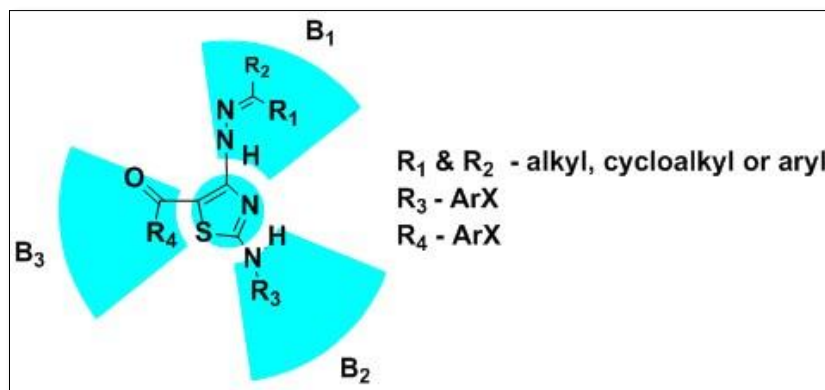


Figure 3.1. Propeller shaped 4-hydrazinothiazole scaffold

Interestingly, our scaffold bears structural similarity with the well-known orally active anticancer drug dasatinib (DAS), used for the treatment of chronic myelogenous leukemia (CML) (Talpez *et al.*, 2006). It is noteworthy that the imbalance in the number of donor-acceptor groups in the structure of our scaffold can impart many intra- and inter molecular interactions that can lead to the formation of multicomponent solid systems. Moreover the structural similarity of the scaffold with DAS, which is prone to form hydrates (Roy *et al.*, 2012), inspired us to study the hydrate/solvate formation in the designed scaffold. It is to be noted that by varying carbonyl components, isothiocyanate or α -halo unit in the structure a vast diversity multiplication can be brought in the 4-hydrazinothiazoles. Due to the easy accessibility of carbonyl compounds, in the present study, variants at the hydrazone site (**B1**) were preferred to generate diverse 4-hydrazinothiazoles for crystal studies.

3.2.1.1. Hydrate formation in 4-alkylidenehydrazinothiazoles

4-alkylidenethyrazinethiazoles, for instance 4-isopropylidenethyrazine thiazoles, (IPHATs) were synthesized by providing acetone as the carbonyl capping for the hydrazone unit in **B1**. Here we have selected two crystal structures from IPHAT class viz; 5-benzoyl-4-isopropylidenethyrazino-2-phenylaminothiazole (IPHAT-1) and 5-(4-chlorobenzoyl)-4-isopropylidenethyrazino-2-phenylamino thiazole (IPHAT-2). Diffraction quality crystals of both the compounds were obtained by slow evaporation of aqueous ethanolic solutions over a period of 3-4

weeks. When analysing the crystal structures of IPHAT members, we observed that both the systems evolved as monohydrates (Figure 3.2) belonging to the non-centrosymmetric space group $P2_1/c$, a common space group observed for pharmaceuticals, with number of molecules per unit cell $Z = 4$.

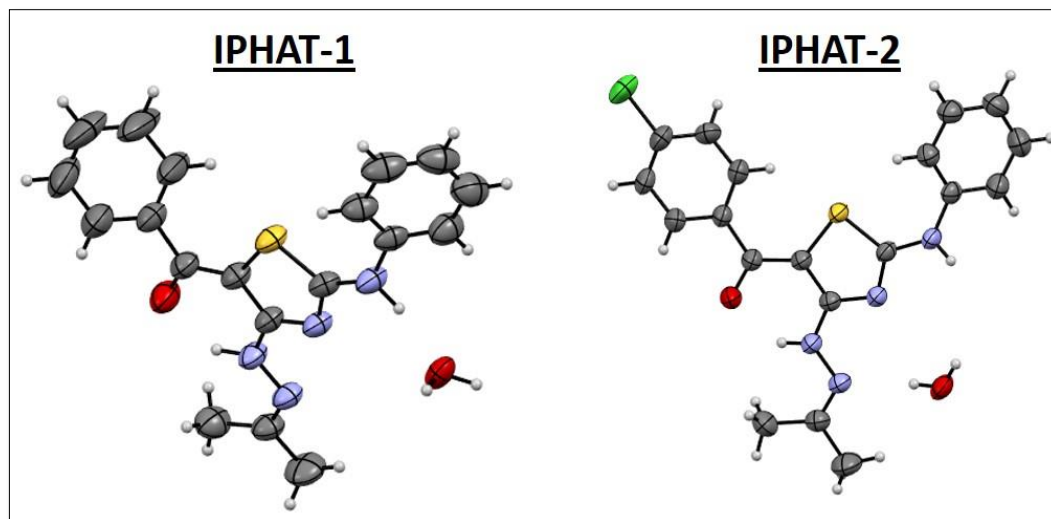


Figure 3.2. ORTEP diagram of IPHAT monohydrates

Even though the molecules formed monohydrates as in the case of DAS, it was interesting to note that the constituent water molecule possessed markedly different bonding interactions. In DAS hydrate dimers are formed by triagonally H-bonded water molecules where as in IPHAT the dimer formation occurred through a tetragonally H-bonded water molecule (Figure 3.3). The water to water H-bond observed in the crystal motivated us to study the IPHAT crystal hydrates in detail for the following reasons.

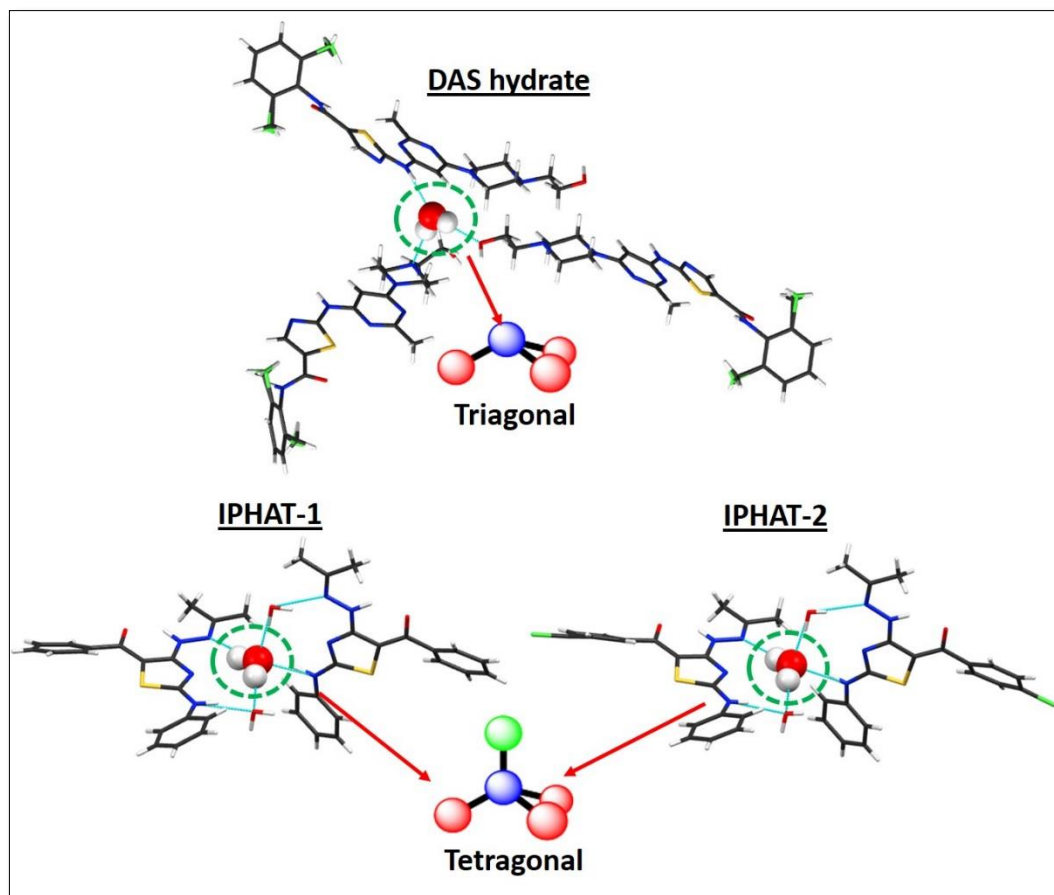


Figure 3.3. H-bonding interactions formed by water molecules in DAS hydrate and IPHAT

Water is an important constituent in many fundamental biological processes (Ball, 2008; Chaplin, 2006) including protein folding (Levy & Onuchic, 2006; Thirumalai *et al.*, 2011) and the activation of G-coupled receptors (Yuan *et al.*, 2014). Owing to the role of water pores in selective transport of ions/protons in proteins such as aquaporins (Moon *et al.*, 1993; Sui *et al.*, 2001; Tajkhorshid *et al.*, 2002) and bacteriorhodopsin (Bondar *et al.*, 2011; Gerwert *et al.*, 2014), in membranes such as Gramicidin A (Akeson & Deamer, 1991; Kelkar & Chattopadhyay, 2007; Woolley & Wallace, 1992) and in enzymes such as cytochrome oxidase C (Belevich *et al.*, 2006; Kaila *et al.*, 2010; Kornblatt, 1998; Wikström *et al.*, 2003), one dimensional (1D) water chains/wires and the design of their synthetic hosts hold enormous research interest. Albeit the implicit significance of water pores, biomimetic design of synthetic water channels (Barboiu & Gilles, 2013) kept low pace, except for a few complex architectures

inspired by aquaporin water (Agre, 2004; Agre *et al.*, 2002) or influenza A proton channel (Pinto *et al.*, 1997; Schnell & Chou, 2008). Both inorganic and organic molecules have proven as host lattices for water in restricted environments. The huge potential of organic molecules, which have a tendency to crystallize as hydrate (Amorín *et al.*, 2011; Desiraju, 2007; Desiraju *et al.*, 2011; Hollingsworth, 2002; Mascal *et al.*, 2006; Natarajan *et al.*, 2013; Wang *et al.*, 2013) and the factors stabilizing the hydrates (Infantes *et al.*, 2007) all provide cue to mimic natural systems among which urea based (Ma *et al.*, 2009; Turner *et al.*, 2006) or imidazole based (Cheruzel *et al.*, 2003; Hoque *et al.*, 2013; Le Duc *et al.*, 2011) were demonstrated as functional channels for ions or water (protons) whereas calixpyrroles (Kumar & Panda, 2014) were reported to stabilize 1D water chains. In yet another perspective, water in hydrates has been utilized as a design element in crystal engineering (Babu & Nangia, 2006; Varughese & Desiraju, 2010). Hence, along with the pharmaceutical interest aiming at an expansion of the crystal database of organic hydrates we decided to study solid structural landscapes of IPHAT in detail.

The basic building block in IPHAT crystal appeared as a butterfly-shaped dimer (Figure 3.4) formed by the antiperiplanar arrangement of thiazole rings pushing the C=O in **B**₃ to the exterior and aligning **B**₁ and **B**₂ to accommodate water molecules in between. The packing coefficients of IPHAT-1 was calculated to be 0.680 and that of IPHAT-2 was found to be 0.690.

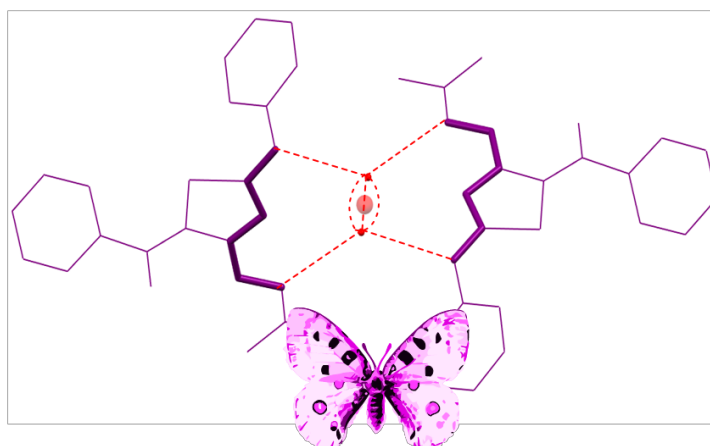


Figure 3.4. Butterfly shaped dimer formed by IPHAT

The H-bonding associations (Table 3.1), as anticipated, followed Etters' rules (Etter, 1990) where both intra- and inter-molecular bonds were observed (Figure 3.5). H-bonding in IPHAT-1 and IPHAT-2 indicate distances in the range of 2.6-2.9 Å (dD⋯A). The oxygen atom of each water molecule in IPHAT-1 and IPHAT-2 was simultaneously H-bonded to NH in **B**₂ (dO⋯H 1.898 Å in IPHAT-1 and 2.064 Å in IPHAT-2) and to neighbouring water molecules (dO⋯H 1.920 Å in IPHAT-1 and 1.963 Å in IPHAT-2) in a *zig-zag* manner.

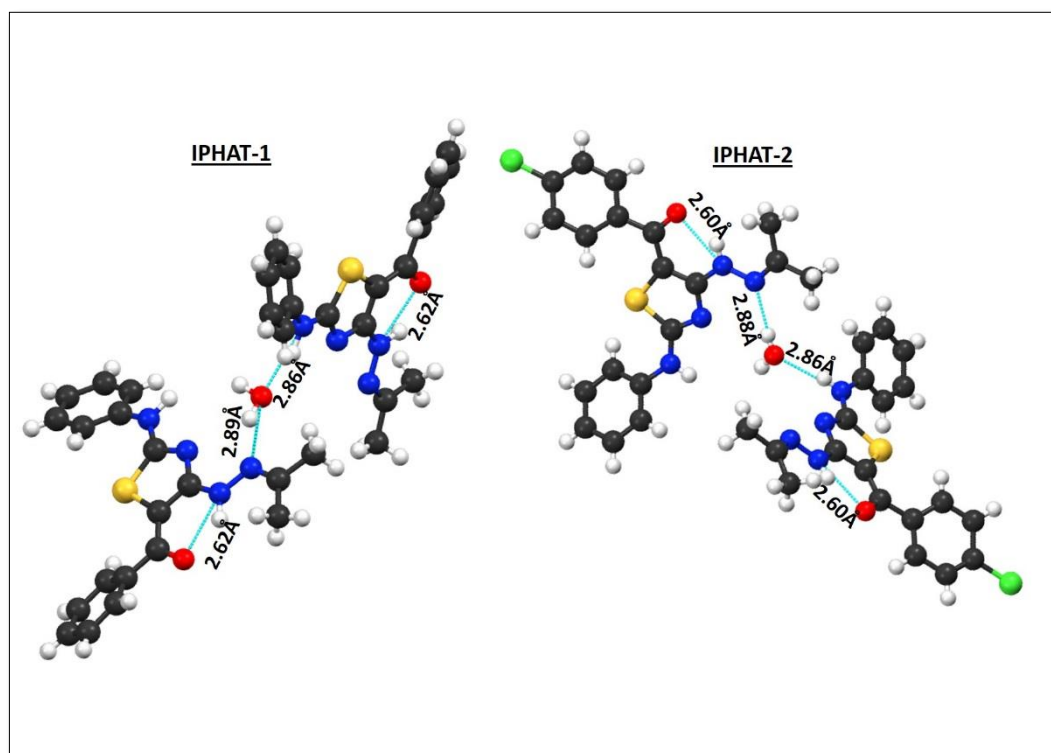


Figure 3.5. Intra- and inter-molecular H-bonding interactions in IPHAT with dD⋯A

These H-bonded water molecules (dO–O 2.864 Å in IPHAT-1 and 2.847 Å in IPHAT-2) form infinite 1D water chains in the respective crystal lattice with O–O distances comparable to that observed in aquaporin water channels (2.8 Å)

Compound	D–H...A	D–H/ Å	H...A)/Å	D...A/ Å	D–H...A/ deg
IPHAT-1	N(3)-H(3)...O(1)	1.000	1.858	2.626	131.05
	N(2)-H(2)...O(1')	1.003	1.898	2.868	161.96
	O(1')-H(1')...N(4)#1	0.947	2.011	2.891	153.68
	O(1')-H(1'')...O(1')#1	0.955	1.920	2.864	169.67
	N(1)-H(1)...O(2)#2	0.822	2.064	2.867	165.61
IPHAT-2	N(3)-H(3)...O(1)	0.852	1.906	2.606	138.49
	O(2)-H(2B)...N(4)	0.793	2.096	2.882	171.39
	O(2)-H(2A)...O(2)#2	0.891	1.963	2.847	171.72
	C(12)-H(12)...N(1)	0.930	2.370	2.920	117.80

^a Symmetry codes: (#1) –x+1, y-1/2, -z+1/2; (#2) –x+1, y+1/2, -z+3/2.

(Eriksson *et al.*, 2013; Tajkhorshid *et al.*, 2002) (Figure 3.6).

Table 3.1. H-bonding interactions in IPHAT-1 and IPHAT-2 (D=donor atom; A= acceptor atom)^a

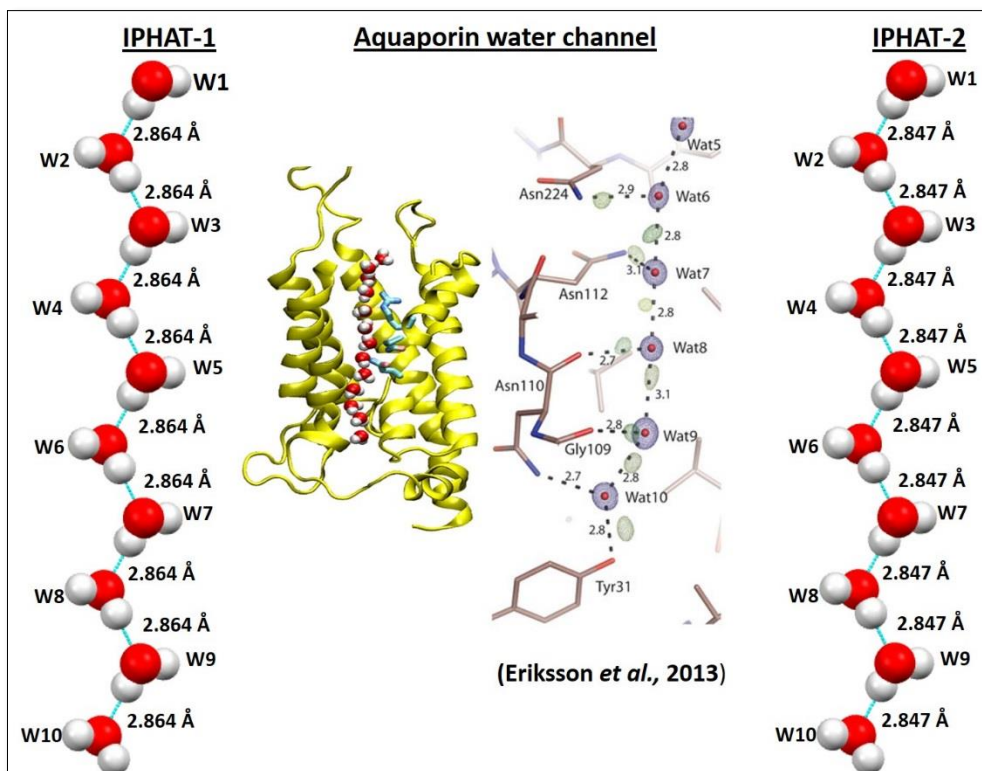


Figure 3.6. Comparison of 1D water chains in aquaporin and IPHAT

Recurrent water chains were observed in the expanded crystal landscape of solid state assemblies with interplanar distances of 9.097 Å and 9.829 Å in IPHAT-1 and IPHAT-2 respectively. Moreover we have found that the water chains in the unit cell are attaining opposite dipolar orientations (Figure 3.7) as in the case of reported imidazole quartet (Turner et al., 2006).

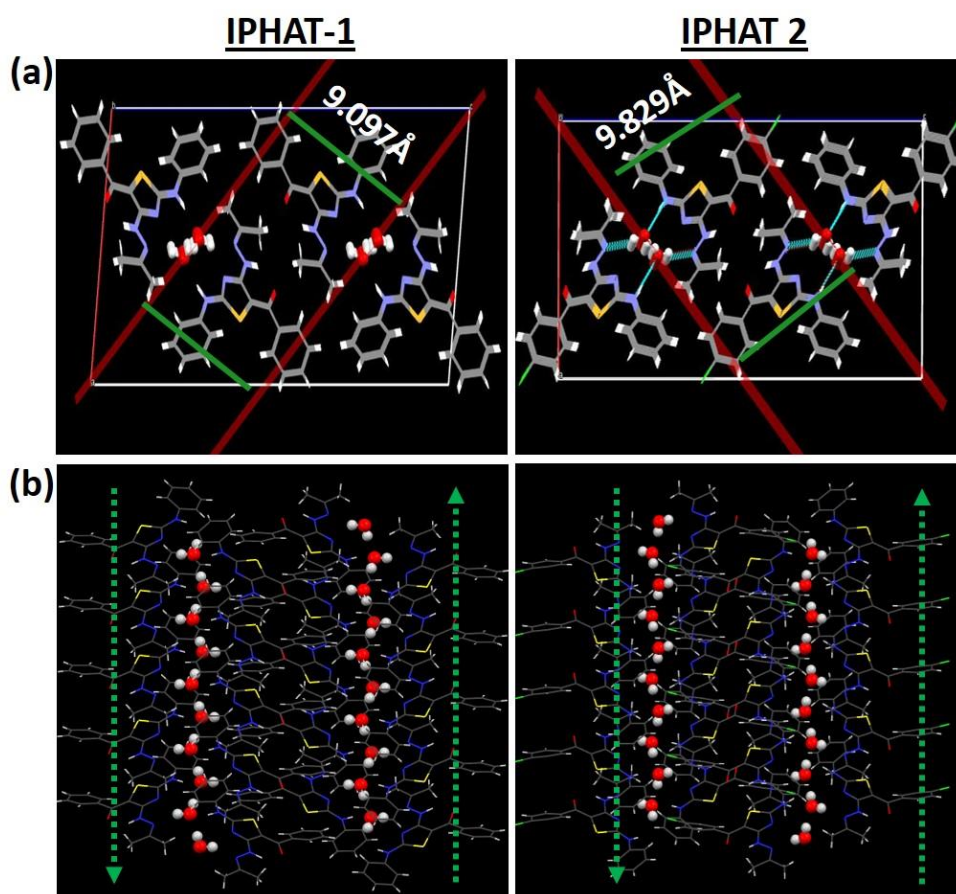


Figure 3.7. (a) Parallel water chains in the crystal lattice of IPHAT monohydrates, (b) Dipolar orientation of water molecules

Coming to the 3D structure, planar arrangement of layered stacks with an interlayer distance of 4.854 Å were generated along *ac* plane such that thiazole hub and the phenyl rings on **B₂** and **B₃** (intercentroidal distances 4.956 Å and 4.854 Å in IPHAT-1 and IPHAT-2 respectively) were disposed at the extremities of a columnar structure. Very interestingly we noticed the formation of a nitrogen rich channel (NRC) resembling a left-handed helix which enclosed tetrahedral H-bonded water molecules as a single file (Figure 3.8).

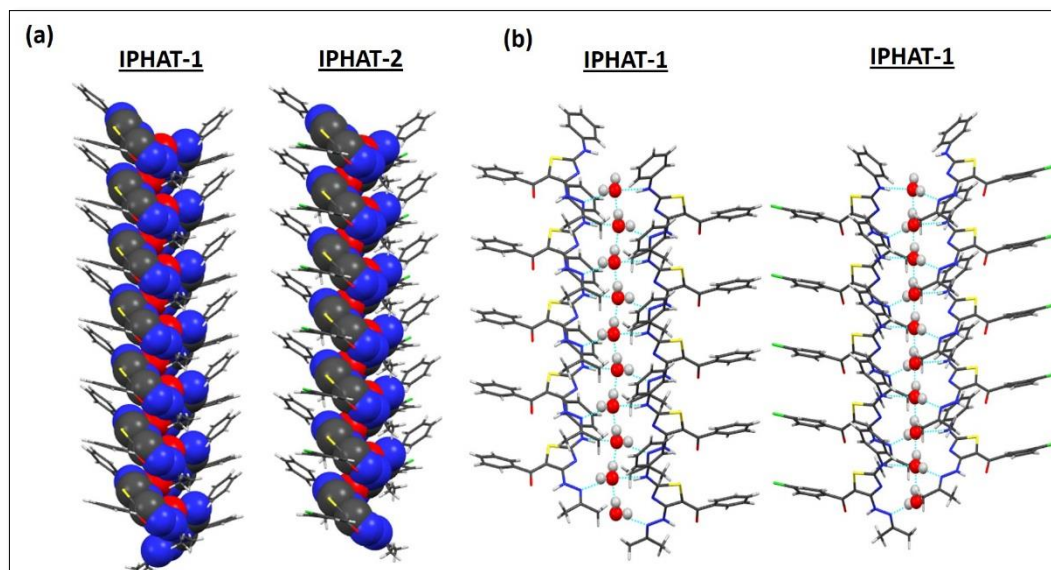


Figure 3.8. (a) View of N-rich left handed helix enclosing 1D water wire in IPHAT, (b) Single file water chain observed in the crystal lattice

It was interesting to note that H-bonding between water molecules and the NRC defined a graph set $R_3^3(10)$. The water channel super structures were stabilized by interlayer π - π stacking interactions between thiazole moieties, those between phenyl rings, along with the strong hydrophobic van der Waals interaction between the methyl groups in the isopropylidene unit (Figure 3.9a). Apart from these, the strong intramolecular H-bonding existed between the C=O in **B**₃ and NH on **B**₁, in a graph set $S(6)$, (dO...H 1.858 Å in IPHAT-1 and 1.906 Å in IPHAT-2 respectively) which synergistically contributed to the stability of these assemblies. The observed hydrophobic gateway formed by aryl ring in **B**₂ and alkyl groups in **B**₁ housing the water in a single file arrangement further may be correlated to hydrophobic gating in biological channels (Aryal *et al.*, 2015) and may be highly significant to regulate the flow of solvent/ions. The area enclosing water wire in the NRC was calculated and was found to be ~ 34 Å² units in both IPHAT-1 and IPHAT-2 (Figure. 3.9b) which is typically formed by isopropylidene and phenyl subunits.

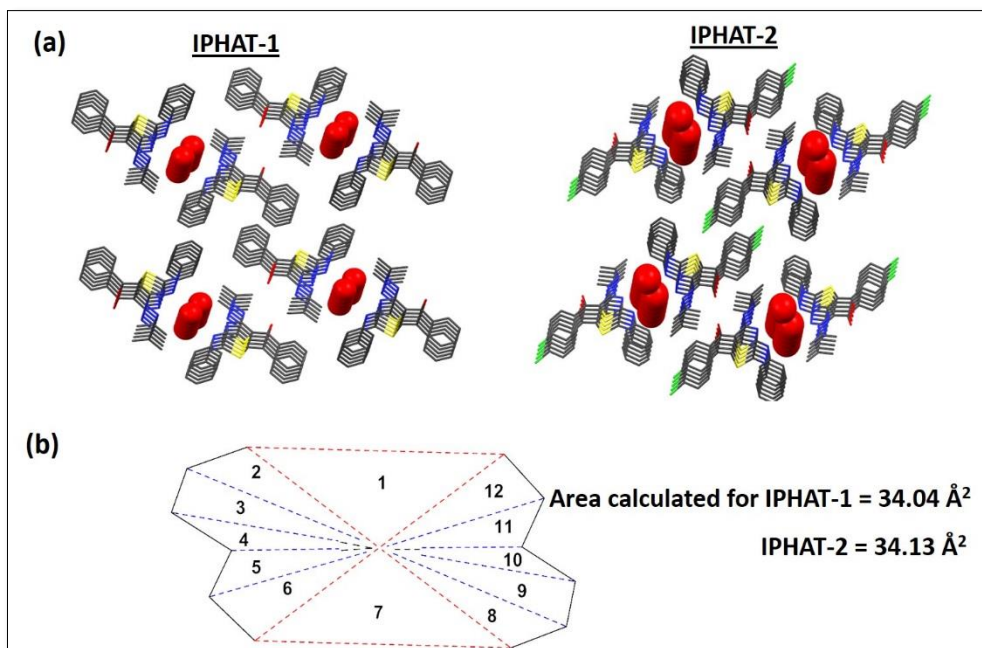


Figure 3.9. (a) View of packing diagram of IPHAT crystal lattice, (b) N-rich channel area enclosing water molecules; Area of triangles was calculated using Heron's formula (Dunham, 1990) ($\Delta = \sqrt{s(s-a)(s-b)(s-c)}$ where $s = \frac{a+b+c}{2}$)

The interesting features observed in the molecular arrangement of IPHAT motivated us to expand the studies to the other classes of designed scaffold. We were interested i) to study the critical role of hydrazone substituents on NRC dimensions ii) to probe the influence of hydrophobic linings in water channel formation and finally and iii) to formulate guidelines regarding predictability of guest encapsulations and hence tunability of the channels.

3.2.1.2. Solvate/hydrate formation in 4-arylidenehydrazinothiazoles

The crystal structure of a representative example from 4-benzylidenehydrazinothiazoles (BzHATs) was generated and the influence of aryl group at the *C4* position was studied in detail. Benzaldehyde was chosen as the carbonyl component in **B1** for the synthesis of BzHAT and diffraction grade crystals were grown under previous conditions. For the present study, the crystal structure was developed for the derivative- 4-benzylidenehydrazino-5-(4-chlorobenzoyl)-2-phenylaminothiazole (BzHAT-2). While examining the crystal landscape, it was found that the hydrate formation was not preferred in the case of BzHAT-2 due to

an apparently constricted NRC ($\sim 28 \text{ \AA}^2$) by the close proximities of **B**₁ and **B**₂. Instead, a molecule of ethanol was accommodated between **B**₂ and **B**₃ to afford BzHAT-2.EtOH where intramolecular H-bonding between the C=O (**B**₃) and NH (**B**₁) was intact ($dO\cdots H$ 2.086 \AA) as observed in IPHAT. We further attempted growing crystals of the same derivative from aqueous methanol (1:1) which on examination turned out to be a methanolate (BzHAT-2.MeOH) where intramolecular H-bonding between the C=O (**B**₃) and NH (**B**₁) deviated by an infinitesimally small difference ($dO\cdots H$ 2.088 \AA) when compared with that in BzHAT-2.EtOH. Both the crystals were found to be isostructural and crystallized in monoclinic crystal systems, solved and refined in the space group $P2(1)/n$ with packing coefficients 0.638 and 0.636 respectively. The solvent molecules aligned between **B**₂ and **B**₃ and were enclosed inside a hydrophobic cavity formed by phenyl rings and acted as bridge for thiazole dimer formation (Figure 3.10a). The crystal packing structure analysis showed a centrosymmetric hexameric arrangement for the solvent molecules in chair conformation (Arunachalam *et al.*, 2007; Little *et al.*, 2015) and the NRC in the super structures of both methanolate and ethanolate comprised an area of 27-28 \AA^2 (Figure 3.10b) and were apparently constricted when compared with that in IPHAT accounting for the absence of water wire.

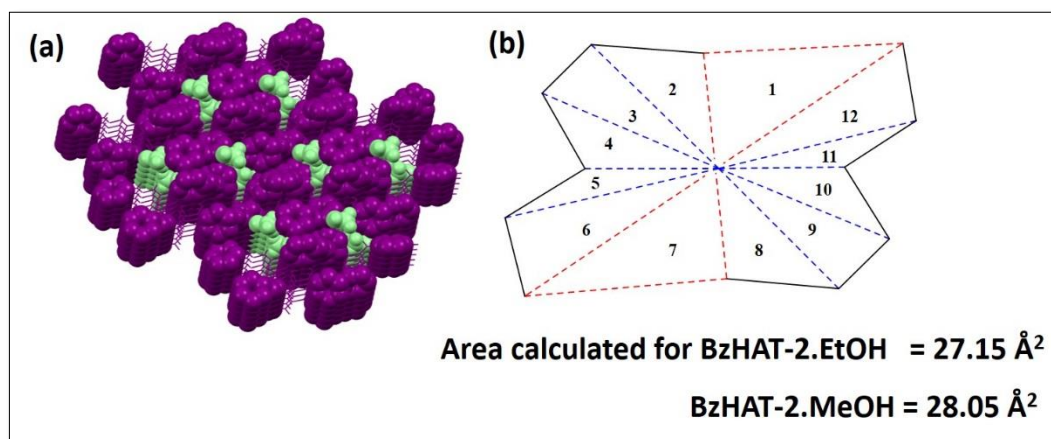


Figure 3.10. (a) Solvent molecules enclosed in the hydrophobic cavity formed by phenyl rings in the crystal lattice of BzHAT, (b) NRC area enclosing solvent molecules; Area of triangles was calculated using Heron's formula (Dunham, 1990)

$$(\Delta = \sqrt{s(s-a)(s-b)(s-c)} \text{ where } s = \frac{a+b+c}{2})$$

Both methanol and ethanol formed two H-bonds (Table 3.2) in their respective crystals - (i) oxygen atom of solvent acting as acceptor and NH in **B₂** (dO...H 1.954 Å in BzHAT-2.MeOH and 1.907 Å in BzHAT-2.EtOH) as donor, and (ii) a bifurcated bond where C=O in **B₃** as acceptor and OH in solvent as donor at a distance of 1.900 Å and 1.997 Å respectively (Figure 3.11) by *cooperative effect* (Ceccarelli et al., 1981) as shown by majority of monoalcoholic systems.

Table 3.2. H-bonding interactions in BzHAT-2. EtOH and BzHAT-2.MeOH

(D=donor atom; A= acceptor atom)^a

Compound	D-H...A	D-H/ Å	H...A/ Å	D...A/ Å	D-H...A/ deg
BzHAT-2.MeOH	N(2)-H(2A)...O(1')#1	0.860	1.950	2.811	174.39
	N(3)-H(3A)...O(1)	0.860	2.090	2.706	128.24
	O(1')-H(1')...O(1)	0.820	1.900	2.719	176.52
	N(3)-H(3)...O(1)	0.861	2.086	2.714	129.37
BzHAT-2.EtOH	O(2)-H(2)...O(1)#2	0.820	1.997	2.740	150.33
	N(1)-H(1)...O(2)	0.860	1.907	2.767	178.11
	N(24)-H(24)...O(26)	0.859	2.033	2.676	130.95

^a Symmetry codes: (#1) $-x+3/2, y+1/2, -z+1/2$; (#2) $-x+1/2, y+1/2, -z+1/2$.

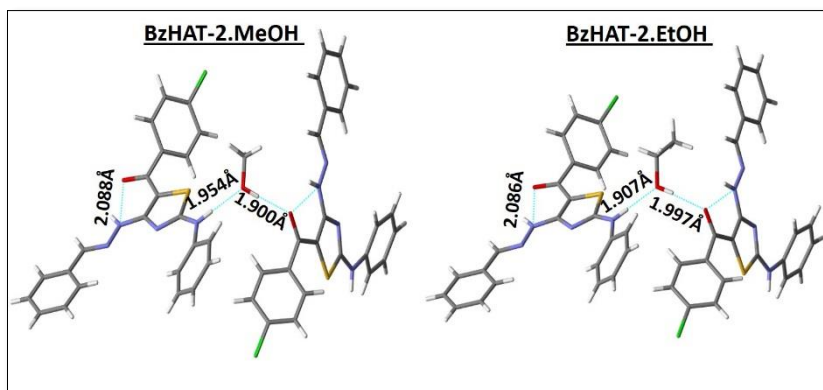


Figure 3.11. H-bonding interactions in BzHAT-2. alcoholates

The NRC channels were observed to be forming a *herringbone* type arrangement along the *bc* plane with interchain separations of 14.844 Å and 16.416 Å in BzHAT-2.MeOH and BzHAT-2.EtOH respectively whereas along the *ac* plane the molecules were arranged in layers with an interlayer distance of 16.189 Å and 16.416 Å in BzHAT-2.MeOH and BzAHT-2.EtOH respectively (Figure 3.12).

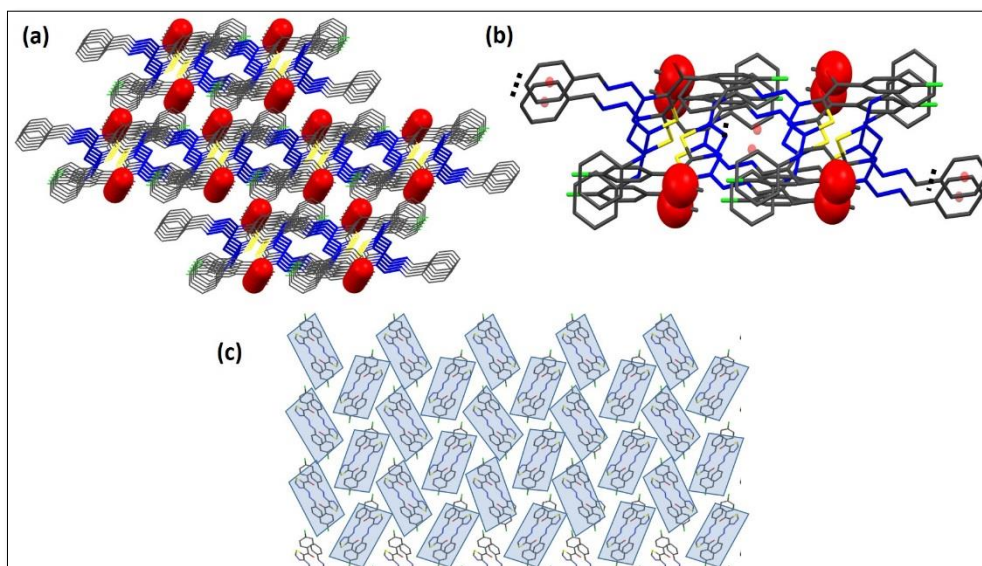


Figure 3.12. (a) Supramolecular assembly of BzHAT alcoholates in the *ac* plane, (b) Centroid-centroid distance between adjacent layers marked with black dotted line, (c) *Herringbone* arrangement of NRC of BzHAT-2.alcoholates

The interlayer distance was almost four fold enhanced when compared to that in IPHAT probably due to the bulky solvent molecules. The alcoholic oxygen atoms defined a parallel triangular wave symmetry in the *bc* plane with an O-O

distance of ~ 9.7 Å. (9.712 in BzHAT-2.MeOH and 9.773 in BzHAT-2.EtOH) (Figure 3.13a), whereas the S atoms of thiazole rings aligned *anti* to the **B**₂ NH, and formed a regular parallel ‘Z’ like arrangement in the superstructure (Figure 3.13b).

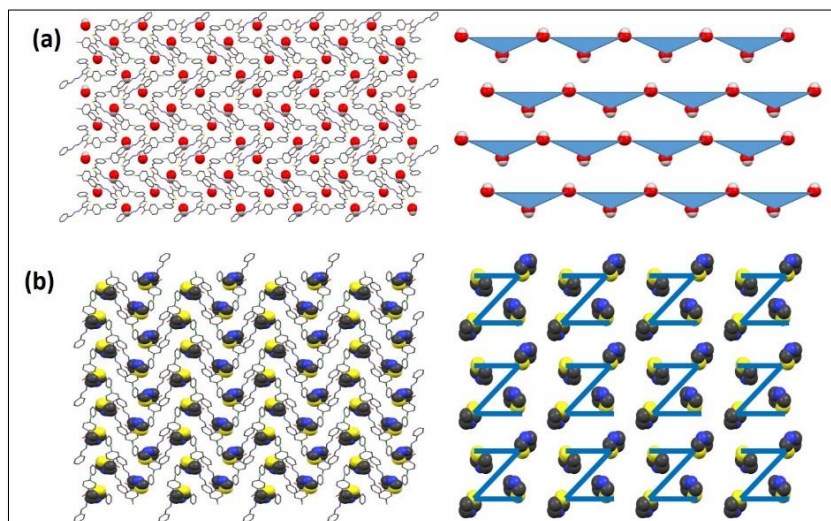


Figure 3.13. (a) Triangular wave arrangement of solvent molecules in molecular packing of BzHAT alcoholate along *bc* plane, (b) ‘Z’ like arrangement of thiazole S atoms in the plane

The variations in channel dimensions and subsequent guest encapsulations substantiate our hypothesis on the probable role of hydrazone substituent on the channel formation and tunability. To further strengthen our hypothesis, a cyclohexyl unit was provided as the hydrazone capping and the variations in channel formations and dimensions were investigated.

3.2.1.3. 4-Cycloalkylidenehydrazinothiazoles

Diffraction quality crystals of 4-cyclohexylidene-5-benzoyl-2-phenylamino-1,3-thiazole (CyHAT-1) from aqueous ethanol (1:1) appeared in triclinic crystal system, solved and refined in the space group *P*-1 with a packing coefficient of 1.26. The asymmetric unit of the crystal contained two chemically identical but crystallographically different molecules bonded together by inter molecular H-bonding (Figure 3.14) in a graph set $R_2^2(8)$.

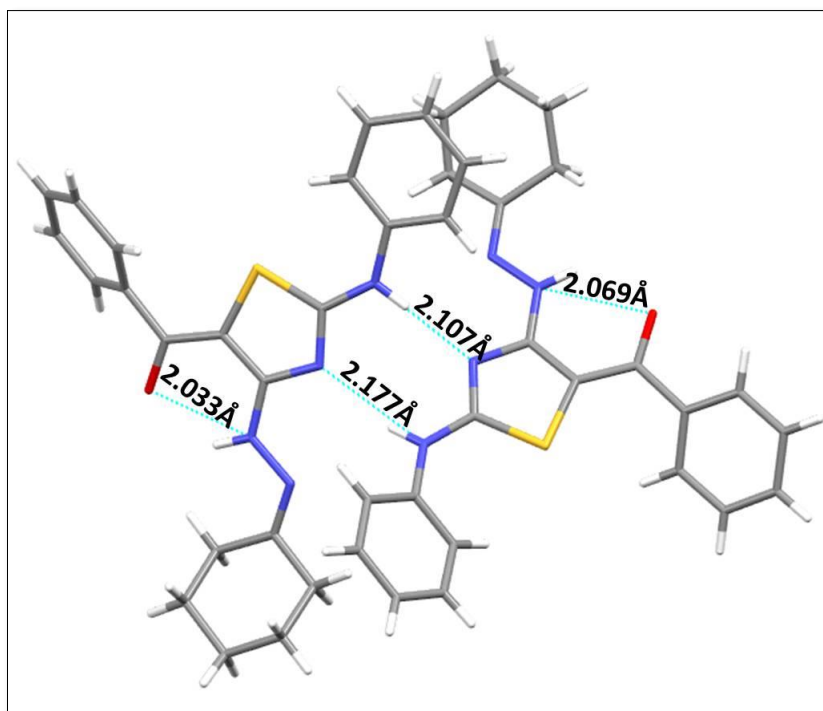


Figure 3.14. View of H-bonding interactions (dashed line) in CyHAT along *a* axis

The thiazole N atoms acted as H-bond acceptors whereas the **B₁** NH acted as H-bond donors ($\sim 2.1 \text{ \AA}$, $\text{dN}\cdots\text{H}$) to orient the rings such that S atoms in the dimeric unit were oppositely aligned to generate a pincer-shaped NRC with thiazole N-N distance of 10.362 \AA (Figure 3.15). However, intramolecular H-bonding (Table 3.3) between the C=O (**B₃**) and NH (**B₁**) was intact and the bond distances ($\text{dO}\cdots\text{H}$ 2.069 or 2.033 \AA) were higher than that in IPHAT derivatives and lower than in BzHAT systems. The water/solvent inclusion in the channels was not observed probably due to open structure of the channel and hence establishing the role of NRC.

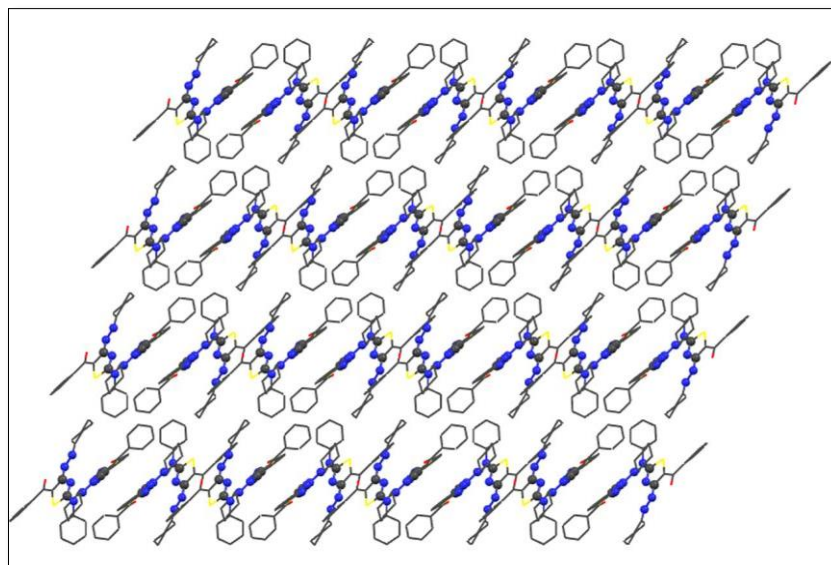


Figure 3.15. Pincer-shaped channels of CyHAT-1 viewed along *ac* plane; N and C atoms in the channel are shown in ball and stick representation; All H atoms are omitted for clarity of view

Table 3.3. H-bonding interactions in CyHAT-1 (D=donor atom; A= acceptor atom)^a

Compound	D–H...A	D–H/ Å	H...A/ Å	D...A/ Å	D–H...A/ deg
CyHAT-1	N(12)-H(12)...N(23))#1	0.861	2.177	3.001	160.26
	N(22)-H(22)...N(13)	0.860	2.107	2.945	164.73
	N(14)-H(14)...O(16)	0.859	2.069	2.678	127.30

^a Symmetry codes: (#1) –x, –y, –z

A calixarene type of arrangement was observed for the molecules when viewed along *a* axis and layers were formed along *ac* plane with an interlayer distance of 12.649 Å and in which thiazole rings faced each other with a S-S distance of 4.218 and 4.630 Å in alternate layers (Figure 3.16).

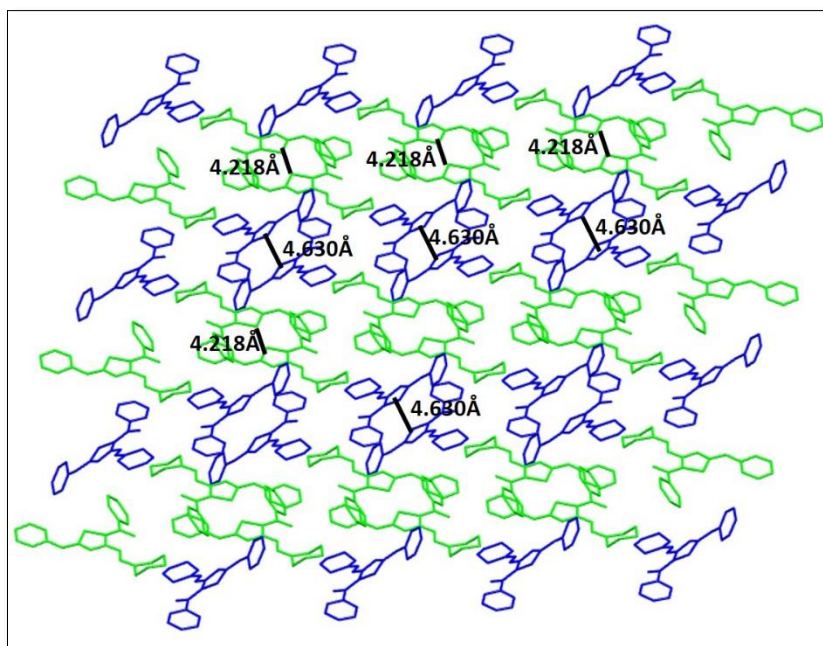


Figure 3.16. Calixarene type of arrangement of CyHAT-1 along a axis; Thiazole S-S distance is marked with a black line; All the atoms are shown in capped stick representation

Moreover a continuous hydrophobic channel formed by the cyclohexane unit in **B₁** and the phenyl ring on **B₃** observed along c axis resembled cyclohexane ring in its chair form (Figure 3.17) was observed as in the case of organic porous materials (Tian *et al.*, 2012).

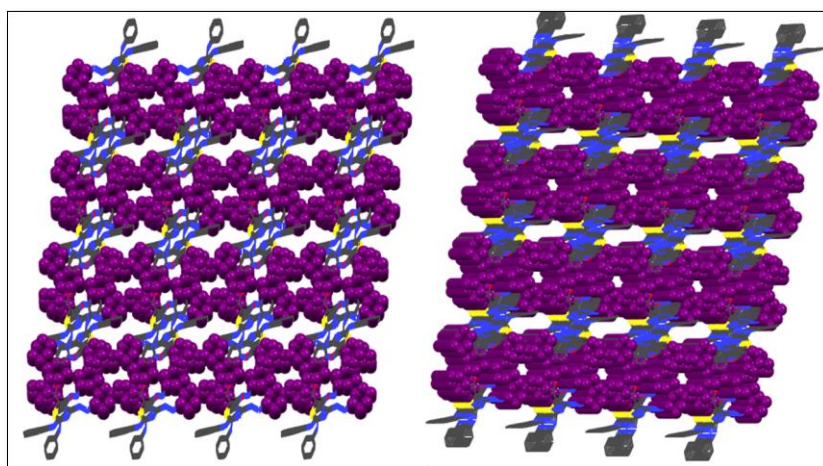


Figure 3.17. Views of hydrophobic cavity observed along c axis of CyHAT-1 crystal packing; Cyclohexane unit and phenyl ring (purple colour) on **B₃** are in CPK representation

These unique molecular skeletons which assemble predominantly through H-bonding and π - π stacking to generate unique channels is expected to serve as suitable starting points for the design and development of synthetic biomimetic channels based on thiazole core. This aspect is currently being explored in our laboratories and is not further discussed in this thesis. Having gathered preliminary, yet significant knowledge on the crystalline structures of HAT we next proceeded with the prediction of properties which are highly relevant for qualifying the candidates for their appropriateness in drug discovery schedule.

3.2.2. ‘Drug-likeness’ of 4-hydrazinothiazoles: ADME property calculation

The introduction of Lipinski’s ‘Rule of five’ (RO5) (Lipinski, 2004) lend a hand to the medicinal chemist to understand the ‘drug-likeness’ of biologically active small molecules and the application of which has gained wide acceptance as an approach to reduce the later stage attrition in drug discovery and development. Hence, one of the key trends in the modern pharmaceutical industry is the calculation of pharmacokinetic properties (PK) with the aim of filtering candidate molecules that are unlikely to survive later stages of drug development. ‘Drug-likeness’ of compounds is measured in terms of their ADME (absorption, distribution, metabolism, excretion) and toxicity properties that can ensure the completion of human Phase I clinical trials. To this end *in silico* ADME screening has been implemented in the drug discovery phase, especially in the early stages of discovery, for a cost effective elimination of poor candidates. The computational methods in prediction of PK properties are mainly focusing on general ‘drug-likeness’ by applying RO5 (Table 3.4) for calculating the pharmaceutically relevant descriptors. Since oral ingestion is the preferred route of administration for most of the drugs, computational filtering process is also applied in the prediction of intestinal absorption.

Table 3.4. The preferred range of physical descriptor values in Lipinski's RO5

Descriptor	Preferred Range
Molecular weight (MW)	≤ 500
Calculated logP (ClogP)	≤ 5
H-bond donor	≤ 5
H-bond acceptors	≤ 10

Motivated by the preliminary results on the aurora inhibiting nature of 4-hydrazinotiazoles, we decided to study the 'drug-likeness' of the designed library of compounds in this family. In the present study QikProp was used for the ADME property prediction by calculating physically significant descriptors and pharmaceutically relevant properties. Among the 120 derivatives studied, 65% of the molecules were found to obey the RO5 without any failure while the remaining compounds had one violation in the descriptor values which is acceptable. The molecular weight (MW) of all the molecules analysed from the library were in a range of 350-488 Da. All the structures were predicted with one H-bond donor and 5-7 H-bond acceptor functionalities in an aqueous solution. The octanol/water partition coefficient (logP) is a measure of the lipophilicity of compounds and the calculated values of the compounds were found to be falling under the recommended range (≤ 5) for 78 derivatives from the designed 120 member library of compounds whereas the remaining 42 were violating the rule with logP values in the range of 5-6.

High oral bioavailability is a key concern in the development of bioactive molecules as therapeutic agents. The measure of polar surface area (PSA) and the number of rotatable bonds are found to be good predictors of oral bioavailability (Veber *et al.*, 2002). The literature suggest that molecules with less than 10 rotatable bonds and PSA less than 140 Å² are observed with good bioavailability. The

analysis of our molecules showed that all the molecules were having rotatable bonds in the recommended range and it was found that 96 % of the molecules are having a PSA of $<132 \text{ \AA}^2$ and thus predicted with good bioavailability. The molecules in all the four classes (IPHAT, IBHAT, CyHAT and BzHAT) with p-nitrophenyl substitution at both C2 and C5 of 2-aminothiazole core exceeded the PSA value probably due to the polarizing ability of the electron withdrawing $-\text{NO}_2$ group. Table 3.5 shows the predicted values of physical descriptors for the top scored ligands from all four classes of compounds in 3LAU active site.

Screening of oral absorption ability of compounds related to intestinal membrane permeability is an important part of assessing oral bioavailability. Caco-2 (Colon carcinoma) cell monolayers and MDCK (Madin-Darby canine kidney) cells are widely used as the model for membrane permeability properties of new chemical entities. The calculated Caco-2 cell permeability of 4-hydrazinothiazole suggested that 66% of the compounds in the library had great permeability ($>500 \text{ nm/s}$). It was observed that 4-nitrophenyl substitution at R₃ and R₄ led to lowest predicted oral bioavailability in the tested library of molecules. Permeability across blood-brain barriers (BBB) is a crucial factor determining effectiveness of central nervous system drugs (CNS) or CNS side effects of various drugs. The analysis of the library of molecules predicted that all the molecules possessed QPlogBB values in the recommended range (-3.0-1.2) with an exception of one molecule in the IPHAT family (R₃ & R₄ = 4-nitrophenyl) which had a slightly lower predicted value (-3.12) than the recommended range. Table 3.6 shows the predicted membrane permeability values of top scored ligands from all four classes of 4-hydrazinothiazoles in 3LAU active site.

Table 3.5. The physical descriptors of top scored ligands of 4-hydrazinothiazoles in 3LAU

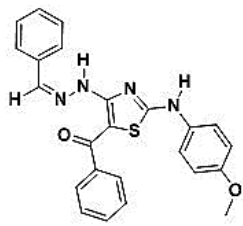
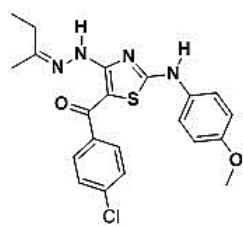
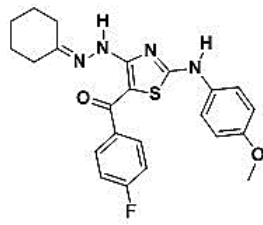
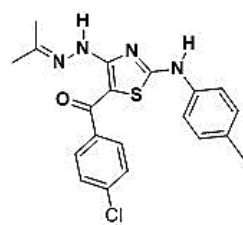
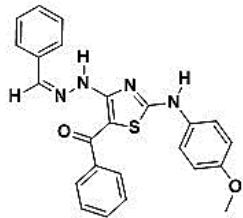
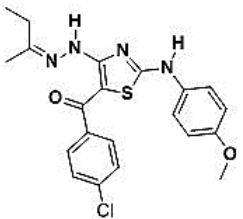

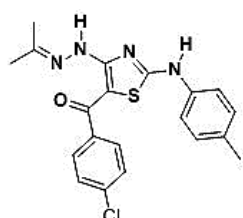
Entry	Structure	QPlogP (-2.0- 6.5) ^a	H-bond donor (0.0-6.0) ^a	H-bond acceptor (2.0- 20.0) ^a	No. of rotatable bonds (0.0-15) ^a	PSA(7.0- 200) ^a
1		4.89	1.0	6.2	9	78.16
2		4.85	1.0	5.7	9	84.98
3		4.97	1.0	5.7	8	84.29
4		4.91	1.0	5.0	7	78.49
^a Recommended range of properties						

Table 3.6. The predicted permeability properties of top scored ligands of 4-hydrazinothiazoles in 3LAU

Entry	Structure	QPPcaco (<25 poor, >500 great) ^a	QPPMDCK (<25 poor, >500 great) ^a	QPlogBB (-3.0-1.2) ^a
1		1615.05	1133.14	-0.74
2		1456.69	2279.85	-0.63
3		1411.51	1677.58	-0.64
4		1206.02	1999.58	-0.63
^a Recommended range of properties				

In addition to the calculation of pharmaceutically relevant properties, the percentage similarity of the tested ligands with an existing library of 1712 drug

molecules were also calculated using the software. Interestingly, we have found that within the ligands tested, the cyclohexylidene and benzylidene class of compounds in which R₃/R₄ with 4-nitrophenyl or 4-methoxyphenyl substitution showed similarity with gefitinib, a drug used for the treatment of certain breast and lung cancer, with a percentage of similarity ranging from 79.2-86.9% (Figure 3.18a). Moreover two derivatives in the cyclohexylidene class in which R₃/R₄ with 4-nitrophenyl showed a similarity towards raloxifene used in the prevention of osteoporosis in post-menopausal women (Figure 3.18b).

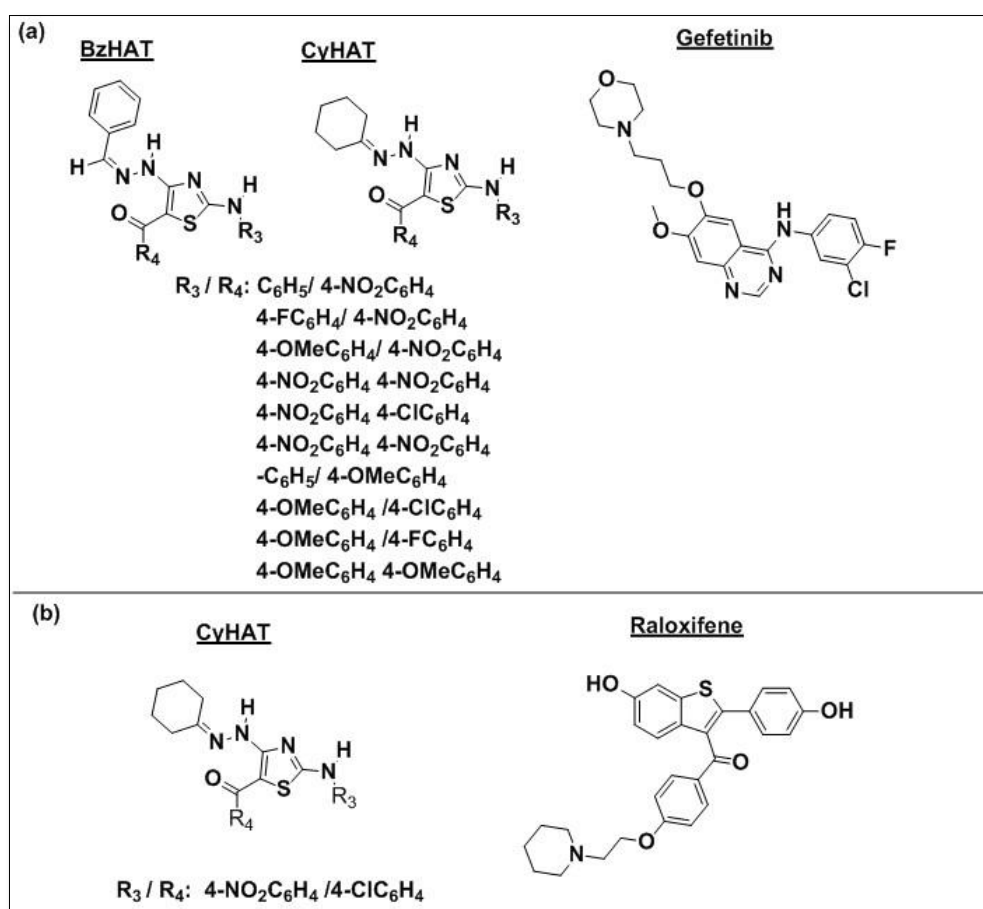


Figure 3.18. (a) The derivatives of BzHAT and CyHAT having similarity with gefitinib; (b) Derivatives of CyHAT showing similarity with raloxifene

The *in silico* evaluation of the ADME properties of the designed library of compounds further strengthened the potential of the 4-hydrazinothiazoles as a drug design scaffold which was further evaluated by *in vitro* anticancer screening experiments.

3.2.3. *In vitro* anticancer screening of 4-hydrazinothiazoles

Normal human cells have a limited life span and the dead cells are continuously replaced by new ones. Any irregularity in this programmed cell death or apoptosis lead to the uncontrolled multiplication of cells which is referred to as cancer. The conventional anticancer drugs has a factor of toxicity with different effects on different cell lines and are able to kill these rapidly dividing cells. In the anticancer drug discovery the preclinical screening is necessary to prioritize novel compounds for further development. *In vitro* cell culture assays (Monks *et al.*, 1991) are commonly used to evaluate the anticancer activity of new drug candidates and the ability of the tested compounds to inhibit the growth of cancer cells established either from human or animal tumors is taken as an indication of potential *in vivo* therapeutic efficacy.

To experimentally investigate the effect of 4-hydrazinothiazoles on tumor cell growth, in the present study, selected compounds from the synthesized library of 4-hydrazinothiazoles were screened for their anticancer activity against six human cancer cell lines (Table 3.7) using SRB (Sulforhodamine B) assay (Skehan *et al.*, 1990) and the studies were carried out at ACTREC, Mumbai. The anticancer drug Adriamycin (ADR) was used as a positive control for the comparison of the results.

Table 3.7. Cell lines used for the anticancer screening

Name of cell line	Name of panel
MCF-7	Breast
SW-620	Colon
HL-60	Leukemia
OVCAR-3	Ovary
SK-MEL-2	Melanoma
A549	Lung

From the synthesized library of 4-hydrazinothiazoles, thirteen compounds were screened individually for their anticancer activity and five compounds were screened in a mixture. Three consecutive experiments were carried out at four different concentrations of the compounds to access their ability to inhibit human cancer cell lines and the average dose response data was used to calculate three different parameters GI (Growth Inhibition), TGI (Total Growth Inhibition) and LC (Lethal Concentration). The screening results suggested that the breast cancer cell line, MCF-7, to be more fragile towards our tested compounds and all the tested compounds were showing $GI_{50} < 40 \mu\text{g/mL}$. The preliminary screening identified one isobutylidene (IBHAT-6) and one benzylidenehydrazinothiazole (BzHAT-5) (R_3 : 4-OMeC₆H₄ & R_4 : H) as active against MCF-7 (Figure 3.19a) and the cyclohexylidene (CyHAT-4) (R_3 : 4-OMeC₆H₄ & R_4 : H) counterpart as active against A549 (Figure 3.19b) with GI_{50} =2.32, 8.16 and 1.61 $\mu\text{g/mL}$ respectively. The GI_{50} values obtained for the tested compounds in six cancer cell lines are given in Table 3.8.

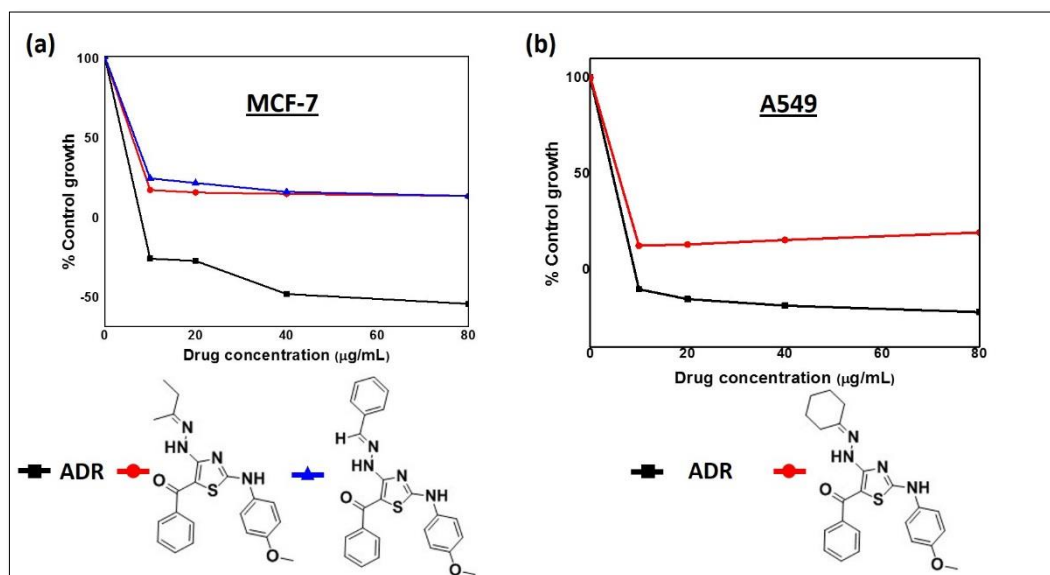
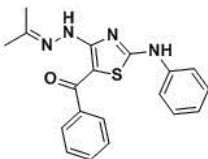
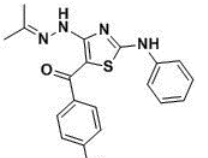
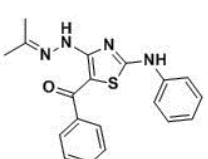
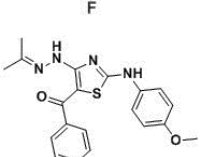
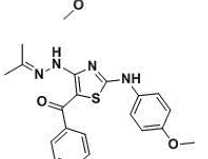
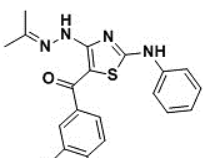
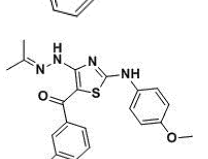
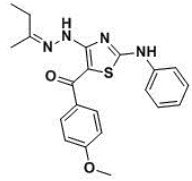
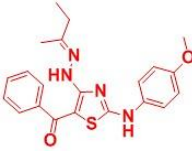
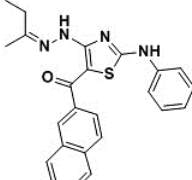
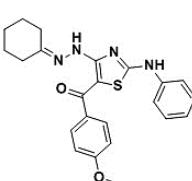
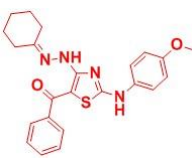
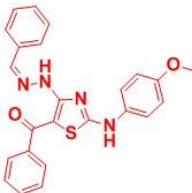


Figure 3.19. Growth inhibition curve of active compounds against (a) MCF-7; b) A549

Table 3.8. *In vitro* screening results of tested compounds^a

Sl. no.	Compound tested	GI ₅₀ value (µg/mL)					
		MCF-7	SW620	HL-60	A549	OVCAR-3	SK-MEL-2
1		31.29	>100	>100	>100	>100	>100
2		34.31	>100	>100	>100	>100	>100
3		34.42	>100	>100	>100	>100	>100
4		26.98	>100	35.59	29.95	59.7	>100
5		34.57	77.16	32.64	56.6	>100	>100
6		17.14	>100	50.07	64.15	66.7	91.7
7		16.51	>100	49.26	>100	95.4	>100

8		41.00	>100	>100	42.75	26.9	>100
9		2.32^a	39.12	29.26	11.52	55.02	35.14
10		24.87	>100	41.19	92.3	>100	>100
11		88.50	>100	48.4	96.8	>100	>100
12		16.27	29.70	35.40	1.61^a	22.70	22.70
13		8.16^a	43.06	37.36	27.60	36.09	30.80
^a Active compound							

The identified active compounds could be considered as structural analogues of DAT1, a well-known anticancer agent reported in the literature (Sengupta *et al.*, 2005) and we found that the analogues from all the four classes of 4-hydrazinothiazoles were active ($GI_{50} < 10 \mu\text{g/mL}$) or potentially active ($GI_{50} < 40 \mu\text{g/mL}$) against the tested cell lines. The activity of the compounds correlated with the predicted property similarity with anticancer drug gefetinib. The GI_{50} values obtained for the active compounds are shown in Figure 3.20.

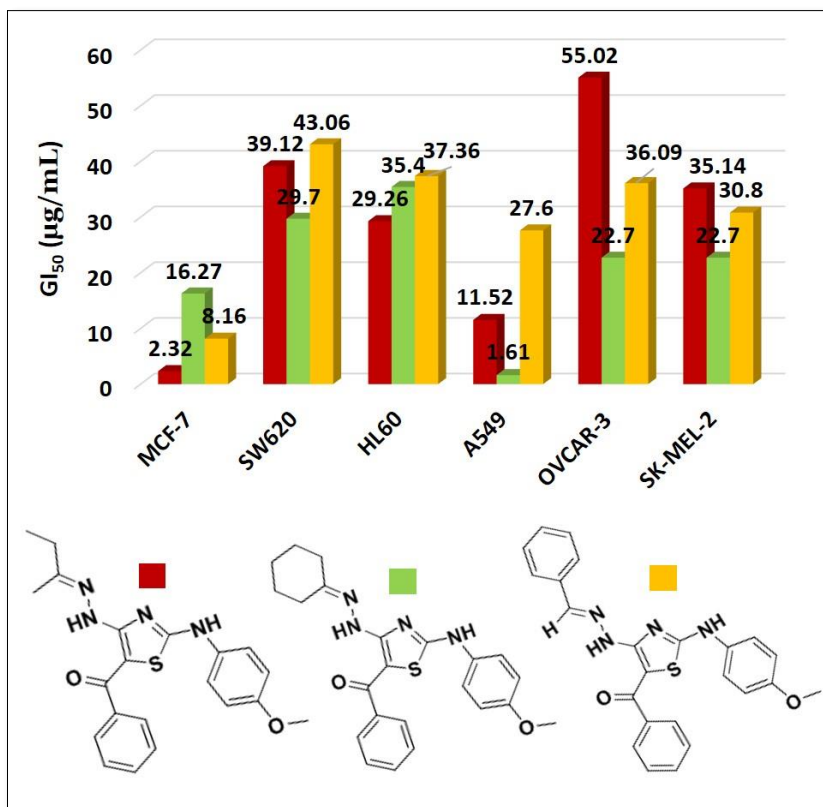


Figure 3.20. GI₅₀ chart of the active compounds in six cancer cell lines

The *in vitro* anticancer screening indicated that most of the compounds tested from 4-hydrazinothiazoles had a <50µg/mL dose-response towards the breast, leukemia and lung cancer cell lines whereas the colon, ovarian and skin melanoma cancer cells were found to be less prone to the tested compounds.

3.3. Experimental Details

3.3.1. Single crystal X-ray diffraction

Diffraction quality crystals of IPHAT-1 (C₁₉H₂₀N₄O₂S), IPHAT-2 (C₁₉H₁₉ClN₄O₂S) and CyHAT-1 (C₂₂H₂₂N₄OS) were developed from 1:1 EtOH/H₂O mixture by slow evaporation at room temperature. A similar procedure was followed for the development of BzHAT-2.EtOH (C₂₅H₂₃ClN₄O₂S) and BzHAT-2.MeOH (C₂₄H₂₁ClN₄O₂S) from aqueous ethanol (1:1) and aqueous

methanol (1:1) respectively. The crystals with 0.25 x 0.20 x 0.15 mm (IPHAT-1) and 0.30 x 0.20 x 0.20 mm (IPHAT-2), 0.25 x 0.20 x 0.15 (BzHAT-2.EtOH), 0.25 x 0.20 x 0.20 (BzHAT-2.MeOH) and 0.50 x 0.15 x 0.15 (CyHAT-1) were used for the XRD measurements and structural refinement.

Diffraction data were collected on Bruker Kappa APEX-II single crystal X-ray diffractometer equipped with graphite-monochromated Mo-K α radiation ($\lambda = 0.71073 \text{ \AA}$) for molecules IPHAT-1, BzHAT-2 and CyHAT-1. Enraf Nonius CAD4-MV31 single crystal X-ray diffractometer with graphite-monochromated Mo-K α radiation source ($\lambda = 0.71073 \text{ \AA}$) was used for the data collection of IPHAT-2. Crystallographic details for crystals were collected at T = 296 K (IPHAT-1, BzHAT), T = 293 K (IPHAT-2) and T = 302 K (CyHAT-1). Least-squares global refinement was used for the calculation of crystal cell constants. The structures were solved by direct methods using SHELXS and were refined by constrained full least-squares on F^2 with SHELXTL (Sheldrick, 1997). Graphics were generated using X-ray crystal analysis software, MERCURY 3.3. Packing coefficients of the compounds were calculated as:

$$\text{Packing coefficient} = \frac{Z \times \text{Volume/atom}}{\text{Unit cell volume}}$$

Where Z is the number of molecules per unit cell. The volume/atom was determined using the crystallographic software Olex-2. Summary of structural data for the molecules is provided in Table 3.9. All the crystal data were submitted to CCDC (The Cambridge Crystallographic Data Centre) and reference numbers are provided to enable the readers to access complete details of structure refinement.

Table 3.9. Summary of crystallographic data and structure refinement summary

Compound	IPHAT-1	IPHAT-2	BzHAT-2. MeOH	BzHAT-2. EtOH	CyHAT-1
CCDC reference	1002352	1002353	1052981	1052982	1052983
Formula weight	368.48	402.89	464.96	478.98	390.49
Space group	$P2_1/c$	$P2_1/c$	$P2(1)/n$	$P2(1)/n$	$P -1$
Crystal system	Monoclinic	Monoclinic	Monoclinic	Monoclinic	Triclinic
$a/\text{\AA}$	14.450 (5)	14.858 (5)	9.6388 (3)	9.6720 (2)	11.987 (16)
$b/\text{\AA}$	4.956 (5)	4.854 (10)	16.1889 (4)	16.4163 (3)	12.649 (16)
$c/\text{\AA}$	26.730 (5)	26.819 (8)	14.8442 (5)	15.2160 (3)	14.39 (2)
α (°)	90.0	90.0	90.0	90.0	102.66 (3)
β (°)	96.3 (5)	90.2 (10)	91.1 (10)	90.8 (10)	106.82 (2)
γ (°)	90.0	90.0	90.0	90.0	93.196 (12)
$V/\text{\AA}^3$	1902.68 (2)	1934.19 (10)	2315.90 (12)	2415.73 (8)	2021.00 (5)
ρ_{cald}	1.286	1.384	1.334	1.317	1.283
Z	4	4	4	4	4
Goodness-of-fit	1.094	1.025	1.036	1.055	0.605
R_I (all data)	0.0964	0.0612	0.0421	0.0515	0.1780
wR_2 [for $I > 2\sigma(I)$]	0.1826	0.1098	0.0897	0.1028	0.1079
Reflections (collected/independent)	12978/3337	13987/3394	17752/4084	17553/4119	8003/1748

3.3.2. ADME property calculation

All the ligand structures used in this study were constructed using the graphical tool, Maestro 9.6 available in Schrodinger LLC. Geometry optimization and partial atomic charge assignment of ligands were done with the help of Ligprep (Schrodinger LLC) using the Optimized Potentials for Liquid Simulations-all atom (OPLS-AA) force field. All the pharmaceutically relevant properties and physical descriptors of the optimized ligands were calculated using Qikprop 3.5 available in Schrodinger LLC. The recommended ranges for the descriptors were derived by comparing those with 95% known drugs. The physical descriptor values such as MW, octanol/water partition coefficient, H-bond donor/acceptor were compared with classical Lipinski's RO5. The oral bioavailability was calculated using Caco-2 and MDCK cell membrane models available in the software. The property similarity search of the compounds was done with a default library of 1712 known drug molecules to identify five similar orally available drug molecules.

3.3.3. *In vitro* anticancer screening

The compounds were screened for their anticancer activity using the colorimetric Sulforhodamine B (SRB) assay following the general protocol (Skehan *et al.*, 1990). The ability of the aminoxanthane dye (bright-pink) is used for measuring the cellular protein content. Six human cancer cell lines namely MCF-7, SW-620, HL-60, A549, OVCAR-3 and SK-MEL-2 were selected from the NCI's (National Cancer Institute) cell line panel. Three consecutive screening experiments were carried out for each compound in a 96 well plate (5×10^3 cells/well). The dose-response in each of the experiments was measured at four different concentrations (10, 20, 40 and 80 $\mu\text{g/mL}$) of the compounds in DMSO or alcohol and in each experiment Adriamycin was used as a positive control at the same concentration levels. The percentage growth was evaluated spectrophotometrically against controls that are not treated with test compounds. Using the seven absorbance measurements [time zero, (Tz), control growth, (C), and test growth in the presence of drug at the five concentration levels (Ti)], the

percentage growth was calculated at each of the drug concentrations levels. Percentage growth inhibition was calculated as

$$\frac{(Ti - Tz)}{(C - Tz)} \times 100 \text{ for } Ti \geq Tz \text{ and } \frac{(Ti - Tz)}{(Tz)} \times 100 \text{ for } Ti < Tz$$

Three dose response parameters were calculated for each experimental agent. Growth inhibition of 50 % (GI₅₀) was calculated from [(Ti-Tz)/(C-Tz)] x 100 = 50, which is the drug concentration resulting in a 50% reduction in the net protein increase (as measured by SRB staining) in control cells during the drug incubation. The drug concentration resulting in total growth inhibition (TGI) was calculated from Ti = Tz. The LC₅₀ (concentration of drug resulting in a 50% reduction in the measured protein at the end of the drug treatment as compared to that at the beginning) indicating a net loss of cells following treatment was calculated from [(Ti-Tz)/Tz] x 100 = -50. Values were calculated for each of these three parameters and compounds with GI₅₀ < 10µg/mL were considered to be active and a marginal value of 40µg/mL was set for potentially active molecules.

3.4. Conclusions

In conclusion, the crystalline forms from the four classes of 4-hydrazinotiazoles were studied by taking representative examples. The role of hydrazone moiety in the formation of unique nitrogen rich channels and the crystal packing arrangement were studied in detail. We found that the unique molecular assemblies formed by H-bonding and π - π stacking interactions can serve as suitable starting points for the design and development of synthetic channels for water/ions based on thiazole core. The *in silico* calculation of the pharmaceutically relevant properties of the designed 120 member library of molecules identified them to be with ADME properties in the recommended range for orally active drug molecules which suggest the ‘drug-likeness’ of the molecules. The experimental screening of thirteen compounds in six human cancer cell lines had identified two structural analogues of DAT1 as active against MCF-7 and one against A549 cancer cell lines.

Moreover, the *in vitro* screening has identified the tested compounds to be more prone toward breast, leukemia and lung cancer cell lines than towards colon, ovarian and skin melanoma cancer cells which were studied.

CHAPTER 4

VIRTUAL SCREENING OF 4-BENZYLIDENEHYDRAZINOTHIAZOLES IN AURORA KINASE PROTEINS

4.1. Background

The modern anticancer drug discovery is driven by pharmaceutically relevant macromolecular biological targets, often proteins, with significant roles in cellular signalling pathways. With the availability of a wide range of target proteins and large number of potentially active chemical compounds, the conventional methods of drug discovery becomes all the more risky to identify compounds with the right combination of selectivity and activity. Hence, considering the drawbacks, the time and cost expensive conventional methods in drug discovery have been replaced with computer aided drug design (CADD) over the past three decades (Jorgensen, 2004). The computational methods permeates through all the aspects of modern drug discovery (Sliwoski *et al.*, 2014) and can be broadly classified in to structure-based or ligand-based methods. Ligand-based drug design (LBDD) is indirect and based on the similarity of the ligand to previously known active ligands whereas structure-based drug design (SBDD) is a direct method that utilizes the information of both the target and the ligand for the prediction of the activity of a new chemical entity. Earlier by 2000, using the SBDD methods, about 42 compounds have reached clinical trials and seven compounds have become approved and marketed as drugs (Hardy and Malikayil, 2003).

Molecular docking is one of the most frequently used SBDD strategies due to its wide range of applications in the analysis of molecular recognition events such as binding energetics, molecular interactions and induced conformational changes. One of the main uses of this method is the screening of virtual compound libraries

known as virtual high-throughput screening (vHTS) for the identification of ‘hits’ from the library of compounds and further for the lead generation and optimization. This SBDD approach exploits the molecule’s ability to interact with a specific protein and to exert a desired biologic effect depending on its ability to favourably interact with a particular binding site on that protein. It is based on the hypothesis that the molecules that share those favourable interactions will be having similar biological effects and thereby novel compounds can be elucidated through the careful analysis of a protein’s binding site. The vHTS relies on large compound libraries and their impact on target proteins.

Protein phosphorylation, the addition of a phosphate group to one of the amino acid side chains of a protein, act as a molecular switch that turn the functioning of a protein and has been recognized as a global regulator of cellular activity (Cohen, 1982). The transfer of phosphates on to the proteins is catalysed by various enzymes that have certain common structural characteristics and falls in to one family of proteins called protein kinases (Ubersax and Ferrell Jr, 2007). Deregulation of these kinase activities leads to the aberrant phosphorylation of proteins which in turn drive to the hallmarks of cancer such as unchecked cell growth and proliferation. In clinical oncology, protein kinases constitute the second largest group of drug targets and are considered to be the major drug targets of the twenty first century (Cohen, 2002; Rask-Andersen *et al.*, 2014; Zhang *et al.*, 2009). So far different classes of kinase proteins have been studied as targets in anticancer drug development (Lapenna and Giordano, 2009) of which aurora kinases have gained much attraction (Carvajal *et al.*, 2006).

4.1.1. Structure and function of AURK-A and AURK-B

Aurora kinases (AURKs) are subgroup of serine/threonine protein kinases that are essential for accurate and equal segregation of genetic materials from parent to daughter cells and are overexpressed in a variety of tumor cell lines including (but not limited to) breast, colon, ovary and skin (Mountzios *et al.*, 2008; Nikonova *et al.*, 2013). There are three human homologues of Aurora kinases A, B and C with

difference in cell function during the mitosis of which AURK-A and AURK-B have been extensively studied for their efficiency as target for anticancer drug development (Andrews, 2005; Dar *et al.*, 2010; Kollareddy *et al.*, 2012). All the three classes of AURK are having an amino acid sequence length ranging from 309-403 with an N-terminal domain of β -pleated sheets and a C-terminal domain of α -helices. The catalytic C-domain of AURK-A and B are 71% identical with the conservation of amino acid residues. Adenosine triphosphate (ATP) is the natural ligand and the phosphate donor in AURK and the binding site for the ligand is lined by 26 amino acid residues. The C-terminal domain of AURKs are having conserved homology and all the Aurora proteins contain a destruction box, or D-box sequencing PxxRxxL recognized by APC/C (anaphase-promoting complex/cyclosome) at the C-terminal that mediates the proteasome degradation of a D-box containing protein. A conserved KEN motif, spanning 11-18 residues is present in both AURK-A and B which acts as a Cdh1 (Cadherin-1)-dependent APC recognition signal. Destruction also requires a short region in the N-terminal, which contains the A-box (activation domain) which is conserved in vertebrate Aurora kinases and contains a Ser53, which is phosphorylated during M phase. Mutation of Ser53 to aspartic acid, which can mimic the effects of phosphorylation, completely blocks Cdh1-dependent destruction of Aurora A. Figure 4.1 depicts the structures of AURK-A and B (Bolanos-Garcia, 2005; Libertini *et al.*, 2010).

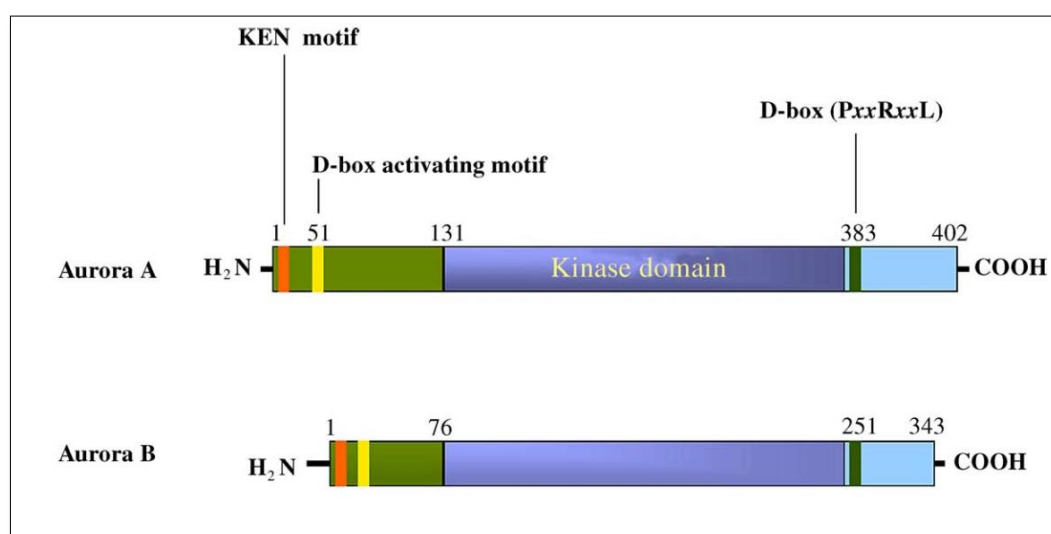


Figure 4.1. Domain organisation of AURK-A and B

AURK-A regulates the cell cycle events occurring from late S phase through M phase which include centrosome maturation, mitotic entry, centrosome separation, bipolar-spindle assembly, chromosome alignment, cytokinesis and mitotic exit. Whereas AURK-B is involved in chromosome segregation, spindle-checkpoint and cytokinesis. The phosphorylation of the threonine residue, Thr288, present in the activation loop of AURK is essential for the activity of the protein. The less conservative N-terminal domain of the AURKs determines selectivity during protein-protein interactions and this domain is believed to be involved in substrate binding and cellular localization. The small molecules which are able to occupy the catalytic binding site of AURK can affect the enzymatic activity of proteins and thereby induce the cell mitosis. It is to be noted that since AURKs are only expressed and activated during mitosis, drugs that target these proteins will not be having any adverse effect towards non-proliferating cells. Furthermore, alteration in p53 pathways are common in human cancers and it is found that cells lacking a p53-mediated post-mitotic checkpoint are highly responsive to Aurora inhibition. Last but not least, since AURK inhibitors do not bind to tubulin, they do not induce neuropathy, which is one of the main side effects of classical antimitotic drugs. All these factors increase the therapeutic index of aurora inhibitors in cancer treatment.

4.1.2. Different modes of kinase inhibition

The hydrophobic cleft alias hinge region formed between the N-lobe and C-lobe acts as the ATP-binding site in the protein kinases in such a way that the adenine moiety of ATP is H-bonded with hinge region and the phosphate backbone will be oriented towards the solvent exposure region. A set of conserved residues in the catalytic domain catalyses the transfer of γ -phosphate of ATP to the hydroxyl oxygen of Serine (Ser), Threonine (Thr) or Tyrosine (Tyr) residue of protein substrate bind to the hydrophobic cleft. Majority of the protein kinases share a common DFG (Asp-Phe-Gly) motif in the ATP site that can exist in two conformations (DFG-in and DFG-out) in response to the phosphorylation. Inhibitors which are able to stabilize the inactive DFG-out conformation are

considered to be superior in terms of specificity than the inhibitors with DFG-in conformation. The 2D (Two dimensional) diagram of ATP binding site of protein kinases is shown in Figure 4.2. The inhibitors that are bound to the ATP binding site through H-bonding interactions with the hinge region will block the protein-protein interaction between the AURK-A and cofactor or the substrate to be phosphorylated and are termed as Type I inhibitors. If the inhibitor is bound to the ATP binding site exploiting the H-bonding interactions, and the DFG residues in the activation loop are folded away from the binding site then, the phosphate group transfer will be blocked and such type of inhibition is termed as Type II inhibition.

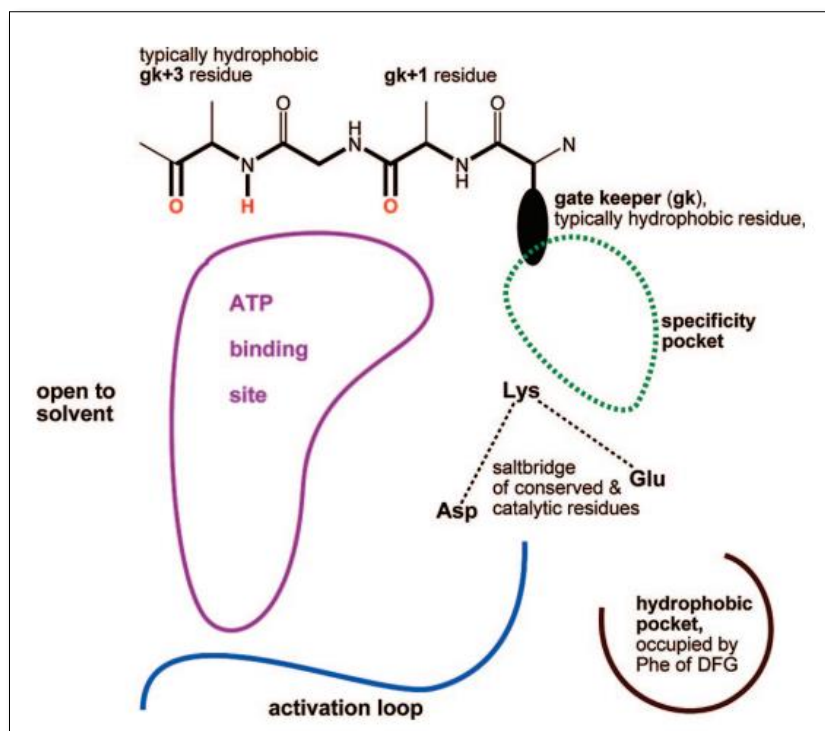


Figure 4.2. 2D representation of the kinase binding site (Ghose *et al.*, 2008)

The clearly established role for the AURKs in mitosis and the evidence of their overexpression in a number of cancers continue to motivate the researchers to develop novel small molecule inhibitors of these proteins and make use of it as a powerful antitumor strategy. With ample background on different modes of AURK inhibitions, coupled with the promising preliminary docking result from the designed 120 member library of 4-hydrazinothiazoles in AURK protein active site,

we were encouraged to proceed with the detailed study of binding interactions with an expanded library of compounds.

4.2. Results and Discussion

4.2.1. Expansion of virtual library

The designed trivariant scaffold (diversity elements at *C2*, *C5* and *C4* of thiazole ring) allows for a wide range of diversity multiplication in its structure and by exploring the possibilities of diversity at *C4*, four classes of 4-hydrazinothiazoles were designed. These include isopropylidene (IPHAT), isobutylidene (IBHAT), cyclohexylidene (CyHAT) and benzylidene (BzHAT) family of molecules by varying the carbonyl components. Among these classes, benzylidene family of 4-hydrazinothiazoles has still wider scope of introducing more number of functional groups at the *C4*, owing to the presence of phenyl ring. Hence BzHAT family was chosen for the expansion of virtual library and for further molecular docking studies in AURK pockets. The unsubstituted phenyl rings have been designated as **A**, **B** and **C** in the core structure for the expansion of virtual library of 4-benzylidenehydrazinothiazole (Figure 4.3) and monosubstituted benzenoids (ortho, meta and para) were chosen as the functional group variants. For the present study, a virtual library of 22500 ($R_1 \times R_2 \times R_3$: 36x25x25) ligands of BzHAT was designed by choosing different combinations of functional groups as given in Table 4.1. The functional groups for the designed library was chosen by considering the commercial availability of reagents for the synthesis of 4-benzylidenehydrazinothiazoles by the optimized [4+1] route. The designed structures in the expanded library were then optimized using OPLS force field and the 3D geometries thus obtained were used for further studies.

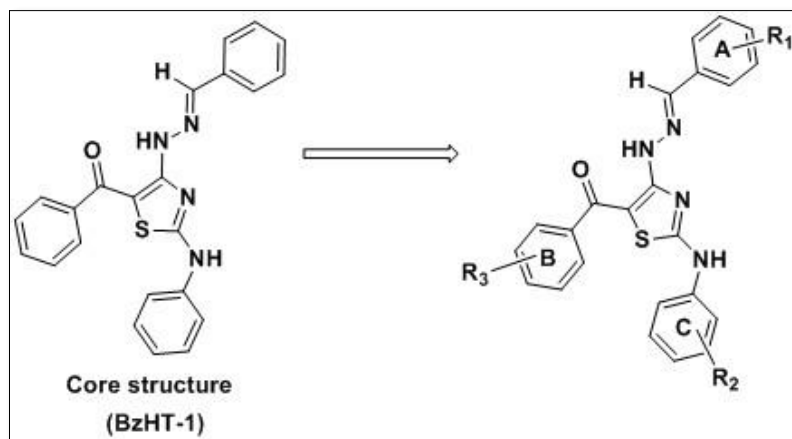


Figure 4.3. The structure of the core compound used for the expansion of virtual library

Table 4.1. List of functional groups used for the expansion of virtual library

R₁ (o/m/p)	R₂ (o/m/p)	R₃ (o/m/p)
H	H	H
-CH ₃	-CH ₃	-CH ₃
-OCH ₃	-OCH ₃	-OCH ₃
-OCH ₂ CH ₃	-OCH ₂ CH ₃	-OCH ₂ CH ₃
-F	-F	-F
-Cl	-Cl	-Cl
-Br	-Br	-Br
-I	-I	-I
-NO ₂	-NO ₂	-NO ₂
-OH	-	-
-CHO	-	-
-COOH	-	-
-NH ₂	-	-

4.2.2. *In vitro* anticancer screening of BzHATs

As mentioned previously, *in vitro* anticancer screening of the tested 4-hydrazinothiazoles (BzHATs) has identified a derivative of 4-benzylidenehydrazinothiazole, **BzHAT-5** ($R_1=H$, $R_2=4-OMeC_6H_4$ & $R_3=H$) as active against breast cancer cell line MCF-7 in micromolar concentrations. It was found that the molecule is having potential activity against all the other five cancer cell lines (A549, SW-620, HL-60, SK-MEL-2, OVCAR-3) tested. Motivated by the preliminary results obtained for the BzHAT derivative, eight more derivatives from the expanded library were screened for their anticancer activity against the previously tested six human cancer cell lines- MCF-7, SW620, HL-60, A549, OVCAR-3 and SK-MEL-2. It was found that all the eight compounds tested were responsive towards MCF-7 cell lines and are having a $GI_{50} < 50 \mu g/mL$. From the set of compounds tested, we have found that halogen substitution on ring **A** or **B** reduces the dose response of the compounds towards the tested cancer cell lines whereas methyl or nitro substitution increases the dose responsiveness of the compounds. The molecules were screened by SRB assay using Adriamycin as positive control and the studies were done at ACTREC, Mumbai. The structure of the derivatives that were screened for their anticancer activity along with the corresponding GI_{50} values in different cell lines are listed in Table 4.2. The experimental screening results suggest that 4-benzylidenehydrazinothiazole with – Me substitution on both ring **A** and **B** is responsive ($GI_{50} < 35 \mu g/mL$) towards all the cell lines tested except the leukemia cell line HL-60 (Figure 4.4).

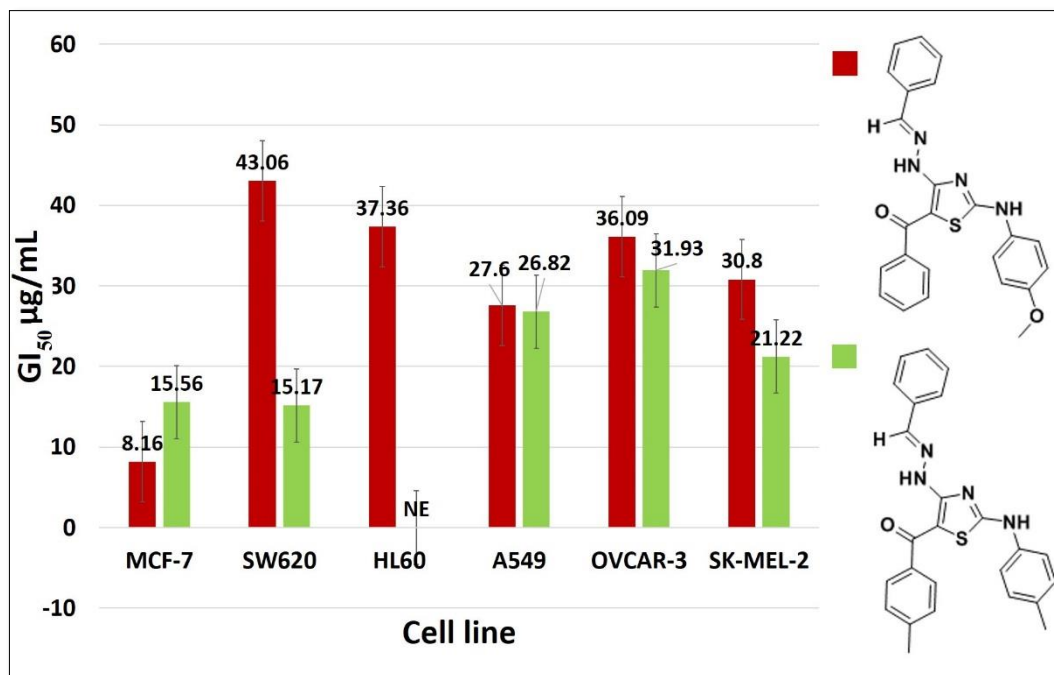
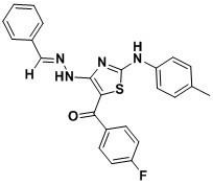
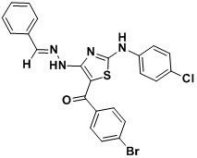
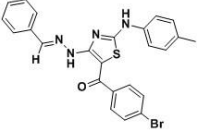
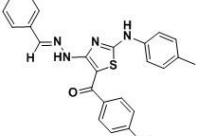
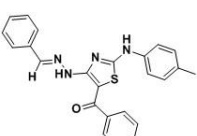
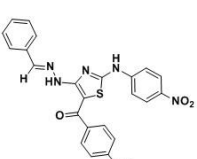


Figure 4.4. Comparison of GI₅₀ values of active compound and methyl derivative of BzHAT

Table 4.2. *In vitro* screening results of tested BzHAT derivatives

Sl. no.	Compound tested	GI ₅₀ value (µg/mL)					SK-MEL-2
		MCF-7	SW620	HL-60	A549	OVCAR-3	
1		43.55	>100	>100	>100	>100	>100
2		30.62	>100	>100	>100	>100	45.62

3		38.46	>100	>100	>100	>100	>100
4		38.04	>100	>100	>100	>100	68.85
5		40.58	>100	>100	>100	>100	>100
6		27.00	53.26	>100	75.40	>100	64.89
7		15.56	15.17	NE [#]	26.82	31.93	21.22
8		18.69	>100	>100	22.35	47.43	35.29
<hr/> [#] Not examined							

The phase contrast microscopic images showing morphological changes observed in cells exposed to methyl compound along with the control are given in Figure 4.5. It was found that the cells exposed to the BzHAT derivative lost their normal morphology and shape. The cells treated with the compound was observed to be more rounded and less adherent than the control.

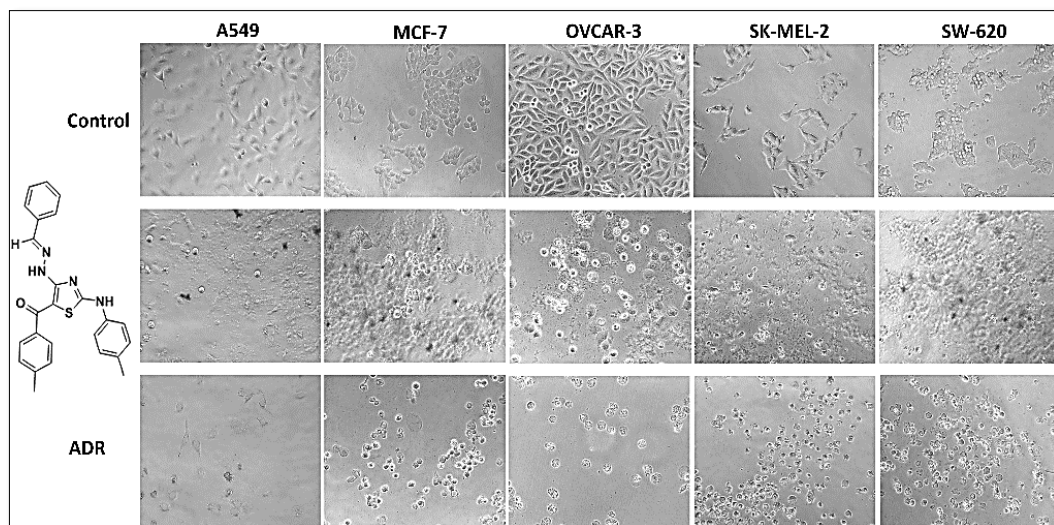
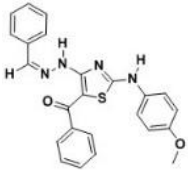
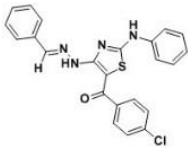
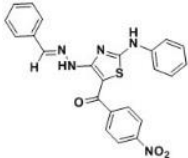
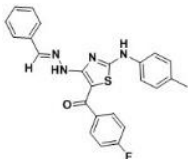
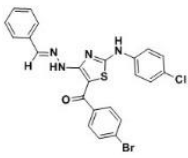
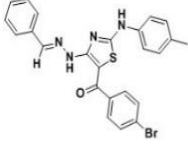
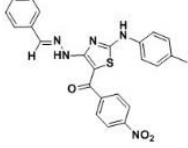


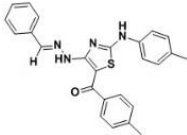
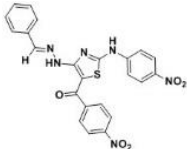
Figure 4.5. Phase contrast images of cell lines treated with methyl derivative of BzHAT

4.2.3. *In silico* ADME property calculation

The ‘drug-likeness’ of the expanded library of 4-benzylidenehydrazinothiazoles were studied by the *in silico* ADME prediction using Qikprop. It was found that the molecular weight of 99% designed molecules were in the range of 398-724 in comparison with the inbuilt library of orally active drug molecules. All the molecules in the library were predicted with 1-2 H-bond donor and 5-8 H-bond acceptor functionalities in aqueous solution which is within that recommended by RO5. Lipophilicity of the molecules calculated as a function of octanol/water partition coefficient was found to be in the range of 2.5-6.5 for 92% of the molecules whereas for 8% of the molecules it exceeded the value. Polar surface area of the molecules were found to be in the range of 74-193 Å² which is very much in the recommended range for drug molecules and the results predict the good oral bioavailability of the designed molecules. It was found that the calculated number of rotatable bonds of the molecules are also well within the recommended range. Table 4.3 shows the calculated values of physical descriptors of BzHAT molecules that were screened for their anticancer activity.

Table 4.3. The physical descriptors of BzHAT derivatives screened for anticancer activity

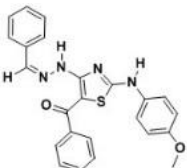
Entry	Structure	QPlogP (-2.0- 6.5) ^a	H-bond donor (0.0-6.0) ^a	H-bond acceptor (2.0- 20.0) ^a	No. of rotatable bonds (0.0-15) ^a	PSA(7.0 -200) ^a
1		4.89	1.0	6.2	9	78.16
2		5.59	1.0	5.5	8	67.69
3		4.38	1.0	6.5	9	112.61
4		5.65	1.0	5.5	8	67.68
5		6.16	1.0	5.5	8	67.69
6		5.98	1.0	5.5	8	67.69
7		4.69	1.0	6.5	9	112.61

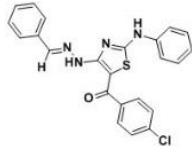
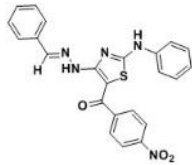
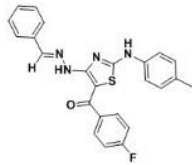
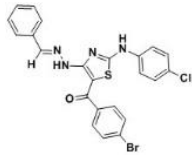
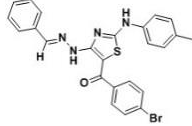
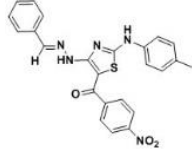
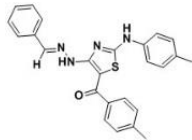
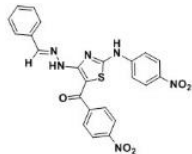
8		5.83	1.0	5.5	8	72.79
9		3.66	1.0	7.5	10	157.53

^a Recommended range of properties

The intestinal membrane permeability properties, an indirect measure of oral absorption ability of the compounds, were calculated using Caco-2 (Colon carcinoma) cell monolayers and MDCK (Madin-Darby canine kidney) cell models. The calculated results suggested that 99% of the molecules had both Caco-2 cell and MDCK cell permeability above 500 nm/s which would suggest a good oral absorption of the molecules. It was observed that most of the derivatives with nitro group substitution at R₁, R₂ or R₃ had lowest predicted oral bioavailability. Permeability across blood-brain barriers (BBB) of 99% of the designed molecules were found to be in the recommended range (-3.0-1.2). Table 4.4 shows the predicted membrane permeability values of BzHAT molecules that were screened for their anticancer activity.

Table 4.4. The predicted permeability properties of BzHAT derivatives screened for anticancer activity

Entry	Structure	QPPcaco (<25 poor, >500 great) ^a	QPPMDCK (<25 poor, >500 great) ^a	QPlogBB (-3.0-1.2) ^a
1		1615.05	1133.14	-0.74

2		1886.51	3320.22	-0.49
3		224.22	134.56	-1.78
4		1889.79	2433.06	-0.56
5		1884.60	8805.88	-0.32
6		1885.55	3568.09	-0.50
7		224.19	134.53	-7.3
8		1406	928	-0.91
9		26.69	13.48	-7.38
<hr/> ^a Recommended range of properties <hr/>				

The calculated ADME properties of the molecules indicated that pharmaceutically relevant properties of 90% of the molecules in the designed library are well within the recommended range for drug molecules which would suggest the ‘drug-likeness’ of the tested compounds and justify the potential of the system in drug discovery.

4.2.4. *In silico* binding studies of 4-benzylidenehydrazinothiazoles

The *in vitro* anticancer screening of synthesized derivatives of BzHAT has proven that all the tested compounds are having potential growth inhibitory activity against MCF-7 cell lines. We correlated our results with the protein overexpression in breast cancer cell lines which are reported with overexpression of AURK proteins. This prompted us to conduct a detailed study of interactions of the designed library of BzHAT molecules in AURK proteins. The *in silico* binding studies were carried out in the active sites of six AURK-A isomers and one AURK-B protein crystal structures obtained from the protein data bank (PDB). The details of the protein crystal structures are given in Table 4.5.

Table 4.5. Details of the protein crystal structures used for molecular docking

Class of protein	PDB ID	Resolution (Å)	Chain length
AURK-A	2BMC	2.6	306
AURK-A	2X6D	2.8	285
AURK-A	3E5A	2.3	268
AURK-A	3COH	2.7	268
AURK-A	3HA6	2.3	268
AURK-A	3UOK	2.9	279
AURK-B	4AF3	2.7	292

All the X-ray crystal structures obtained for the protein inhibitor complex were optimized prior to the docking studies using protein preparation and refinement utility provided by Schrodinger LLC and partial atomic charges were

assigned using OPLS-AA force field. The predicted binding modes of the co-crystallized ligands in the active sites of the respective proteins by re-docking were in cross correlation with the interactions obtained from the PDB data bank and thus the docking protocol has been validated (Figure 4.6).

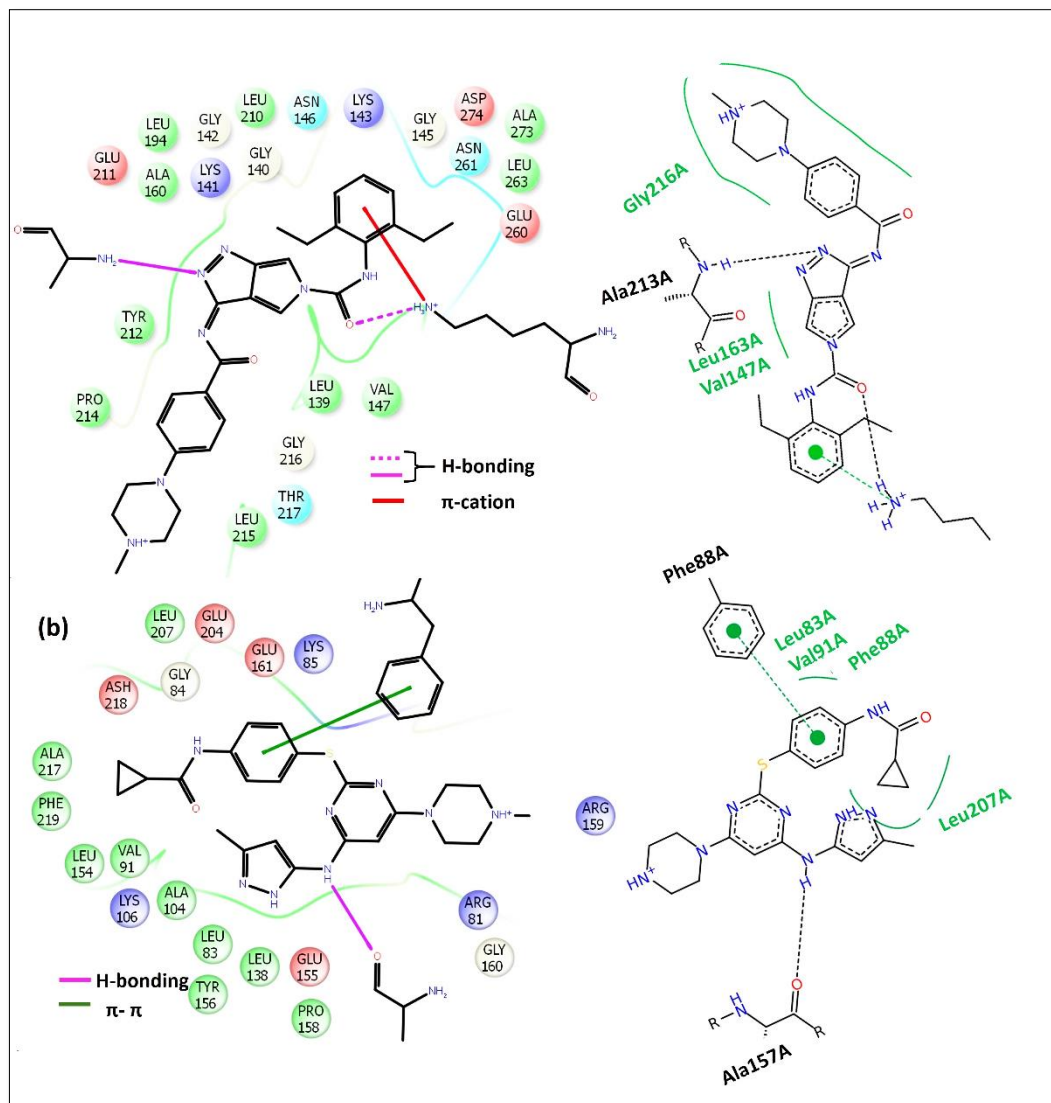


Figure 4.6. The predicted 2D interaction diagram of native ligands in active sites of (a) 2BMC, (b) 4AF3; The interactions obtained by X-ray diffraction are shown on the right side of the figure

4.2.4.1. Binding interactions of the core structure

The core molecule, **BzHAT-1**, selected for the expansion of BzHAT library had unsubstituted benzenoid rings **A**, **B** and **C**. The *in silico* binding studies of **BzHAT-1** in the active sites of 2BMC protein (Figure 4.7a) showed that the molecule was bound to the front pocket I (FP-I) located between solvent exposed loop and the DFG-motif of the hydrophobic front cleft of ATP binding site with DFG-out like conformation. The molecule was bound to the cleft in such a way that ring **B** occupied in the adenine pocket (AP) of ATP and was completely enclosed by the hydrophobic residues of the hinge whereas ring **A** and ring **C** were in the solvent exposure regions of the protein. The molecule was found to be non-hinge binder *i.e.*, no H-bonding interactions were predicted with the hinge residues, whereas the –NH at the C4 of thiazole ring was acting as a H-bond donor to the gate area (GK) residue Ala273 ($d_{A..H}=2.6\text{\AA}$) similar to that reported in bisindolyl maleimide based PDK1 (3-phosphoinositide dependent protein kinase-1) inhibitor LY333531 (Komander *et al.*, 2004). In 2X6D protein, the molecule bound to the same hydrophobic front cleft of the hinge region where the molecule was H-bonded to Arg137 ($d_{A..H}=2.6\text{\AA}$) and ring **C** formed π - π stacking interaction with the same residue with a DFG-in (active) conformation (Figure 4.7b). The core molecule occupied the FP-I of 3COH with ring **B** in the AP and ring **A** in the phosphate binding pocket as in the case of 2BMC (Figure 4.7c). The molecule was stabilized in the pocket by H-bonding interactions between C2 –NH and Leu139 residue of the β_2 sheet with a distance of $d_{A..H}=2.5\text{\AA}$. Moreover a π - π stacking interaction was observed between Tyr219 of αD in the C-lobe with an inactive DFG-out conformation. In 3E5A, the molecule occupied the FP-I (Figure 4.7d) with a 180° ring flip of the thiazole ring which resulted in hydrophobic enclosure of ring **A** and **C** whereas ring **B** was completely exposed to the solvents. The molecule appeared to be stabilized in the binding pocket through π - π stacking interaction between thiazole ring and Phe144 of the G-loop with active DFG-in conformation. In 3HA6, the core molecule was bound to the front cleft (Figure 4.7e) of the hinge region (ring **B**) and extended towards the gate area (ring **A** and **C**) due to the conformational change of G-loop especially Phe144 and Lys143 residues. The

DFG-motif of the protein attained an active conformation by the binding of molecule. The binding pose of the molecule was stabilized by π -cation interaction formed between ring **B** and Lys162 in the β_3 sheet along with H-bonding ($d_{A..H}$ = 2.2 Å) with –N at C4. The molecule was further observed with π - π stacking interaction of ring **C** with DFG+1 residue Trp277 in the catalytic loop.

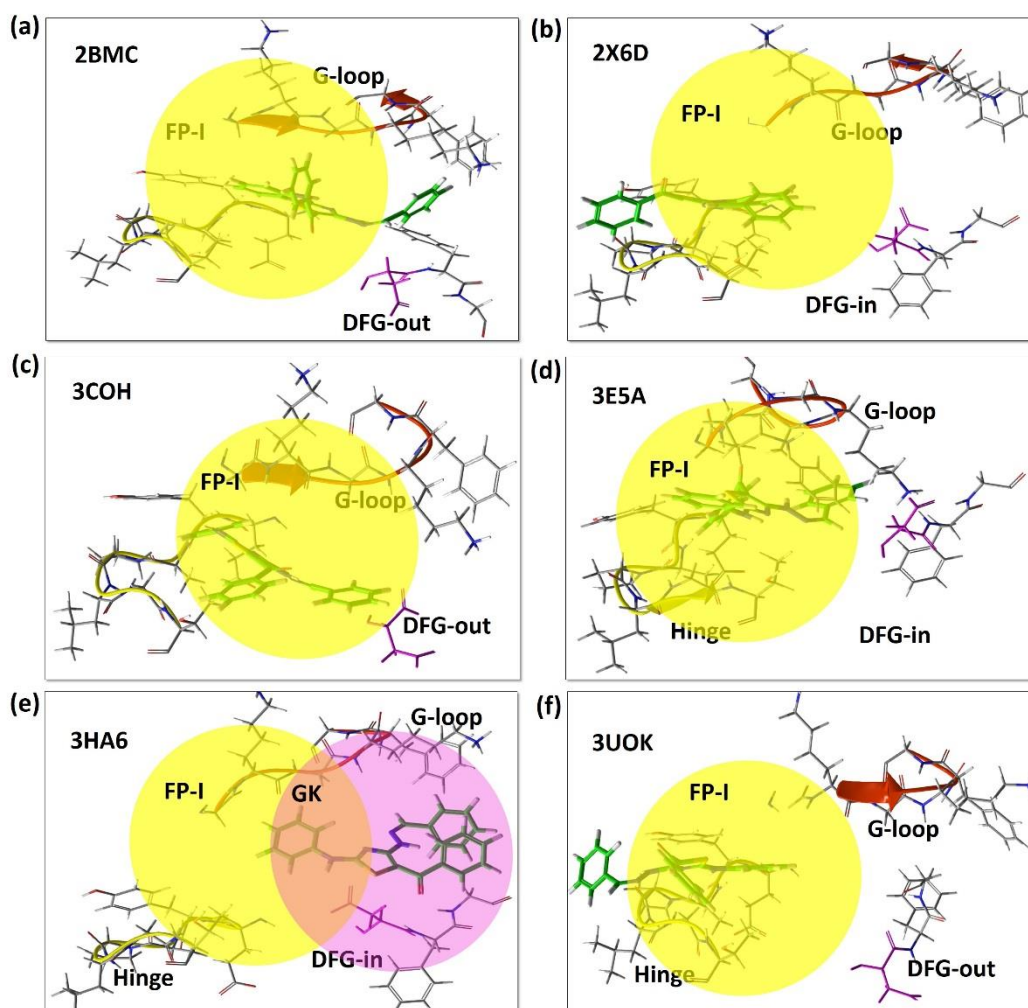


Figure 4.7. The 3D binding site of **BzHAT-1** (core structure) in AURK-A proteins; Asp residue of DFG-motif is shown in purple colour and the ligand C-atoms are shown in green colour; FP-I(yellow) and gate area (purple) are represented in coloured spheres

In 3UOK, the molecule was found to be hinge binder, the C2 –NH was H-bonded to Ala213 ($d_{A..H}$ = 2.1 Å) of the hinge region of the protein with DFG-out conformation (Figure 4.7f). The molecule occupied the front pocket of the ATP

4.2.4.2. Binding interactions of the active compound, 5-benzoyl-4-benzylidenehydrazino-2-(4-methoxyphenylamino)thiazole

The *in vitro* anticancer screening of the synthesized members from the library of 4-benzylidenehydrazinothiazole proved the dose responsiveness of the tested derivatives against breast cancer cell line MCF-7 with an average GI_{50} value of 28 $\mu\text{g/mL}$. The experimental screening of nine molecules from the synthesized library has identified an active compound ($R_1=\text{H}$, $R_2=\text{p-OMe}$, and $R_3=\text{H}$) from the BzHAT library with $GI_{50} < 10 \mu\text{g/mL}$. The reported overexpression of aurora proteins in breast cancer cells motivated us to select the derivative as a ‘hit’ for the detailed binding site interaction studies of BzHAT library of compounds in the active sites of the aurora family of proteins. The molecule was bound to the FP-I of the 2BMC protein and as in the case of the core structure. The molecule was found to be a hinge binder with H-bonding interaction between Ala213 of the active site and C2 –NH of the ligand at a distance of 2.0Å ($d_{\text{A..H}}$). Apart from this –NH at the C4 of the thiazole ring was H-bonded to Leu139 ($d_{\text{A..H}}=1.9\text{\AA}$) and the C=O was forming a salt bridge with Arg137 which also contributed to the affinity of the compound towards the binding pocket. It was observed that ring **A** and **C** were completely exposed to the solvents whereas ring **B** was in the hydrophobic enclosure of adenine binding pocket with DFG-out conformation. The predicted binding pocket and the interactions of the molecule are comparable with a pyridoindole Aurora inhibitor TAK-901 in phase I trial and Adriamycin, a well-known anticancer drug in the market. In 2X6D, where the DFG-motif is adopting an active conformation, the molecule demonstrated an ATP competitive Type I binding mode through H-bonding interactions between Ala213 of the hinge region and C2 –NH of the ligand at a distance of 2.3Å ($d_{\text{A..H}}$) with ring **B** occupying the adenine pocket. Further, the molecule was stabilized by π - π stacking interaction of ring **B** with Arg137 residue. The comparison of binding interactions of the molecules with known aurora inhibitors identified that the binding mode of the compound was comparable with CCT137690, an imidazopyridine derivative. In 3COH, the molecule was found to be a hinge binder through H-bonding interaction with the Ala213 of the hinge region through the p-OMe ($d_{\text{A..H}}=2.0\text{\AA}$) substituent on

the ring **B**. Here the molecule was located in FP-I of the protein and was further stabilized in the pocket through H-bonding interaction of C2 –NH with Leu139 ($d_{A..H}=2.0\text{\AA}$) residue of β_2 sheet. Ring **C** occupied in the ribose binding site of ATP formed a π - π stacking interaction with Tyr219 of the C-lobe. Comparison of the docked structures obtained for well-known kinase inhibitor imatinib and the drug Adriamycin in the proteins were found to be having the same binding pocket of the protein with similar binding interactions. The active molecule was bound to the hinge region of the 3E5A protein with H-bonding interaction between C2 –NH and Pro214 with a distance of 2.1\AA ($d_{A..H}$) in a Type I manner. The ring **B** was exposed to the solvent regions of the protein whereas ring **A** and **C** were completely buried in the hydrophobic residues of the protein. The binding mode of the compound was found to be comparable with a highly selective 2-aminothiazole containing AURK-A inhibitor, VX-689. In 3HA6 protein, the molecule was bound to the hinge region in Type I manner through H-bonding interaction between p-OMe and Ala213 ($d_{A..H}=2.0\text{\AA}$). Here the binding pocket of the molecule extended towards the gate area as in the case of core structure **BzHAT-1** and the molecule was stabilized by π -cation interaction between ring **A** and Ly162 of β_3 sheet. The binding pose of the molecule was found to be similar to that of imatinib and a thiazole containing aurora inhibitor SNS-314. The molecule was bound to 3UOK active site in Type I interaction mode where the C2 –NH of the ligand was H-bonded to Ala213 of the hinge region. Further, the ligand was stabilized by a salt bridge formed between –N at C4, C=O and Arg137 residue, π - π stacking between ring **C** and Arg220. The kinase inhibitors imatinib and VX-689 are found to be bound to the same binding pocket of the compound with similar interactions. Figure 4.9 shows the 3D binding mode of the active molecules in tested AURK-A proteins.

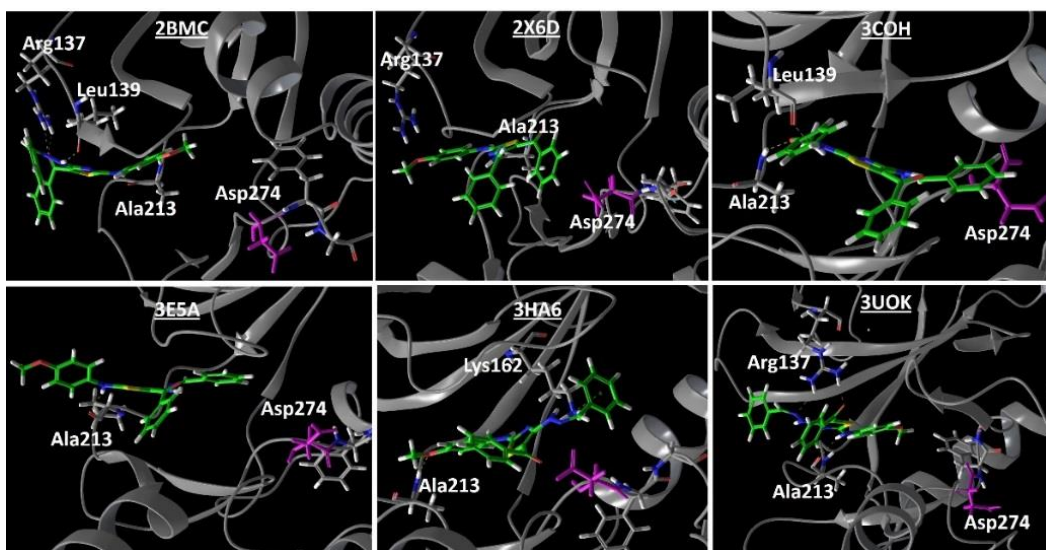


Figure 4.9. The 3D binding site of the **BzHAT-5** (active molecule) in AURK-A proteins; Asp residue of DFG-motif is shown in purple colour and the ligand C-atoms are shown in green colour

In all the cases the binding of the molecules in the hydrophobic front pocket resembled the binding mode of the well-known 2-aminothiazole containing anticancer drug dasatinib in Abl (Abelson murine leukemia) kinase (Tokarski *et al.*, 2006). As in the case of dasatinib, 2-aminothiazole part of the active compound which include ring **B** was found to be the hinge binder and occupied in the adenine binding pocket. Ring **A** and **C** of the compound were pointing towards ribose site or phosphate binding site whereas in dasatinib substitution at the C5 of thiazole was extending towards the back cleft of the protein binding site (Figure 4.10).

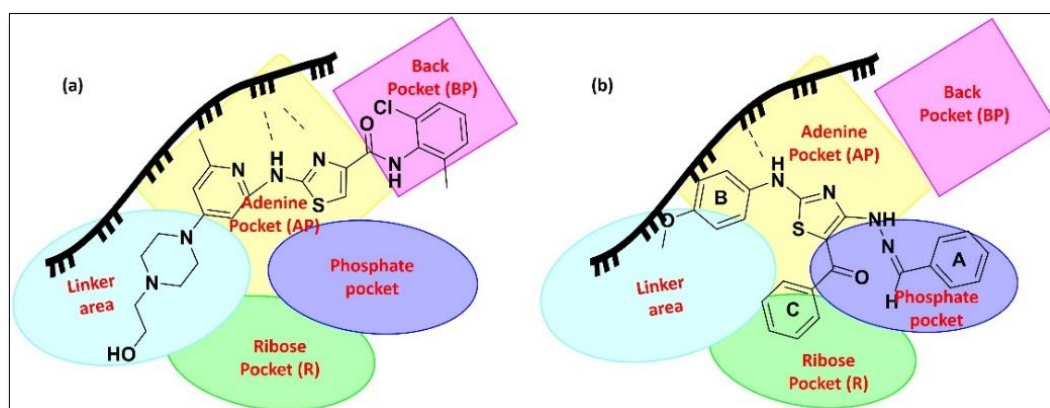


Figure 4.10. Binding modes of (a) dasatinib in the active site of c-Abl, (b) **BzHAT-5** in the active site of AURK-A

The binding site prediction of the active compound in 4AF3 (AURK-B) showed that the molecule is a hinge binder which is H-bonded to the hinge region through C=O of the ligand and it was found that the ring **B** was pushed towards the solvent exposure region of the protein. Both ring **C** along with the thiazole ring occupied the adenine pocket whereas and ring **A** was towards the phosphate binding site of the protein where the DFG-motif is in the inactive form (Figure 4.11). The binding mode of the molecule resembled that of a quinazoline derivative of aurora inhibitor ZM447439.

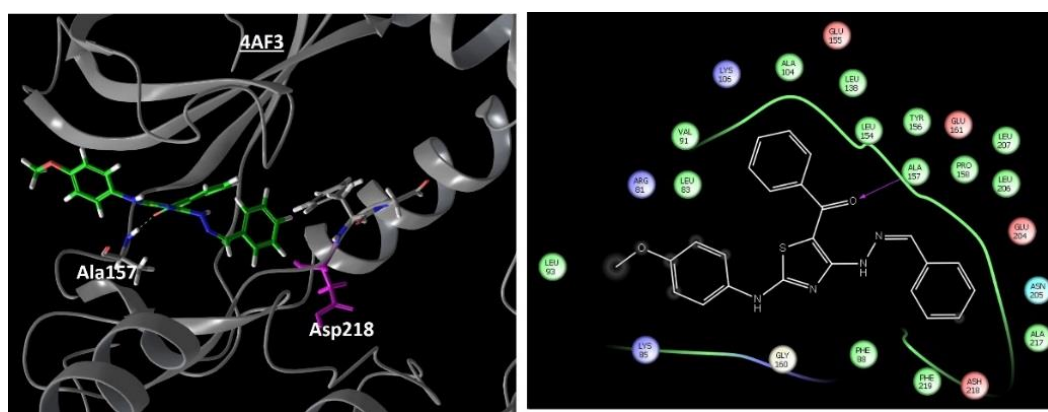


Figure 4.11. The 3D binding site of **BzHT-5** (active molecule) in AURK-B protein 4AF3; Asp residue of DFG-motif is shown in purple colour and the ligand C-atoms are shown in green colour; The 2D interaction diagram of the molecule is given in the right hand side of the figure

The binding studies of the active compound in the tested aurora proteins proved the potential of the molecule to act as ATP competitive inhibitor in both AURK-A and B. In both classes of proteins the molecule was predicted as acting as H-bond donor (AURK-A) or H-bond acceptor (AURK-B) which would bind to the hinge region. With the promising *in silico* binding results by selecting the active compound viz; 5-benzoyl-4-benzylidenehydrazino-2-(4-methoxyphenylamino)thiazole BzHT-5, as the ‘hit’ we then proceeded with the study of effect of substituent at ring **A** and **C** of active compound on protein binding as our preliminary studies on hit to lead generation and optimization.

4.2.4.3. Effect of substitution on ring A of active compound 5-benzoyl-4-benzylidenehydrazino-2-(4-methoxyphenylamino)thiazole

It was identified that the selected 'hit' molecule bound to the hydrophobic pocket formed by the hinge residues where ring **B** of the compound was completely immersed in the pocket whereas both ring **A** and **C** were exposed to the solvents. The influence of substitution on ring **A** was next studied using the list of substituents as given in Table 4.3. Substitution on ring **A** resulted in low docking score for the derivatives in the 2BMC protein as the binding of the molecules shifted with a distance of $\sim 9\text{\AA}$ (with respect to thiazole core) from the Ala213 residue of the hinge region and extended towards the gate area of the protein. Irrespective of the substituent on ring **A**, the derivatives were bound to the hinge region through H-bonding between Ala213 residue and the $-\text{OMe}$ ($d_{\text{A...H}} \sim 2.4\text{\AA}$) substitution on ring **B**. It was also observed that the orientation (para, meta and ortho) of substituents on ring **A** has little effect on the binding interactions of the molecules as all of the three derivatives were attaining a similar binding pose in the 2BMC active site. In 2X6D, ring **A** with bulky groups such as $-\text{OEt}$ or $-\text{Br}$ and highly electron withdrawing groups such as $-\text{NO}_2$ and $-\text{CHO}$ at the para position resulted in binding of the derivatives to the DFG-motif through the hydrazone $-\text{NH}$. Whereas all the other substituents showed the similar interaction pattern as that of the active compound and were bound to the FP-I of the active site of the protein with a slight shift of $\sim 8\text{\AA}$ in thiazole core position towards the linker. It was observed that in 3COH, the substituents on ring **A** had shifted the compound slightly towards the gate area of the active site of protein as in the case of 2BMC. No marked difference was observed in the binding pattern with change in substituent. In 3E5A, the effect of substitution on ring **A** followed the same trend as in the case of 2X6D where the substituents $-\text{OEt}$, $-\text{Br}$, $-\text{NO}_2$ and $-\text{COOH}$ has extended the binding of molecules toward the gate area through π - π interaction of aromatic rings **A**, **B** or **C** with Phe144 residue of G-loop. Whereas all other derivative were bound to the FP-I of the protein active site. In 3HA6, protein the $-\text{OH}$ and $-\text{OMe}$ substituted compounds were found to be shifted more towards the linker region of the FP-I though all the

other derivatives were found to be in the gate area and with a similar interaction pattern as shown by active compound.

It was found that the substitution on ring **A** of the active compound had a remarkable effect on the binding pattern of the compounds in proteins with DFG-in conformation. In the active state of the protein the molecules with substitution on ring **A** was found to be mainly occupying the gate area of the protein and interacting with the residues in G-loop and/or activation loop. However, in proteins with DFG-motif in the inactive form, the derivatives of the active compound was bound to the hinge region as in the case of the active compound but the binding is slightly extended towards the gate area. Figure 4.12 shows the ring **A** substituent effect on the binding pattern of active compound in tested AURK-A proteins.

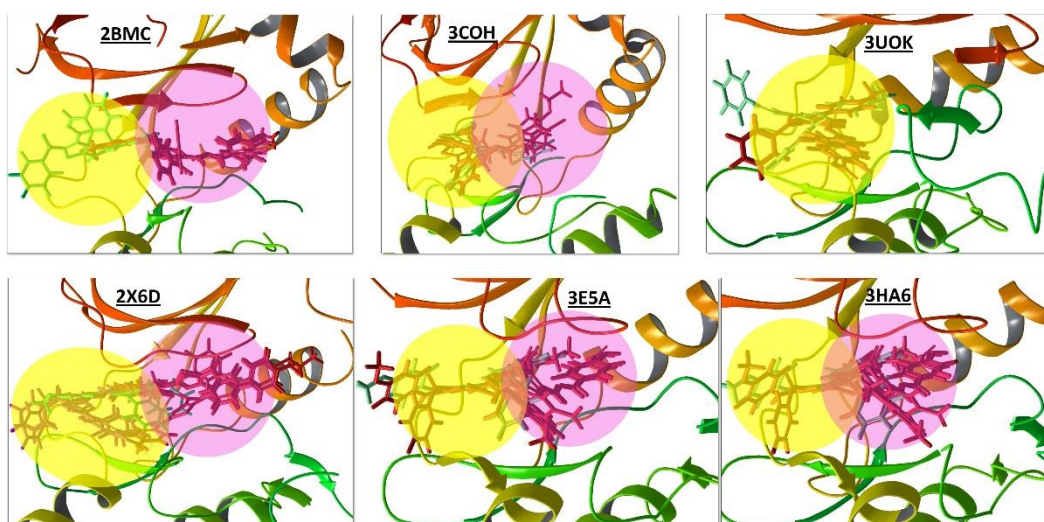


Figure 4.12. Effect of ring **A** substitution on the binding pattern of **BzHAT-5** (green) in AURK-A proteins; FP-I (yellow) and gate area (purple) region of active site are represented in coloured spheres

The substitution on ring **A** of active compound had no marked effect on the binding of derivatives in the active site of AURK-B protein. The molecules were observed to be binding to the front cleft of the hinge region and simultaneously to the Lys85 residue of the G-loop through π -cation interaction (Figure 4.13).

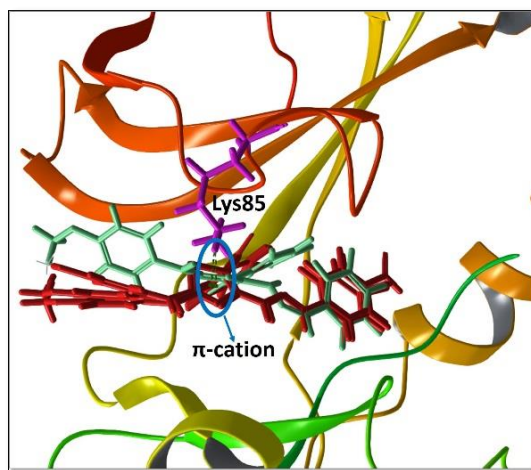


Figure 4.13. Effect of ring A substitution on the binding pattern of **BzHAT-5** (green) in AURK-B protein

4.2.4.4. Effect of substitution on ring C of active compound 5-benzoyl-4-benzylidenehydrazino-2-(4-methoxyphenylamino)thiazole

In comparison with the active compound in 2BMC protein active site substitution of ring C with – NO₂, -OMe and -Br has shifted the binding of the derivatives towards the gate area where the molecules interact with the DFG-motif through H-bonding irrespective of the orientation of substituent on the ring. The binding of all other derivatives of the active compound were found to be comparable with that of active compound. It was observed that in derivatives with meta and ortho ethoxy/methyl substituents on ring C, the binding site had shifted towards the gate keeper (GK) area whereas in halogens the meta substituent was found to be a GK binder. In 2X6D, no substitution or orientation effect was observed for the derivatives which were occupying the FP-I of protein active site. It was observed that in 3COH the substituents on ring C had shifted the compound slightly towards the gate area of the active site of protein as in the case of 2BMC. But substitution/orientation had little effect on the binding pattern of derivatives. In 3E5A also -NO₂, -OMe and -Br substitution resulted in the shift of binding area towards the GK but the change was less pronounced when compared with that of the ring A substitution. The other derivatives occupied exactly the same binding site of the active compound with similar interaction pattern. Here also substituent orientation had no effect on the binding of compounds. The substitution effect was

absent in the case of 3HA6 protein since all are binding in the same binding pocket as that of active compound whereas orientation of the substituents has found to be having remarkable effect on the binding pocket determination of derivatives. Derivatives with ortho halo substituents on ring **C** was found to be more shifted to FP-I with hinge interaction whereas the ortho substitution of other substituents bound to the DFG/DFG+1 residue in the GK. In 3UOK active site, all derivatives were found to be in FP-I as in the case of active compound with similar interactions irrespective of the orientation of the substituents. It was observed that derivatives of active compound with substitution on ring **C** had a tendency to extend the binding site towards the gate area of protein active site irrespective of the conformation of DFG-motif. In the active state of the protein, the molecules with substitution on ring **A** was found to be mainly occupying the gate area of the protein and interacting with the residues in G-loop and/or activation loop. Figure 4.14 shows the ring **C** substituent effect on the binding pattern of active compound in tested AURK-A proteins.

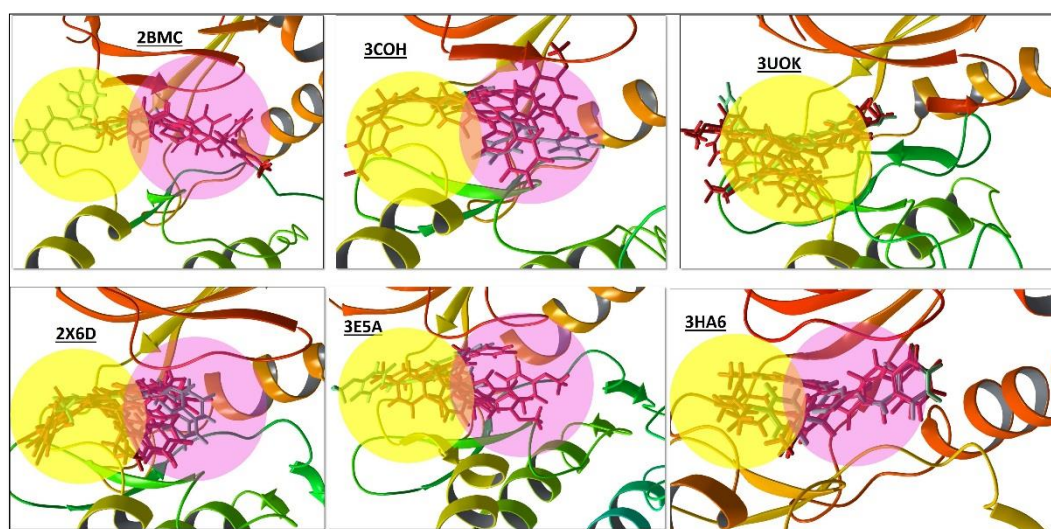


Figure 4.14. Effect of ring **C** substitution on the binding pattern of **BzHAT-5** (green) in AURK-A proteins; FP-I (yellow) and gate area (purple) region of active site are represented in coloured spheres

In 4AF3 protein, the substitution and orientation effects were found to be remarkable in the case of $-\text{NO}_2$ and $-\text{Br}$ substituents. In both the cases changes in para substitution resulted in the binding of corresponding derivative towards the

gate area through interaction with Phe88 residue of G-loop and the ortho and meta substituted derivatives were found to be hinge binders through interaction with Ala157 residue. All other derivatives were found to be occupying the same binding pocket as that by the active compound irrespective of their orientation. Figure 4.15 represents the substituent and orientation effect of $-\text{NO}_2$ and $-\text{Br}$ derivatives of active compound in 4AF3.

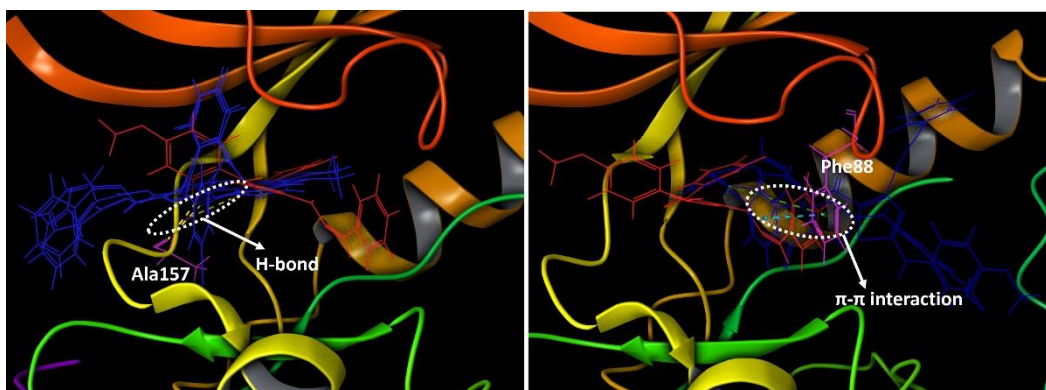


Figure 4.15. Substituent and orientation effect of $-\text{NO}_2$ and $-\text{Br}$ derivatives of **BzHAT-5** (red) in 4AF3; Hinge binding ortho and meta derivatives (blue) are shown in left and G-loop binding para derivatives (blue) are shown in right

4.3. Conclusions

In conclusion, utilizing the possibility of diversity multiplication in our designed scaffold (**HAT**) an expanded virtual library of 22500 members of 4-benzylidenehydrazinothiazole was designed and their optimized 3D structures were created. The ADME property prediction of the library of compounds showed 90% compounds to be having pharmaceutically relevant properties in the recommended range. The dose responsiveness of a set of synthesized compounds in BzHAT library was studied using SRB assay. The *in vitro* screening has identified eight compounds as promisingly active and one compound was identified as active against breast cancer cell line MCF-7. The *in silico* binding studies of the active compound in AURK protein binding sites identified it as an ATP competitive Type I inhibitor irrespective of the class of proteins. By selecting the active compound as ‘hit’ we have initiated the hit to lead generation and optimization procedure in the

designed library by studying the effect of ring (**A** and **C**) substituents on the binding of compounds. It was found that the effect of ring **A** substitution on the binding site and interaction pattern to be more pronounced in AURK-A proteins with DFG-in conformation whereas ring **C** substitution had an impact on the binding of all the tested AURK-A proteins irrespective of the conformation of DFG-motif. In AURK-B, ring **A** substitution had no remarkable effect on the binding pattern while the change in binding site of the derivatives was observed with $-\text{NO}_2$ and $-\text{Br}$ substitution on ring **C**. The expansion of the virtual library of the tetravariant scaffold **HAT** and the lead optimization procedure is continuing in our laboratories and is not further discussed in this thesis.

The drug discovery process being a time consuming one, along with our small molecule research we have initiated preliminary studies on the development of a carrier system based on dendrimers. Due to its wide acceptance for drug, gene and other biomolecule delivery applications, polyamidoamine (PAMAM) dendrimer was our primary choice. To contribute to our long term goal of developing a multifunctional carrier system based on PAMAM, the possibility of introducing heterocyclic ring systems on to the periphery of PAMAM dendrimers was investigated. Owing to our specific interest in 2-aminothiazole core, we have next proceeded with the design and development of a PAMAM-2-aminothiazole conjugate and will be discussed in part B of this thesis.

PART B

*Design and synthesis of a dendrimeric nanoprobe based
on 2-aminothiazole template*

Specific Objectives of Part B

- Design of PAMAM -2-aminothiazole conjugate with tunable sites.
- Formulation of divergent synthetic strategy, chemical synthesis and characterization of conjugate.
- Development of the conjugate as fluorescent nanoprobe.
- Photophysical studies on the conjugate to evaluate its potential as a fluorescent probe.
- Molecular dynamics simulation of the conjugate under different pH and solvent conditions.

CHAPTER 5

PAMAM DENDRIMERS AS MULTIFUNCTIONAL CARRIERS IN BIOMEDICAL APPLICATIONS

5.1. Introduction

Chemotherapy is one of the effective treatment techniques used in cancer therapy. But, the conventional chemotherapy is often afflicted by the low therapeutic index of anticancer agents due to their high plasma concentration that leads to the lack of sensitivity of the drugs used. Therefore researchers in this field are focused much towards the development of chemotherapeutics that can either passively or actively target cancerous cells. The abnormal angiogenesis occurring in tumor tissues results in the fast development of vasculature in contrast to that in healthy tissues which causes hyperpermeability of the endothelial cells of the inherent pores in the vessel walls (~400nm) of tumor. This characteristic feature of the tumor tissue is termed as enhanced permeability and retention (EPR) effect. One of the effective ways to achieve the passive targeting of tumor cells is found to be the use of nanocarriers as drug delivery systems (DDS) that utilizes this characteristic features of tumor biology (Maeda *et al.*, 2000). The intracellular gaps in tumor vasculature allow the extravasation of these DDS from the blood plasma to tumor tissues. The size of the carriers used for the targeting plays a critical role in the efficacy of such systems. Usually drug carriers with diameter larger than 3 nm (to prevent rapid clearance by the kidneys) but smaller than 200 nm (to avoid the reticuloendothelial system (RES)) are considered to be ideal for targeting. The surface properties of the drug carrier are yet another crucial factor which determines their biocompatibility, biodistribution and retention of the DDS within the circulatory system. Thus, in recent years, research is heading towards the surface modifications of nanocarriers to control their biological properties in a desirable fashion and make them multifunctional to perform various therapeutic and diagnostic functions simultaneously (Torchilin, 2012). In this context conjugation

of nanocarrier scaffolds with multiple copies of targeting ligands, drugs and dyes has become a popular approach for achieving the aim of theranostics materials useful for both diagnosis and treatment of diseases. Different nanocarriers (Kumari *et al.*, 2015) are reported in the literature such as liposomes, micelles and polymeric nanoparticles to name a few, among which dendrimers have a significant position owing to their unique structural features. The higher degree of control over the highly branched structure and the ability to tailor properties mark dendrimers different from polymers and made them ideal for targeted drug-delivery, macromolecular carriers, surface engineering and biomimetic applications.

5.1.1. Dendrimers and their unique structural features

The term dendrimer is derived from Greek words *dendron* meaning ‘tree’ and *meros* meaning ‘part’. The core, the interior and the end groups are the three basic architectural features of dendrimers and the physical as well as chemical properties, the overall size, shape and flexibility are strongly influenced by each one of this architectural components (Figure 5.1) that exhibits a specific function, and at the same time, defines unique properties for these monodisperse nanostructures (Klajnert and Bryszewska, 2000).

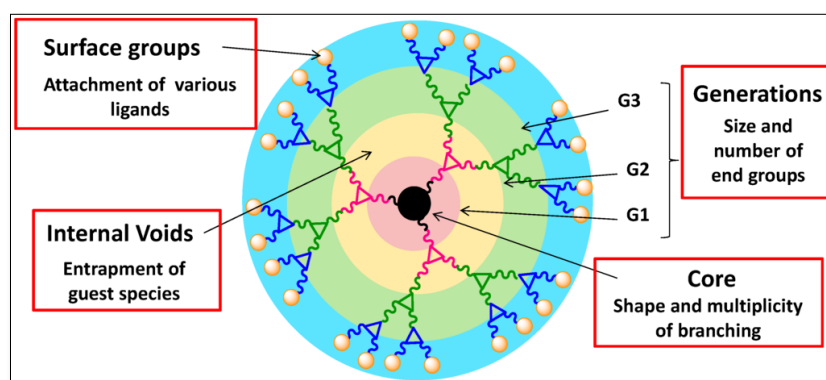


Figure 5.1. Schematic representation of structural components of dendrimer architecture (Sharma and Kakkar, 2015)

The core is positioned at the centre and is responsible for the shape, directionality and multiplicity of the dendrimer. The branched wedges that are

attached to the core constitute the interior and the number of branched points encountered upon moving outward from the core to the periphery represent the generation number. The number of generations is the deciding factor of branching density which determines the amplification of the peripheral functionalities and thereby the globularity of the structure which offer internal cavities for the encapsulation of guest molecules. The end groups present at the periphery of dendrimeric structure, when appropriately functionalized, will allow for the modulation of interfacial properties and the interaction with the surrounding environment and thus act as tunable handles enabling the design of multifunctional dendrimers. Moreover, they are the reactive gates for the controlled release of encapsulated guest molecules from the interior of the dendrimer.

The high level of control achievable over the architecture of dendrimers, their size, shape, branching length and density and their surface functionality, make these compounds ideal carriers in biomedical applications such as drug delivery, gene transfection and imaging applications either by encapsulation into the interior or by attachment to the dendrimer surface. This also facilitates tailoring the properties of the carrier to meet the specific demands for its therapeutic applications. In the molecular dimensions, globular conformation and compartmentalized structure make these symmetrical three dimensional macromolecular architectures as mimics of certain globular proteins and enzymes and are often referred to as *artificial enzymes* (Darbre and Reymond, 2006; Javor *et al.*, 2007). Their unique architecture and terminal groups amenable to wide chemistries make them an excellent platform for covalent/supramolecular modification and hence the best among all the nanodevices (Petros and DeSimone, 2010; Wolfbeis, 2015) known for different applications (Wu *et al.*, 2015; Zhu and Shi, 2013). To be more specific, in cancer nanomedicine dendrimers have found application in almost all the stages starting from prevention, diagnosis, monitoring and control to therapy (Figure 5.2).

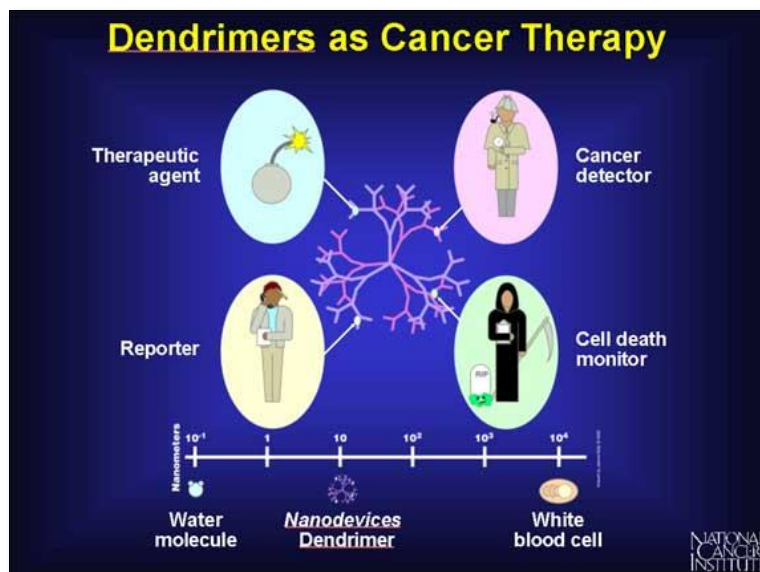


Figure 5.2. Applications of dendrimers in cancer therapy

5.1.2. PAMAM dendrimer in biomedical applications

Being one of the most wide spread topologies observed in nature spanning from meter (tree branches and roots) to nanometer dimension (glycogen and amylopectin), dendrimers rule the supramolecular regime ever since their synthesis was reported by Tomalia (Tomalia *et al.*, 1985) (polyamidoamine), Vögtle (Buhleier *et al.*, 1978) and Meijer (Sijbesma *et al.*, 1997) (polypropylene imine) earlier in 2000. Among various dendrimeric structures studied for biomedical applications, poly(amidoamine) (PAMAM) dendrimers hold specific interest due to their compact size, high surface charge density and ability to penetrate across the intestinal epithelial barrier. The comparatively high biocompatibility and solubility of PAMAM becomes an add-on advantage when considering the biological applications. These were originally developed by Tomalia, *et al.* (1985) with an ethylenediamine core bearing amido amine branching units and are commercially available as cationic full generations with amine termini and anionic half generations with carboxylic acid terminal functionalities. These molecules are available in nanometre dimension growing from 1.1nm-12.4nm in diameter (generation 1-10) (Tomalia, 2005). The chemical structure of PAMAM generation 3 is shown in Figure 5.3.

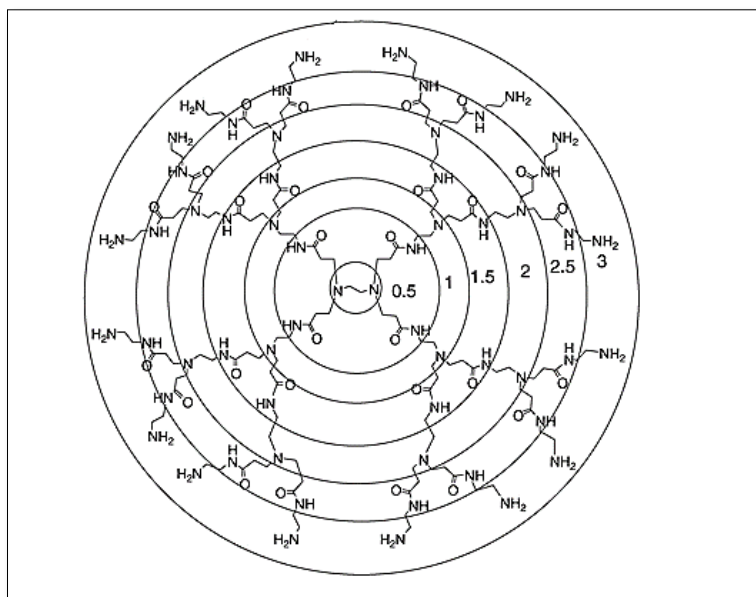


Figure 5.3. Chemical structure of PAMAM generation 3

Considering their size resemblance with biomolecules such as insulin (~3 nm), cytochrome C (~4nm) and haemoglobin (~5.5nm), PAMAM dendrimers have found wide spread applications in the biomedical field. For example, the use of different generations of modified PAMAM as protein and peptide mimics (Liu and Breslow, 2003; Yang *et al.*, 2013) are widely studied in immunodiagnostics. Drug delivery is another application where PAMAM dendrimers have made a superior position. There are many reports available for the use of these molecules as solubility enhancers of hydrophobic drug molecules by utilizing the interaction between dendrimer and the drug molecule (Svenson and Chauhan, 2008; Tekade *et al.*, 2008). The use of PAMAM dendrimers as carriers for the targeted delivery of anticancer drugs through non-covalent interactions, covalent binding and spacer mediated conjugates (D'Emanuele and Attwood, 2005; Kesharwani and Iyer, 2015; Menjoge *et al.*, 2010) is also well documented. The PAMAM dendrimers have offered great potential to develop materials with improved therapeutic efficacy including target specificity, controlled drug release, lower therapeutic doses and minimum exposure to normal tissues and the applications of these nanomaterials and their modifications further extend to the field of cancer diagnosis (Qiao and Shi, 2015; Wolinsky and Grinstaff, 2008), gene delivery (Pack *et al.*, 2005; Yang

et al., 2015), photodynamic therapy (Tao *et al.*, 2013) and neutron capture therapy (Kobayashi and Brechbiel, 2005) to cite a few.

5.1.3. Fluorescent dendritic nanoprobe (FDNs)

Bioimaging is an essential tool in biological research to visualize the morphological details of the cells. The common imaging modalities used in the clinical studies rely on photons with wavelengths ranging from gamma emission to infrared with the exception of MRI (magnetic resonance imaging) which uses magnetic properties of atomic nuclei with half-integer spin. The high energy photons used in these imaging techniques are found to be potentially harmful because of the reactions they can trigger in the cells. But, photons in the visible and infrared wavelengths are found to be possessing no or little damage to cells due to their low penetration power. Thus, the fluorescence imaging techniques are considered to be more reliable which in the last ten years has become an essential tool in preclinical studies extending in the macroscopic to the microscopic range, and attaining as further as sub-cellular resolution (Mérián *et al.*, 2012). Apart from this, the inherent superiorities such as high sensitivity, high selectivity, convenience and non-destructive nature made this optical imaging modality a widely accepted one in biomedical applications (Azhdarinia *et al.*, 2012). The technique relies on a probe that emit light on excitation with suitable wavelength. Since nanostructure-based detection platforms have many advantages over traditional approaches in terms of sensitivity, signal stability and multiplexing capability, research in this field is more on the design and development of fluorescent nanostructures (FNSs) as fluorescent probes in bioimaging (Liu *et al.*, 2011).

FNSs are widely classified into three classes - organic FNSs, inorganic FNSs and organic/inorganic hybrid FNSs (Figure 5.4). Control over the functionalization stoichiometry together with less potential toxicity effects and reproducibility are very important for implementing these fluorescent nanoprobe to real world applications. In this case, most of the fluorescent nanoprobe studied such as silica nanoparticles, quantum dots and carbon dots are failures either in

terms of their toxicity effect or reproducibility and use of these molecular systems is not recommended for many applications (Wolfbeis, 2015). Thus the development of size tunable, multifunctional fluorescent systems with superior photostability and desirable pharmacokinetic behaviour is a need of the hour and in this regard organic FNSs are gaining much importance due to the synthetic feasibility and thereby the reproducibility and photostability.

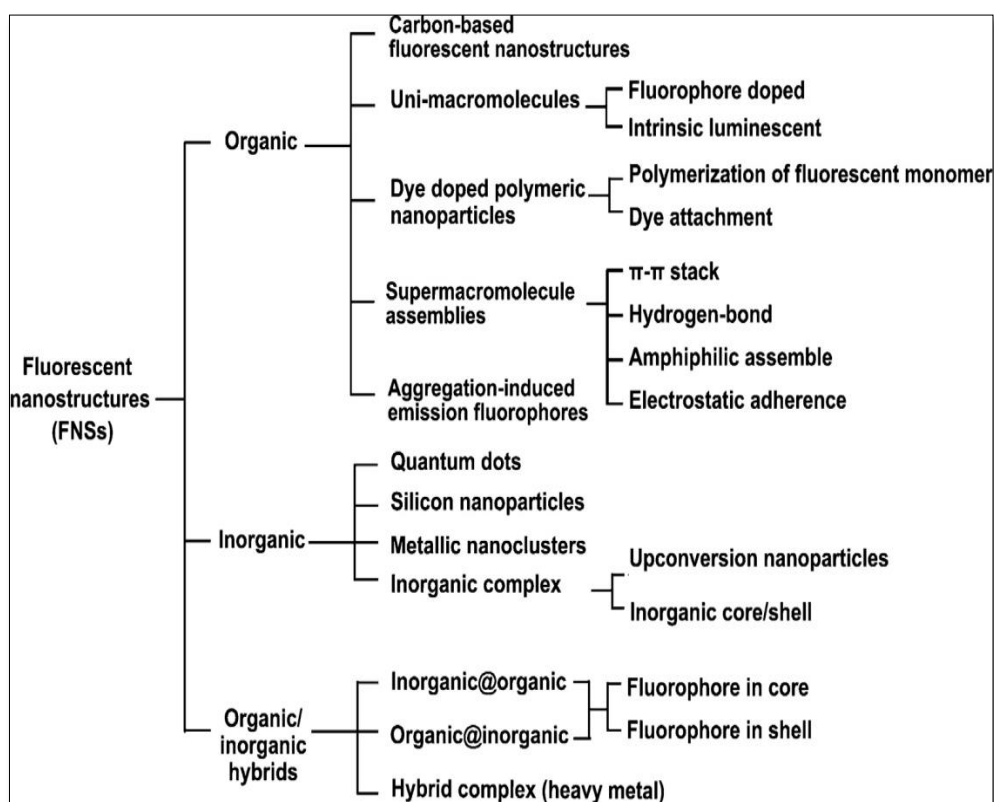


Figure 5.4. Classification of FNSs based on their chemical composition (Chen and Yin, 2014)

Multifunctionality, monodispersity, biocompatibility and tunable chemical properties of dendrimers make them superior among all the other organic molecules. Research in the field of development of dendrimer based FNSs/fluorescent dendritic nanoprobes (FDN) is taking a fast pace in the recent years (Kim *et al.*, 2013; Oesterling and Müllen, 2007; Reilly *et al.*, 2015). Among various dendrimers, the non-toxic nature and biocompatibility of PAMAM dendrimers make them an excellent scaffold for biomedical applications. Moreover, the surface amino groups on PAMAM provide useful moieties for the functional

modification of dendrimers since they allow covalent coupling reactions under mild conditions in a controlled fashion. Although the intrinsic fluorescence of this class of dendrimer seems to be promising for straight monitoring of biological changes (Lee *et al.*, 2004; Pistolis *et al.*, 1997; Wang and Imae, 2004), the real world applications of the same is limited by their low quantum yield (QY). There are a number of reports available on the derivatization of PAMAM dendrimers with fluorescent dyes to track targeting and cellular internalization (Lesniak *et al.*, 2013; Thomas *et al.*, 2010), in protein labelling (Wängler *et al.*, 2008), in ion sensing (Lamy *et al.*, 2012) and theranostic applications (Krasia-Christoforou and Georgiou, 2013; Kukowska-Latallo *et al.*, 2005). The severe drawbacks of traditional small molecule organic fluorophores such as lack of targeting efficacy, poor solubility and cell leakage can be successfully overcome by the use of fluorescent dendritic nanoprobe. But as mentioned before, the practical applications of these FNSs are limited because of the low fluorescent properties when compared to small organic dye molecules especially in terms of QY and life time. Thus the researchers in this field are working on the development of novel FDNs with fluorescent properties essential for imaging and having superior biocompatibility.

5.1.4. Molecular dynamics simulation studies on dendrimers

Molecular dynamics (MD) is a force-field based simulation method used for understanding the atomic level mechanism of physical phenomena at nonzero temperatures on a picosecond timescale. It calculates the time dependent behaviour of molecular systems and in recent years this computational tool has attained considerable interest in biomedical field as it can provide detailed information about the fluctuations and conformational changes occurring in biomacromolecules (Karplus and McCammon, 2002). Molecular interactions being the key factor controlling the biological functions, the study of the macromolecular structures is essential in the understanding of biology. Thus, the MD method is now routinely used to investigate the structure, dynamics and thermodynamics of biological

molecules and their complexes. Moreover it has become a major tool in the design of novel bioactive molecules and to study their mode of action.

One of the great challenges in nanomedicine is the development of novel carriers with maximum therapeutic potential and minimum side-effects for drug and gene delivery. Dendrimers being one of the top most architectures used in biomedical applications, understanding the structural properties of dendrimers in solution is important as the dendrimer structure is tightly linked with function. The size, shape, effective charge, and terminal chemistry of the dendrimers, which can be tuned by the surroundings, such as temperature, pH, and salt ions, play significant roles in their application as delivery vectors. In this regard MD simulations on these factors affecting the structure of dendrimer could facilitate the progress in understanding the delivery process of these bioactive molecules (Cagin *et al.*, 2000; Han *et al.*, 2005).

PAMAM dendrimer being one of the most studied class of dendrimers, MD simulations has been carried out for getting a clear understanding of its 3D structure in solutions (Lee *et al.*, 2006). Three ionic states are reported for PAMAM at different pH ranges and there are reports on the pH responsive conformational changes on the structure (Chen *et al.*, 2000; Maiti *et al.*, 2005). Therefore the dynamics of the structure at different pH conditions and their dependence on the dendrimer's behaviour and functions gained much attention from the researchers (Liu *et al.*, 2009; Maiti and Goddard, 2006). Understanding the interaction between drugs and dendrimers at the molecular level is crucial to optimize the use of the systems as carrier where MD simulations of dendrimer–drug systems are found to be a suitable choice for such optimizations. The structural differences in the interior pockets of the dendrimer exhibit interesting physicochemical implications for the host–guest behaviour and MD simulations has found complementary role in the design and optimization of such dendrimer based host–guest systems (Miklis *et al.*, 1997; Tanis and Karatasos, 2009). The globular shape of dendrimers leads to multivalency at the surface and shielding effects at the core which facilitate the application of the molecules in different fields. Hence, the determination of the 3D

structures and the change in topology due to surface modifications are very significant. The study of dynamics of functional group conjugation on PAMAM dendrimer surface and the possible molecular interactions arising therein are gaining much importance in the recent past with respect to their biomedical applications (Ma, 2013). Since the understanding of interactions involved in the drug delivery process can be used in the development of highly efficient and low toxicity carriers, the dynamics simulation studies can help in the rational design of dendrimer size, shape, or surface properties for applications in nanomedicine.

Coming to the field of medicinal chemistry, as already discussed heterocyclic compounds are the corner stones and thus the effective targeting and delivery of the heterocyclic systems to the diseased site have much significance in the field of medicine. However, despite their versatility and potential, low solubility, degradation, fast clearance rates and non-specific toxicity limit the wider applications and further development of such compounds into market drugs. To overcome these drawbacks and to improve the pharmacokinetic/pharmacodynamics properties of heterocycles, one of the explorable strategies would be nanovectorization of such compounds on to suitable nanocarriers. Our interest being in heterocyclic ring systems especially 2-aminothiazole based ones and motivated by our preliminary findings on the 2-aminothiazole based **HAT** systems in drug discovery we set out our plans for the design and development of multifunctional PAMAM based carriers these systems. As a preliminary step, we planned for the covalent immobilization of 2-aminothiazole template on PAMAM dendrimer and the study of the behaviour of such systems by MD simulations.

CHAPTER 6

DESIGN, SYNTHESIS AND MD SIMULATIONS OF PAMAM-2-AMINOTHIAZOLE CONJUGATE

6.1. Background

As mentioned in previous sections, heterocyclic ring compounds find applications in diverse fields of science and are an inseparable part of human life. The ability of the heterocyclic compounds to manifest the substituents around a core scaffold in a defined three dimensional manner is one of the striking structural features that keeps them on the top of all the synthetic organic scaffolds discovered so far. Moreover, due to their ability to hydrogen bond, alter polarity, solubility, and their electronic and optical properties, heterocycles serve as unique scaffolds in all kinds of organic compounds of interest in electronics, biology, optics, pharmacology and materials science. In pharmacology, the wide-spread applications of heterocycles range from antibacterial, antifungal, anti-HIV, antitubercular, antimalarial, anti-inflammatory to anticancer activity.

Considering the importance of this class of compounds, heterocyclic systems and their vectorization onto nanocarriers attract researchers from both medicine and materials science disciplines (Martins *et al.*, 2015). With an expanding database on various properties and applications of heterocyclic systems, especially related to their bioactivity (Dua *et al.*, 2011), the choice of the vector and effective strategies for linking the vector-heterocycle becomes significant and highly reliant on the application. For example, in nanomedicine and allied fields encapsulation is the common strategy (Pérez-Herrero and Fernández-Medarde, 2015) used for nanovectorization of heterocyclic ring systems. However, the unique properties of nanocarriers that would arise from covalent conjugation (Zhang *et al.*, 2008) can further expand the applicability of such nanovector conjugates in diverse fields.

Our interest being in 2-aminothiazole based heterocyclic ring systems, along with our small molecule research we are aiming at the covalent vectorization of this heterocyclic rings on to nanocarriers. PAMAM dendrimer being one of the most explored class of nanocarriers in different applications, the nanovectorization of heterocyclic ring systems on to the periphery of PAMAM have great significance from an application point of view. Thus, to contribute to the long term goal of developing a multifunctional carrier system based on PAMAM, the possibility of introducing heterocyclic ring systems on to the periphery of PAMAM dendrimers was investigated. Owing to the specific interest in 2-aminothiazole core, as a very first step, we have designed a PAMAM conjugate bearing 2-aminothiazole on the periphery as shown in Figure 6.1.

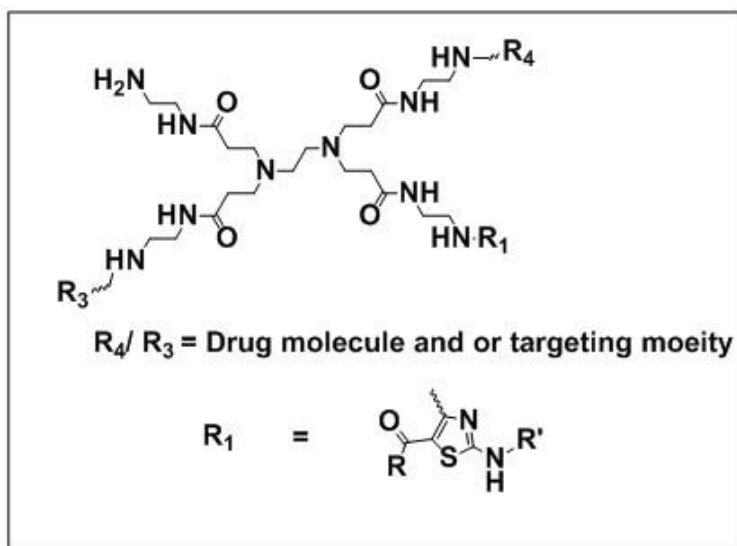


Figure 6.1. Designed PAMAM-2-aminothiazole conjugate

Since the PAMAM dendrimers are available commercially, it was felt worth exploring PAMAM modification so as to have a divergent approach. Albeit the well proven biocompatibility of PAMAM dendrimers (Svenson and Tomalia, 2012) very less is explored on their covalent modification with biologically relevant heterocycles for applications as prodrug and/or theranostics. This may, in part be due to the lack of novel and reliable strategies for their covalent nanovectorization on to the dendrimer periphery. In this regard, we hypothesised the construction of 2-aminothiazole ring on PAMAM periphery using [4+1] ring closure for thiazole

ring formation. Depending on the synthons employed, the attachment of the dendrimer to C2, C4 or C5 of thiazole ring was envisaged as in Figure 6.2.



Figure 6.2. Designed divergent strategies for PAMAM-2-aminothiazole conjugate

A common synthon that can be used for the synthesis of diverse heterocycles on the PAMAM periphery would be further interesting and in the present work we have initiated an effort to develop such a versatile platform for the synthesis of PAMAM-heterocyclic conjugate following a divergent synthetic strategy.

6.2. Results and Discussions

6.2.1. Design of PAMAM based versatile synthon for heterocyclic ring construction

The search for a common platform for synthesis of heterocycles has identified a biguanidine analogue amidinothiourea (ATU) as a useful synthon in the construction of a number of heterocyclic ring systems such as triazole (Yerande *et*

al., 2014a), imidazole (Kaila *et al.*, 2009), thiazole (Binu *et al.*, 1998), oxadiazole (Yerande *et al.*, 2014b) and triazine (Glotova *et al.*, 2004). PAMAM being our choice of interest as nanocarriers, the vectorization of an amidinothiourea fragment on to the periphery of PAMAM might be a breakthrough for the divergent construction of a number of heterocyclic rings of interest on to a well-proven biocompatible nanovector. With this aim in mind, we have designed an amidinothiourea conjugated PAMAM (**PAMAM-ATU**) dendrimer which can theoretically be used for the construction of various heterocycles with the appropriate choice of reagents during the cyclization step as shown in Figure 6.3.

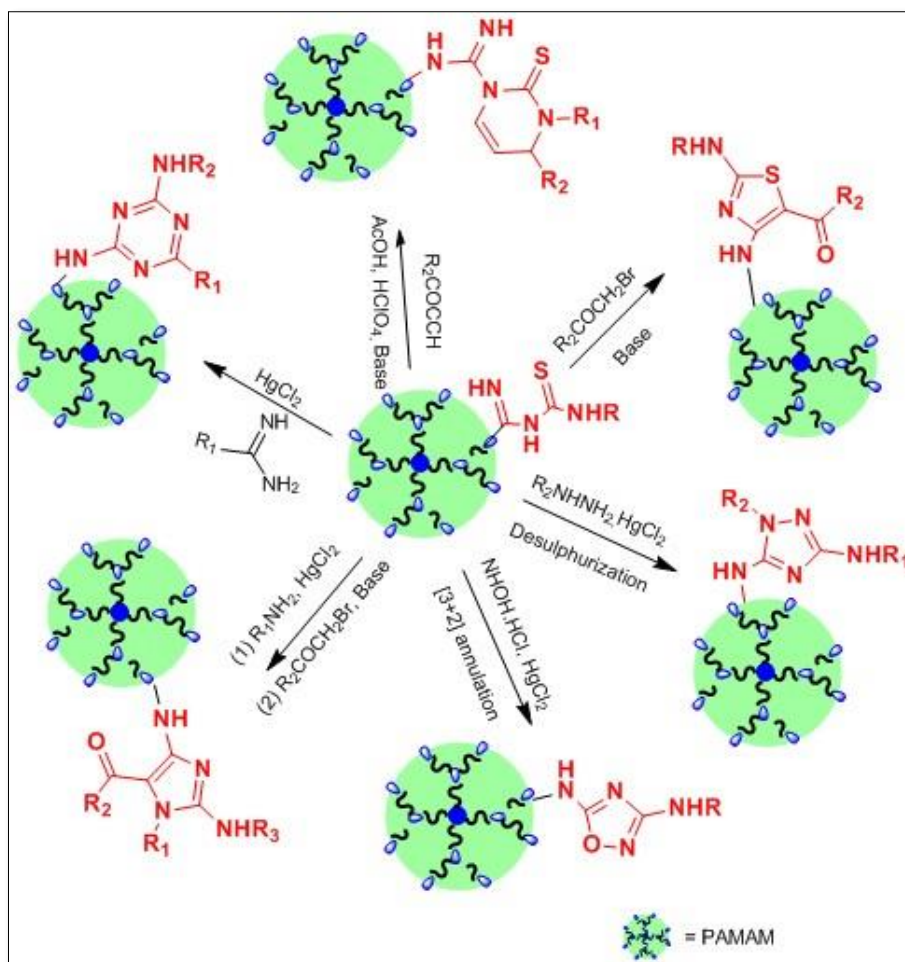
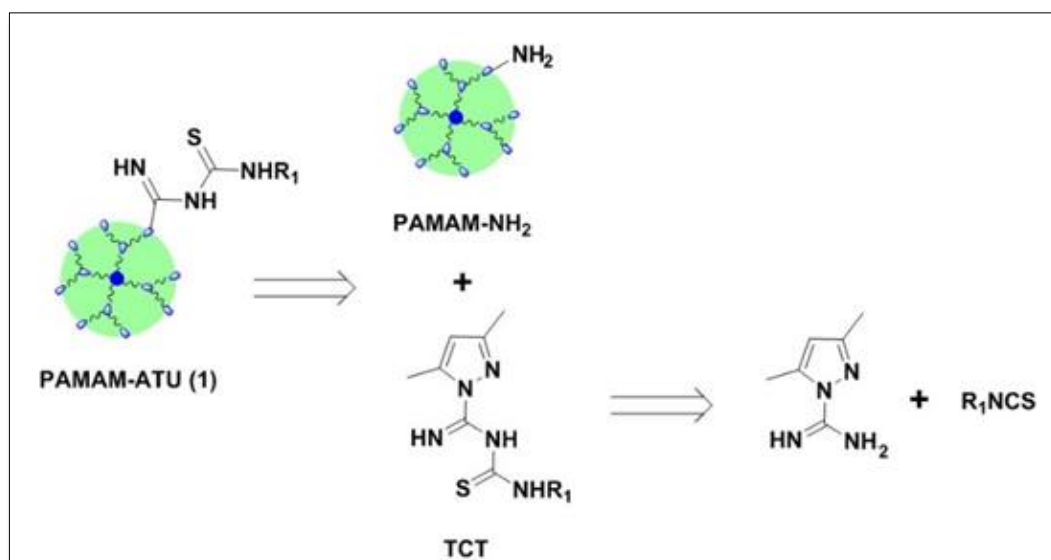


Figure 6.3. PAMAM dendrimer bearing amidinothiourea unit as a universal platform for nanovectorization of diverse heterocycles

6.2.2. Retrosynthesis of amidinothiourea conjugated PAMAM

In our envisioned divergent strategy, we aimed at achieving the covalent anchoring of an amidinothiourea fragment on to the PAMAM periphery and the synthesis of which was designed by retrosynthetic analysis (Scheme 6.1). The retrosynthesis of the designed **PAMAM-ATU** showed that the construction of such a synthon would be possible by a thiocarbamoylamidine transfer to the primary amino groups of PAMAM. Since the dendrimer possess multiple nucleophilic sites with varying reactivity, the choice of reagents and reaction conditions are critical to the synthesis of the proposed amidinothiourea unit. In this regard a regiospecific reagent which would attack the terminal amine would be the best choice, for which an amidine transfer strategy using thiocarbamoylamidine transfer agent (TCT) (Jenardanan *et al.*, 1997) was felt worth examining. Our rationale for choosing TCT strategy was further encouraged by the facile synthesis of the transfer reagent (Scott and Reilly, 1952) accomplished from commercially available 3,5-dimethyl-1-amidinopyrazole and diverse set of isothiocyanates. Further, the solid phase synthon for 2,4-diaminothiazole synthesis has also been accomplished on polystyrene (Sreejalekshmi *et al.*, 2006) using the TCT strategy.

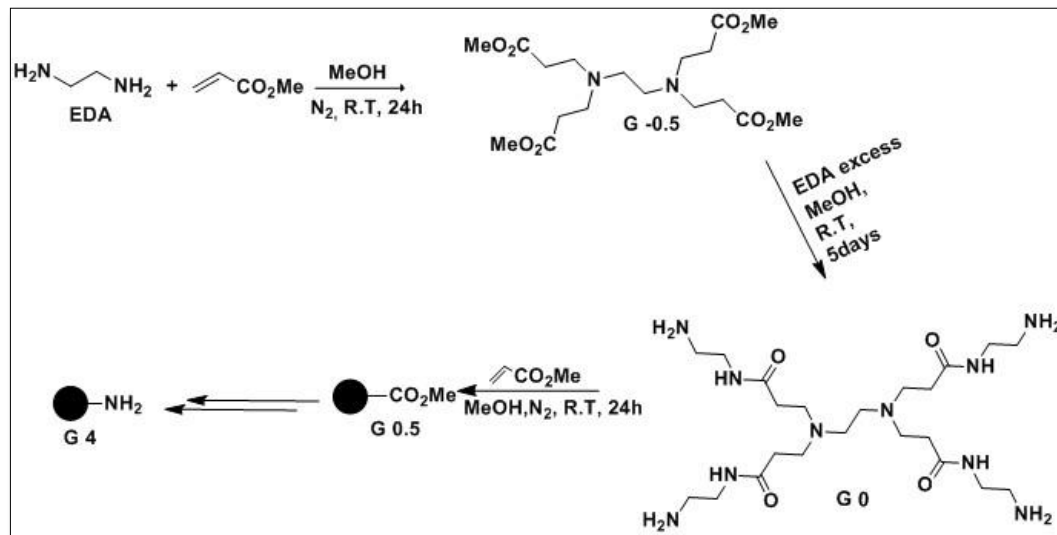


Scheme 6.1. Retrosynthesis of amidinothiourea conjugated PAMAM (**PAMAM-ATU**)

Moreover the proposed regiospecific thiocarbamoylamidine transfer on to primary amino groups of PAMAM would ensure selective modification of dendrimer terminals through **R₁** and hence would have profound influence on dendrimer properties.

6.2.3. Validation of retrosynthetic routes to PAMAM-ATU

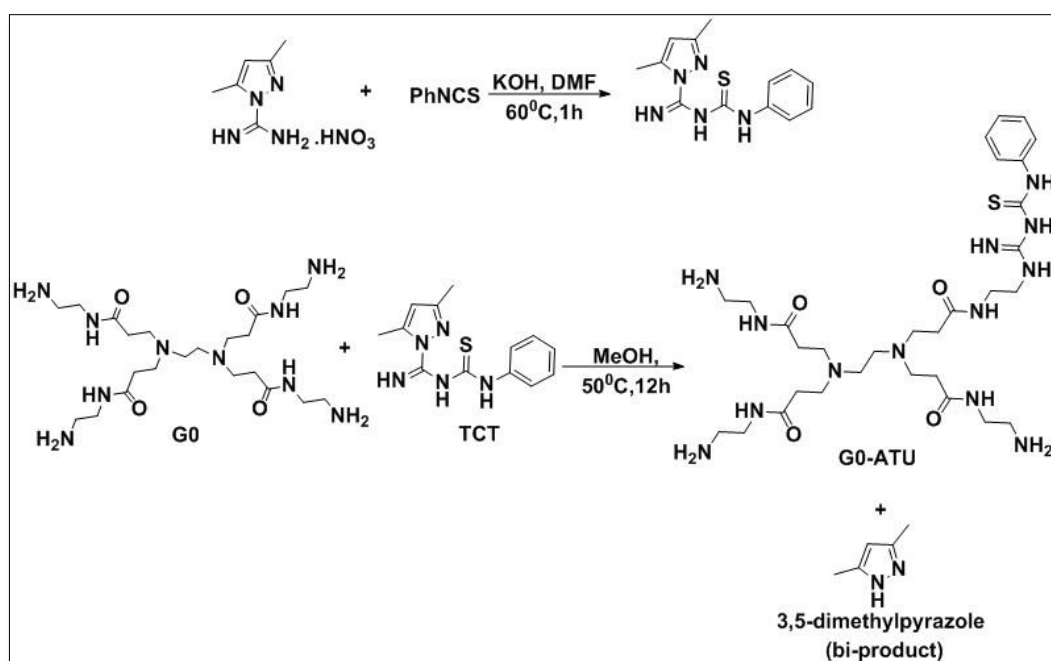
The divergent synthesis of amine terminated PAMAM with ethylenediamine (EDA) core was carried out following the reported procedure (Esfand and Tomalia, 2001) in which the first step was the Michael addition of primary amine to methyl acrylate which resulted in the formation of half generation PAMAM (G-0.5) with ester termini. The multiester formed on amidation with excessive EDA gave the full generation PAMAM (G0) with amine termini and the reactions were continued for the synthesis of higher generations as shown in Scheme 6.2.



Scheme 6.2. Divergent synthesis of amino terminated PAMAM

To test our hypothesised divergent synthesis of **PAMAM-ATU**, we have chosen the synthesized PAMAM G0 with four terminal amino groups. The formation of G0 was confirmed by spectroscopic techniques and the number of terminal amino groups were estimated by potentiometric titration (Mullen *et al.*,

2012) which was calculated to be 3 ± 1 . The thiocarbamoylamidine transfer agent, 1-(N-phenylthiocarbamoyl)amidino-3,5-dimethylpyrazole, was obtained from the reaction between 1-amidino-3,5-dimethylpyrazole and phenylisothiocyanate as reported earlier by Jenardanan *et al.* in 1997. The treatment of one of the terminal amino groups with 1equiv. of TCT, resulted in the formation of the desired compound **G0-ATU** with the elimination of 3,5-dimethyl pyrazole. The reactions were carried out in four different polar solvents (DMF, DMAc, MeOH and ACN) and the optimized reaction procedure for the thiocarbamoylamidine transfer along with the literature procedure for the preparation of TCT are shown in Scheme 6.3. The viscous liquid obtained was purified by column chromatography using sephadex LH-20 and characterized using spectroscopic techniques and molecular mass determination. The thiocarbamoyl transfer reaction was confirmed by the presence of C=S stretching and C-H bending corresponding to monosubstituted benzenoids at 1095 and 819 cm^{-1} respectively along with amide I (1631 cm^{-1}) and amide II (1543 cm^{-1}) band of PAMAM. The ^1H NMR spectra accounted for five aromatic protons in a range of $\delta=6.93$ to 7.55 ppm and molecular mass as determined by MALDI-TOF analysis was found to be 693, as expected for PAMAM G0 with one of the arms bearing a phenylthiocarbamoylamidine unit.



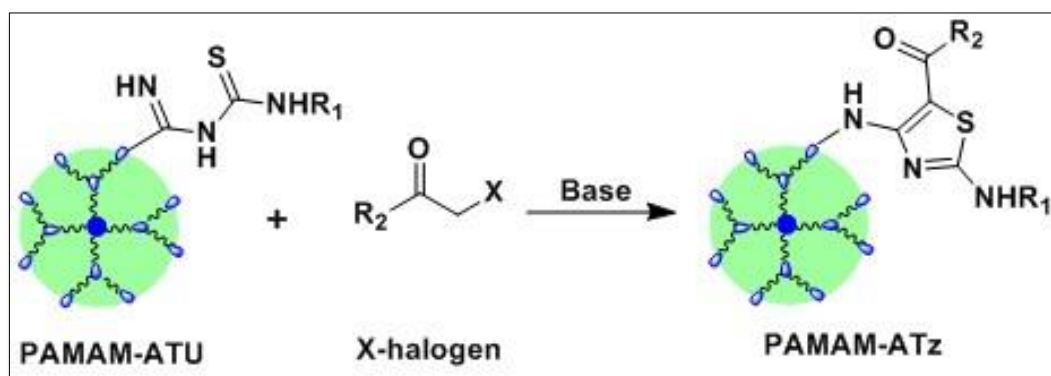
Scheme 6.3. Divergent synthesis of **G0-ATU**

The results suggested the success of our synthetic strategy to build an amidinothiourea platform on PAMAM dendrimer and establish the utility of TCT for modifying amine terminated PAMAM dendrimers. Higher generations of PAMAM (G1-G4) were also subjected to the TCT strategy and in all the cases the thiocarbamoylamidine transfer was confirmed by the characteristic peaks obtained in IR spectra of the resulted compounds and also by the formation of 3,5-dimethyl pyrazole. To establish the functional group diversity and the generality of the synthesis, we next used 4-nitrophenylisothiocyanate for the preparation of TCT agent and the corresponding transfer reaction was carried out on PAMAM G0 following the same procedure as already discussed. The transfer reaction was confirmed by recording IR spectrum of the viscous liquid (G0-ATU-2), obtained after petroleum ether wash, which showed the characteristic nitro group stretching frequencies (1583 and 1325 cm^{-1}), the C-N stretch (847 cm^{-1}) along with the amide I and amide II band of PAMAM. The presence of pyrazole in the petroleum wash also indicated the transfer reaction to be successful. Thus a mild and efficient reaction procedure was established for the synthesis of a PAMAM based amidinothiourea synthon. To the best of our knowledge, such a conjugate with potential as a versatile synthon for diverse heterocyclic rings on to the periphery of PAMAM has been accomplished for the first time. With the commercial availability of a number of isothiocyanates, the designed synthetic route provides a feasible way to obtain an amidinothiourea conjugated PAMAM with diverse functional groups (through **R₁**) attached to the periphery of the PAMAM.

6.2.4. Synthesis of PAMAM-2-aminothiazole conjugate

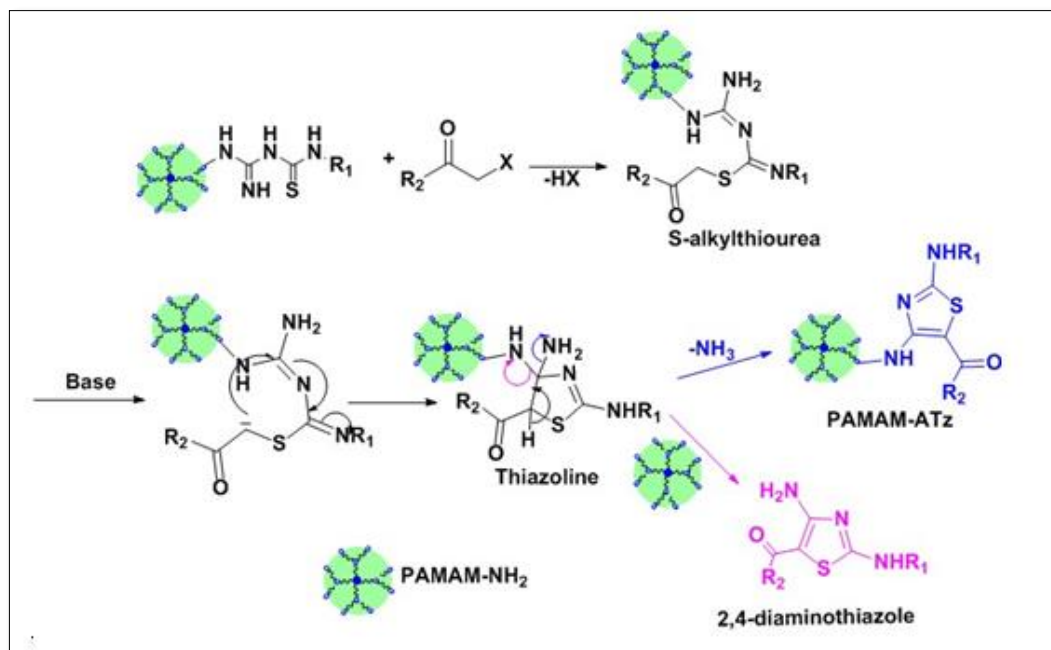
With the successful synthesis of C-N-C-S unit tethered to PAMAM, our next aim was the construction of 2-aminothiazole on to PAMAM periphery using **PAMAM-ATU** as a precursor for the thiazole ring synthesis. In this context, Hantzsch thiazole synthesis using thioamides and thioureas are widely explored for 2-aminothiazole synthesis but Rajasekharan *et al.* (1986) has established a mild and efficient [4+1] ring synthesis for 2,4-diaminothiazole from suitably substituted amidinothioureas and α -haloketones. The successful anchoring of amidinothiourea

on PAMAM dendrimer has provided the C-N-C-S unit for thiazole ring construction and based on the literature data available on the solid phase aminothiazole synthesis (Sreejalekshmi, *et al.*, 2006), we planned for achieving the nanovectorization of 2-aminothiazole template onto PAMAM by covalent modification as shown in Scheme 6.4. Here the **PAMAM-ATU** conjugate would act as the C-N-C-S fragment donor whereas the C5 of the thiazole could be a contribution from active methylene compounds, say α -haloketones. It is to be noted that the designed synthetic route provide a 2-aminothiazole conjugated PAMAM with two sites for diversity multiplication/property tuning in its structure which could be afforded from commercially available isothiocyanates and α -haloketones.



Scheme 6.4. Synthetic route to 2-aminothiazole conjugated PAMAM G0

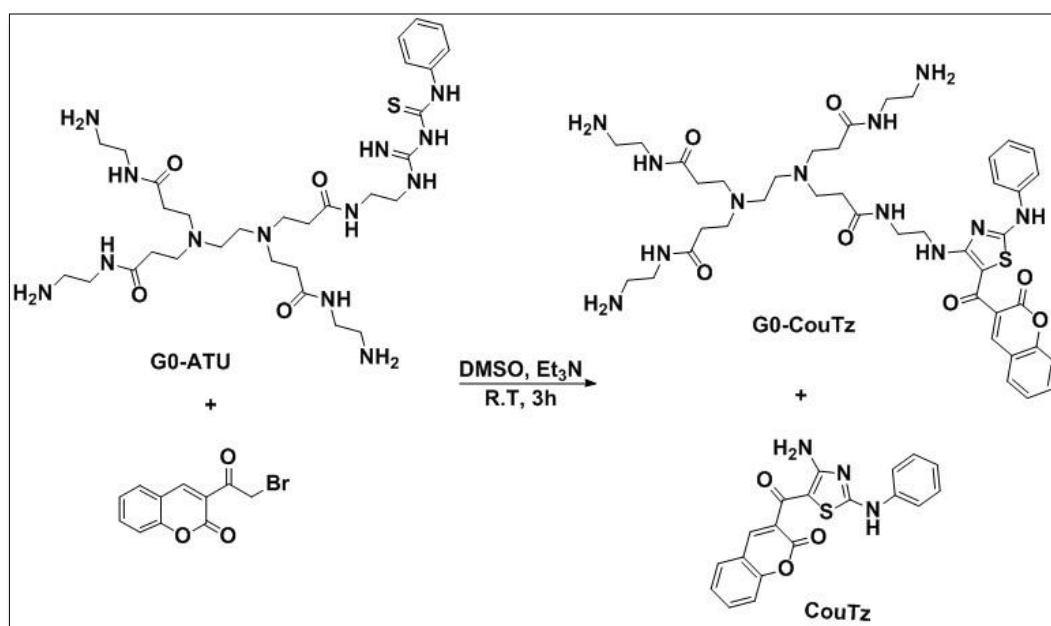
The heterocyclization is expected to proceed through S-alkylation of the thiocarbamoyl unit that result in the formation of an acyclic S-alkylthiourea intermediate. The cyclisation of this intermediate in presence of base can result in the formation of five membered thiazoline which on competitive eliminative aromatization could afford the 2-aminothiazole ring. Such an elimination may result in the formation of either 2-aminothiazole conjugated PAMAM (**PAMAM-ATz**) as the lone product or as a mixture with 2,4-diaminothiazole as the bi-product. Scheme 6.5 gives the mechanistic insight to the hypothesized heterocyclization leading to **PAMAM-ATz**.



Scheme 6.5. Mechanism of heterocyclization of **PAMAM-ATU**

To test the hypothesis, the amidinothiourea conjugate **G0-ATU** in DMSO was reacted with p-nitrophenacylbromide and p-chlorophenacylbromide (in two separate reactions) at room temperature in the presence of organic base Et₃N for 3h. The IR spectra of the respective purified products obtained after the reaction was identified with the characteristic amide I and amide II bands of PAMAM along with the nitro group/ C-Cl stretching frequencies. The amide I and amide II bands of p-nitrophenyl substituted **PAMAM-ATz** was observed at 1646 and 1552 cm⁻¹ respectively whereas that for the p-chlorophenyl substituted product was found to be at 1632 and 1589 cm⁻¹. The product formations were further confirmed by the characteristic nitro group stretching frequencies at 1544 and 1348 cm⁻¹, the C-N stretch at 847 cm⁻¹ for p-nitrophenyl and Ar-Cl stretching at 1090 cm⁻¹ for p-chlorophenyl substituted **PAMAM-ATz**. Along with the realization of the nanovectorization of aminothiazole on to PAMAM, it is to be noted that our strategy succeeded in the accomplishing a divariant conjugate **PAMAM-ATz**, which offers the flexibility of tuning dendrimer property by varying isothiocyanate (**R**₁ during formation of **PAMAM-ATU**) and α-halo compounds (**R**₂ during cyclization), both of which are commercially available in large numbers.

Among many properties of PAMAM conjugates with commercial implications, one which requires amplification would be its fluorescence (Chen and Yin, 2014; Soršak *et al.*, 2015), which is mostly quenched in solvents hence impairing practical application of such conjugates. Thus along with the successful vectorization of the well-recognized drug discovery fragment, 2-aminothiazole on to PAMAM, we set out with yet another objective to explore the possibilities of developing useful photophysical properties on the dendrimer. To this end, the simplest strategy would be to introduce a photounit during the thiazole formation step, for which we preferred a coumarin ring, primarily because of its wide occurrence in laser dyes (Trenor *et al.*, 2004) and interesting photophysical properties. We were further stimulated by the dearth of synthetic routes to coumarin conjugated dendrimers and studies on their photophysics (Adronov *et al.*, 2000). Thus by using 3-bromoacetylcoumarin as the active methylene component in the cyclization of **G0-ATU**, we synthesized coumarinoyl-2-aminothiazole conjugated PAMAMG0 (**G0-CouTz**) under optimized conditions (Scheme 6.6).



Scheme 6.6. Chemical synthesis of coumarinoyl-2-aminothiazole conjugated PAMAM

The desired product was obtained as a minor one (yield= 25%) along with the formation of 5-coumarinoyl-2,4-diaminothiazole (**CouTz**) as expected from the

mechanism. The identity of column purified **G0-CouTz** was confirmed by spectroscopic techniques and molecular mass determination. The ^1H NMR spectrum of the conjugate accounted for the aromatic protons and amide protons in a range of $\delta=7.03$ to 7.65 ppm and the characteristic coumarinoyl $-\text{CH}$ proton was observed at $\delta=8.46$ ppm as a singlet. Further the molecular mass as determined by MALDI-TOF analysis was found to be 861, as expected for **G0-CouTz**. The molecular size of the thiazole conjugate was determined by AFM analysis. The topographic image of **G0-CouTz** showed grain shaped particles with an average diameter of 120 nm along the minor axis and 260 nm along the major axis (Figure 6.4) indicating unique folding of the dendrimer arms, possibly due to non-covalent interactions.

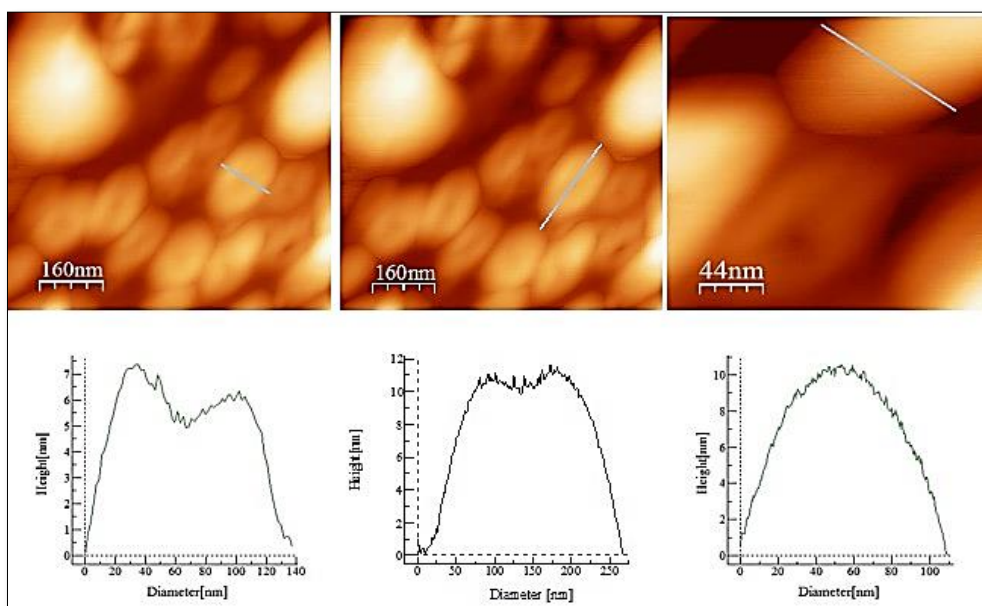


Figure 6.4. Topographic AFM images ($1\mu\text{m} \times 1\mu\text{m}$) and corresponding cross sectional analysis of **G0-CouTz** on mica surface

The synthesized **G0-CouTz** exhibited solid state green emission along with excellent photophysical properties in presence of solvents whereas the precursor **G0-ATU** was found to be non-fluorescent in nature. The luminescence properties of the thiazolyl conjugate could be thought of as a synergistic contribution from coumarin unit, the thiazole bridge with an amino substituent on C2 and PAMAM. Since, the fate and function of the dendrimer conjugate depends

on the chemistry and structure of the solvated form of the conjugate we have carried out molecular dynamics (MD) simulations of **G0-ATz** to rationalize the observations.

6.2.5. Molecular dynamics simulation studies on PAMAM-CouTz

The microstructure and surface properties of dendrimers and their conjugates determine their potential behaviour and applicability. The comprehensive understanding of the structure and dynamics of the dendrimer conjugates is highly significant in order to use them in various applications. Experimental diffraction techniques such as small angle neutron scattering (SANS) and small angle X-ray scattering (SAXS) have helped to elucidate the effect of important variables such as the generation, surface functionalization, and pH on the microstructure of dendrimer (Caminade *et al.*, 2005). But, due to the presence of numerous energetically favourable conformations and their rapid interchange in solutions there is a gap in the atomic level determination of position of functional surface group and their interactions by the diffraction techniques. In order to overcome this researchers are focusing on the computational simulation studies of such conjugate to elucidate relevant information about the variables that affect the properties of the dendrimer conjugate. Since the structure and gyration radius of the dendrimer depends on the pH and solvent conditions, in the present study, we have investigated the effect of these two parameters on the structure and conformation of the PAMAM G0 and the newly developed **G0-CouTz** conjugate.

6.2.5.1. Structural minimization of G0 and G0-CouTz

PAMAM dendrimers are polyelectrolytes and in aqueous solution protonation can take place at termini (primary amines) and/or at branch points (tertiary amines) depending on the pH of the solution. At low pH (≤ 4) all the primary as well as tertiary amines are found to be protonated whereas at physiological pH 7.4 only the primary amines in PAMAM are reported to be

protonated and at high pH (≥ 10) the dendrimer exists in the neutral form (Maiti *et al.*, 2005). To study the change in the interaction and dynamics of the dendrimer and dendrimer conjugate, structure minimization was carried out with MacroModel at the different protonation levels and the minimized structures were used as the input structure for the molecular dynamics (MD) studies. The minimization of the structures were carried out in water with a convergent threshold of energy 0.05 J/Åmol (RMS gradient of energy) in 5000 iterative steps. The minimization of the structures at all the three pH (4, 7.4 and 10) were carried out with different force fields MM2, MMFF, MMFFs, AMBER and OPLS-2005. In all the cases the lowest energy for the minimized structure was obtained with OPLS-2005 and hence those structure were selected for further studies. The energy minimized conformational structures of PAMAM G0 and G0-CouTz at different protonation levels are given in Figure 6.5.

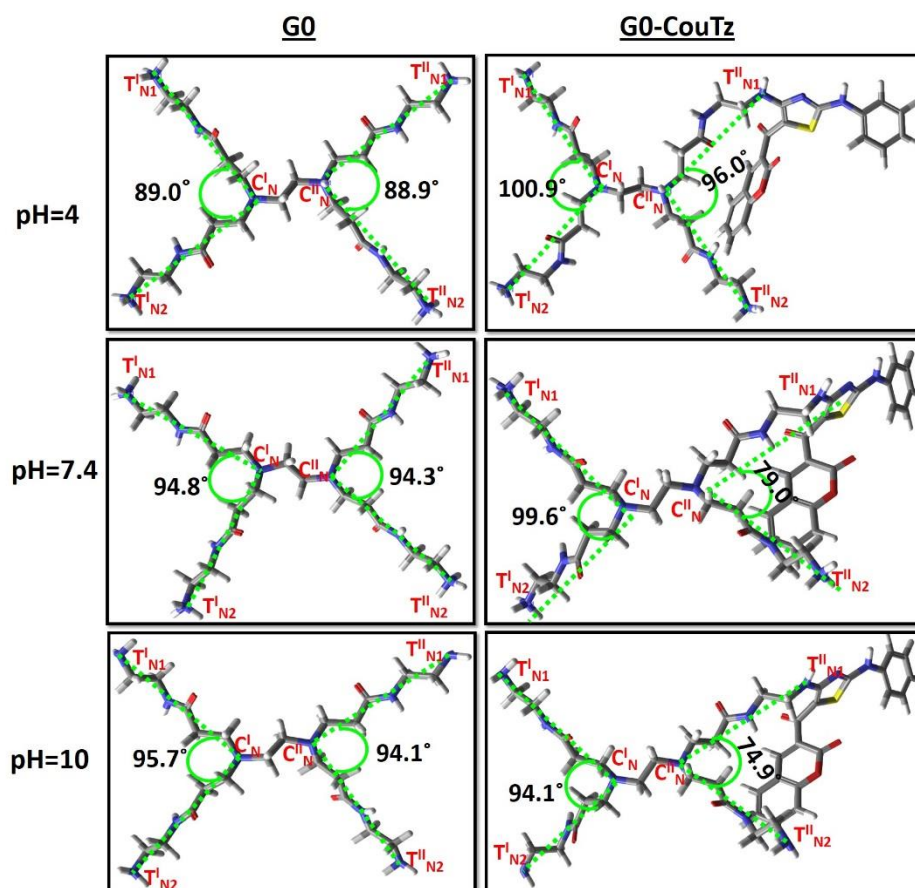


Figure 6.5. Energy minimized structures of G0 and G0-CouTz at pH 4, 7.4 and 10; Angle between the branching point and terminal N atoms of arms are represented

At pH 4, both the primary (T^I_N and T^{II}_N) as well as the tertiary (C^I_N and C^{II}_N) N-atoms are reported to be in the protonated state. The minimized structure of the unmodified dendrimer shows that the terminal N-atoms are inclined to the branch point N at an angle of $\sim 89^\circ$ with the two branching points (C^I_N and C^{II}_N) in the opposite plane with a dihedral angle of 180° . The distance between the terminal amino groups and the branching point was observed to be 8.74 \AA units. At the same pH, in **G0-CouTz**, where one of the terminal amino groups was modified with coumarinoyl-2-aminothiazole moiety, we have observed an increase in the angle between the terminals and the branching points ($\angle T^I_{N1}C^I_N T^I_{N2} = 100^\circ$ and $\angle T^{II}_{N1}C^{II}_N T^{II}_{N2} = 96^\circ$). Here also C^I_N and C^{II}_N are occupying the opposite planes and the distances between the terminal and core N-atoms were found to be $T^I_{N1}C^I_N = 8.75$, $T^I_{N2}C^I_N = 8.37$, $T^{II}_{N1}C^{II}_N = 8.23$ and $T^{II}_{N2}C^{II}_N = 8.75 \text{ \AA}$ units. The coumarinoyl moiety was occupying the space between the arms and was stabilized by π -cation interaction between the positively charged C^{II}_N and the coumarin ring.

At physiological pH (7.4) in the minimized structure of the G0, the angle formed between the N-atoms of terminal amino (T^I_{Ni} and T^{II}_{Ni}) groups and the branching point N-atoms of EDA core (C^I_N and C^{II}_N) was found to be $\sim 94^\circ$ and the terminal amino groups were away from the branching point at an average distance of 8.72 \AA units. The dihedral angle between C^I_N and C^{II}_N was found to be reduced to $\sim 161^\circ$. But, in the structure **G0-CouTz**, the angle between the unmodified arms and the corresponding branching point ($\angle T^I_{N1}C^I_N T^I_{N2}$) was slightly increased to 99° when compared to that in G0 whereas that formed by the branching point bearing the modified arm ($\angle T^{II}_{N1}C^{II}_N T^{II}_{N2}$) was reduced to 79° . The distance between the terminal amino groups of unsubstituted arms and branching point was retained in the conjugate also whereas, the terminal amino groups T^{II}_{N1} and T^{II}_{N2} were found to be at a distance of 8.40 and 8.48 \AA from C^{II}_N respectively and the coumarinoyl moiety was pushed away from the C^{II}_N probably due to the electrostatic repulsion between the N-atom atom and the π electrons of the coumarin ring.

At high pH (10), where none of the N-atoms are protonated, the minimized structure of the dendrimer G0 the terminal N-atoms were inclined to the core N with an angle of 95° with C^I_N and C^{II}_N dihedral angle of 158°. The distance between the terminal amino groups and the branching points was found to be ~8.80 Å units. In the structure of **G0-CouTz** the <T^I_{N1}C^I_NT^I_{N2} is reduced to 94° and <T^{II}_{N1}C^{II}_NT^{II}_{N2} to 74° with C^I_N and C^{II}_N dihedral angle of 157°. The distances T^I_{N1}C^I_N, T^I_{N2}C^I_N, T^{II}_{N1}C^{II}_N and T^{II}_{N2}C^{II}_N were found to be 8.63, 8.44, 8.35 and 8.46 Å units respectively. The coumarinoyl moiety was pushed away from the C^{II}_N probably due to the electrostatic repulsion between the N-atom atom and the π electrons of the coumarin ring as in the case of pH 7.4. The results obtained for the minimization are summarised in Table 6.1. The results clearly reveals the structural changes occurring in different protonated states of dendrimer and conjugate.

Table 6.1. Distances and angles obtained for minimized structures of G0 and G0-CouTz

pH	Structure	Distance (Å)				Angle (°)		Dihedral angle (°)
		T ^I _{N1} C ^I _N	T ^I _{N2} C ^I _N	T ^{II} _{N1} C ^{II} _N	T ^{II} _{N2} C ^{II} _N	T ^I _{N1} C ^I _N T ^I _{N2}	T ^{II} _{N1} C ^{II} _N T ^{II} _{N2}	
4	G0	8.74	8.75	8.75	8.74	89.0	88.9	180.0
	G0-CouTz	8.75	8.37	8.23	8.75	100.9	96.0	177.9
7.4	G0	8.70	8.76	8.67	8.76	94.8	94.3	161.2
	G0-CouTz	8.68	8.73	8.40	8.48	99.6	79.0	157.5
10	G0	8.62	8.70	8.46	8.70	95.7	94.1	158.2
	G0-CouTz	8.63	8.44	8.35	8.46	94.1	74.9	157.3

Using these minimized structures of G0 and G0-CouTz we then proceeded with the MD simulations to predict the time dependent behaviour of the conjugates with respect to solvent and pH of the solution.

6.2.5.2. Effect of solvent on the structure and dynamics of G0

In order to study the effect of solvents on the structure and dynamics of the lowest generation PAMAM G0 with four terminal amino groups, MD simulations have been carried out with two different solvent models- water and DMSO. The simulation quality structures were obtained using respective solvent models at physiological pH. The simulations were carried out for 5ns using Desmond in an orthorhombic periodic box of volume 10^3\AA^3 in presence of Cl^- counter ions. The studies were performed using isothermal-isobaric ensemble NPT at temperature of 300K and pressure of 1.013bar. Figure 6.6 shows the snapshots of PAMAM G0 in water and DMSO at the beginning (0ns), after 2.5ns and at the end of 5ns simulations.

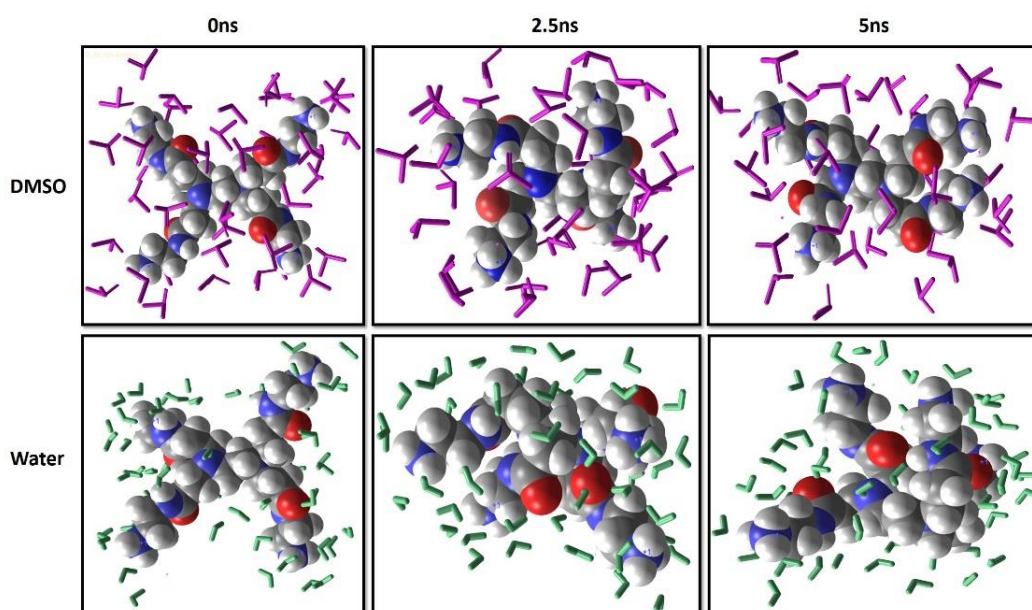


Figure 6.6. Snapshots of G0 during simulations in DMSO and water at pH7.4; DMSO (purple) and water (aquamarine) molecules at the vicinity of 3\AA distance are displayed

A quantitative estimate of the dendrimer size can be described by mean square radius of gyration (R_g^2). For a dendrimer with N atoms, the mean square radius of gyration is given

$$R_g^2 = \frac{1}{M} \sum_{k=1}^N [m_k(r_k - r_{\text{mean}})^2]$$

where r_{mean} is the centre of dendrimer, $(r_k - r_{\text{mean}})$ is the distance of k^{th} atom from the centre, m_k is the mass of the k^{th} atom and M is the molar mass of dendrimer. The time-evolution of R_g (Figure 6.7) of G0 reveals that the molecule had a comparatively larger size in DMSO than in water.

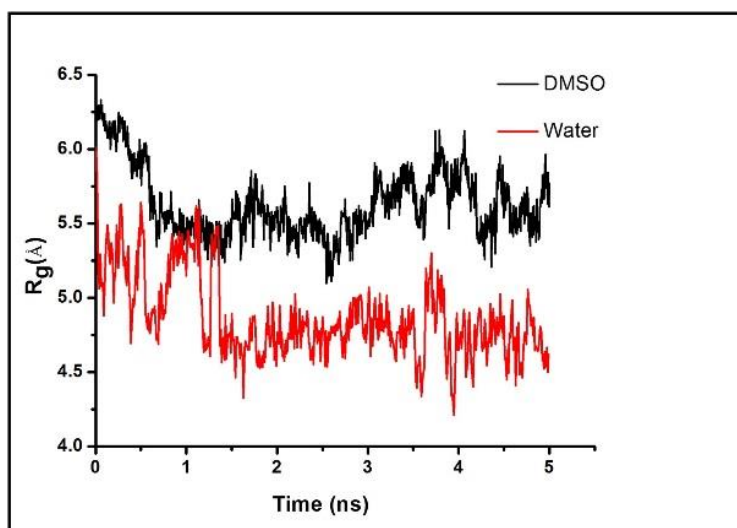


Figure 6.7. Time-evolution of radius of gyration of G0 in DMSO and water during the course of 5ns molecular dynamics simulations

The value of mean radius of gyration was found to be 5.63 ± 0.23 in DMSO where as in water the value was found to be 4.78 ± 0.23 . The difference in the size of the dendrimer may be due to the extent of flexibility of the arms which can be attributed to the variation in the intramolecular interaction energy (E_{int}). The time-evolution of various energy components of G0 (E_{intG0}) in DMSO and water are given in Figure 6.8.

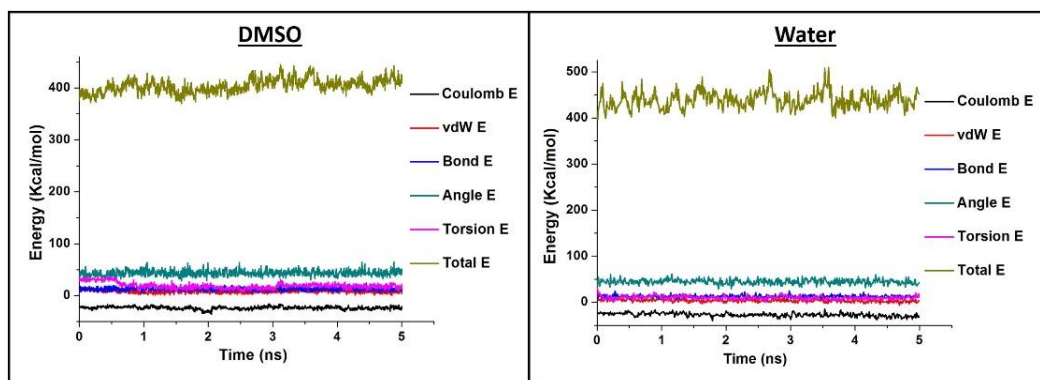


Figure 6.8. Variation of energy components of G0 in DMSO and water during the course of molecular dynamics simulations

The mean value of the distances between the core and terminal N-atoms were found to be 7.70 ± 0.31 and 7.12 ± 0.11 in DMSO and water respectively which correlates with the R_g values obtained in the respective solvents. We have also observed that the change in shape of G0 dendrimer is more pronounced in case of water than in DMSO.

6.2.5.3. Effect of solvent on the structure and dynamics of G0-CouTz

The dynamics simulations of **G0-CouTz** at pH 7.4 showed that in DMSO the molecule tend to attain a more open structure where the coumarinoyl-2-aminothiazole moiety at the periphery ($T^{\text{II}}_{\text{N1}}$) was extended outwards from the core after 5ns where as in water that was inclined towards the space between the arms of dendrimer and was stabilized by π -cation interaction between $T^{\text{II}}_{\text{N2}}$ and coumarin ring (Figure 6.9).

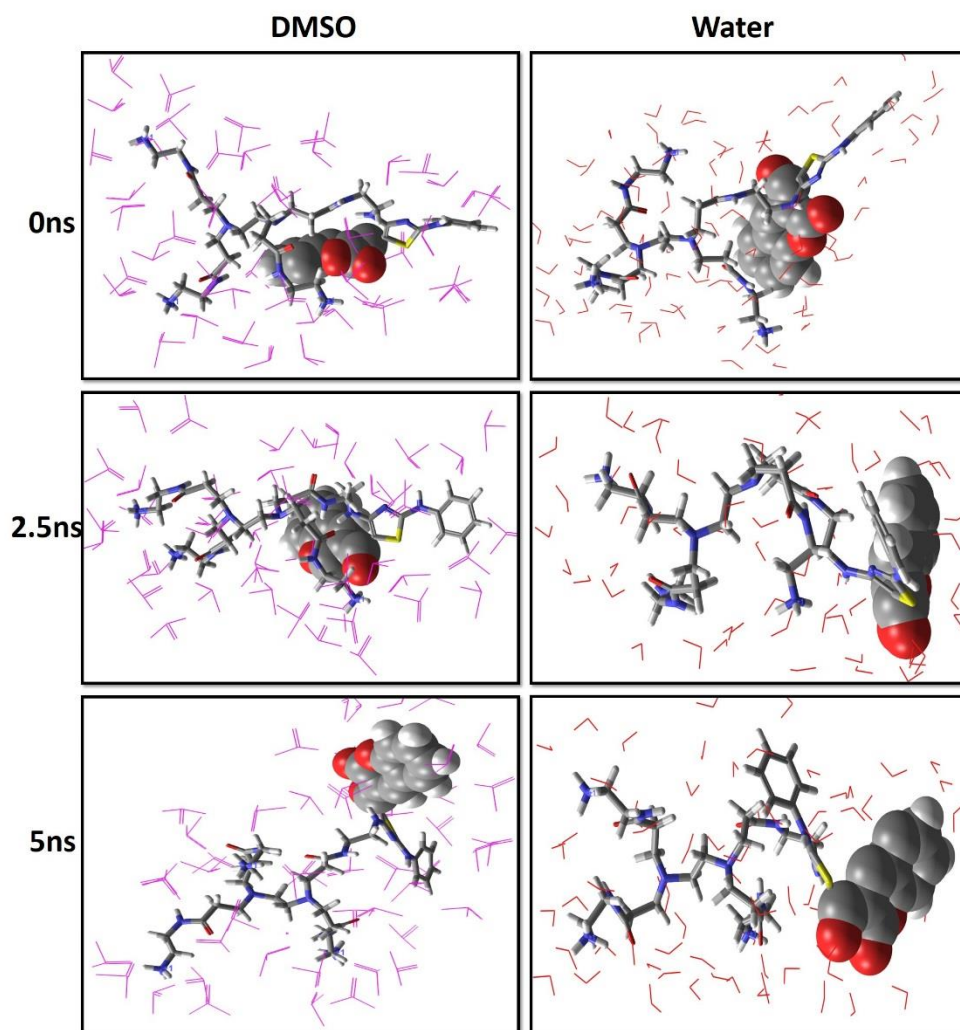


Figure 6.9. Snapshots of G0-CouTz during simulations in DMSO and water at pH7.4; DMSO (purple) and water (red) molecules at the vicinity of 3Å distance are displayed

The changes observed in the distance between the core and the modified terminal N-atom ($C_{N}^{II}T_{N1}^{II}$) and the including angle ($\angle T_{N1}^{II}C_{N}^{II}T_{N2}^{II}$) during the course of simulations are given in Figure 6.10.

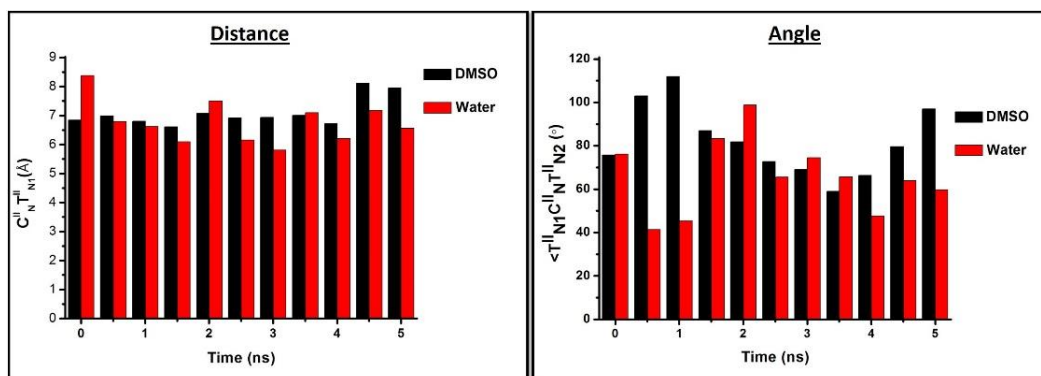


Figure 6.10. Time-evolution of the distance and angle between the core and modified terminal N-atom

In DMSO, after 5ns, the distance between the core N-atom and the functionalized N-atom increased by 1.1 Å unit whereas in water, the distance was reduced by 0.16 Å unit. In both the solvents the change in the angle between the arms were more pronounced. In DMSO, the increment in the included angle was found to be $\sim 21^\circ$ whereas in water the angle reduced by $\sim 16^\circ$. The change observed in the angle is mainly due to the difference in the intramolecular interactions of **G0-CouTz** in the solvents. Time-evolution of intramolecular H-bonding interactions observed in the conjugate is given in Figure 6.11.

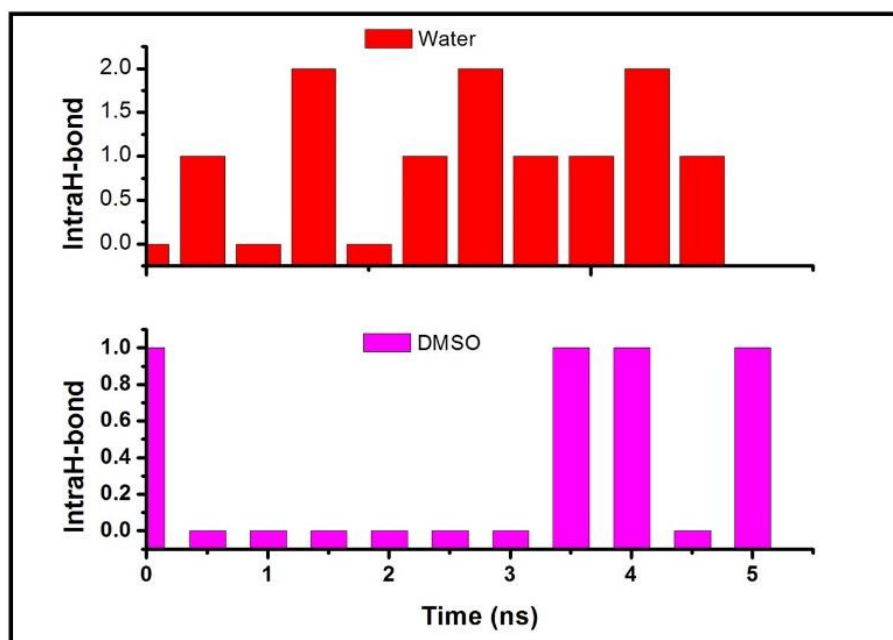


Figure 6.11. Time-evolution of intramolecular H-bonding interactions formed in **G0-CouTz** in DMSO and water

As in the case of G0, the conjugate also had more flexibility in water than in DMSO as indicated by the various E_{int} profile (Figure 6.12). The values of distances and angles obtained after 5ns simulation is shown in Table 6.2.

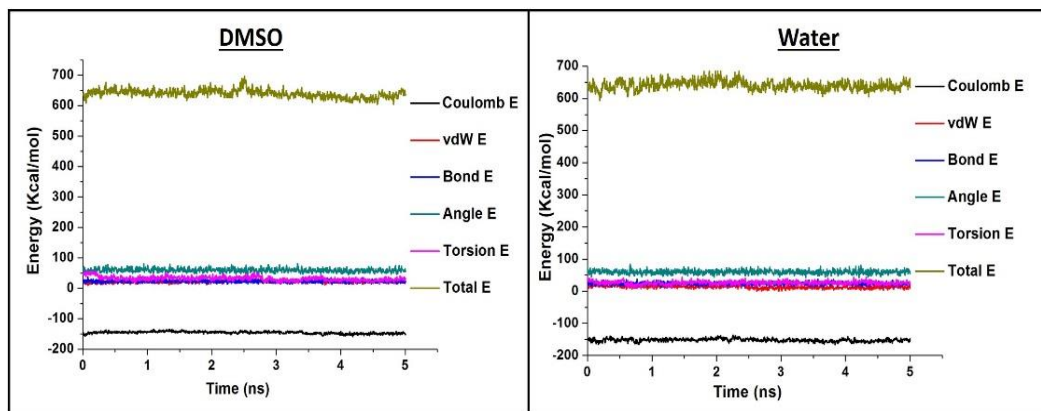


Figure 6.12. Variation of energy components of **G0-CouTz** in DMSO and water during the course of molecular dynamics simulations

Table 6.2. Distances and angles obtained for **G0-CouTz** after 5ns of simulations

Solvent	Distance (Å)				Angle (°)		Dihedral angle (°)
	T ^I _{N1} C ^I _N	T ^I _{N2} C ^I _N	T ^{II} _{N1} C ^{II} _N	T ^{II} _{N2} C ^{II} _N	T ^I _{N1} C ^I _N T ^I _{N2}	T ^{II} _{N1} C ^{II} _N T ^{II} _{N2}	
DMSO	8.17	5.50	7.94	7.03	97.06	109.9	-127.3
Water	6.88	6.81	6.55	6.54	38.7	59.6	87.3

The time-evolution of R_g (Figure 6.13) of **G0-CouTz** revealed that the molecule attained a comparatively large size in DMSO than in water. The mean radius of gyration was found to be 7.00 ± 0.29 and 6.25 ± 0.36 in DMSO and water respectively.

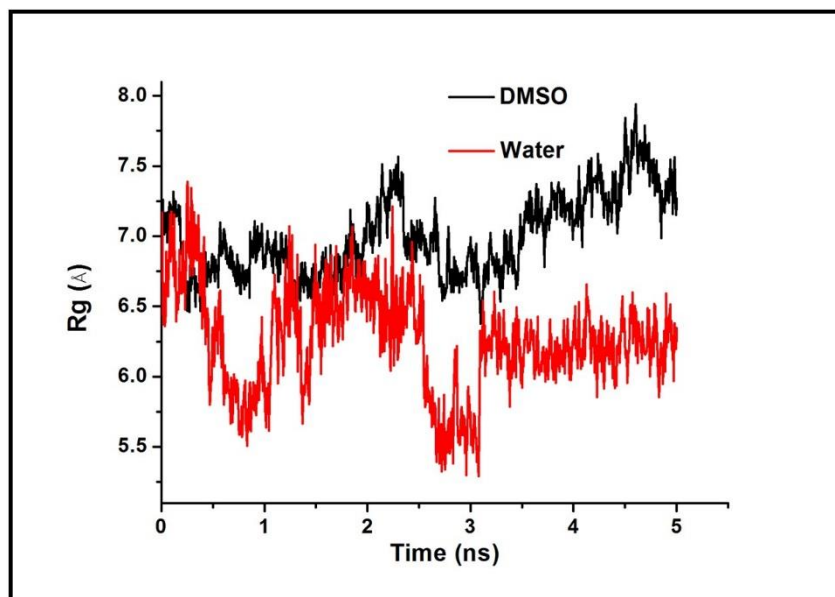


Figure 6.13. Time-evolution of radius of gyration of **G0-CouTz** in DMSO and water during the course of 5ns molecular dynamics simulations

The results obtained from MD confirmed the solvent dependent nature of the conjugate with a more open structure in DMSO with an increase in the radius of gyration. Under neutral pH, in water, the thiazole bearing arm was in close contact with unsubstituted arms of the dendrimer through π -cation interaction ($\sim 5\text{\AA}$) which imparted them a spiral-like structure. Whereas in DMSO, the conjugate at the end of 5ns, hardly showed any interactions with the free arms. The study revealed that the two ring systems- coumarin at *C5* and phenyl at *C2* in the thiazole ring attain parallel to perpendicular orientation with one another and the conjugate attained a completely open structure.

6.2.5.4. Effect of pH on the structure and dynamics of G0

The experimental studies have proven that PAMAM dendrimers are present in different protonation levels depending on the pH of the solution and the gyration radius of dendrimers changes as function of pH. Hence, in the present study, we have decided to study the difference in the structure and interactions of G0 and **G0-CouTz** at three different pH values- 4, 7.4 and 10 in aqueous solution.

The MD simulations were carried out in G0 for 5ns using an NPT ensemble at 300K and 1.013bar pressure in an orthorhombic box with $10 \times 10 \times 10 \text{ \AA}^3$ dimension. At acidic pH (pH=4), when the core as well as the terminal N-atoms are protonated the dendrimeric shape of the molecule was retained after 5ns. This may be due to the electrostatic repulsion between the positively charged N-atoms of the molecule which reduces the intramolecular H-bonding between the arms of the dendrimer. At physiological pH (pH=7.4), when only the terminal N-atoms are protonated, the flexibility of the arms of the dendrimer were more pronounced and it overcome the electrostatic repulsion between the atoms and trying to attain more compact structure through intramolecular H-bonding between the arms of the dendrimer. At higher pH all the N-atoms were found to be non-protonated after 5ns of simulations the dendrimer is observed to attain a completely compact structure with intramolecular H-bonding. The snapshots of the structures obtained for G0 during the MD simulations at different pH conditions is given in Figure 6.14 and the time-evolution of radius of gyration (Figure 6.15) revealed that the size of the dendrimer after 5ns was in the order pH4 (5.38 ± 0.31) > pH7.4(4.62 ± 0.27) > pH10(4.20 ± 0.25).

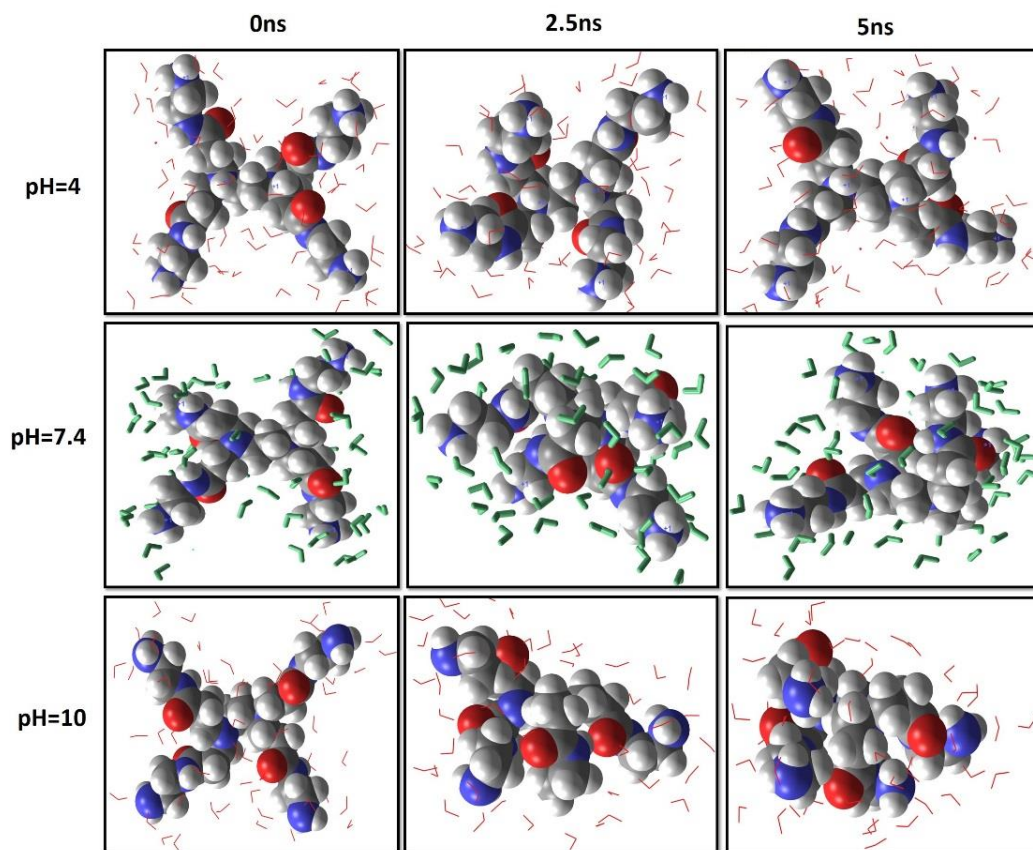


Figure 6.14. Snapshots of G0 during simulations under different pH in water. Water (red/aquamarine) molecules at the vicinity of 3Å distance are displayed

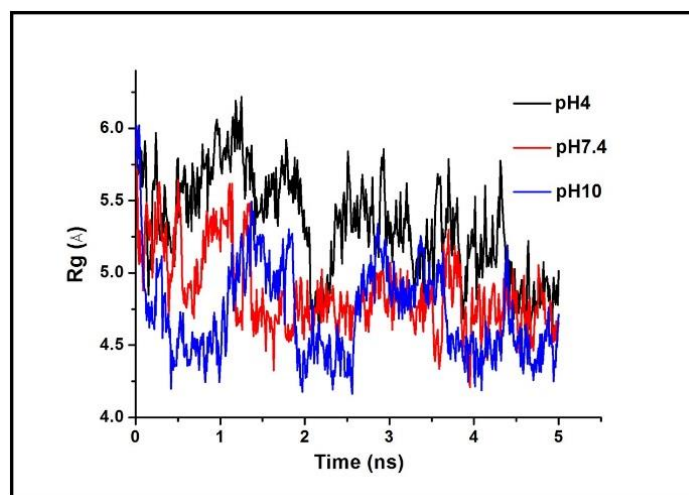


Figure 6.15. Time-evolution of radius of gyration of G0 in under different pH conditions during the course of 5ns molecular dynamics simulations

The total E_{int} of the dendrimer followed the same order which suggested that the flexibility of the dendrimer arms increase as the pH of the solution increases. The intramolecular H-bonding interactions were also pH dependent as shown in Figure 6.16.

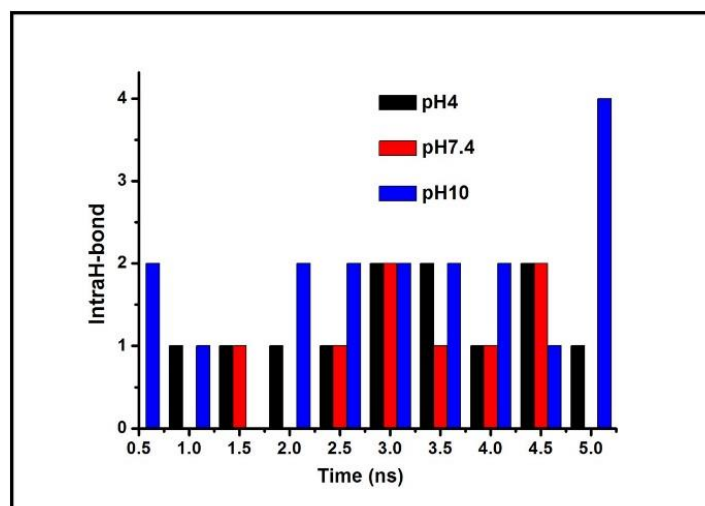


Figure 6.16. Time-evolution of intramolecular H-bonding interactions formed in G0 in water under different pH

The results obtained clearly proved the dependence of shape of the dendrimer on the pH of the solution.

6.2.5.5. Effect of pH on the structure and dynamics of G0-CouTz

The MD simulations of the conjugate **G0-CouTz** under the same experimental conditions revealed that the shape of the conjugate was changing during the course of simulations. Under all the tested pH conditions it was observed that as the time progressed the coumarinoyl ring at the C5 of the thiazole at the termini of dendrimer tend to move away from the cavity and at the end of 5ns, occupied the periphery (Figure 6.17). Here also the more compact structure was obtained at pH 10 primarily due to the intramolecular H-bonding interaction between the arms of the dendrimer under this pH. The mean values of different energy components along with the standard deviation obtained for the conjugate at different pH is given in Table 6.3.

Table 6.3. Mean values of various energy components of **G0-CouTz** obtained during MD simulation

Energy component	pH4	pH7.4	pH10
Coulomb E	-100.92±5.6	-152.0±4.6	-151.53±5.7
vdW E	18.00±4.1	13.3±4.4	14.87±4.8
Bond E	23.61±3.9	23.53±4.0	23.83±4.0
Angle E	60.46±6.0	59.85±5.9	58.27±5.8
Torsion E	21.47±4.7	26.38±5.0	39.11±6.0
Total E	669.96±20.2	641.10±14.0	743.0±12.5

The total E_{int} profile obtained at different pH revealed that the flexibility of the conjugate was higher at pH 10 as in the case of G0.

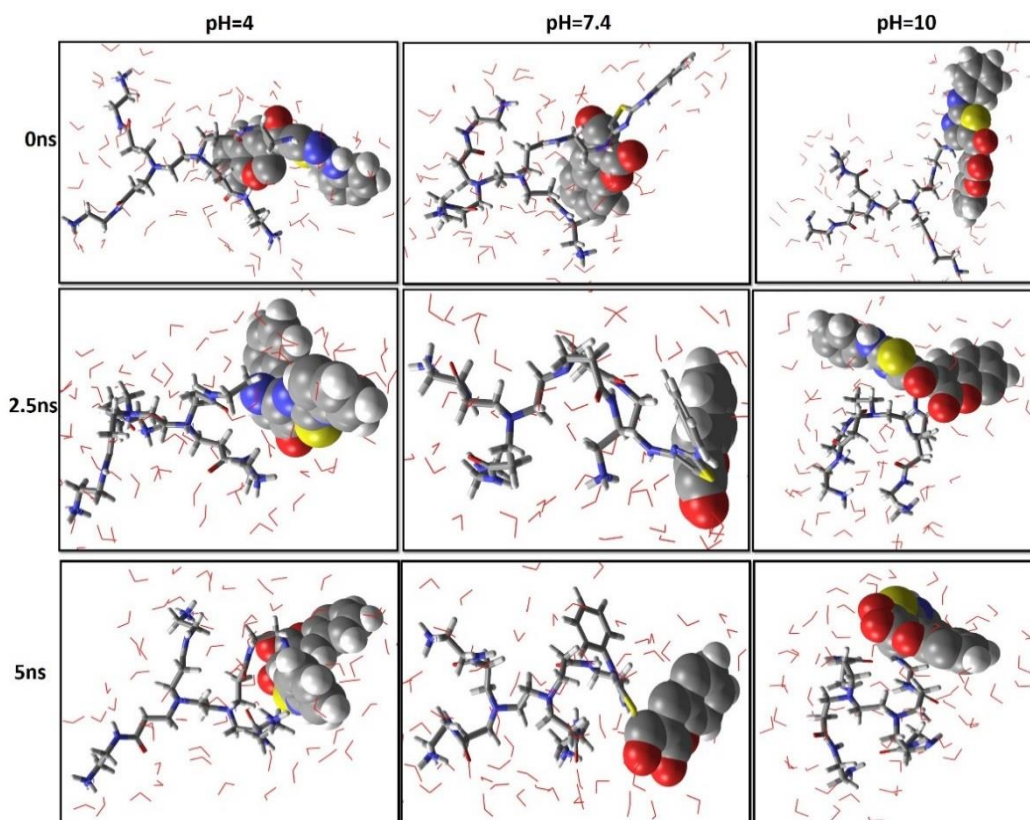


Figure 6.17. Snapshots of **G0-CouTz** during simulations under different pH in water; Water (red) molecules at the vicinity of 3 Å distance are displayed and the coumarin ring is represented in the CPK model for clarity

The size determination during the simulation revealed that the conjugate had a lower size at pH10 with mean $R_g = 5.73 \pm 0.3$ Å units whereas at pH 4 and 7.4 the mean value was found to be 6.54 ± 0.3 and 6.25 ± 0.3 respectively. Figure 6.18 shows the time-evolution of R_g during the course of MD simulations.

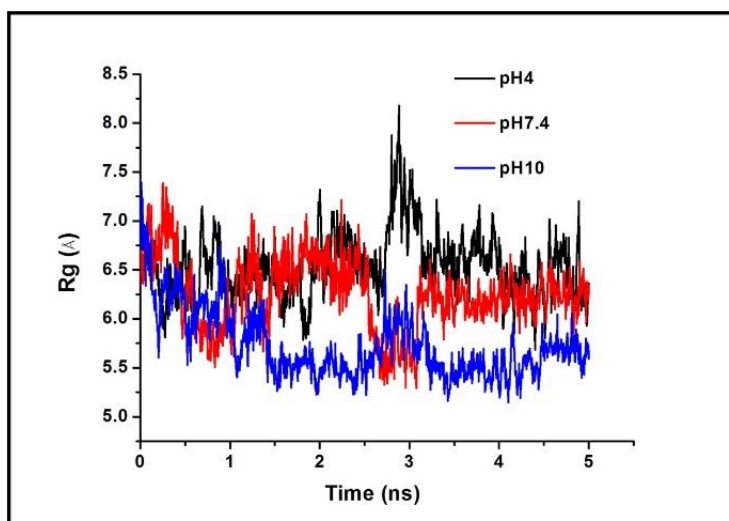


Figure 6.18. Time-evolution of radius of gyration of **G0-CouTz** in under different pH conditions during the course of 5ns molecular dynamics simulations

The structures obtained after 5ns simulation showed that under all pH conditions the coumarinoylthiazole unit migrated away from the dendrimer core. Table 6.4 gives the values of distances and angles obtained after 5ns simulation under different pH.

Table 6.4. The values of distances and angles obtained in **G0-CouTz** after 5ns at different pH

pH	Distance (Å)				Angle (°)		Dihedral angle (°)
	T ^I _{N1} C ^I _N	T ^I _{N2} C ^I _N	T ^{II} _{N1} C ^{II} _N	T ^{II} _{N2} C ^{II} _N	T ^I _{N1} C ^I _N T ^I _{N2}	T ^{II} _{N1} C ^{II} _N T ^{II} _{N2}	
4	6.94	8.42	6.08	7.64	123.3	89.6	165.7
7.4	6.88	6.81	6.54	6.55	38.7	59.6	87.3
10	7.89	7.02	6.30	5.95	105.5	61.5	-81.2

At acidic pH, the thiazole ring formed π -cation interaction with the protonated core N-atom and thereby pushing the substituents at C2 and C5 of the ring outwards and consequently R_g of the conjugate at this pH was increased. Under

physiological pH, the coumarin moiety formed π -cation interaction with the terminal charged N-atom which caused the bending of the modified arm. This led to a reduced cavity space between the arms of the dendrimer. Whereas at pH 10, the conjugate was stabilized by intra molecular H-bonding interactions between the arms of the molecule, thus attaining a globular like structure with reduced R_g . The internal cavity radius observed in the conjugate which can be indirectly determined by the angle between the arms of the dendrimer after the simulation was in the order of pH4>pH7.4>pH10. The information about the internal cavity radius and its pH dependent variation observed for the conjugate can be utilized to determine the encapsulation efficiency and thereby the release mechanism of suitable guest molecules.

6.3. Experimental Details

6.3.1. General reagent information

Aminoguanidine nitrate, acetyl acetone, methyl acrylate, isothiocyanates, 3-bromoacetyl coumarin, 4-nitrophenacylbromide and 4-chlorophenacylbromide were purchased from Aldrich chemical company. Triethylamine, ethylenediamine and solvents were purchased from Merck chemicals and were purified using standard methods before use. Sephadex LH-20 for column chromatography and deuterated solvents for NMR spectroscopy were obtained from Aldrich chemical company.

6.3.2. General analytical information

Purity of the compounds were checked using TLC on silica coated plates obtained from Merck, India and spots were visualized under UV light or in iodine chamber. All the synthesized compounds were characterized by spectroscopic techniques (NMR, MS, IR). NMR spectra were recorded using Bruker AV III 500 MHz FT NMR spectrometer using appropriate deuterated solvents. Molecular mass

determination was carried out using Bruker Ultraflex-TOF and ESI/HRMS using Thermoscientific Exactive Orbitrap mass spectrometer. Infrared (IR) spectra were obtained using Perkin Elmer Spectrum 100 FT-IR spectrometer.

6.3.3. General computational details

The chemical structures of the dendrimer and the conjugate was drawn using the graphical interface Maestro available in Schrodinger software suite. The charges on the dendrimer at different protonation levels were added manually and the stable conformations at different pH were obtained using MacroModel minimization panel available in the software suite. The minimizations were carried out using different force fields MM2, MMFF, MMFFs, AMBER and OPLS-2005 and OPLS-2005 has been chosen as the optimized one considering the energy of the optimized structure. All the minimizations were done in water as the solvent using PRCG minimization method with convergent threshold of energy 0.05 J/Åmol (RMS gradient of energy) in 5000 iterative steps. The minimized structure obtained using MacroModel was taken for the molecular dynamics simulations.

All the MD simulations were carried out using Desmond (version 4.5) for 5ns with a time step of 2fs. The preparation of the structures for simulation studies were done in selected solvents (DMSO and water) with the inbuilt solvent models available in the software. For the studies in water, TIP3P solvent model was used for modelling water molecules. We have selected orthorhombic box with a buffer size of 10Å for the MD simulations. All the simulations were carried out using an isothermal-isobaric ensemble (NPT) at 300K and 1.01325bar pressure using OPLS-2005 force field.

6.4. Synthesis

6.4.1. Synthesis of PAMAM G0

PAMAM G0 was synthesized by Tomalia's divergent method (Esfand and Tomalia, 2001). The half generation (G-0.5) dendrimer was synthesized by reacting EDA with 4 molar excess of methyl acrylate in MeOH at 0°C under N₂ atmosphere for 24h. The solvent was then removed and the dried product was then treated with excess EDA in MeOH under N₂ for 5days. After the completion of the reaction excess EDA was removed by azeotropic distillation using toluene/MeOH (9:1) and excess of toluene was removed by MeOH (10mL). The product obtained was dried under vacuum and purified using column chromatography on Sephadex LH-20 with CH₂Cl₂/MeOH (1:1) as eluent.

(^aCH₂^aCH₂)[N(^bCH₂^cCH₂^dCO^eNH^fCH₂^gCH₂^hNH₂)₂]₂: IR (UATR) ν cm⁻¹: 3344, 3281 (N-H), 2933, 2865 (C-H), 1633 (amide I), 1550 (amide II); ¹H NMR (500 MHz, D₂O): δ (ppm) 2.37-2.34 (m, c), 2.52 (m, a), 2.65-2.63 (m, g), 2.74-2.69 (m, b), 3.17-3.15 (m, f) ; ¹³C NMR (125MHz, D₂O): δ (ppm) 32.7, 39.8, 41.6, 49.2, 50.0, 175.0; ESI-MS (M+H)⁺: 517.4 (50%). The δ values were compared with the literature (Hung *et al.*, 2011) values. The mass spectra was also compared with the reported data (Uclés *et al.*, 2013) and was in complete agreement.

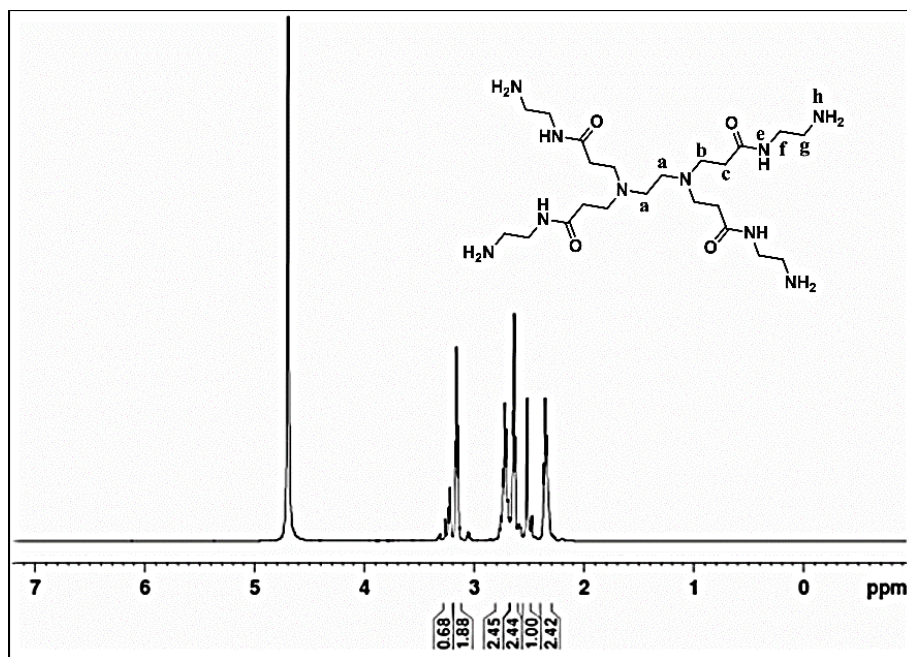


Figure 6.19. ^1H NMR spectrum of PAMAM G0

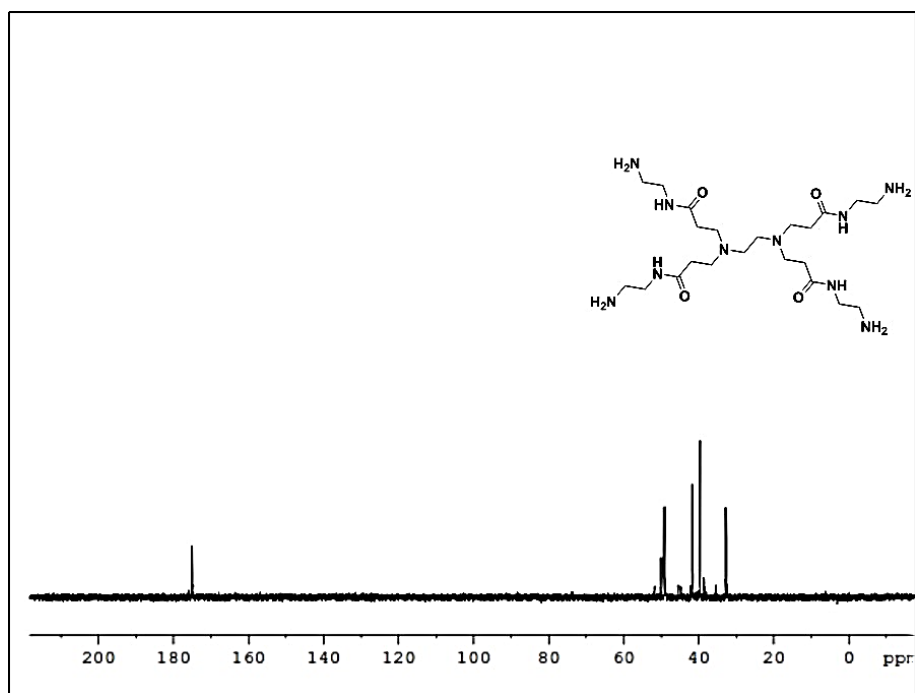


Figure 6.20. ^{13}C NMR spectrum of PAMAM G0

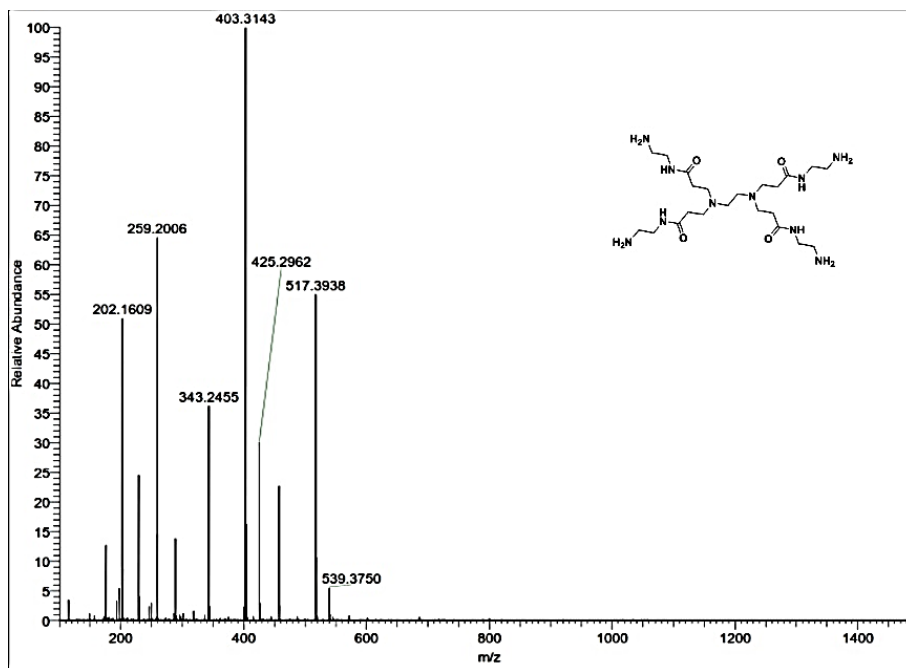


Figure 6.21. ESI-MS spectrum of PAMAM G0

6.4.2. Synthesis of G0-ATU

One of the amino groups of G0 dendrimer was selectively reacted with 1 $equiv.$ of 1-(N-phenylthiocarbamoyl)amidino-3,5-dimethylpyrazole in MeOH at 50°C for 12h. The reaction mixture was then washed with petroleum ether to remove the free 3,5-dimethyl pyrazole and the solvent was removed under reduced pressure. The product obtained was dried under vacuum at room temperature for 24h and purified by column chromatography on Sephadex LH-20 with MeOH as eluent.

C₃₀H₅₅N₁₃O₄S: Viscous liquid (yellow). Yield 68%. IR (UATR) ν cm⁻¹: 3340, 3280 (N-H), 3066 (aromatic C-H), 2940, 2835 (C-H), 1631 (amide I), 1543 (amide II), 1095 (C=S), 819 (aromatic); ¹H NMR (500 MHz, DMSO-d₆): δ (ppm) 2.11-2.19 (m, -NH₂), 2.35-2.42 (m, -NH₂), 2.49-3.72 (m, -CH₂), 6.93-7.55 (m, ArH), 7.60-8.07 (m, -NHC=O), 8.65 (s, =NH), 9.08 (-NHC=S), 9.51 (s, -ArNH); MALDI-TOF MS (M)⁺: 693.4.

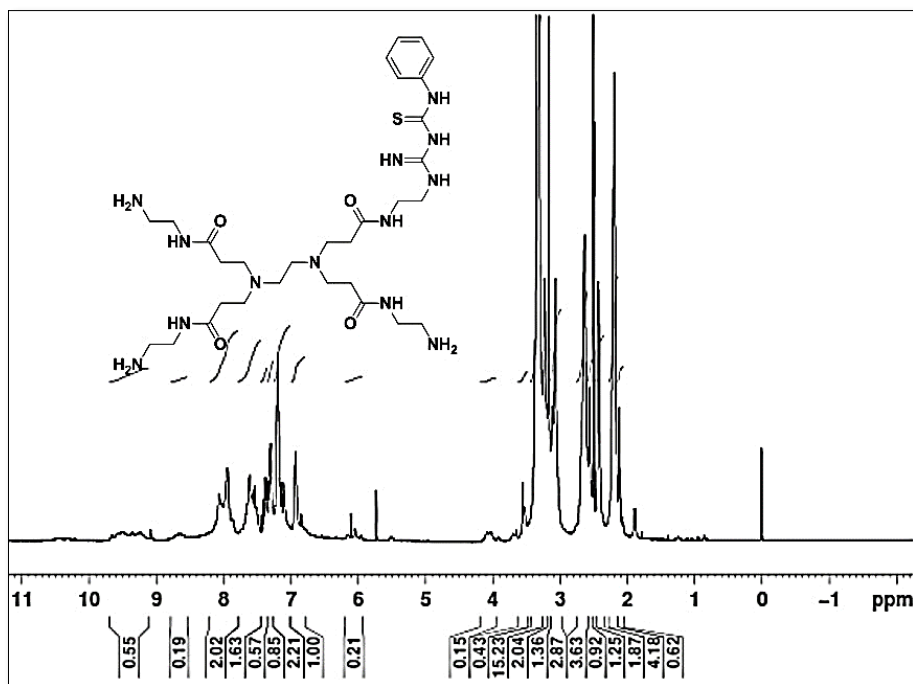


Figure 6.22. ^1H NMR spectrum of **G0-ATU**

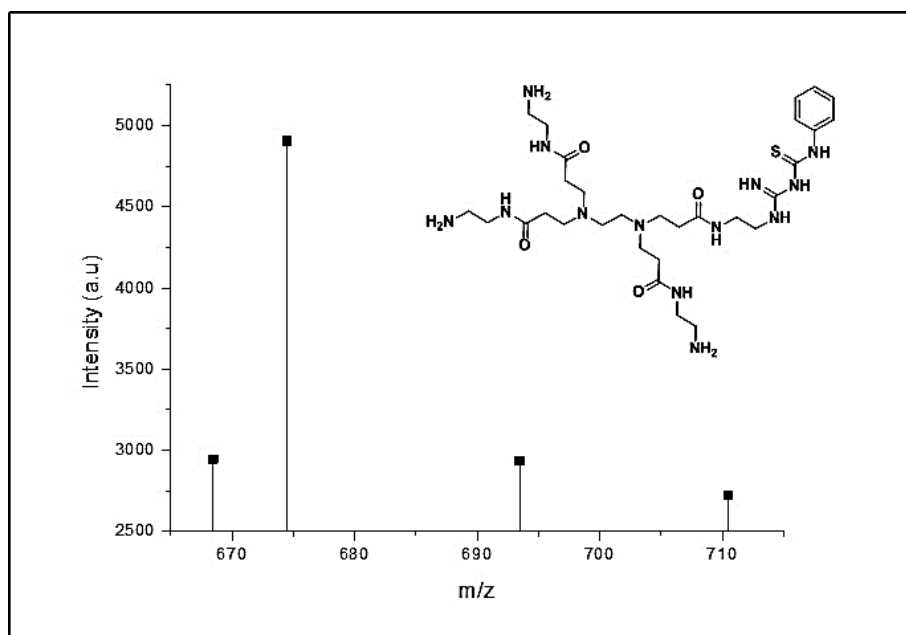


Figure 6.23. MALDI-TOF-MS spectrum of **G0-ATU**

6.4.3. Synthesis of G0-ATU-2

One of the amino groups of G0 dendrimer was selectively reacted with 1 $equiv.$ of 1-(N-(4-nitrophenylthiocarbamoyl))amidino-3,5-dimethylpyrazole in MeOH at 50°C for 12h. The reaction mixture was then washed with petroleum ether to remove the free 3,5-dimethyl pyrazole and the solvent was removed under reduced pressure. The product obtained was dried under vacuum at room temperature for 24h and purified by column chromatography on Sephadex LH-20 with MeOH as eluent.

C₃₀H₅₄N₁₄O₆S: Viscous liquid. Yielded 52%. IR (UATR) ν cm⁻¹: 3359, 3290 (N-H), 3094 (aromatic C-H), 2925, 2841 (C-H), 1625 (amide I), 1596 (amide II), 1108 (C=S), 847 (C-N stretch for ArNO₂), 819 (aromatic).

6.4.4. Synthesis of G0-CouTz

Conjugate **G0-ATU** (1mmol) in DMSO was treated with 3-bromoacetyl coumarin (0.9mmol) in presence of Et₃N (1.12mmol) for 3h at room temperature. The reaction mixture was then added to crushed ice and the precipitate obtained was filtered and dried. The product was purified by column chromatography on Sephadex LH-20 using petroleum ether/EtOAc (1:1) as eluent.

C₄₂H₆₀N₁₂O₆S: Pasty solid (yellow). Yield 25%. IR (UATR) cm⁻¹: 3378, 3269 (N-H), 3068 (aromatic C-H), 2941, 2851 (C-H), 1714 (C=O, lactone), 1636 (amide I), 1546 (amide II), 809 (aromatic); ¹H NMR (500 MHz, CDCl₃) δ (ppm): 0.79-0.81(m, -NH₂), 1.18-3.83 (m, -CH₂), 7.04-7.44 (m, ArH), 7.45-7.64 (m, -NHC=O), 7.76 (s, ArNH), 8.46 (s, coumarin CH); MALDI-TOF MS (M)⁺: 861.0.

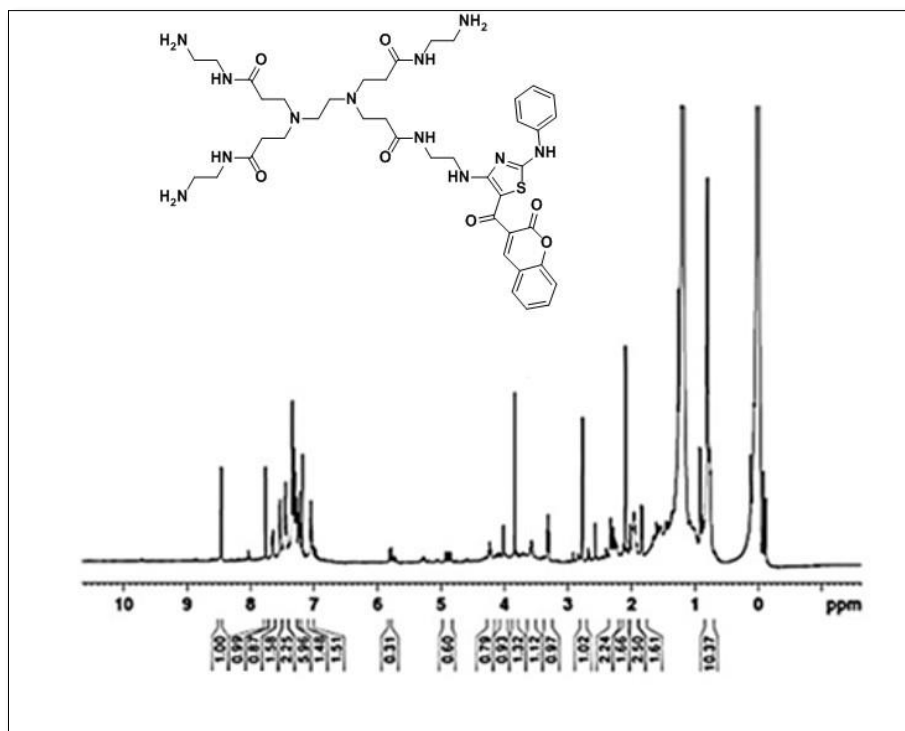


Figure 6.24. ¹H NMR spectrum of **G0-CouTz**

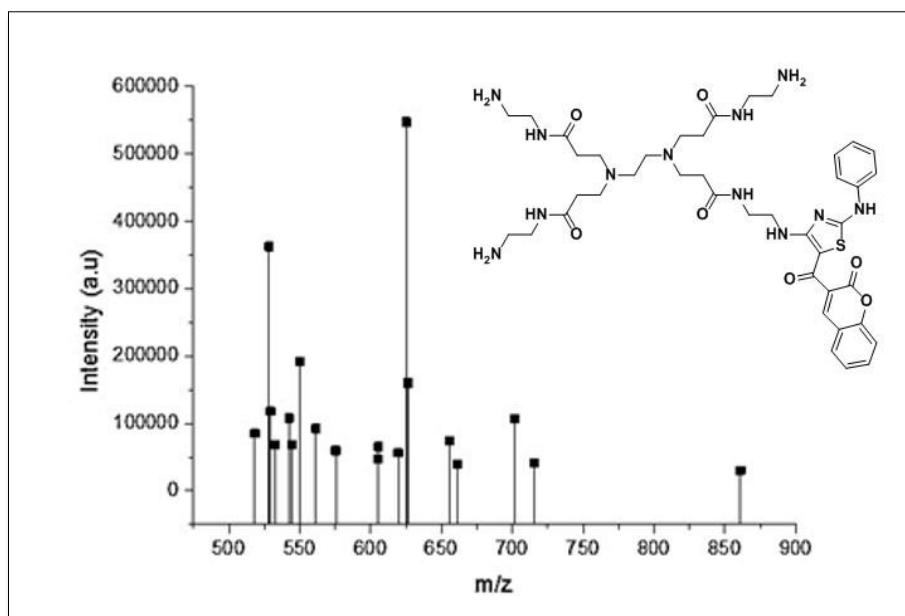


Figure 6.25. MALDI-TOF-MS spectrum of **G0-CouTz**

6.5. Conclusions

In summary, towards an effort to modify the PAMAM periphery with heterocyclic ring systems, we have designed and synthesized PAMAM amidinothiourea conjugate as a potential precursor platform for building diverse heterocycles on to the periphery of PAMAM through divergent covalent amidine transfer chemistry. To demonstrate the applicability of the synthon in heterocyclic nanovectorization we have designed and formulated novel synthetic routes for anchoring of the 2-aminothiazole moiety on to the periphery of PAMAM dendrimer. The 2-aminothiazolyl conjugates were synthesized by a [4+1] ring closure between amidinothiourea conjugated PAMAM and α -haloketone. With an intension of developing the conjugate as a potential nanoprobe for imaging applications PAMAM-coumarinoyl-2-aminothiazole conjugates was synthesized using 3-bromoacetylcoumarin as the haloketone component. The conjugate obtained was identified with green fluorescence. The changes observed in the microstructure of PAMAMG0 and the corresponding PAMAM-coumarinoyl-2-aminothiazolyl conjugate were studied using MD simulation in DMSO and water at different pH conditions. The studies revealed the change in the structural features with a larger radius of gyration in DMSO than in water. The pH dependence studies by MD provided an insight into the change in the cavity radius of the conjugate which is an indication on the encapsulation efficiency enabling use of such systems as carrier for suitable guest moieties.

CHAPTER 7

EVALUATION OF THE POTENCY OF NOVEL FLUORESCENT DENDRIMERIC NANOPROBE (FDN) FOR IMAGING APPLICATIONS

7.1. Background

The design of systems that can change their chemical and/or physical properties with their microenvironment has great significance in science and technologies for developing devices for environment protection and human health. As mentioned in the previous chapter, inherent superiorities such as high sensitivity, high selectivity, convenience, diversity and non-destructive character make fluorescence-based techniques most effective for such molecular devices. The potential of this detection or imaging technique is determined by the physicochemical properties of the fluorophores used. Though low molecular weight organic dye molecules are having high fluorescent intensity and quantum yield, poor solubility, lack of biocompatibility, low photostability and wide emission range have restricted their usage in many of the real world applications especially in biomedical field (Kumar, 2007). Thus, the development of highly fluorescent agents which have advantages over the conventional small molecular fluorescent systems in terms of sensitivity, specificity and signal strength (Koo *et al.*, 2011) has paramount significance in different fields of application. The need for improving the sensitivity and specificity of fluorophores continue to motivate researchers in exploring novel nanostructure based fluorescent probes (Chen and Yin, 2014). Considering the multivalent nature, structural control, comparatively less toxicity effects and the reproducibility of results have given fluorescent dendrimeric nanoprobes (FDNs) a significant position among all the fluorescent nanostructures studied so far.

The ease of modification of the functional groups and the relatively high biocompatibility of PAMAM dendrimers motivated the researchers to use them as medium-sized, bright, photostable platform for the development of FDNs with multiple options of bioconjugation for different imaging or diagnostic applications. Most of the PAMAM based FDNs studied so far are developed by the inclusion or covalent attachment of fluorescent labels. The amenable chemistry of PAMAM dendrimers allows the covalent attachment of the fluorescent compounds to the periphery (Grabchev *et al.*, 2002), to the core (Zhang *et al.*, 2010) or to both the positions (Bojinov *et al.*, 2008). In the present study, with the newly developed divergent synthetic method for PAMAM-2-aminothiazole conjugate we have attempted to impart useful photophysical properties by the introduction of a coumarin ring which is a well-known photounit with wide spread applications in biological activities (Borges *et al.*, 2005; Kontogiorgis & Hadjipavlou-Litina, 2005), laser dyes (Trenor *et al.*, 2004), fluorescence brighteners (Berthiaume *et al.*, 1998) and fluorochromophores (Taziaux *et al.*, 2004), to the periphery of the conjugate. This chapter discusses on the evaluation of the potential of the newly developed coumarinoyl-2-aminothiazole conjugated PAMAM (**G0-CouTz**) its photophysical properties in an attempt to demonstrate it for imaging applications. The absorption, emission, quantum yield, photostability and fluorescence lifetime were studied and are discussed in the following sections.

7.2. Results and Discussion

7.2.1. Absorption characteristics of the conjugates

The UV-visible absorption spectrum of PAMAM G0 in DMF exhibited absorption maxima corresponding to the $n-\pi^*$ transition at 276nm which is in correlation with the literature value (López-Cabaña *et al.*, 2015). Whereas amidinothiourea substitution on one of the arms of G0 resulted in red shift of the peak to 284nm with the appearance of a shoulder peak at 313nm. The absorption spectra of conjugate, **G0-CouTz**, showed two absorption bands with λ_{max} value of

294 (band I) and 380nm (band II) in which the latter one would be certainly from the $n-\pi^*$ transition of the coumarinoyl moiety (Gangopadhyay *et al.*, 2015) attached to the C5 of the thiazole ring. The absorption spectra of the compounds in DMF are shown in Figure 7.1.

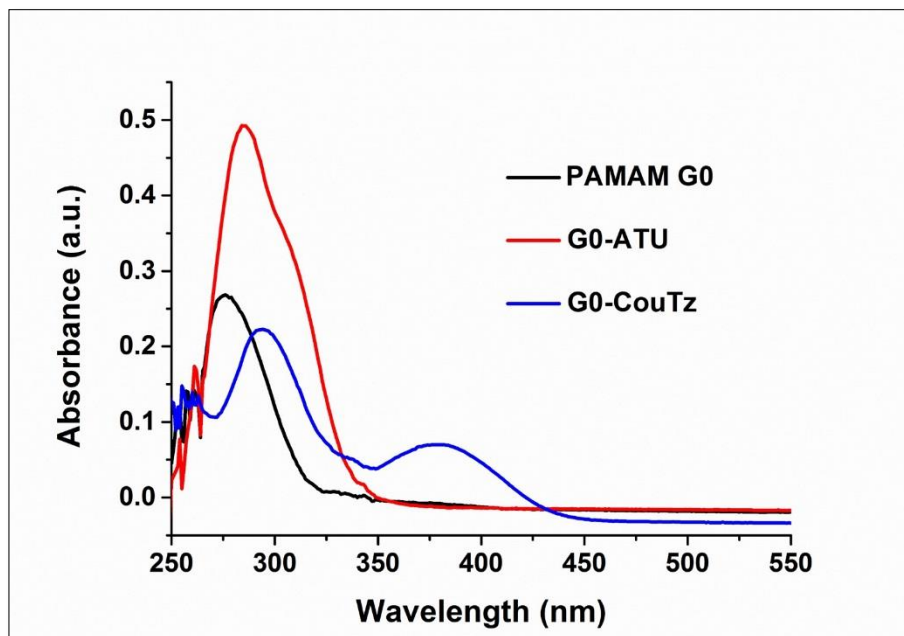


Figure 7.1. Comparison of UV-visible absorption spectra of PAMAM G0 and the conjugates in DMF

The thiazole moiety in the conjugate **G0-CouTz** can be considered as a π -bridge between the dendrimer and the photounit. The frontier molecular orbital (FMO) analysis of the conjugate revealed a π -polarized framework obtained on the periphery of PAMAM by the construction of the coumarinoyl-2-aminothiazole. The HOMO (highest occupied molecular orbital) was found to be localized on the 2-aminothiazole template whereas the LUMO (lowest unoccupied molecular orbital) was found to be localized on the coumarin moiety at C5 of the thiazole ring which suggested a possible charge transfer from the donor to acceptor (Figure 7.2.)

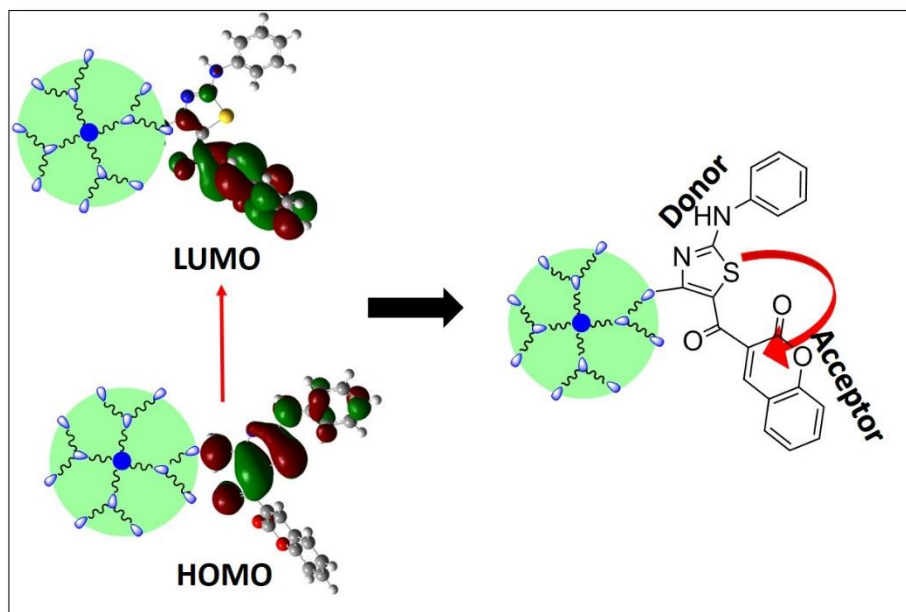


Figure 7.2. Schematic representation of possible charge transfer in **G0-CouTz**

It was observed that the absorption peaks of the conjugate was affected by the nature of the solvents. The maximum absorption wavelength (λ_{max}) of the band I and II of **G0-CouTz** in neat solvents along with relevant solvents parameters (Marcus, 1993) are summarized in Table 7.1. In nonpolar solvents, the absorptions were found to be at 286 and 369nm which corresponds to the $n-\pi^*$ transitions of dendrimer and coumarin moiety respectively. The polychlorinated solvents (CHCl_3 and DCM) used have little or no effect on the absorption band II whereas the absorption peak of the dendrimer, *i.e.*, band I, was slightly red shifted (5nm) in these solvents. In electron pair donating (EPD) solvents (Acetone, DMF and DMSO), a bathochromic shift was observed for both the bands with increase in polarity of solvents. In this group of solvents, the maximum shift was observed for DMSO where the λ_{max} values were found to be 298 (band I) and 383nm (band II). Figure 7.3 represents the comparison of the absorption spectra of compounds in three representative solvents.

Table 7.1. Solvatochromic shift in the absorption spectra of **G0-CouTz**

Solvent	λ_1 (nm)	λ_2 (nm)	α^a	β^b	π^{*c}
Cyclohexane	286	369	0.00	0.00	0.00
Hexane	286	368	0.00	0.00	-0.04
Toluene	291	369	0.00	0.11	0.54
CHCl ₃	291	370	0.20	0.10	0.58
DCM	291	369	0.13	0.10	0.82
Acetone	-	374	0.08	0.43	0.71
DMF	293	380	0.00	0.69	0.88
ACN	288	369	0.19	0.40	0.75
DMSO	298	383	0.00	0.76	1.00

^a Hydrogen bond donation ability of solvent ^b Hydrogen bond acceptance ability of solvent ^c polarity parameter

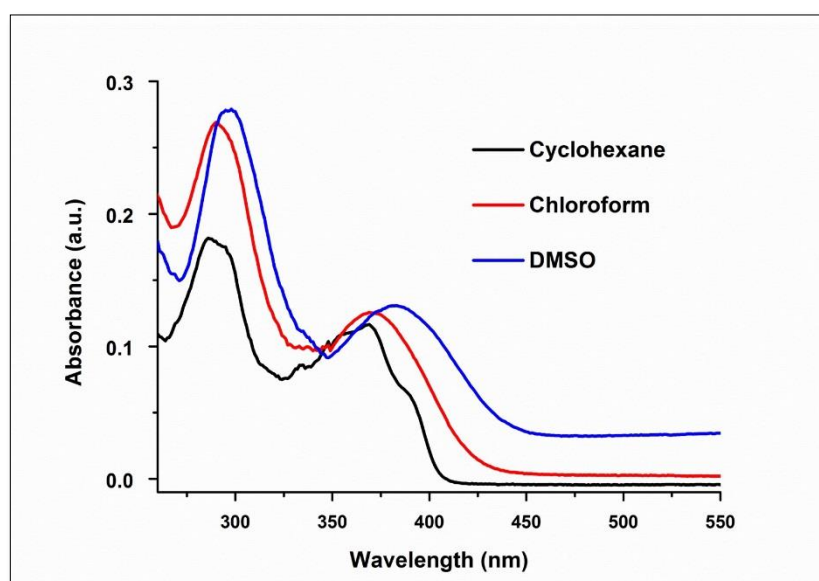


Figure 7.3. UV-visible absorption spectra of **G0-CouTz** in different solvents

The conjugate was found to be exhibiting a red shift of 12 and 14nm in wavelength maxima of band I and II respectively, when recorded in least polar cyclohexane to most polar DMSO. It is to be noted that the solvatochromic shifts observed in the absorption bands of the conjugate is affected by the HBA (Hydrogen bond acceptance) abilities and polarity/polarizability of the solvents (high values of β and π^*).

7.2.2. Emission characteristics of the conjugate

As mentioned in the previous chapter, the coumarinoyl-2-aminothiazole conjugate of PAMAM G0 (**G0-CouTz**) was showing a bright green fluorescence in the solid state. Enthused by the observation, we next proceeded with fluorescence emission studies of the conjugate in detail. The emission spectra of PAMAM G0 (1 μ M) in DMSO at the excitation wavelength of 298nm was observed with an emission maxima of 441nm with a fluorescence intensity of 1.24×10^4 . The conjugation of an amidinothiourea unit on to the periphery of PAMAM had no effect on the emission wavelength of the dendrimer but a decrease in the fluorescence intensity of the molecule (0.79×10^4) was observed when compared with the unmodified dendrimer. Whereas the emission spectra of the conjugate **G0-CouTz** (1 μ M) at an excitation wavelength of 294nm was observed with λ_{em} at 557nm with an intensity of 2.59×10^5 . The detailed analysis of the fluorescence emission of the conjugate in different solvents identified the potential of **G0-CouTz** as a solvent polarity indicator. The conjugate was observed with positive fluorescence solvatochromism (Figure 7.4) in presence of the solvents listed in Table 7.1. Coumarin dyes are well known examples of compounds showing solvatochromism due to change in the dipole moment in the ground and excited state (Ravi *et al.*, 1995). Since in the conjugate **G0-CouTz**, the periphery of the PAMAM dendrimer is having a π -rich framework a difference in the polarization of the conjugate in the excited state with polarizability of the solvents is expected. The emission maxima of the conjugate shifted from 467 to 557nm as the solvent changed from non-polar cyclohexane to polar DMSO. The emission spectra obtained for the conjugate in nine different solvents are shown in Figure 7.5.



Figure 7.4. Photographs of solid state green fluorescence (left) and positive solvatochromism obtained for **G0-CouTz** conjugate at an excitation wavelength of 365nm

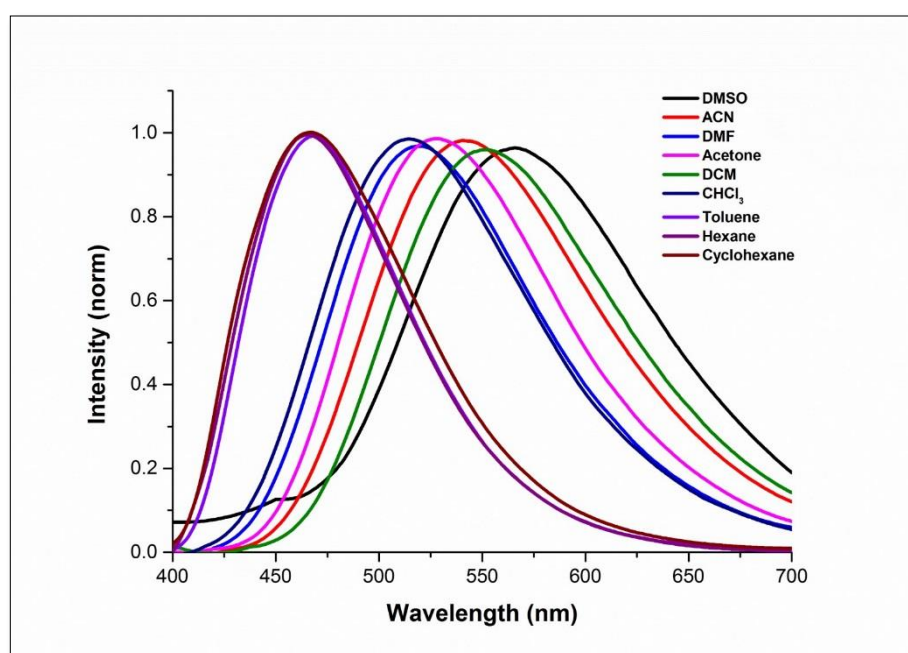


Figure 7.5. Emission spectra of **G0-CouTz** (1μM) in different solvents

With the absorption and emission spectral of the conjugate in hand, we next examined its Stokes shift (difference in band maxima of excitation and emission) values which are critical to the evaluation of fluorophore for bioimaging applications. Since large Stokes shift can separate the emission and excitation lights well and increase the sensitivity of fluorescence detection, the possible self-

quenching as well as fluorescence detection errors due to the excitation source will be efficiently avoided when such probes are used. Thus fluorescent probes with fluorescence tunability and large Stokes shifts (particularly those with Stokes shifts >80nm) are very promising, since in that case low background interference in bioimaging can be achieved (Bochkov *et al.*, 2013). Interestingly, we have found that along with the tuning of the fluorescence with polarity of solvents, the conjugate exhibited high to exceptionally large Stokes shift values in the solvents as listed in Table 7.2 where the values change from 98 to 175nm as the solvent changes from non-polar cyclohexane to polar DMSO.

Table 7.2. Stokes shift values calculated for **G0-CouTz** in different solvents

Solvent	λ_{abs} (nm)	λ_{em} (nm)	Stokes shift (nm)
Cyclohexane	369	467	98
Hexane	368	465	97
Toluene	369	472	103
CHCl ₃	369	514	136
DCM	368	515	146
Acetone	368	525	151
DMF	380	543	163
CH ₃ CN	369	543	171
DMSO	383	557	175

The fluorescence solvatochromism was better explained by Lippert-Mataga plot (Mataga *et al.*, 1956). The plot (Figure 7.6) of Stokes shift (cm⁻¹) versus solvent orientation polarizability furnished a linear fit ($R^2= 0.95$) and we anticipate

that this sensitivity to solvent polarity could be an attribute arising from the thiazole π -bridged coumarin moiety on the periphery of PAMAM.

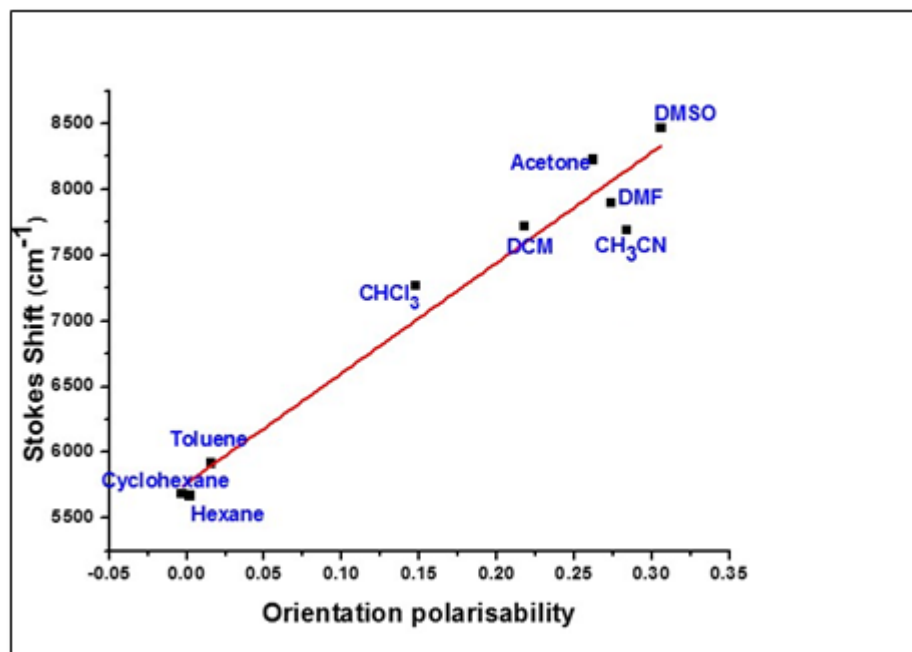


Figure 7.6. Lippert-Mataga plot of **G0-CouTz**

The absorption properties of **the conjugate** was almost independent on the solvent properties, which indicated that the electronic ground-state is not experiencing a particular stabilization by the employed solvent. But, the shift in the emission maxima was consistent with a process after excitation, which leads to an excited state where its energy was decreased in solvents with high π^* .

For any photoluminescent species, the quantum yield (QY) of its luminescence is a basic property, and its measurement is an important step in the characterization of the species. Fluorescence quantum yield (ϕ_f) is the ratio of photons emitted to that absorbed and that for the conjugate was calculated using quinine sulphate ($\phi_f = 0.55$) as the standard at an excitation wavelength of 366nm (Brouwer, 2011). The conjugate was observed with moderate to good QY in all the solvents tested where the maximum quantum yield was observed in toluene ($\phi_f = 0.77$). In dichloromethane, the conjugate with single arm of G0 modified with coumarinoyl-2-aminothiazole was observed with QY of 0.09. This value, which

was the lowest for our conjugate was found to be higher than that reported (Grabchev et al., 2002) for PAMAM G0 labelled with 1,8-naphthalimide (well-known dye) in all the four arms, where the QY varied from 0.01-0.08 depending on the substitution on naphthalimide ring.

Fluorescence lifetime being another significant criteria for selection of fluorophores in single-molecule fluorescence spectroscopy, we next investigated the fluorescence decay of the conjugate using time-correlated single-photon counting (TCSPC) at an excitation wavelength of 340nm. The decay profile of the conjugate in the solvents is given in Figure 7.7 which suggested a two component decay in all the solvents tested. The summarized results of ϕ_f and life time of the conjugate in the tested solvents is listed in Table 7.3.

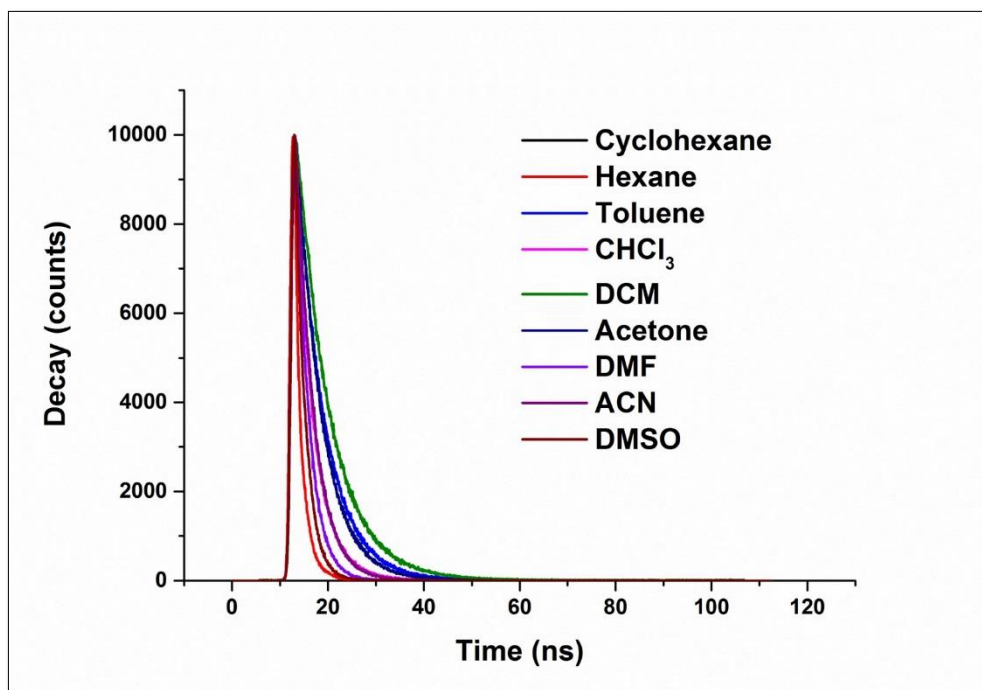


Figure 7.7. Fluorescence decay profile of **G0-CouTz** in different solvents

The photostability of the conjugate was studied in DMSO (excellent Stokes shift) by continuous irradiation of the solution with two UV lamps (16W) at a wavelength of 365nm for 2h. The fluorescence intensity (FI) of the solution was measured at an interval of 15min and it was found that the conjugate was

photostable up to 1.5h as the FI remains almost constant and after that the intensity got dropped drastically (Figure 7.8).

Table 7.3. Fluorescence lifetime and QY of **G0-CouTz**

Solvent	ϕ_f	Life time (ns)	
		τ_1	τ_2
Cyclohexane	0.22	2.5	10.1
Hexane	0.12	0.56	2.2
Toluene	0.77	2.7	10.9
CHCl ₃	0.23	1.7	4.3
DCM	0.09	3.3	13.3
Acetone	0.20	2.5	10.3
DMF	0.15	1.2	4.7
CH ₃ CN	0.20	1.7	3.7
DMSO	0.05	9.9	3.9

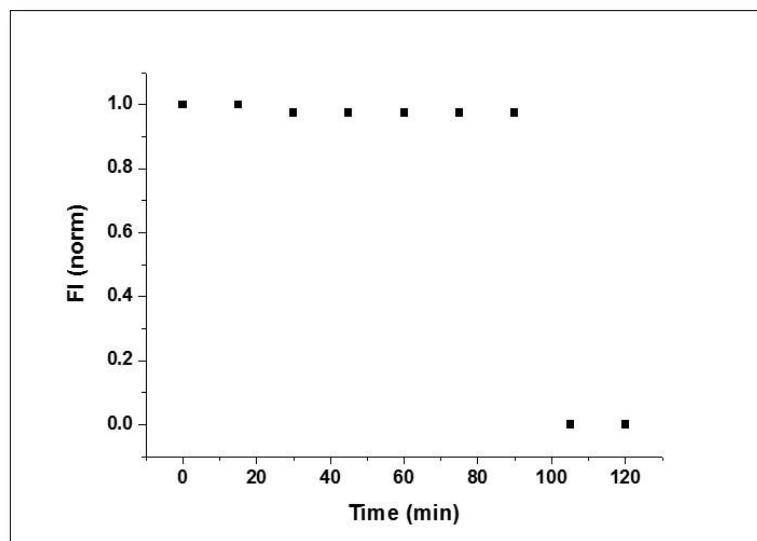


Figure 7.8. Change in fluorescence intensity with time at an irradiation wavelength of 365nm

7.3. Experimental Details

7.3.1. UV-Vis absorption studies

Varian Cary 100 Bio UV-Vis spectrophotometer was used for UV-Vis spectroscopy measurements. Spectroscopic grade solvents obtained from Merck chemicals/ Spectrochem were used for the studies without further purification. All the absorption spectra were recorded with 10^{-5} M concentration of compounds.

7.3.2. Fluorescence emission studies

All the fluorescence studies were carried out using Horiba Jobin Yvon Fluoromax-4 spectrometer and molecules were excited at their absorption maximum. The studies were carried out using 10^{-6} M concentration of the compounds. The photographs of the solid-state fluorescence and fluorescence solvatochromism were taken inside the UV chamber with a lamp of wavelength 365nm. The quantum yields of the samples were calculated with quinine sulphate as the standard at an excitation wavelength of 366nm using the equation,

$$\Phi_f^i = \frac{F^i f_s n_i^2}{F^s f_i n_s^2} \Phi_f^s$$

where F^i is the integrated area of sample, F^s is the integrated area of standard, n_i is the refractive index of sample solution, n_s is the refractive index of standard solution and f_x is the absorption factor ($f_x = 1 - 10^{-A_x}$, A =absorbance).

Fluorescence life time of the samples were analysed using time-correlated single-photon counting (TCSPC) with preset number of counts of 10000 photons at an excitation wavelength of 340nm. The photostability of the conjugate was investigated in a photo reactor equipped with two 16W UV lamps of 365nm wavelength. The sample solution in DMSO (10^{-6} M) was kept inside the reactor and the emission spectra of the sample solution was recorded at an interval of 15min up to 2h.

7.4. Conclusions

In summary, the synthesized coumarinoyl-2-aminothiazole-PAMAM conjugate, **G0-CouTz** was highly soluble in most of the organic solvents and was found to be an excellent a solvent polarity indicator as revealed from the fluorescence emission studies. This would further suggest the potential to develop the conjugate as labelling agents for cell membranes, protein binding sites and liposomes. The conjugate was identified with positive solvatochromism with emission maxima ranging from 467 to 557nm depending upon the polarity of the solvent. The Stokes shift values of the conjugate were found to be exceptionally high ranging from 98 to 175nm with moderate to good quantum yield (0.05-0.77). The photophysical studies of the conjugate has indicated the potential of the conjugate to be developed as a fluorescent dendrimeric nanoprobe. To the best of our knowledge our system achieved highest value of Stokes shift and quantum yield reported ever in a PAMAM system and our laboratories are further expanding the study to develop the FDN conjugate for imaging applications.

CHAPTER 8

CONCLUSIONS AND FUTURE PERSPECTIVES

8.1. Conclusions

Motivated by the importance of heterocyclic scaffolds in the bioactive chemical space, a novel 2-aminothiazole based template has been designed for small molecule drug design. PAMAM, being one of the best biocompatible carrier for biomedical applications, a divergent synthetic strategy for the development of PAMAM-2-aminothiazole conjugate has been developed in the present work. To summarise the results the key conclusions of the present work are as follows.

A novel 2-aminothiazole template based small molecule drug design scaffold, 4-hydrazinothiazoles, had been designed and developed with immense scope of diversity multiplication around the core. An efficient two-step as well as *one-pot* sequential multicomponent synthesis following a [4+1] ring closure were accomplished and optimized for the highly substituted scaffold. Utilizing the diversity components around the 2-aminothiazole core, four families of the identified scaffold were designed and representative members from each family were synthesized and structural elucidation was carried out using spectroscopic techniques. Solid-state screening of the synthesized compounds identified unique nitrogen rich channels in the crystal packing of the molecules which has the potential to serve as a suitable starting point for the development of thiazole based synthetic channels. The role of hydrazone moiety in the formation of these channels and thereby the control over the solvate formation was established using representative examples.

The anticancer activity of the molecules was evaluated by *in vitro* anticancer screening of synthesized molecules against six human cancer cell lines. The molecules were found to be more prone towards breast, lung and leukemia

cancer cell lines and two structural analogues of DAT1, a well-known anticancer agent, were identified as active against MCF-7 and one against A549 cell lines was identified from a library of twenty one compounds screened.

Molecular docking studies with a 120 member virtual library of the designed scaffold has identified AURK family of proteins as a promising target for the newly developed drug design scaffold, 4-hydrazinothiazoles. Structure based ligand docking of a library of 22500 molecules of 4-benzylidenehydrazinothiazole identified the novel library of molecules as ATP competitive Type I AURK inhibitors. In an effort towards lead generation, the effect of ring substituents on the binding of the compounds in AURK A and B protein active sites was studied using hydrazone analogue of DAT1 viz; 5-benzoyl-4-benzylidenehydrazino-2-(4-methoxyphenylamino)thiazole as the hit. Ring C substitution had a substantial effect on the binding interaction of the compounds in both AURK A and AURK B proteins whereas ring A substitution was pronounced effect in AURKA protein with DFG-in conformation. ADME property prediction of the library of molecules had proven the 'drug-likeness' of the scaffold and $-\text{NO}_2$ group substitution was predicted with lowest oral bioavailability.

Being interested in nanovectorization of heterocyclic ring compounds on to PAMAM periphery, novel synthetic routes for achieving a potential versatile synthon, amidinothiourea conjugated PAMAM, for building diverse heterocycles on PAMAM periphery was designed and formulated. The utility of the synthon in heterocycle-PAMAM conjugate development was demonstrated by the synthesis of a bivariant PAMAMG0-2-aminothiazole conjugate following a [4+1] ring closure between amidinothiourea conjugated PAMAMG0 and α -haloketone. The use of the novel divergent conjugate in tuning of properties was demonstrated by the development of PAMAMG0-coumarinoyl-2-aminothiazole conjugate with green solid-state fluorescence which showed exciting photophysical properties such as bright fluorescence, high Stokes shift and moderate to good quantum yield

in solution state. Studies on the novel conjugate were carried out to identify the potential of developing a fluorescent nanoprobe.

The solvent dependence and pH dependence on the microstructure of PAMAMG0 and the PAMAM-coumarinoyl-2-aminothiazolyl conjugate were evaluated using MD simulations in DMSO and water at three different pH conditions. The studies revealed the swelling of the molecules in DMSO with larger radius of gyration. The pH dependence studies have proven a larger internal cavity radius of the conjugate at lower pH which can be utilized in using the conjugate for encapsulation of suitable guest moieties.

In summary, in the present work we have developed a novel small molecule anticancer drug design scaffold based on 2-aminothiazole template and identified it as a promising ATP competitive Type I Aurora inhibitor by molecular docking studies. We have succeeded in the development of a 2-aminothiazole template on to a very useful biocompatible nanocarrier PAMAM and in the development of a PAMAM-2-aminothiazole conjugate with excellent photophysical properties which have the potential to be developed as a nanoprobe for bioimaging applications.

8.2. Future Perspectives

The designed 4-hydrazinothiazole was found to be an excellent scaffold with large possibility of structural alterations. The virtual library of the template can be expanded further and can be screened in the active sites of different target proteins. Apart from these single crystal XRD studies on the template can be extended further to use such supramolecular synthons in the development of biomimetic membranes and water/ion channels. The designed PAMAM-thiazolyl conjugate has the potential to be developed as a carrier for drug molecules either by utilizing the internal cavity or by peripheral conjugation to the free amino groups. The large Stokes shift values and extremely good quantum yields obtained for the fluorescent dendrimeric probe based on PAMAM-coumarinoyl thiazole

can be made use in imaging application and the studies are in progress in our laboratory.

REFERENCES

1. Aaltonen, J., Allesø, M., Mirza, S., Koradia, V., Gordon, K. C., & Rantanen, J. (2009). Solid form screening—a review. *European Journal of Pharmaceutics and Biopharmaceutics*, 71(1): 23-37.
2. Adronov, A., Gilat, S. L., Frechet, J. M., Ohta, K., Neuwahl, F. V., & Fleming, G. R. (2000). Light harvesting and energy transfer in laser-dye-labeled poly (aryl ether) dendrimers. *Journal of the American Chemical Society*, 122(6): 1175-1185.
3. Agre, P. (2004). Aquaporin water channels (Nobel lecture). *Angewandte Chemie International Edition*, 43(33): 4278-4290.
4. Agre, P., King, L. S., Yasui, M., Guggino, W. B., Ottersen, O. P., Fujiyoshi, Y., *et al.* (2002). Aquaporin water channels—from atomic structure to clinical medicine. *The Journal of Physiology*, 542(1): 3-16.
5. Ahluwalia, G. S., Jayaram, H. N., Plowman, J. P., Cooney, D. A., & Johns, D. G. (1984). Studies on the mechanism of action of 2- β -d-ribofuranosylthiazole-4-carboxamide—V: Factors governing the response of murine tumors to tiazofurin. *Biochemical Pharmacology*, 33(8): 1195-1203.
6. Akeson, M., & Deamer, D. W. (1991). Proton conductance by the gramicidin water wire. Model for proton conductance in the F1F0 ATPases? *Biophysical Journal*, 60(1): 101-109.
7. Al-Omary, F. A., Hassan, G. S., El-Messery, S. M., & El-Subbagh, H. I. (2012). Substituted thiazoles V. Synthesis and antitumor activity of novel thiazolo [2, 3-b] quinazoline and pyrido [4, 3-d] thiazolo [3, 2-a] pyrimidine analogues. *European Journal of Medicinal Chemistry*, 47: 65-72.
8. Al-Said, M. S., Ghorab, M. M., Al-Dosari, M. S., & Hamed, M. M. (2011). Synthesis and in vitro anticancer evaluation of some novel hexahydroquinoline derivatives having a benzenesulfonamide moiety. *European Journal of Medicinal Chemistry*, 46(1): 201-207.
9. Amir, M., Ali, I., Hassan, M., & Mulakayala, N. (2014). Design, synthesis, and biological evaluation of hydrazone Incorporated 1, 2, 4-triazines as anticonvulsant agents. *Archiv der Pharmazie*, 347(12): 958-968.
10. Amorín, M., Llamas-Saiz, A. L., Castedo, L., & Granja, J. R. (2011). Three-dimensional water channel embedded in an α , γ -cyclic octapeptide-derived organic porous material. *Crystal Growth & Design*, 11(8): 3351-3357.

11. Andersen, C. B., Wan, Y., Chang, J. W., Riggs, B., Lee, C., Liu, Y., *et al.* (2008). Discovery of selective aminothiazole aurora kinase inhibitors. *ACS Chemical Biology*, 3(3): 180-192.
12. Andrews, P. D. (2005). Aurora kinases: shining lights on the therapeutic horizon? *Oncogene*, 24(32): 5005-5015.
13. Andronnikova, G., Usol'tseva, S., Nikolaeva, S., Anoshina, G., Nifontov, V., & Emelina, É. (1988). Synthesis and antitumor activity of 2-hydrazinothiazole derivatives. *Pharmaceutical Chemistry Journal*, 22(11): 835-837.
14. Arbitrario, J. P., Belmont, B. J., Evanchik, M. J., Flanagan, W. M., Fucini, R. V., Hansen, S. K., *et al.* (2010). SNS-314, a pan-Aurora kinase inhibitor, shows potent anti-tumor activity and dosing flexibility *in vivo*. *Cancer Chemotherapy and Pharmacology*, 65(4): 707-717.
15. Arunachalam, M., Suresh, E., & Ghosh, P. (2007). Synthesis and X-ray crystallographic investigation of a novel indole-based cryptand: structure of a sandwiched cyclic S 6 hexameric methanol cluster. *Tetrahedron Letters*, 48(16): 2909-2913.
16. Aryal, P., Sansom, M. S., & Tucker, S. J. (2015). Hydrophobic gating in ion channels. *Journal of Molecular Biology*, 427(1): 121-130.
17. Auerbach, C., & Falconer, D. (1949). A new mutant in the progeny of mice treated with nitrogen mustard. *Nature*, 163(4148): 678-678.
18. Ayati, A., Emami, S., Asadipour, A., Shafiee, A., & Foroumadi, A. (2015). Recent applications of 1, 3-thiazole core structure in the identification of new lead compounds and drug discovery. *European Journal of Medicinal Chemistry*, 97: 699-718.
19. Azhdarinia, A., Ghosh, P., Ghosh, S., Wilganowski, N., & Sevic-Muraca, E. M. (2012). Dual-labeling strategies for nuclear and fluorescence molecular imaging: a review and analysis. *Molecular Imaging and Biology*, 14(3): 261-276.
20. Babu, N. J., & Nangia, A. (2006). Multiple z'in carboxylic acid-pyridine trimer synthon and kagomé lattice in the structure of 5-methylpyrazine-2, 3-dicarboxylic acid. *Crystal Growth & Design*, 6(9): 1995-1999.
21. Ball, P. (2008). Water as an active constituent in cell biology. *Chemical Reviews*, 108(1): 74-108.

22. Barboiu, M., & Gilles, A. (2013). From natural to bioassisted and biomimetic artificial water channel systems. *Accounts of Chemical Research*, 46(12): 2814-2823.
23. Belevich, I., Verkhovsky, M. I., & Wikström, M. (2006). Proton-coupled electron transfer drives the proton pump of cytochrome c oxidase. *Nature*, 440(7085): 829-832.
24. Benitez, A., Ross, L. O., Goodman, L., & Baker, B. (1960). Potential anticancer agents. 1 XXXVI. alkylating agents derived from 5-aminouracil. *Journal of the American Chemical Society*, 82(17): 4585-4591.
25. Beraldo, H., & Gambino, D. (2004). The wide pharmacological versatility of semicarbazones, thiosemicarbazones and their metal complexes. *Mini Reviews in Medicinal Chemistry*, 4(1): 31-39.
26. Berthiaume, M. D., Raleigh, W. J., & Uriarte, R. J. (1998). Fluorescent brightening of cosmetic compositions, *US5830446 A*.
27. Bharti, S. K., Nath, G., Tilak, R., & Singh, S. (2010). Synthesis, antibacterial and anti-fungal activities of some novel Schiff bases containing 2, 4-disubstituted thiazole ring. *European Journal of Medicinal Chemistry*, 45(2): 651-660.
28. Bhat, S., Shim, J. S., & Liu, J. O. (2013). Tricyclic thiazoles are a new class of angiogenesis inhibitors. *Bioorganic & Medicinal Chemistry Letters*, 23(9): 2733-2737.
29. Binu, R., Thomas, K., Jenardanan, G., & Rajasekharan, K. (1998). Synthesis and cyclization of 1-(N-nitroamidino) thioureas to 2, 4-diaminothiazoles. *Organic Preparations and Procedures International*, 30(1): 93-96.
30. Bleicher, K. H., Böhm, H.-J., Müller, K., & Alanine, A. I. (2003). Hit and lead generation: beyond high-throughput screening. *Nature Reviews Drug Discovery*, 2(5): 369-378.
31. Blum, R. H., Carter, S. K., & Agre, K. (1973). A clinical review of bleomycin—a new antineoplastic agent. *Cancer*, 31(4): 903-914.
32. Bochkov, A. Y., Akchurin, I. O., Dyachenko, O. A., & Traven, V. F. (2013). NIR-fluorescent coumarin-fused BODIPY dyes with large Stokes shifts. *Chemical Communications*, 49(99): 11653-11655.
33. Bohacek, R. S., McMartin, C., & Guida, W. C. (1996). The art and practice of structure-based drug design: A molecular modeling perspective. *Medicinal Research Reviews*, 16(1): 3-50.

34. Bojinov, V. B., Georgiev, N. I., & Nikolov, P. S. (2008). Design and synthesis of core and peripherally functionalized with 1, 8-naphthalimide units fluorescent PAMAM dendron as light harvesting antenna. *Journal of Photochemistry and Photobiology A: Chemistry*, 197(2): 281-289.
35. Bolanos-Garcia, V. M. (2005). Aurora kinases. *The International Journal of Biochemistry & Cell Biology*, 37(8): 1572-1577.
36. Bollag, D. M., McQueney, P. A., Zhu, J., Hensens, O., Koupal, L., Liesch, J., *et al.* (1995). Epothilones, a new class of microtubule-stabilizing agents with a taxol-like mechanism of action. *Cancer Research*, 55(11): 2325-2333.
37. Bondar, A.-N., Fischer, S., & Smith, J. C. (2011). Water pathways in the bacteriorhodopsin proton pump. *The Journal of Membrane Biology*, 239(1-2): 73-84.
38. Borges, F., Roleira, F., Milhazes, N., Santana, L., & Uriarte, E. (2005). Simple coumarins and analogues in medicinal chemistry: occurrence, synthesis and biological activity. *Current Medicinal Chemistry*, 12(8): 887-916.
39. Brouwer, A. M. (2011). Standards for photoluminescence quantum yield measurements in solution (IUPAC Technical Report). *Pure and Applied Chemistry*, 83(12): 2213-2228.
40. Buhleier, E., Wehner, W., & Vogtle, F. (1978). Cascade-chain-like and nonskid-chain-like syntheses of molecular cavity topologies. *Synthesis-Stuttgart*, (2): 155-158.
41. Butler, M. S., Robertson, A. A., & Cooper, M. A. (2014). Natural product and natural product derived drugs in clinical trials. *Natural Product Reports*, 31(11): 1612-1661.
42. Cagin, T., Wang, G., Martin, R., Breen, N., & Goddard III, W. A. (2000). Molecular modelling of dendrimers for nanoscale applications. *Nanotechnology*, 11(2): 77.
43. Cai, J., Zhang, S., Zheng, M., Wu, X., Chen, J., & Ji, M. (2012). Design, synthesis, and in vitro antiproliferative activity of novel Dasatinib derivatives. *Bioorganic & Medicinal Chemistry Letters*, 22(2): 806-810.
44. Caminade, A.-M., Laurent, R., & Majoral, J.-P. (2005). Characterization of dendrimers. *Advanced Drug Delivery Reviews*, 57(15): 2130-2146.
45. Carraro, F., Pucci, A., Naldini, A., Schenone, S., Bruno, O., Ranise, A., *et al.* (2004). Pyrazolo [3, 4-d] pyrimidines endowed with antiproliferative

- activity on ductal infiltrating carcinoma cells. *Journal of Medicinal Chemistry*, 47(7): 1595-1598.
46. Carvajal, R. D., Tse, A., & Schwartz, G. K. (2006). Aurora kinases: new targets for cancer therapy. *Clinical Cancer Research*, 12(23): 6869-6875.
 47. Carvalho, C., Santos, R. X., Cardoso, S., Correia, S., Oliveira, P. J., Santos, M. S., *et al.* (2009). Doxorubicin: the good, the bad and the ugly effect. *Current Medicinal Chemistry*, 16(25): 3267-3285.
 48. Carvalho, F. S., Burgeiro, A., Garcia, R., Moreno, A. J., Carvalho, R. A., & Oliveira, P. J. (2014). Doxorubicin-induced cardiotoxicity: From bioenergetic failure and cell death to cardiomyopathy. *Medicinal Research Reviews*, 34(1): 106-135.
 49. Ceccarelli, C., Jeffrey, G., & Taylor, R. (1981). A survey of OH-O hydrogen bond geometries determined by neutron diffraction. *Journal of Molecular Structure*, 70: 255-271.
 50. Cejudo, R., Alzuet, G., González-Alvarez, M., García-Gimenez, J., Borrás, J., & Liu-González, M. (2006). DNA cleavage reaction induced by dimeric copper (II) complexes of N-substituted thiazole sulfonamides. *Journal of Inorganic Biochemistry*, 100(1): 70-79.
 51. Chaplin, M. (2006). Do we underestimate the importance of water in cell biology? *Nature Reviews Molecular Cell Biology*, 7(11): 861-866.
 52. Chen, L., Chu, X.-j., Lovey, A., & Zhao, C. (2005). 4-Aminothiazole derivatives, *US20060014958 A1*.
 53. Chen, M., & Yin, M. (2014). Design and development of fluorescent nanostructures for bioimaging. *Progress in Polymer Science*, 39(2): 365-395.
 54. Chen, R., Wierda, W. G., Chubb, S., Hawtin, R. E., Fox, J. A., Keating, M. J., *et al.* (2009). Mechanism of action of SNS-032, a novel cyclin-dependent kinase inhibitor, in chronic lymphocytic leukemia. *Blood*, 113(19): 4637-4645.
 55. Chen, W., Tomalia, D. A., & Thomas, J. L. (2000). Unusual pH-dependent polarity changes in PAMAM dendrimers: evidence for pH-responsive conformational changes. *Macromolecules*, 33(25): 9169-9172.
 56. Cheruzel, L. E., Pometun, M. S., Cecil, M. R., Mashuta, M. S., Wittebort, R. J., & Buchanan, R. M. (2003). Structures and solid-state dynamics of one-dimensional water chains stabilized by imidazole channels. *Angewandte Chemie*, 115(44): 5610-5613.

57. Chimenti, F., Bizzarri, B., Maccioni, E., Secci, D., Bolasco, A., Fioravanti, R., *et al.* (2007). Synthesis and in vitro activity of 2-thiazolylhydrazone derivatives compared with the activity of clotrimazole against clinical isolates of *Candida* spp. *Bioorganic & Medicinal Chemistry Letters*, 17(16): 4635-4640.
58. Cohen, P. (1982). The role of protein phosphorylation in neural and hormonal control of cellular activity. *Nature*, 296: 613-620.
59. Cohen, P. (2002). Protein kinases—the major drug targets of the twenty-first century? *Nature Reviews Drug Discovery*, 1(4): 309-315.
60. Collins, I., & Workman, P. (2006). New approaches to molecular cancer therapeutics. *Nature Chemical Biology*, 2(12): 689-700.
61. Congiu, C., & Onnis, V. (2013). Synthesis and biological evaluation of novel acylhydrazone derivatives as potential antitumor agents. *Bioorganic & Medicinal Chemistry*, 21(21): 6592-6599.
62. Cukurovali, A., Yilmaz, I., Gur, S., & Kazaz, C. (2006). Synthesis, antibacterial and antifungal activity of some new thiazolylhydrazone derivatives containing 3-substituted cyclobutane ring. *European Journal of Medicinal Chemistry*, 41(2): 201-207.
63. Da, K., Abelman, W., Craver, L., & Burchenal, J. (1948). The use of nitrogen mustards in the palliative treatment of cancer. *Cancer*, 1: 634-6456.
64. Dar, A. A., Goff, L. W., Majid, S., Berlin, J., & El-Rifai, W. (2010). Aurora kinase inhibitors—rising stars in cancer therapeutics? *Molecular Cancer Therapeutics*, 9(2): 268-278.
65. Darbre, T., & Reymond, J.-L. (2006). Peptide dendrimers as artificial enzymes, receptors, and drug-delivery agents. *Accounts of Chemical Research*, 39(12): 925-934.
66. Das, D., Sikdar, P., & Bairagi, M. (2016). Recent developments of 2-aminothiazoles in medicinal chemistry. *European Journal of Medicinal Chemistry*, 109: 89-98.
67. Das, J., Chen, P., Norris, D., Padmanabha, R., Lin, J., Moquin, R. V., *et al.* (2006). 2-aminothiazole as a novel kinase inhibitor template. Structure-activity relationship studies toward the discovery of N-(2-chloro-6-methylphenyl)-2-[[6-[4-(2-hydroxyethyl)-1-piperazinyl]]-2-methyl-4-pyrimidinyl] amino]-1, 3-thiazole-5-carboxamide (dasatinib, BMS-354825) as a potent pan-Src kinase inhibitor. *Journal of Medicinal Chemistry*, 49(23): 6819-6832.

68. De las Heras, F. G., Alonso, R., & Alonso, G. (1979). Alkylating nucleosides. 1. Synthesis and cytostatic activity of N-glycosyl (halomethyl)-1, 2, 3-triazoles. A new type of alkylating agent. *Journal of Medicinal Chemistry*, 22(5): 496-501.
69. DeGraw, J., & Goodman, L. (1964). Alkylating agents derived from indole. IV. Synthesis of the 5-Nitrogen mustard of indole-3-carboxylic acid1a. *Journal of Medicinal Chemistry*, 7(2): 213-215.
70. D'Emanuele, A., & Attwood, D. (2005). Dendrimer–drug interactions. *Advanced Drug Delivery Reviews*, 57(15): 2147-2162.
71. Deng, Z.-L., Du, C.-X., Li, X., Hu, B., Kuang, Z.-K., Wang, R., *et al.* (2013). Exploring the biologically relevant chemical space for drug discovery. *Journal of Chemical Information and Modeling*, 53(11): 2820-2828.
72. Denisova, A., & Andronnikova, G. (1995). Bromination of 4-substituted thiazolylhydrazones. *Chemistry of Heterocyclic Compounds*, 31(7): 863-867.
73. Desiraju, G. R. (2007). Crystal engineering: a holistic view. *Angewandte Chemie International Edition*, 46(44): 8342-8356.
74. Desiraju, G. R., Vittal, J. J., & Ramanan, A. (2011). *Crystal engineering: a textbook*: World Scientific.
75. Dillman, R. O., Johnson, D. E., Shawler, D. L., & Koziol, J. A. (1988). Superiority of an acid-labile daunorubicin-monoclonal antibody immunoconjugate compared to free drug. *Cancer Research*, 48(21): 6097-6102.
76. Du, J.-Z., Du, X.-J., Mao, C.-Q., & Wang, J. (2011). Tailor-made dual pH-sensitive polymer–doxorubicin nanoparticles for efficient anticancer drug delivery. *Journal of the American Chemical Society*, 133(44): 17560-17563.
77. Dua, R., Shrivastava, S., Sonwane, S., & Srivastava, S. (2011). Pharmacological significance of synthetic heterocycles scaffold: a review. *Advances in Biological Research*, 5(3): 120-144.
78. Dudkin, V. Y., Wang, C., Arrington, K. L., Fraley, M. E., Hartman, G. D., Stirdivant, S. M., *et al.* (2012). Pyridyl aminothiazoles as potent Chk1 inhibitors: optimization of cellular activity. *Bioorganic & Medicinal Chemistry Letters*, 22(7): 2613-2619.
79. Dunham, W. (1990). *Journey through genius: the great theorems of mathematics*. Wiley: New York.

80. Easmon, J., Pürstinger, G., Thies, K.-S., Heinisch, G., & Hofmann, J. (2006). Synthesis, structure-activity relationships, and antitumor studies of 2-benzoxazolyl hydrazones derived from alpha-(N)-acyl heteroaromatics. *Journal of Medicinal Chemistry*, 49(21): 6343-6350.
81. El-Gaby, M. S., Micky, J. A., Taha, N. M., El-Sharief, S., & Marwa, A. (2002). Antimicrobial activity of some novel thiourea, hydrazine, fused pyrimidine and 2-(4-substituted) anilinobenzoazole derivatives containing sulfonamido moieties. *Journal of the Chinese Chemical Society*, 49(3): 407-414.
82. El-Messery, S. M., Hassan, G. S., Al-Omary, F. A., & El-Subbagh, H. I. (2012). Substituted thiazoles VI. Synthesis and antitumor activity of new 2-acetamido-and 2 or 3-propanamido-thiazole analogs. *European Journal of Medicinal Chemistry*, 54: 615-625.
83. Eriksson, U. K., Fischer, G., Friemann, R., Enkavi, G., Tajkhorshid, E., & Neutze, R. (2013). Subangstrom resolution X-ray structure details aquaporin-water interactions. *Science*, 340(6138): 1346-1349.
84. Esfand, R., & Tomalia, D. (2001). *Dendrimers and Other Dendritic Polymers*. Wiley: New York.
85. Etter, M. C. (1990). Encoding and decoding hydrogen-bond patterns of organic compounds. *Accounts of Chemical Research*, 23(4): 120-126.
86. Ferrandina, G., Mariani, M., Andreoli, M., Shahabi, S., Scambia, G., & Ferlini, C. (2012). Novel drugs targeting microtubules: the role of epothilones. *Current Pharmaceutical Design*, 18(19): 2793-2803.
87. Francini, C. M., Fallacara, A. L., Artusi, R., Mennuni, L., Calgani, A., Angelucci, A., *et al.* (2015). Identification of aminoimidazole and aminothiazole derivatives as Src family kinase inhibitors. *ChemMedChem*, 10(12): 2027-2041.
88. Gaies, E., Jebabli, N., Trabelsi, S., Salouage, I., Charfi, R., Lakhal, M., *et al.* (2012). Methotrexate side effects: review article. *Journal of Drug Metabolism and Toxicology*. doi: 10.4172/2157-7609.1000125.
89. Gangopadhyay, M., Singh, T., Behara, K. K., Karwa, S., Ghosh, S., & Singh, N. P. (2015). Coumarin-containing-star-shaped 4-arm-polyethylene glycol: targeted fluorescent organic nanoparticles for dual treatment of photodynamic therapy and chemotherapy. *Photochemical & Photobiological Sciences*, 14(7): 1329-1336.

90. Gardner, C. R., Walsh, C. T., & Almarsson, Ö. (2004). Drugs as materials: valuing physical form in drug discovery. *Nature Reviews Drug Discovery*, 3(11): 926-934.
91. Gemma, S., Savini, L., Altarelli, M., Tripaldi, P., Chiasserini, L., Coccone, S. S., *et al.* (2009). Development of antitubercular compounds based on a 4-quinolyldiazone scaffold. Further structure–activity relationship studies. *Bioorganic and Medicinal Chemistry*, 17(16): 6063-6072.
92. Gerwert, K., Freier, E., & Wolf, S. (2014). The role of protein-bound water molecules in microbial rhodopsins. *Biochimica et Biophysica Acta (BBA)-Bioenergetics*, 1837(5): 606-613.
93. Ghose, A. K., Herbertz, T., Pippin, D. A., Salvino, J. M., & Mallamo, J. P. (2008). Knowledge based prediction of ligand binding modes and rational inhibitor design for kinase drug discovery. *Journal of Medicinal Chemistry*, 51(17): 5149-5171.
94. Glotova, T., Protsuk, N., Kanitskaya, L., Dolgushin, G., & Lopyrev, V. (2004). Reactions of α -acetylenic ketones with n-3-amidinothioureas. 1. Synthesis and properties of new derivatives of 1, 3-thiazine. *Chemistry of Heterocyclic Compounds*, 40(12): 1595-1599.
95. Goette, D. K. (1981). Topical chemotherapy with 5-fluorouracil: A review. *Journal of the American Academy of Dermatology*, 4(6): 633-649.
96. Gomha, S. M., Abdulla, M. M., & Abou-Seri, S. M. (2015). Identification of novel aminothiazole and aminothiadiazaole conjugated cyanopyridines as selective CHK1 inhibitors. *European Journal of Medicinal Chemistry*, 92: 459-470.
97. Gorczynski, M. J., Leal, R. M., Mooberry, S. L., Bushweller, J. H., & Brown, M. L. (2004). Synthesis and evaluation of substituted 4-aryloxy- and 4-arylsulfanyl-phenyl-2-aminothiazoles as inhibitors of human breast cancer cell proliferation. *Bioorganic and Medicinal Chemistry*, 12(5): 1029-1036.
98. Grabchev, I., Qian, X., Bojinov, V., Xiao, Y., & Zhang, W. (2002). Synthesis and photophysical properties of 1, 8-naphthalimide-labelled PAMAM as PET sensors of protons and of transition metal ions. *Polymer*, 43(21): 5731-5736.

99. Grant, D. J. (1999). Theory and origin of polymorphism. *Drugs and the Pharmaceutical Sciences*, 95: 1-33.
100. Green, D. A., Antholine, W. E., Wong, S. J., Richardson, D. R., & Chitambar, C. R. (2001). Inhibition of malignant cell growth by 311, a novel iron chelator of the pyridoxal isonicotinoyl hydrazone class effect on the r2 subunit of ribonucleotide reductase. *Clinical Cancer Research*, 7(11): 3574-3579.
101. Greenfield, R. S., Kaneko, T., Daues, A., Edson, M. A., Fitzgerald, K. A., Olech, L. J., *et al.* (1990). Evaluation in vitro of adriamycin immunoconjugates synthesized using an acid-sensitive hydrazone linker. *Cancer Research*, 50(20): 6600-6607.
102. Griffiths, G., Scaerou, F., Midgley, C., McClue, S., Tosh, C., Jackson, W., *et al.* (2008). Anti-tumor activity of CYC116, a novel small molecule inhibitor of Aurora kinases and VEGFR2. *Cancer Research*, 68(9 Supplement): 5644-5644.
103. Gupta, G. P., & Massagué, J. (2006). Cancer metastasis: Building a framework. *Cell*, 127(4): 679-695.
104. Gupton, J. (2006). Pyrrole natural products with antitumor properties. In M. Lee (Ed.), *Heterocyclic Antitumor Antibiotics* (Vol. 2, pp. 53-92): Springer Berlin Heidelberg.
105. Hall, M. D., Salam, N. K., Hellawell, J. L., Fales, H. M., Kensler, C. B., Ludwig, J. A., *et al.* (2009). Synthesis, activity, and pharmacophore development for isatin- β -thiosemicarbazones with selective activity toward multidrug-resistant cells. *Journal of Medicinal Chemistry*, 52(10): 3191-3204.
106. Hamamichi, N., Natrajan, A., & Hecht, S. M. (1992). On the role of individual bleomycin thiazoles in oxygen activation and DNA cleavage. *Journal of the American Chemical Society*, 114(16): 6278-6291.
107. Han, M., Chen, P., & Yang, X. (2005). Molecular dynamics simulation of PAMAM dendrimer in aqueous solution. *Polymer*, 46(10): 3481-3488.
108. Hardy, L. W., & Malikayil, A. (2003). The impact of structure-guided drug design on clinical agents. *Current Drug Discovery*, 3: 15-20.
109. Hartwell, L. H., & Kastan, M. B. (1994). Cell cycle control and cancer. *Science*, 266(5192): 1821-1828.
110. Hassan, G. S., El-Messery, S. M., Al-Omary, F. A., & El-Subbagh, H. I. (2012). Substituted thiazoles VII. Synthesis and antitumor activity of certain

- 2-(substituted amino)-4-phenyl-1,3-thiazole analogs. *Bioorganic & Medicinal Chemistry Letters*, 22(20): 6318-6323.
111. Heiniger, B., Gakhar, G., Prasain, K., Hua, D. H., & Nguyen, T. A. (2010). Second-generation substituted quinolines as anticancer drugs for breast cancer. *Anticancer Research*, 30(10): 3927-3932.
 112. Hirai, H., Shimomura, T., Kobayashi, M., Eguchi, T., Taniguchi, E., Fukasawa, K., *et al.* (2010). Biological characterization of 2-aminothiazole-derived Cdk4/6 selective inhibitor in vitro and in vivo. *Cell Cycle*, 9(8): 1590-1600.
 113. Holla, B. S., Malini, K., Rao, B. S., Sarojini, B., & Kumari, N. S. (2003). Synthesis of some new 2, 4-disubstituted thiazoles as possible antibacterial and anti-inflammatory agents. *European Journal of Medicinal Chemistry*, 38(3): 313-318.
 114. Hollingsworth, M. D. (2002). Crystal engineering: from structure to function. *Science*, 295(5564): 2410-2413.
 115. Hoque, M. N., Basu, A., & Das, G. (2013). Pyridine–urea-based anion receptor: formation of cyclic sulfate–water hexamer and dihydrogen phosphate–water trimer in hydrophobic environment. *Crystal Growth & Design*, 14(1): 6-10.
 116. Hrubý, M., Koňák, Č., & Ulbrich, K. (2005). Polymeric micellar pH-sensitive drug delivery system for doxorubicin. *Journal of Controlled Release*, 103(1): 137-148.
 117. Huang, L.-F., & Tong, W.-Q. T. (2004). Impact of solid state properties on developability assessment of drug candidates. *Advanced Drug Delivery Reviews*, 56(3): 321-334.
 118. Hung, W.-I., Hung, C.-B., Chang, Y.-H., Dai, J.-K., Li, Y., He, H., *et al.* (2011). Synthesis and electroactive properties of poly (amidoamine) dendrimers with an aniline pentamer shell. *Journal of Materials Chemistry*, 21(12): 4581-4587.
 119. Ignat, A., Lovasz, T., Vasilescu, M., Fischer-Fodor, E., Tatomir, C. B., Cristea, C., *et al.* (2012). Heterocycles 27. Microwave assisted synthesis and antitumour activity of novel phenothiazinyl-thiazolyl-hydrazine derivatives. *Archiv der Pharmazie*, 345(7): 574-583.
 120. Infantes, L., Fábíán, L., & Motherwell, W. S. (2007). Organic crystal hydrates: what are the important factors for formation. *CrystEngComm*, 9(1): 65-71.

121. Javor, S., Delort, E., Darbre, T., & Reymond, J.-L. (2007). A peptide dendrimer enzyme model with a single catalytic site at the core. *Journal of the American Chemical Society*, 129(43): 13238-13246.
122. Jenardanan, G., Francis, M., Deepa, S., & Rajasekharan, K. (1997). 1-(N-Arylthiocarbamoyl) amidino-3, 5-dimethyl Pyrazoles-Preparation and Use in Heterocycle Synthesis. *Synthetic Communications*, 27(19): 3457-3462.
123. Jiang, J. B., Hesson, D., Dusak, B., Dexter, D., Kang, G., & Hamel, E. (1990). Synthesis and biological evaluation of 2-styrylquinazolin-4 (3H)-ones, a new class of antimitotic anticancer agents which inhibit tubulin polymerization. *Journal of Medicinal Chemistry*, 33(6): 1721-1728.
124. Jordan, V. C. (2003). Antiestrogens and selective estrogen receptor modulators as multifunctional medicines. 1. Receptor interactions. *Journal of Medicinal Chemistry*, 46(6): 883-908.
125. Jorgensen, W. L. (2004). The many roles of computation in drug discovery. *Science*, 303(5665): 1813-1818.
126. Juneja, M., Vanam, U., Paranthaman, S., Bharathan, A., Keerthi, V. S., Reena, J. K., *et al.* (2013). 4-Amino-2-arylamino-5-indoloyl/cinnamoylthiazoles, analogs of topsentin-class of marine alkaloids, induce apoptosis in HeLa cells. *European Journal of Medicinal Chemistry*, 63: 474-483.
127. Jung, F. H., Pasquet, G., Lambert-van der Brempt, C., Lohmann, J.-J. M., Warin, N., Renaud, F., *et al.* (2006). Discovery of novel and potent thiazoloquinazolines as selective Aurora A and B kinase inhibitors. *Journal of Medicinal Chemistry*, 49(3): 955-970.
128. Kaila, J. C., Baraiya, A. B., Pandya, A. N., Jalani, H. B., Vasu, K. K., & Sudarsanam, V. (2009). A convenient synthesis of di- and trisubstituted 2-aminoimidazoles from 1-amidino-3-trityl-thioureas. *Tetrahedron Letters*, 50(27): 3955-3958.
129. Kaila, V. R., Verkhovsky, M. I., & Wikström, M. (2010). Proton-coupled electron transfer in cytochrome oxidase. *Chemical Reviews*, 110(12): 7062-7081.
130. Kalani, K., Yadav, D. K., Khan, F., Srivastava, S. K., & Suri, N. (2012). Pharmacophore, QSAR, and ADME based semisynthesis and in vitro evaluation of ursolic acid analogs for anticancer activity. *Journal of Molecular Modeling*, 18(7): 3389-3413.
131. Kamal, A., Dastagiri, D., Ramaiah, M. J., Reddy, J. S., Bharathi, E. V., Reddy, M. K., *et al.* (2011). Synthesis and apoptosis inducing ability of new

anilino substituted pyrimidine sulfonamides as potential anticancer agents. *European Journal of Medicinal Chemistry*, 46(12): 5817-5824.

132. Kamal, A., Rao, A. S., Vishnuvardhan, M., Reddy, T. S., Swapna, K., Bagul, C., *et al.* (2015). Synthesis of 2-anilinopyridyl–triazole conjugates as antimetabolic agents. *Organic and Biomolecular Chemistry*, 13(17): 4879-4895.
133. Kandpal, B., Meshram, J., Mohanram, I., & Shaikh, A. (2015). Evaluation of newly synthesized quinazolinone derivatives of hydrazones as potent anti-inflammatory and antibacterial agents. *Medicinal Chemistry Research*, 24(4): 1419-1426.
134. Kaplánek, R., Jakubek, M., Rak, J., Kejík, Z., Havlík, M., Dolenský, B., *et al.* (2015). Caffeine–hydrazones as anticancer agents with pronounced selectivity toward T-lymphoblastic leukaemia cells. *Bioorganic Chemistry*, 60: 19-29.
135. Karegoudar, P., Karthikeyan, M. S., Prasad, D. J., Mahalinga, M., Holla, B. S., & Kumari, N. S. (2008). Synthesis of some novel 2, 4-disubstituted thiazoles as possible antimicrobial agents. *European Journal of Medicinal Chemistry*, 43(2): 261-267.
136. Karplus, M., & McCammon, J. A. (2002). Molecular dynamics simulations of biomolecules. *Nature Structural & Molecular Biology*, 9(9): 646-652.
137. Keen, N., & Taylor, S. (2004). Aurora-kinase inhibitors as anticancer agents. *Nature Reviews Cancer*, 4(12): 927-936.
138. Kelkar, D. A., & Chattopadhyay, A. (2007). The gramicidin ion channel: a model membrane protein. *Biochimica et Biophysica Acta (BBA)-Biomembranes*, 1768(9): 2011-2025.
139. Kerns, E. H., & Di, L. (2003). Pharmaceutical profiling in drug discovery. *Drug Discovery Today*, 8(7): 316-323.
140. Kesharwani, P., & Iyer, A. K. (2015). Recent advances in dendrimer-based nanovectors for tumor-targeted drug and gene delivery. *Drug Discovery Today*, 20(5): 536-547.
141. Khan, K. M., Irfan, M., Ashraf, M., Taha, M., Saad, S. M., Perveen, S., *et al.* (2015). Synthesis of phenyl thiazole hydrazones and their activity against glycation of proteins. *Medicinal Chemistry Research*, 24(7): 1-9.
142. Kidwai, M., Venktaramanan, R., Mohan, R., & Sapra, P. (2002). Cancer chemotherapy and heterocyclic compounds. *Current Medicinal Chemistry*, 9(12): 1209-1228.

143. Kim, K. S., Kimball, S. D., Cai, Z.-w., Rawlins, D. B., Misra, R. N., Poss, M. A., *et al.* (2001). Aminothiazole inhibitors of cyclin dependent kinases, *US6262096 B1*.
144. Kim, K. S., Kimball, S. D., Misra, R. N., Rawlins, D. B., Hunt, J. T., Xiao, H.-Y., *et al.* (2002). Discovery of aminothiazole inhibitors of cyclin-dependent kinase 2: synthesis, X-ray crystallographic analysis, and biological activities. *Journal of Medicinal Chemistry*, 45(18): 3905-3927.
145. Kim, Y., Kim, S. H., Tanyeri, M., Katzenellenbogen, J. A., & Schroeder, C. M. (2013). Dendrimer probes for enhanced photostability and localization in fluorescence imaging. *Biophysical Journal*, 104(7): 1566-1575.
146. King, T. P., Zhao, S. W., & Lam, T. (1986). Preparation of protein conjugates via intermolecular hydrazone linkage. *Biochemistry*, 25(19): 5774-5779.
147. Kitchen, D. B., Decornez, H., Furr, J. R., & Bajorath, J. (2004). Docking and scoring in virtual screening for drug discovery: methods and applications. *Nature Reviews Drug Discovery*, 3(11): 935-949.
148. Klajnert, B., & Bryszewska, M. (2000). Dendrimers: properties and applications. *Acta Biochimica Polonica*, 48(1): 199-208.
149. Knowles, J., & Gromo, G. (2003). Target selection in drug discovery. *Nature Reviews Drug Discovery*, 2(1): 63-69.
150. Knox, P., O'sullivan, M., & Lentfer, H. (2003). Piperidinyl-thiazole carboxylic acid derivatives as angiogenesis inhibitors, *US20060135501 A1*.
151. Kobayashi, H., & Brechbiel, M. W. (2005). Nano-sized MRI contrast agents with dendrimer cores. *Advanced Drug Delivery Reviews*, 57(15): 2271-2286.
152. Koehn, F. E., & Carter, G. T. (2005). The evolving role of natural products in drug discovery. *Nature Reviews Drug Discovery*, 4(3): 206-220.
153. Kollareddy, M., Zheleva, D., Dzubak, P., Brahmikshatriya, P. S., Lepsik, M., & Hajdich, M. (2012). Aurora kinase inhibitors: progress towards the clinic. *Investigational New Drugs*, 30(6): 2411-2432.
154. Komander, D., Kular, G. S., Schüttelkopf, A. W., Deak, M., Prakash, K., Bain, J., *et al.* (2004). Interactions of LY333531 and other bisindolyl maleimide inhibitors with PDK1. *Structure*, 12(2): 215-226.

155. Kontogiorgis, C. A., & Hadjipavlou-Litina, D. J. (2005). Synthesis and antiinflammatory activity of coumarin derivatives. *Journal of Medicinal Chemistry*, 48(20): 6400-6408.
156. Koo, H., Huh, M. S., Ryu, J. H., Lee, D.-E., Sun, I.-C., Choi, K., *et al.* (2011). Nanoprobes for biomedical imaging in living systems. *Nano Today*, 6(2): 204-220.
157. Kornblatt, J. A. (1998). The water channel of cytochrome c oxidase: inferences from inhibitor studies. *Biophysical Journal*, 75(6): 3127-3134.
158. Krasia-Christoforou, T., & Georgiou, T. K. (2013). Polymeric theranostics: using polymer-based systems for simultaneous imaging and therapy. *Journal of Materials Chemistry B*, 1(24): 3002-3025.
159. Kukowska-Latallo, J. F., Candido, K. A., Cao, Z., Nigavekar, S. S., Majoros, I. J., Thomas, T. P., *et al.* (2005). Nanoparticle targeting of anticancer drug improves therapeutic response in animal model of human epithelial cancer. *Cancer Research*, 65(12): 5317-5324.
160. Kumar, B. S., & Panda, P. K. (2014). 1D water chain stabilized by meso-expanded calix [4] pyrrole. *CrystEngComm*, 16(37): 8669-8672.
161. Kumar, C. S. (2007). *Nanomaterials for biosensors*: John Wiley & Sons.
162. Kumar, N., Chauhan, L. S., Sharma, C. S., Dashora, N., & Bera, R. (2014). Synthesis, analgesic and anti-inflammatory activities of chalconyl-incorporated hydrazone derivatives of mefenamic acid. *Medicinal Chemistry Research*, 26(6): 1-11.
163. Kumar, P., Shrivastava, B., Pandeya, S. N., Tripathi, L., & Stables, J. P. (2012). Design, synthesis, and anticonvulsant evaluation of some novel 1, 3 benzothiazol-2-yl hydrazones/acetohydrazones. *Medicinal Chemistry Research*, 21(9): 2428-2442.
164. Kumari, P., Ghosh, B., & Biswas, S. (2015). Nanocarriers for cancer-targeted drug delivery. *Journal of Drug Targeting*, 24(3): 1-13.
165. La Regina, G., Bai, R., Coluccia, A., Famiglini, V., Pelliccia, S., Passacantilli, S., *et al.* (2014). New pyrrole derivatives with potent tubulin polymerization inhibiting activity as anticancer agents including hedgehog-dependent cancer. *Journal of Medicinal Chemistry*, 57(15): 6531-6552.
166. Lai, P.-S., Lou, P.-J., Peng, C.-L., Pai, C.-L., Yen, W.-N., Huang, M.-Y., *et al.* (2007). Doxorubicin delivery by polyamidoamine dendrimer conjugation and photochemical internalization for cancer therapy. *Journal of Controlled Release*, 122(1): 39-46.

167. Lamy, C. M., Sallin, O., Loussert, C., & Chatton, J.-Y. (2012). Sodium sensing in neurons with a dendrimer-based nanoprobe. *ACS Nano*, 6(2): 1176-1187.
168. Landry, Y., & Gies, J. P. (2008). Drugs and their molecular targets: an updated overview. *Fundamental & Clinical Pharmacology*, 22(1): 1-18.
169. Lapenna, S., & Giordano, A. (2009). Cell cycle kinases as therapeutic targets for cancer. *Nature Reviews Drug Discovery*, 8(7): 547-566.
170. Le Duc, Y., Michau, M., Gilles, A., Gence, V., Legrand, Y. M., van der Lee, A., *et al.* (2011). Imidazole-quartet water and proton dipolar channels. *Angewandte Chemie*, 123(48): 11568-11574.
171. Lee, F. Y., Borzilleri, R., Fairchild, C. R., Kim, S.-H., Long, B. H., Reventos-Suarez, C., *et al.* (2001). BMS-247550 a novel epothilone analog with a mode of action similar to paclitaxel but possessing superior antitumor efficacy. *Clinical Cancer Research*, 7(5): 1429-1437.
172. Lee, F. Y., Covello, K. L., Castaneda, S., Hawken, D. R., Kan, D., Lewin, A., *et al.* (2008). Synergistic antitumor activity of ixabepilone (BMS-247550) plus bevacizumab in multiple in vivo tumor models. *Clinical Cancer Research*, 14(24): 8123-8131.
173. Lee, H., Baker, J. R., & Larson, R. G. (2006). Molecular dynamics studies of the size, shape, and internal structure of 0% and 90% acetylated fifth-generation polyamidoamine dendrimers in water and methanol. *The Journal of Physical Chemistry B*, 110(9): 4014-4019.
174. Lee, W. I., Bae, Y., & Bard, A. J. (2004). Strong blue photoluminescence and ECL from OH-terminated PAMAM dendrimers in the absence of gold nanoparticles. *Journal of the American Chemical Society*, 126(27): 8358-8359.
175. Lesniak, W. G., Mishra, M. K., Jyoti, A., Balakrishnan, B., Zhang, F., Nance, E., *et al.* (2013). Biodistribution of fluorescently labeled PAMAM dendrimers in neonatal rabbits: effect of neuroinflammation. *Molecular Pharmaceutics*, 10(12): 4560-4571.
176. Levy, Y., & Onuchic, J. N. (2006). Water mediation in protein folding and molecular recognition. *Annual Review of Biophysics and Biomolecular Structure*, 35: 389-415.
177. Li, C.-M., Lu, Y., Narayanan, R., Miller, D. D., & Dalton, J. T. (2010). Drug metabolism and pharmacokinetics of 4-substituted methoxybenzoyl-aryl-thiazoles. *Drug Metabolism and Disposition*, 38(11): 2032-2039.

178. Li, X., Lu, X., Xing, M., Yang, X.-H., Zhao, T.-T., Gong, H.-B., *et al.* (2012). Synthesis, biological evaluation, and molecular docking studies of N, 1, 3-triphenyl-1H-pyrazole-4-carboxamide derivatives as anticancer agents. *Bioorganic & Medicinal Chemistry Letters*, 22(11): 3589-3593.
179. Li, Y., Xu, Y., Qian, X., & Qu, B. (2004). Naphthalimide–thiazoles as novel photonucleases: molecular design, synthesis, and evaluation. *Tetrahedron Letters*, 45(6): 1247-1251.
180. Libertini, S., Abagnale, A., Passaro, C., Botta, G., & Portella, G. (2010). Aurora A and B kinases-targets of novel anticancer drugs. *Recent patents on anti-cancer drug discovery*, 5(3): 219-241.
181. Lin, H.-Y., Li, Z.-K., Bai, L.-F., Baloch, S. K., Wang, F., Qiu, H.-Y., *et al.* (2015). Synthesis of aryl dihydrothiazol acyl shikonin ester derivatives as anticancer agents through microtubule stabilization. *Biochemical Pharmacology*, 96(2): 93-106.
182. Lindauer, M., & Hochhaus, A. (2014). *Small molecules in oncology*. Springer: New York.
183. Lipinski, C. A. (2004). Lead-and drug-like compounds: the rule-of-five revolution. *Drug Discovery Today: Technologies*, 1(4): 337-341.
184. Little, M. A., Briggs, M. E., Jones, J. T., Schmidtman, M., Hasell, T., Chong, S. Y., *et al.* (2015). Trapping virtual pores by crystal retro-engineering. *Nature Chemistry*, 7(2): 153-159.
185. Liu, J., Yang, X., He, X., Wang, K., Wang, Q., Guo, Q., *et al.* (2011). Fluorescent nanoparticles for chemical and biological sensing. *Science China Chemistry*, 54(8): 1157-1176.
186. Liu, L., & Breslow, R. (2003). Dendrimeric pyridoxamine enzyme mimics. *Journal of the American Chemical Society*, 125(40): 12110-12111.
187. Liu, Y., Bryantsev, V. S., Diallo, M. S., & Goddard Iii, W. A. (2009). PAMAM dendrimers undergo pH responsive conformational changes without swelling. *Journal of the American Chemical Society*, 131(8): 2798-2799.
188. López-Cabaña, Z., Valdés, O., Vergara, C., Camarada, M., Nachtigall, F., González-Nilo, F., *et al.* (2015). Photophysical studies of the interactions of poly (amidoamine) generation zero (PAMAM G0) with copper and zinc ions. *Journal of Luminescence*, 164: 23-30.

189. Lu, B., & Atala, A. (2014). Small molecules and small molecule drugs in regenerative medicine. *Drug Discovery Today*, 19(6): 801-808.
190. Lu, Y., Li, C.-M., Wang, Z., Chen, J., Mohler, M. L., Li, W., *et al.* (2011). Design, synthesis, and SAR studies of 4-substituted methoxybenzoyl-aryl-thiazoles analogues as potent and orally bioavailable anticancer agents. *Journal of medicinal chemistry*, 54(13): 4678-4693.
191. Ma, L., Harrell Jr, W. A., & Davis, J. T. (2009). Stabilizing guanosine-sterol ion channels with a carbamate to urea modification in the linker. *Organic Letters*, 11(7): 1599-1602.
192. Ma, X. D., Yang, S. Q., Gu, S. X., He, Q. Q., Chen, F. E., De Clercq, E., *et al.* (2011). Synthesis and anti-HIV activity of aryl-2-[(4-cyanophenyl) amino]-4-pyrimidinone hydrazones as potent Non-nucleoside reverse transcriptase inhibitors. *ChemMedChem*, 6(12): 2225-2232.
193. Ma, Y.-q. (2013). Theoretical and computational studies of dendrimers as delivery vectors. *Chemical Society Reviews*, 42(2): 705-727.
194. Madadi, N. R., Zong, H., Ketkar, A., Zheng, C., Penthala, N. R., Janganati, V., *et al.* (2015). Synthesis and evaluation of a series of resveratrol analogues as potent anti-cancer agents that target tubulin. *Medicinal Chemical Communications*, 6(5): 788-794.
195. Maeda, H., Wu, J., Sawa, T., Matsumura, Y., & Hori, K. (2000). Tumor vascular permeability and the EPR effect in macromolecular therapeutics: a review. *Journal of Controlled Release*, 65(1): 271-284.
196. Mahajan, A., Kremer, L., Louw, S., Guéradel, Y., Chibale, K., & Biot, C. (2011). Synthesis and in vitro antitubercular activity of ferrocene-based hydrazones. *Bioorganic & Medicinal Chemistry Letters*, 21(10): 2866-2868.
197. Mahboobi, S., Sellmer, A., Höcher, H., Eichhorn, E., Bär, T., Schmidt, M., *et al.* (2006). [4-(Imidazol-1-yl) thiazol-2-yl] phenylamines. A novel class of highly potent colchicine site binding tubulin inhibitors: synthesis and cytotoxic activity on selected human cancer cell lines. *Journal of Medicinal Chemistry*, 49(19): 5769-5776.
198. Maiti, P. K., & Goddard, W. A. (2006). Solvent quality changes the structure of G8 PAMAM dendrimer, a disagreement with some experimental interpretations. *The Journal of Physical Chemistry B*, 110(51): 25628-25632.

199. Maiti, P. K., Cagin, T., Lin, S.-T., & Goddard, W. A. (2005). Effect of solvent and pH on the structure of PAMAM dendrimers. *Macromolecules*, 38(3): 979-991.
200. Makam, P., Thakur, P. K., & Kannan, T. (2014). *In vitro* and *in silico* antimalarial activity of 2-(2-hydrazinyl) thiazole derivatives. *European Journal of Pharmaceutical Sciences*, 52: 138-145.
201. Malumbres, M., & Barbacid, M. (2009). Cell cycle, CDKs and cancer: a changing paradigm. *Nature Reviews Cancer*, 9(3): 153-166.
202. Manivel, P., & Khan, F. N. (2009). Synthesis of some new 2, 4-disubstituted hydrazinethiazoles and 2, 5-disubstituted thiazolidinones. *Phosphorus, Sulfur, and Silicon*, 184(11): 2910-2922.
203. Manvar, A., Bavishi, A., Radadiya, A., Patel, J., Vora, V., Dodia, N., *et al.* (2011). Diversity oriented design of various hydrazides and their *in vitro* evaluation against Mycobacterium tuberculosis H37 Rv strains. *Bioorganic & Medicinal Chemistry Letters*, 21(16): 4728-4731.
204. Mao, J., Wang, Y., Wan, B., Kozikowski, A. P., & Franzblau, S. G. (2007). Design, Synthesis, and pharmacological evaluation of mefloquine-based ligands as novel antituberculosis agents. *ChemMedChem*, 2(11): 1624-1630.
205. Marcus, Y. (1993). The properties of organic liquids that are relevant to their use as solvating solvents. *Chemical Society Reviews*, 22(6): 409-416.
206. Martins, P., Jesus, J., Santos, S., Raposo, L. R., Roma-Rodrigues, C., Baptista, P. V., *et al.* (2015). Heterocyclic anticancer compounds: recent advances and the paradigm shift towards the use of nanomedicine's tool box. *Molecules*, 20(9): 16852-16891.
207. Mascal, M., Infantes, L., & Chisholm, J. (2006). Water oligomers in crystal hydrates—what's news and what isn't? *Angewandte Chemie International Edition*, 45(1): 32-36.
208. Mataga, N., Kaifu, Y., & Koizumi, M. (1956). Solvent effects upon fluorescence spectra and the dipolemoments of excited molecules. *Bulletin of the Chemical Society of Japan*, 29(4): 465-470.
209. Melink, T. J., Von Hoff, D. D., Kuhn, J. G., Hersh, M. R., Sternson, L. A., Patton, T. F., *et al.* (1985). Phase I evaluation and pharmacokinetics of tiazofurin (2- β -d-ribofuranosylthiazole-4-carboxamide, NSC 286193). *Cancer Research*, 45(6): 2859-2865.

210. Meng, X.-Y., Zhang, H.-X., Mezei, M., & Cui, M. (2011). Molecular docking: a powerful approach for structure-based drug discovery. *Current Computer-aided Drug Design*, 7(2): 146-157.
211. Menjoge, A. R., Kannan, R. M., & Tomalia, D. A. (2010). Dendrimer-based drug and imaging conjugates: design considerations for nanomedical applications. *Drug Discovery Today*, 15(5): 171-185.
212. Mérian, J., Gravier, J., Navarro, F., & Texier, I. (2012). Fluorescent nanoprobes dedicated to in vivo imaging: from preclinical validations to clinical translation. *Molecules*, 17(5): 5564-5591.
213. Miklis, P., Cag˘in, T., & Goddard, W. A. (1997). Dynamics of Bengal Rose encapsulated in the Meijer dendrimer box. *Journal of the American Chemical Society*, 119(32): 7458-7462.
214. Misra, R. N., Xiao, H.-y., Kim, K. S., Lu, S., Han, W.-C., Barbosa, S. A., *et al.* (2004). N-(cycloalkylamino) acyl-2-aminothiazole inhibitors of cyclin-dependent kinase 2. N-[5-[[[5-(1, 1-dimethylethyl)-2-oxazolyl] methyl] thio]-2-thiazolyl]-4-piperidinecarboxamide (BMS-387032), a highly efficacious and selective antitumor agent. *Journal of Medicinal Chemistry*, 47(7): 1719-1728.
215. Monks, A., Scudiero, D., Skehan, P., Shoemaker, R., Paull, K., Vistica, D., *et al.* (1991). Feasibility of a high-flux anticancer drug screen using a diverse panel of cultured human tumor cell lines. *Journal of the National Cancer Institute*, 83(11): 757-766.
216. Moon, C., Preston, G. M., Griffin, C. A., Jabs, E. W., & Agre, P. (1993). The human aquaporin-CHIP gene. Structure, organization, and chromosomal localization. *Journal of Biological Chemistry*, 268(21): 15772-15778.
217. Mountzios, G., Terpos, E., & Dimopoulos, M.-A. (2008). Aurora kinases as targets for cancer therapy. *Cancer Treatment Reviews*, 34(2): 175-182.
218. Mullen, D. G., Desai, A., van Dongen, M. A., Barash, M., Baker Jr, J. R., & Banaszak Holl, M. M. (2012). Best practices for purification and characterization of PAMAM dendrimer. *Macromolecules*, 45(12): 5316-5320.
219. Nam, S., Kim, D., Cheng, J. Q., Zhang, S., Lee, J.-H., Buettner, R., *et al.* (2005). Action of the Src family kinase inhibitor, dasatinib (BMS-354825), on human prostate cancer cells. *Cancer Research*, 65(20): 9185-9189.
220. Natarajan, R., Bridgland, L., Sirikulajorn, A., Lee, J.-H., Haddow, M. F., Magro, G., *et al.* (2013). Tunable porous organic crystals: structural scope

- and adsorption properties of nanoporous steroidal ureas. *Journal of the American Chemical Society*, 135(45): 16912-16925.
221. Nettles, J. H., Li, H., Cornett, B., Krahn, J. M., Snyder, J. P., & Downing, K. H. (2004). The binding mode of epothilone A on α , β -tubulin by electron crystallography. *Science*, 305(5685): 866-869.
 222. Newman, A. W., & Byrn, S. R. (2003). Solid-state analysis of the active pharmaceutical ingredient in drug products. *Drug Discovery Today*, 8(19): 898-905.
 223. Nikonova, A. S., Astsaturov, I., Serebriiskii, I. G., Dunbrack Jr, R. L., & Golemis, E. A. (2013). Aurora A kinase (AURKA) in normal and pathological cell division. *Cellular and Molecular Life Sciences*, 70(4): 661-687.
 224. O'Dwyer, P. J., Shoemaker, D. D., Jayaram, H. N., Johns, D. G., Cooney, D. A., Marsoni, S., *et al.* (1984). Tiazofurin: a new antitumor agent. *Investigational New Drugs*, 2(1): 79-84.
 225. Oesterling, I., & Müllen, K. (2007). Multichromophoric polyphenylene dendrimers: toward brilliant light emitters with an increased number of fluorophores. *Journal of the American Chemical Society*, 129(15): 4595-4605.
 226. Ooms, F. (2000). Molecular modeling and computer aided drug design. Examples of their applications in medicinal chemistry. *Current Medicinal Chemistry*, 7(2): 141-158.
 227. Özdemir, A. (2010). Synthesis of some novel hydrazone derivatives and evaluation of their antituberculosis activity. *Marmara Pharmaceutical Journal* 14: 79-83.
 228. Özkay, Y., Tunalı, Y., Karaca, H., & Işıkdag, İ. (2010). Antimicrobial activity and a SAR study of some novel benzimidazole derivatives bearing hydrazone moiety. *European Journal of Medicinal Chemistry*, 45(8): 3293-3298.
 229. Pack, D. W., Hoffman, A. S., Pun, S., & Stayton, P. S. (2005). Design and development of polymers for gene delivery. *Nature reviews Drug discovery*, 4(7): 581-593.
 230. Parker, W. B. (2009). Enzymology of purine and pyrimidine antimetabolites used in the treatment of cancer. *Chemical Reviews*, 109(7): 2880-2893.

231. Patil, S. A., Patil, R., & Miller, D. D. (2012). Indole molecules as inhibitors of tubulin polymerization: potential new anticancer agents. *Future Medicinal Chemistry*, 4(16): 2085-2115.
232. Paul, S., Pragalath, S., Yardily, A., Rajasekharan, K., Reji, T., & Fen, A. (2013). Synthesis of anticancer compounds 2-(4-amino-2-arylaminothiazol-5-oyl)-N-methylbenzimidazoles. *Indian Journal of Chemistry Section B-Organic Chemistry Including Medicinal Chemistry*, 52(4): 560-564.
233. Penthala, N. R., Zong, H., Ketkar, A., Madadi, N. R., Janganati, V., Eoff, R. L., *et al.* (2015). Synthesis, anticancer activity and molecular docking studies on a series of heterocyclic trans-cyanocombretastatin analogues as antitubulin agents. *European Journal of Medicinal Chemistry*, 92: 212-220.
234. Pérez-Herrero, E., & Fernández-Medarde, A. (2015). Advanced targeted therapies in cancer: Drug nanocarriers, the future of chemotherapy. *European Journal of Pharmaceutics and Biopharmaceutics*, 93: 52-79.
235. Peters, G., Van der Wilt, C., Van Moorsel, C., Kroep, J., Bergman, A., & Ackland, S. (2000). Basis for effective combination cancer chemotherapy with antimetabolites. *Pharmacology and Therapeutics*, 87(2): 227-253.
236. Petros, R. A., & DeSimone, J. M. (2010). Strategies in the design of nanoparticles for therapeutic applications. *Nature Reviews Drug discovery*, 9(8): 615-627.
237. Pinto, L. H., Dieckmann, G. R., Gandhi, C. S., Papworth, C. G., Braman, J., Shaughnessy, M. A., *et al.* (1997). A functionally defined model for the M2 proton channel of influenza A virus suggests a mechanism for its ion selectivity. *Proceedings of the National Academy of Sciences*, 94(21): 11301-11306.
238. Pistolis, G., Malliaris, A., Paleos, C., & Tsiourvas, D. (1997). Study of poly (amidoamine) starburst dendrimers by fluorescence probing. *Langmuir*, 13(22): 5870-5875.
239. Prabakaran, M., Grailer, J. J., Pilla, S., Steeber, D. A., & Gong, S. (2009). Amphiphilic multi-arm-block copolymer conjugated with doxorubicin via pH-sensitive hydrazone bond for tumor-targeted drug delivery. *Biomaterials*, 30(29): 5757-5766.
240. Prasanna, D., Kavitha, C., Vinaya, K., Ranganatha, S., Raghavan, S. C., & Rangappa, K. (2010). Synthesis and Identification of a new class of antileukemic agents containing 2-(arylcarboxamide)-(S)-6-amino-4, 5, 6, 7-tetrahydrobenzo [d] thiazole. *European Journal of Medicinal Chemistry*, 45(11): 5331-5336.

241. Prashanth, T., Thirusangu, P., Avin, B. V., Ranganatha, V. L., Prabhakar, B., & Khanum, S. A. (2014). Synthesis and evaluation of novel benzophenone-thiazole derivatives as potent VEGF-A inhibitors. *European Journal of Medicinal Chemistry*, 87: 274-283.
242. Qiao, Z., & Shi, X. (2015). Dendrimer-based molecular imaging contrast agents. *Progress in Polymer Science*, 44: 1-27.
243. Qin, J., Xi, L., Du, J., Liu, H., & Yao, X. (2010). QSAR studies on aminothiazole derivatives as aurora a kinase inhibitors. *Chemical Biology & Drug Design*, 76(6): 527-537.
244. R Solomon, V., & Lee, H. (2011). Quinoline as a privileged scaffold in cancer drug discovery. *Current Medicinal Chemistry*, 18(10): 1488-1508.
245. Raciti, G., Mazzone, P., Raudino, A., Mazzone, G., & Cambria, A. (1995). Inhibition of rat liver mitochondrial monoamine oxidase by hydrazine-thiazole derivatives: structure-activity relationships. *Bioorganic and Medicinal Chemistry*, 3(11): 1485-1491.
246. Radi, M., Dreassi, E., Brullo, C., Crespan, E., Tintori, C., Bernardo, V., *et al.* (2011). Design, synthesis, biological activity, and ADME properties of pyrazolo [3, 4-d] pyrimidines active in hypoxic human leukemia cells: a lead optimization study. *Journal of Medicinal Chemistry*, 54(8): 2610-2626.
247. Rajasekharan, K., Nair, K., & Jenardanan, G. (1986). Studies on the synthesis of 5-acyl-2, 4-diaminothiazoles from amidinothioureas. *Synthesis*(5): 353-355.
248. Rajitha, G., Prasad, K. V., Umamaheswari, A., Pradhan, D., & Bharathi, K. (2014). Synthesis, biological evaluation, and molecular docking studies of N-(α -acetamido cinnamoyl) aryl hydrazone derivatives as antiinflammatory and analgesic agents. *Medicinal Chemistry Research*, 23(12): 5204-5214.
249. Ramírez, J., Svetaz, L., Quiroga, J., Abonia, R., Raimondi, M., Zacchino, S., *et al.* (2015). Synthesis of novel thiazole-based 8, 9-dihydro-7H-pyrimido [4, 5-b][1, 4] diazepines as potential antitumor and antifungal agents. *European Journal of Medicinal Chemistry*, 92: 866-875.
250. Rask-Andersen, M., Zhang, J., Fabbro, D., & Schiöth, H. B. (2014). Advances in kinase targeting: current clinical use and clinical trials. *Trends in Pharmacological Sciences*, 35(11): 604-620.
251. Ravi, M., Soujanya, T., Samanta, A., & Radhakrishnan, T. (1995). Excited-state dipole moments of some Coumarin dyes from a solvatochromic method using the solvent polarity parameter, ENT. *Journal of the Chemical Society, Faraday Transactions*, 91(17): 2739-2742.

252. Reddy, D. S., Hosamani, K. M., Devarajegowda, H. C., & Kurjogi, M. M. (2015). A facile synthesis and evaluation of new biomolecule-based coumarin–thiazoline hybrids as potent anti-tubercular agents with cytotoxicity, DNA cleavage and X-ray studies. *RSC Advances*, 5(79): 64566-64581.
253. Reilly, D. T., Kim, S. H., Katzenellenbogen, J. A., & Schroeder, C. M. (2015). Fluorescent nanoconjugate derivatives with enhanced photostability for single molecule imaging. *Analytical Chemistry*, 87(21): 11048-11057.
254. Reymond, J.-L., Van Deursen, R., Blum, L. C., & Ruddigkeit, L. (2010). Chemical space as a source for new drugs. *Medicinal Chemical Communications*, 1(1): 30-38.
255. Robert, F., Hurwitz, H., Verschraegen, C., Advani, R., Berman, C., Taverna, P., *et al.* (2008). Phase 1 trial of SNS-314, a novel selective inhibitor of aurora kinases A, B, and C, in advanced solid tumor patients. *ASCO Annual Meeting Proceedings*, 2008, pp.14642.
256. Robins, R., Srivastava, P., Narayanan, V., Plowman, J., & Paull, K. (1982). 2-. beta.-D-ribofuranosylthiazole-4-carboxamide, a novel potential antitumor agent for lung tumors and metastases. *Journal of Medicinal Chemistry*, 25(2): 107-108.
257. Rollas, S., & Küçükgülzel, S. G. (2007). Biological activities of hydrazone derivatives. *Molecules*, 12(8): 1910-1939.
258. Romagnoli, R., Baraldi, P. G., Brancale, A., Ricci, A., Hamel, E., Bortolozzi, R., *et al.* (2011). Convergent synthesis and biological evaluation of 2-amino-4-(3', 4', 5'-trimethoxyphenyl)-5-aryl thiazoles as microtubule targeting agents. *Journal of Medicinal Chemistry*, 54(14): 5144-5153.
259. Romagnoli, R., Baraldi, P. G., Carrion, M. D., Cruz-Lopez, O., Lopez Cara, C., Basso, G., *et al.* (2009). 2-Arylamino-4-amino-5-arylthiazoles. "One-pot" synthesis and biological evaluation of a new class of inhibitors of tubulin polymerization. *Journal of Medicinal Chemistry*, 52(17): 5551-5555.
260. Romagnoli, R., Baraldi, P. G., Salvador, M. K., Camacho, M. E., Preti, D., Tabrizi, M. A., *et al.* (2012). Synthesis and biological evaluation of 2-substituted-4-(3', 4', 5'-trimethoxyphenyl)-5-aryl thiazoles as anticancer agents. *Bioorganic and Medicinal Chemistry*, 20(24): 7083-7094.
261. Roy, S., Quiñones, R., & Matzger, A. J. (2012). Structural and physicochemical aspects of dasatinib hydrate and anhydrate phases. *Crystal Growth & Design*, 12(4): 2122-2126.

262. Salehi, M., Amini, M., Ostad, S. N., Riazi, G. H., Assadieskandar, A., Shafiei, B., *et al.* (2013). Synthesis, cytotoxic evaluation and molecular docking study of 2-alkylthio-4-(2, 3, 4-trimethoxyphenyl)-5-aryl-thiazoles as tubulin polymerization inhibitors. *Bioorganic and Medicinal Chemistry*, 21(24): 7648-7654.
263. Salgın-Gökşen, U., Gökhan-Kelekçi, N., Göktaş, Ö., Köysal, Y., Kılıç, E., Işık, Ş., *et al.* (2007). 1-Acylthiosemicarbazides, 1, 2, 4-triazole-5 (4H)-thiones, 1, 3, 4-thiadiazoles and hydrazones containing 5-methyl-2-benzoxazolinones: synthesis, analgesic-anti-inflammatory and antimicrobial activities. *Bioorganic and Medicinal Chemistry*, 15(17): 5738-5751.
264. Schnell, J. R., & Chou, J. J. (2008). Structure and mechanism of the M2 proton channel of influenza A virus. *Nature*, 451(7178): 591-595.
265. Schonbrunn, E., Betzi, S., Alam, R., Martin, M. P., Becker, A., Han, H., *et al.* (2013). Development of highly potent and selective diaminothiazole inhibitors of cyclin-dependent kinases. *Journal of Medicinal Chemistry*, 56(10): 3768-3782.
266. Schrödinger Release 2016-1: *Desmond Molecular Dynamics System, version 4.5*, D. E. Shaw Research, New York, NY, 2016. Maestro-Desmond Interoperability Tools, version 4.5, Schrödinger, New York, NY, 2016.
267. Schrödinger Release 2014-1: *LigPrep, version 2.9*, Schrödinger, LLC, New York, NY, 2014.
268. Scott, F. L., & Reilly, J. (1952). Studies in the pyrazole series. i. halogenation of the 1-guanylpurazoles. *Journal of the American Chemical Society*, 74(18): 4562-4566.
269. Secci, D., Bizzarri, B., Bolasco, A., Carradori, S., D'Ascenzio, M., Rivanera, D., *et al.* (2012). Synthesis, anti-Candida activity, and cytotoxicity of new (4-(4-iodophenyl) thiazol-2-yl) hydrazine derivatives. *European Journal of Medicinal Chemistry*, 53: 246-253.
270. Sedaghat, T., Aminian, M., & Azarkish, M. (2015). New bis-diphenyltin (IV) complexes with oxalyldihydrazone derivatives: Synthesis, characterization and antibacterial activity. *Phosphorus, Sulfur, and Silicon and the Related Elements*, 190(3): 352-359.
271. Sedaghat, T., Aminian, M., Bruno, G., & Rudbari, H. A. (2013). Binuclear organotin (IV) complexes with adipic dihydrazones: Synthesis, spectral characterization, crystal structures and antibacterial activity. *Journal of Organometallic Chemistry*, 737: 26-31.

272. Sengupta, S., Smitha, S. L., Thomas, N. E., Santhoshkumar, T. R., Devi, S. K., Sreejalekshmi, K. G., *et al.* (2005). 4-Amino-5-benzoyl-2-(4-methoxyphenylamino) thiazole (DAT1): a cytotoxic agent towards cancer cells and a probe for tubulin-microtubule system. *British Journal of Pharmacology*, 145(8): 1076-1083.
273. Shah, N. P., Tran, C., Lee, F. Y., Chen, P., Norris, D., & Sawyers, C. L. (2004). Overriding imatinib resistance with a novel ABL kinase inhibitor. *Science*, 305(5682): 399-401.
274. Sharma, A., & Kakkar, A. (2015). Designing dendrimer and miktoarm polymer based multi-tasking nanocarriers for efficient medical therapy. *Molecules*, 20(9): 16987-17015.
275. Sheldrick, G. M. (Ed.). (1997). *SHELXL 97, Program for Crystal Structure Solution and Refinement*; Go ttingen University: Germany.
276. Sherer, C., & Snape, T. J. (2014). Heterocyclic scaffolds as promising anticancer agents against tumours of the central nervous system: Exploring the scope of indole and carbazole derivatives. *European Journal of Medicinal Chemistry*, 97:552-560.
277. Sherr, C. J. (1996). Cancer cell cycles. *Science*, 274(5293): 1672-1677.
278. Shiau, C.-w., & Chen, K.-f. (2015). Aryl amine substituted pyrimidine and quinazoline and their use as anticancer drugs, *US20150246891 A1*.
279. Shimamura, T., Shibata, J., Kurihara, H., Mita, T., Otsuki, S., Sagara, T., *et al.* (2006). Identification of potent 5-pyrimidinyl-2-aminothiazole CDK4, 6 inhibitors with significant selectivity over CDK1, 2, 5, 7, and 9. *Bioorganic & Medicinal Chemistry Letters*, 16(14): 3751-3754.
280. Shujah, S., Muhammad, N., Shah, A., Ali, S., Meetsma, A., & Hussain, Z. (2014). Homobimetallic organotin (IV) complexes with hexadentate Schiff base: Synthesis, crystal structure and antimicrobial studies. *Journal of Organometallic Chemistry*, 759: 19-26.
281. Sidhu, J., Singla, R., Mayank, E., & Jaitak, V. (2015). Indole derivatives as anticancer agents for breast cancer therapy: A review. *Anti-cancer Agents in Medicinal Chemistry*, 16(2):160-173.
282. Siegel, R. L., Miller, K. D., & Jemal, A. (2015). Cancer statistics, 2015. *CA: A Cancer Journal for Clinicians*, 65(1): 5-29.

283. Sijbesma, R. P., Beijer, F. H., Brunsveld, L., Folmer, B. J., Hirschberg, J. K., Lange, R. F., *et al.* (1997). Reversible polymers formed from self-complementary monomers using quadruple hydrogen bonding. *Science*, 278(5343): 1601-1604.
284. Sikic, B. I., Rozenzweig, M., & Carter, S. K. (2013). *Bleomycin chemotherapy*, Elsevier: USA.
285. Silverman, R. B., & Holladay, M. W. (2014). *The organic chemistry of drug design and drug action*, Elsevier: USA.
286. Skehan, P., Storeng, R., Scudiero, D., Monks, A., McMahon, J., Vistica, D., *et al.* (1990). New colorimetric cytotoxicity assay for anticancer-drug screening. *Journal of the National Cancer Institute*, 82(13): 1107-1112.
287. Sliwoski, G., Kothiwale, S., Meiler, J., & Lowe, E. W. (2014). Computational methods in drug discovery. *Pharmacological Reviews*, 66(1): 334-395.
288. Slobbe, P., Ruijter, E., & Orru, R. V. (2012). Recent applications of multicomponent reactions in medicinal chemistry. *MedChemComm*, 3(10): 1189-1218.
289. Small-Molecule Drug Discovery Suite 2014-1: *Glide*, version 6.2, Schrödinger, LLC, New York, NY, 2014.
290. Sondhi, S. M., Dinodia, M., & Kumar, A. (2006). Synthesis, anti-inflammatory and analgesic activity evaluation of some amidine and hydrazone derivatives. *Bioorganic and Medicinal Chemistry*, 14(13): 4657-4663.
291. Song, Y. n., Chen, W., Kang, D., Zhang, Q., Zhan, P., & Liu, X. (2014). "Old friends in new guise": exploiting privileged structures for scaffold re-evolution/refining. *Combinatorial Chemistry & High Throughput Screening*, 17(6): 536-553.
292. Soršak, E., Valh, J. V., Urek, Š. K., & Lobnik, A. (2015). Application of PAMAM dendrimers in optical sensing. *Analyst*, 140(4): 976-989.
293. Sreejalekshmi, K. G. (2010). A Facile, Sequential Multicomponent Approach to N-Aminoamidinothioureas—Versatile Synthons to Bioactive Heterocycles. *Phosphorus, Sulfur, and Silicon*, 185(9): 1830-1837.
294. Sreejalekshmi, K. G., Devi, S. K., & Rajasekharan, K. N. (2006). An efficient protocol for solid phase aminothiazole synthesis. *Tetrahedron Letters*, 47(35): 6179-6182.

295. Sriram, D., Yogeewari, P., & Madhu, K. (2006). Synthesis and in vitro antitubercular activity of some 1-[(4-sub) phenyl]-3-(4-{1-[(pyridine-4-carbonyl) hydrazono] ethyl} phenyl) thiourea. *Bioorganic & Medicinal Chemistry Letters*, 16(4): 876-878.
296. Stockwell, B. R. (2004). Exploring biology with small organic molecules. *Nature*, 432(7019): 846-854.
297. Stubbe, J., Kozarich, J. W., Wu, W., & Vanderwall, D. E. (1996). Bleomycins: a structural model for specificity, binding, and double strand cleavage. *Accounts of Chemical Research*, 29(7): 322-330.
298. Sui, H., Han, B.-G., Lee, J. K., Walian, P., & Jap, B. K. (2001). Structural basis of water-specific transport through the AQP1 water channel. *Nature*, 414(6866): 872-878.
299. Svenson, S., & Chauhan, A. S. (2008). Dendrimers for enhanced drug solubilization. *Nanomedicine*, 3(5): 679-702.
300. Svenson, S., & Tomalia, D. A. (2012). Dendrimers in biomedical applications—reflections on the field. *Advanced Drug Delivery Reviews*, 64: 102-115.
301. Tager, M., & Danowski, T. (1948). Inhibition of the growth of fungi by thiourea derivatives, particularly hydrazine dithiocarbamyl. *The Journal of Infectious Diseases*, 82(2): 126-130.
302. Tajkhorshid, E., Nollert, P., Jensen, M. Ø., Miercke, L. J., O'Connell, J., Stroud, R. M., *et al.* (2002). Control of the selectivity of the aquaporin water channel family by global orientational tuning. *Science*, 296(5567): 525-530.
303. Takimoto, C. H., Lu, Z.-H., Zhang, R., Liang, M. D., Larson, L. V., Cantilena, L., *et al.* (1996). Severe neurotoxicity following 5-fluorouracil-based chemotherapy in a patient with dihydropyrimidine dehydrogenase deficiency. *Clinical Cancer Research*, 2(3): 477-481.
304. Talpaz, M., Shah, N. P., Kantarjian, H., Donato, N., Nicoll, J., Paquette, R., *et al.* (2006). Dasatinib in imatinib-resistant Philadelphia chromosome-positive leukemias. *New England Journal of Medicine*, 354(24): 2531-2541.
305. Tanis, I., & Karatasos, K. (2009). Association of a weakly acidic anti-inflammatory drug (ibuprofen) with a poly (amidoamine) dendrimer as studied by molecular dynamics simulations. *The Journal of Physical Chemistry B*, 113(31): 10984-10993.
306. Tao, X., Yang, Y.-J., Liu, S., Zheng, Y.-Z., Fu, J., & Chen, J.-F. (2013). Poly (amidoamine) dendrimer-grafted porous hollow silica nanoparticles

for enhanced intracellular photodynamic therapy. *Acta Biomaterialia*, 9(5): 6431-6438.

307. Taziaux, D., Soumillion, J.-P., & Jiwan, J.-L. H. (2004). Photophysical and complexing properties of new fluoroionophores based on coumarin 343 linked to rigidified crown-ethers. *Journal of Photochemistry and Photobiology A: Chemistry*, 162(2): 599-607.
308. Tekade, R. K., Kumar, P. V., & Jain, N. K. (2008). Dendrimers in oncology: an expanding horizon. *Chemical Reviews*, 109(1): 49-87.
309. Terstappen, G. C., Schlüpen, C., Raggiaschi, R., & Gaviraghi, G. (2007). Target deconvolution strategies in drug discovery. *Nature Reviews Drug Discovery*, 6(11): 891-903.
310. Thirumalai, D., Reddy, G., & Straub, J. E. (2011). Role of water in protein aggregation and amyloid polymorphism. *Accounts of Chemical Research*, 45(1): 83-92.
311. Thomas, E., Tabernero, J., Fornier, M., Conté, P., Fumoleau, P., Lluch, A., *et al.* (2007). Phase II clinical trial of ixabepilone (BMS-247550), an epothilone B analog, in patients with taxane-resistant metastatic breast cancer. *Journal of Clinical Oncology*, 25(23): 3399-3406.
312. Thomas, N. E., Thamkachy, R., Sivakumar, K. C., Sreedevi, K. J., Louis, X. L., Thomas, S. A., *et al.* (2014). Reversible action of diaminothiazoles in cancer cells Is implicated by the induction of a fast conformational change of tubulin and suppression of microtubule dynamics. *Molecular Cancer Therapeutics*, 13(1): 179-189.
313. Thomas, S. A., Vasudevan, S., Thamkachy, R., Lekshmi, S. U., Santhoshkumar, T. R., Rajasekharan, K. N., *et al.* (2013). Upregulation of DR5 receptor by the diaminothiazole DAT1 [4-amino-5-benzoyl-2-(4-methoxy phenyl amino) thiazole] triggers an independent extrinsic pathway of apoptosis in colon cancer cells with compromised pro and antiapoptotic proteins. *Apoptosis*, 18(6): 713-726.
314. Thomas, T. P., Shukla, R., Kotlyar, A., Kukowska-Latallo, J., & Baker, J. R. (2010). Dendrimer-based tumor cell targeting of fibroblast growth factor-1. *Bioorganic & Medicinal Chemistry Letters*, 20(2): 700-703.
315. Tian, J., Thallapally, P. K., & McGrail, B. P. (2012). Porous organic molecular materials. *CrystEngComm*, 14(6): 1909-1919.
316. Titus, S., & Sreejalekshmi, K. G. (2014). One-pot four-component synthesis of 4-hydrazinothiazoles: novel scaffolds for drug discovery. *Tetrahedron Letters*, 55(40): 5465-5467.

317. Tokarski, J. S., Newitt, J. A., Chang, C. Y. J., Cheng, J. D., Wittekind, M., Kiefer, S. E., *et al.* (2006). The structure of Dasatinib (BMS-354825) bound to activated ABL kinase domain elucidates its inhibitory activity against imatinib-resistant ABL mutants. *Cancer Research*, 66(11): 5790-5797.
318. Tomalia, D. A. (2005). Birth of a new macromolecular architecture: dendrimers as quantized building blocks for nanoscale synthetic polymer chemistry. *Progress in Polymer Science*, 30(3): 294-324.
319. Tomalia, D. A., Baker, H., Dewald, J., Hall, M., Kallos, G., Martin, S., *et al.* (1985). A new class of polymers: starburst-dendritic macromolecules. *Polymer Journal*, 17(1): 117-132.
320. Torchilin, V. P. (2012). Multifunctional nanocarriers. *Advanced Drug Delivery Reviews*, 64: 302-315.
321. Trenor, S. R., Shultz, A. R., Love, B. J., & Long, T. E. (2004). Coumarins in polymers: from light harvesting to photo-cross-linkable tissue scaffolds. *Chemical Reviews*, 104(6): 3059-3078.
322. Tricot, G., Jayaram, H. N., Weber, G., & Hoffman, R. (1990). Tiazofurin: biological effects and clinical uses. *The International Journal of Cell Cloning*, 8(3): 161-170.
323. Trivedi, M., Budihardjo, I., Loureiro, K., Reid, T. R., & Ma, J. D. (2008). Epothilones: a novel class of microtubule-stabilizing drugs for the treatment of cancer. *Future Oncology*, 4(4): 483-500.
324. Turner, D. R., Paterson, M. J., & Steed, J. W. (2006). A conformationally flexible, urea-based tripodal anion receptor: solid-state, solution, and theoretical studies. *The Journal of Organic Chemistry*, 71(4): 1598-1608.
325. Ubersax, J. A., & Ferrell Jr, J. E. (2007). Mechanisms of specificity in protein phosphorylation. *Nature Reviews Molecular Cell Biology*, 8(7): 530-541.
326. Uclés, A., Ulaszewska, M., Hernando, M., Ramos, M., Herrera, S., García, E., *et al.* (2013). Qualitative and quantitative analysis of poly (amidoamine) dendrimers in an aqueous matrix by liquid chromatography–electrospray ionization-hybrid quadrupole/time-of-flight mass spectrometry (LC-ESI-QTOF-MS). *Analytical and Bioanalytical Chemistry*, 405(18): 5901-5914.
327. Usol'tseva, S., & Andronnikova, G. (1994a). Synthesis and properties of thiazole halohydrazones. 1. Synthesis and interaction of 2- α -chlorobenzylidenehydrazino-4-ethoxycarbonyl-thiazole with triethylamine

in the presence of dipolarophiles. *Chemistry of Heterocyclic Compounds*, 30(2): 231-233.

328. Usol'tseva, S., & Andronnikova, G. (1994b). Synthesis and properties of thiazole halohydrazones. 2. Interaction of 2- α -chlorobenzylidenehydrazino-4-ethoxy-carbonylthiazole with nucleophiles. *Chemistry of Heterocyclic Compounds*, 30(2): 234-237.
329. Usol'tseva, S., Andronnikova, G., & Shevyrin, V. (1993). Bromination of 2-thiazolylhydrazones. *Chemistry of Heterocyclic Compounds*, 29(2): 226-230.
330. Varughese, S., & Desiraju, G. R. (2010). Using water as a design element in crystal engineering. Host– guest compounds of hydrated 3, 5-dihydroxybenzoic acid. *Crystal Growth & Design*, 10(9): 4184-4196.
331. Vasantha, K., Basavarajaswamy, G., Rai, M. V., Boja, P., Pai, V. R., Shruthi, N., *et al.* (2015). Rapid 'one-pot' synthesis of a novel benzimidazole-5-carboxylate and its hydrazone derivatives as potential anti-inflammatory and antimicrobial agents. *Bioorganic & Medicinal Chemistry Letters*, 25(7): 1420-1426.
332. Vasudevan, S., Thomas, S. A., Sivakumar, K. C., Komalam, R. J., Sreerekha, K. V., Rajasekharan, K. N., *et al.* (2015). Diaminothiazoles evade multidrug resistance in cancer cells and xenograft tumour models and develop transient specific resistance: Understanding the basis of broad-spectrum vs specific resistance. *Carcinogenesis*. doi: 10.1093/carcin/bgv072.
333. Veber, D. F., Johnson, S. R., Cheng, H.-Y., Smith, B. R., Ward, K. W., & Kopple, K. D. (2002). Molecular properties that influence the oral bioavailability of drug candidates. *Journal of Medicinal Chemistry*, 45(12): 2615-2623.
334. Verma, G., Marella, A., Shaquiquzzaman, M., Akhtar, M., Ali, M. R., & Alam, M. M. (2014). A review exploring biological activities of hydrazones. *Journal of Pharmacy & Bioallied Sciences*, 6(2): 69-80.
335. Vicini, P., Geronikaki, A., Incerti, M., Busonera, B., Poni, G., Cabras, C. A., *et al.* (2003). Synthesis and biological evaluation of benzo [d] isothiazole, benzothiazole and thiazole Schiff bases. *Bioorganic and Medicinal Chemistry*, 11(22): 4785-4789.
336. Vicini, P., Incerti, M., La Colla, P., & Loddo, R. (2009). Anti-HIV evaluation of benzo [d] isothiazole hydrazones. *European Journal of Medicinal Chemistry*, 44(4): 1801-1807.

337. Vogt, D., Weber, J., Ihlefeld, K., Brüggerhoff, A., Proschak, E., & Stark, H. (2014). Design, synthesis and evaluation of 2-aminothiazole derivatives as sphingosine kinase inhibitors. *Bioorganic and Medicinal Chemistry*, 22(19): 5354-5367.
338. Wang, D. M., Kuo, J. W., Kuo, W. T., Hsu, C. F., Wang, M. H., Chang, Y., *et al.* (2014). Synthesis and cellular uptake of p-[123I]-phenyl-aminothiazole (123I-PAT) as a potential agent for targeting tubulin polymerization in tumors. *Journal of Labelled Compounds and Radiopharmaceuticals*, 57(3): 132-135.
339. Wang, D., & Imae, T. (2004). Fluorescence emission from dendrimers and its pH dependence. *Journal of the American Chemical Society*, 126(41): 13204-13205.
340. Wang, H.-H., Qiu, K.-M., Cui, H.-E., Yang, Y.-S., Xing, M., Qiu, X.-Y., *et al.* (2013). Synthesis, molecular docking and evaluation of thiazolyl-pyrazoline derivatives containing benzodioxole as potential anticancer agents. *Bioorganic and Medicinal Chemistry*, 21(2): 448-455.
341. Wang, Y.-T., Tang, G.-M., Wang, J.-H., Wan, W.-Z., Qin, T.-X., Wang, Y.-Q., *et al.* (2013). Dynamic one-dimensional water in a nonporous organic solid with optics response. *CrystEngComm*, 15(37): 7430-7433.
342. Wängler, C., Moldenhauer, G., Saffrich, R., Knapp, E. M., Beijer, B., Schnölzer, M., *et al.* (2008). PAMAM structure-based multifunctional fluorescent conjugates for improved fluorescent labelling of biomacromolecules. *Chemistry—A European Journal*, 14(27): 8116-8130.
343. Welsch, M. E., Snyder, S. A., & Stockwell, B. R. (2010). Privileged scaffolds for library design and drug discovery. *Current Opinion in Chemical Biology*, 14(3): 347-361.
344. Wikström, M., Verkhovsky, M. I., & Hummer, G. (2003). Water-gated mechanism of proton translocation by cytochrome c oxidase. *Biochimica et Biophysica Acta (BBA)-Bioenergetics*, 1604(2): 61-65.
345. Wolfbeis, O. S. (2015). An overview of nanoparticles commonly used in fluorescent bioimaging. *Chemical Society Reviews*, 44(14): 4743-4768.
346. Wolinsky, J. B., & Grinstaff, M. W. (2008). Therapeutic and diagnostic applications of dendrimers for cancer treatment. *Advanced Drug Delivery Reviews*, 60(9): 1037-1055.
347. Woolley, G. A., & Wallace, B. (1992). Model ion channels: gramicidin and alamethicin. *The Journal of Membrane Biology*, 129(2): 109-136.

348. Wu, W., Tang, R., Li, Q., & Li, Z. (2015). Functional hyperbranched polymers with advanced optical, electrical and magnetic properties. *Chemical Society Reviews*, 44(12): 3997-4022.
349. Xiang, M., Cao, Y., Fan, W., Chen, L., & Mo, Y. (2012). Computer-aided drug design: lead discovery and optimization. *Combinatorial Chemistry and High Throughput Screening*, 15(4): 328-337.
350. Xing, M., Zhao, T.-T., Ren, Y.-J., Peng, N.-N., Yang, X.-H., Li, X., *et al.* (2014). Synthesis, biological evaluation, and molecular docking studies of pyrazolyl-acylhydrazone derivatives as novel anticancer agents. *Medicinal Chemistry Research*, 23(7): 3274-3286.
351. Yang, J., Cao, S., Li, J., Xin, J., Chen, X., Wu, W., *et al.* (2013). Staged self-assembly of PAMAM dendrimers into macroscopic aggregates with a microribbon structure similar to that of amelogenin. *Soft Matter*, 9(31): 7553-7559.
352. Yang, J., Zhang, Q., Chang, H., & Cheng, Y. (2015). Surface-engineered dendrimers in gene delivery. *Chemical Reviews*, 115(11): 5274-5300.
353. Yerande, S. G., Baviskar, C. D., Newase, K. M., Wang, W., Wang, K., & Dömling, A. (2014). Mercury (II) Chloride-Mediated Desulphurization of Amidinothiouras: Synthesis and Antimicrobial Activity of 3-Amino-1, 2, 4-triazole Derivatives. *Journal of Heterocyclic Chemistry*, 51(6): 1883-1887.
354. Yerande, S. G., Ghaisas, A. B., Newase, K. M., Wang, W., Wang, K., & Dömling, A. (2014). (3+ 2) Annulation of Amidinothiouras with Binucleophile: Synthesis and Antimicrobial Activity of 3-Phenylamino-5-aryl/alkyl-1, 2, 4-oxadiazole Derivatives. *Journal of Heterocyclic Chemistry*, 51(6): 1752-1756.
355. Yuan, S., Filipek, S., Palczewski, K., & Vogel, H. (2014). Activation of G-protein- coupled receptors correlates with the formation of a continuous internal water pathway. *Nature Communications*. doi: 10.1038/ncomms5733.
356. Zachariae, H. (1990). Methotrexate side effects. *British Journal of Dermatology*, 122(s36): 127-133.
357. Zaharia, V., Ignat, A., Palibroda, N., Ngameni, B., Kuete, V., Fokunang, C. N., *et al.* (2010). Synthesis of some p-toluenesulfonyl-hydrazinothiazoles and hydrazino-bis-thiazoles and their anticancer activity. *European journal of medicinal chemistry*, 45(11): 5080-5085.

358. Zhang, J., Yang, P. L., & Gray, N. S. (2009). Targeting cancer with small molecule kinase inhibitors. *Nature Reviews Cancer*, 9(1): 28-39.
359. Zhang, L., Gu, F., Chan, J., Wang, A., Langer, R., & Farokhzad, O. (2008). Nanoparticles in medicine: therapeutic applications and developments. *Clinical Pharmacology and Therapeutics*, 83(5): 761-769.
360. Zhang, Q., Sha, Y., & Wang, J.-H. (2010). 8-Hydroxyquinoline dansylates modified with PAMAM dendrimer as fluorescent Fe³⁺ sensors. *Molecules*, 15(5): 2962-2971.
361. Zheng, S., Zhong, Q., Jiang, Q., Mottamal, M., Zhang, Q., Zhu, N., *et al.* (2013). Discovery of a series of thiazole derivatives as novel inhibitors of metastatic cancer cell migration and invasion. *ACS Medicinal Chemistry Letters*, 4(2): 191-196.
362. Zheng, S., Zhong, Q., Xi, Y., Mottamal, M., Zhang, Q., Schroeder, R. L., *et al.* (2014). Modification and biological evaluation of thiazole derivatives as novel inhibitors of metastatic cancer cell migration and invasion. *Journal of Medicinal Chemistry*, 57(15): 6653-6667.
363. Zhou, W., Huang, A., Zhang, Y., Lin, Q., Guo, W., You, Z., *et al.* (2015). Design and optimization of hybrid of 2, 4-diaminopyrimidine and arylthiazole scaffold as anticancer cell proliferation and migration agents. *European Journal of Medicinal Chemistry*, 96: 269-280.
364. Zhu, J., & Shi, X. (2013). Dendrimer-based nanodevices for targeted drug delivery applications. *Journal of Materials Chemistry B*, 1(34): 4199-4211.